UNIVERSITY OF CALIFORNIA SAN DIEGO

PolyMOFs: A Novel Class of Polymer-Metal-Organic Framework Hybrid Materials

A dissertation submitted in partial satisfaction of the requirements
for the degree Doctor of Philosophy

in

Chemistry

by

Sergio Ayala Jr.

Committee in charge:

Professor Seth M. Cohen, Chair
Professor Guy Bertrand
Professor Clifford P. Kubiak
Professor Ying Shirley Meng
Professor Tadeusz Molinski

2020

The Dissertation of Sergio Ayala Jr. is approved, and it is acceptable in quality and form for publication on microfilm and electronically:

_____

_____

_____

_____

_____

Chair

University of California San Diego

2020

DEDICATION

To my wife, my son, my parents, my sister and the rest of my family and friends who have supported me throughout this journey, thank you.

TABLE OF CONTENTS

Signature Page iii

Dedication iv

Table of Contents iv

List of Figures viii

List of Schemes xxi

List of Tables xxii

Acknowledgements xxiii

Vita xxvii

Abstract of the Dissertation xxix

Chapter 1: Metal-Organic Frameworks and MOF-Polymer Hybrids 1

1.1 Metal-Organic Frameworks 2

1.2 MOF-Polymer Hybrid Materials 5

1.3 PolyMOFs 12

1.4 Scope of the Dissertation 14

1.5 Acknowledgements 15

1.6 References 15

Chapter 2: UiO-66 polyMOFs with Hierarchical Structure and Porosity 22

2.1 Introduction 23

2.2 Synthesis and Characterization of Polymer Ligands 24

2.3 Synthesis and Characterization of PolyUiO-66 26

2.4 Conclusions 31

2.5 Appendix: Supporting Information 31

2.6 Acknowledgements 52
2.7 References 52
Chapter 3: Applying Isoreticular Chemistry to polyMOFs 55
3.1 Introduction 56
3.2 Results and Discussion – Isoreticular Expansion of polyMOFs 60
3.3 Results and Discussion – PolyMOF Formation from ortho-Substituted Polymer Ligands 68
3.4 Conclusions 73
3.5 Appendix: Supporting Information 74
3.6 Acknowledgements 109
3.7 References 110
Chapter 4: Block co-polyMOFs with Controlled morphologies 113
4.1 Introduction 114
4.2 Synthesis and Characterization of pbdc-8a Block Copolymers 117
4.3 Formation and Morphology Control of UiO-66 BCPMOFs 120
4.4 Synthesis and Characterization of IRMOF-1 Type BCPMOFs 128
4.5 Conclusions 133
4.6 Appendix: Supporting Information 134
4.7 Acknowledgements 193
4.8 References 193
Chapter 5: Multivariate PolyMOFs 198
5.1 Introduction 199
5.2 Synthesis and Characterization of MTV Random Copolymers 202

5.3 Synthesis and Characterization of MTV-polyMOFs 205

5.4 Conclusions and Outlook 211

5.5 Appendix: Supporting Information 213

5.6 Acknowledgements 223

5.7 References 223

LIST OF FIGURES

Figure 1.1. A representation of how different organic linkers and inorganic SBUs can be used to prepare several MOF topologies. (a) H_2bdc and Zn_4O clusters can be combined to produce cubic IRMOF-1 (also referred to as MOF-5) architecture. (b) H_2bdc and $Zr_6(O)_4(OH)_4$ clusters yield a highly interconnected framework, UiO-66. Isoreticular MOFs are achieved 3

Figure 1.2. Schematic representation of postsynthetic modification (PSM) and postsynthetic exchange (PSE). PSM (top) can be achieved on a pre-installed chemical handle. PSE can be achieved by exchanging the metal (bottom left) or the organic linker (bottom right) after MOF formation 5

Figure 1.3. An illustrative representation of MOF mixed-matrix membranes (MMMs) 6

Figure 1.4. The three methods used to graft a polymer onto the surface of a MOF are presented. In a grafting "through" approach (top), the MOF is functionalized with a chemical handle to be copolymerized with a monomer and produce a polymer matrix. In a grafting "from" approach (bottom left), the MOF is functionalized with an initiator to grow polymers directly 8

Figure 1.5. Schematic representation of polymerization through the pores of MOFs. In one approach (top), small molecule monomers like styrene are confined within the pore of a MOF, followed by subsequent polymerization and digestion, to afford polymers with narrow dispersity. Conversely, the MOF can be crosslinked through the pores (bottom) 10

Figure 1.6. An illustrative representation of polymers being used to template the MOF. The synthetic polymer can control the shape of the MOF either through electrostatic interactions (green) or control the size by competitive coordination (red). 12

Figure 1.7. Illustrative example of an amorphous polymer ligand (pbdc-xa) transformed into a polymer-MOF (polyMOF) hybrid material. 13

Figure 2.1. PXRD patterns for UiO-66 polyMOFs prepared from pbdc-*x*a-u ligands 27

Figure 2.2. SEM images of polyUiO-66 prepared from different polymer ligands: a) pbdc-6a-u; b) pbdc-8a-u; c) pbdc-10a (does not form polyUiO-66, only amorphous material). The interlaced morphology found with pbdc-8a-u was also found using fractionated polymer ligands of different M_n: d) pbdc-8a-u_{2800}; e) pbdc-8a-u_{7800}; and f) pbdc-8a-u_{42000} 29

Figure 2.3. N_2 sorption isotherms for polyUiO-66 generated from different polymer ligands. A hysteresis loop was observed for polyMOFs from both: disperse pbdc-8a-u (a), and more uniform, fractionated pbdc-8a-u polymers (b). The hysteric behavior found with all pbdc-8a-u derived samples is indicative of a hierarchal micro- and meso-porous material 30

Figure 2S.1. ^{1}H NMR of pbdc-6e-u. End-group analysis was used to determine number of repeat units and M_n 37

Figure 2S.2. ^{1}H NMR of pbdc-8e-u. End-group analysis was used to determine number of repeat units and M_n 37

Figure 2S.3. ^{1}H NMR of pbdc-10e-u. End-group analysis was used to determine number of repeat units and M_n. 38

Figure 2S.4. ^{1}H NMR of pbdc-8e-u$_{2700}$. End-group analysis was used to determine number of repeat units and M_n. 38

Figure 2S.5. ^{1}H NMR of pbdc-8e-u$_{7800}$. End-group analysis was used to determine number of repeat units and M_n after column chromatography..... 39

Figure 2S.6. ^{1}H NMR of pbdc-8e-u$_{42000}$. End-group analysis was used to determine number of repeat units and M_n after column chromatography 39

Figure 2S.7. GPC traces obtained for a) broad molecular weight pbdc-*x*e-u ligands and b) narrow molecular weight pbdc-8e-u ligands. Negative refraction are solvent markers..... 40

Figure 2S.8. ^{1}H NMR of pbdc-6a-u..... 40

Figure 2S.9. ^{1}H NMR of pbdc-8a-u..... 41

Figure 2S.10. ^{1}H NMR of pbdc-10a-u..... 41

Figure 2S.11. ^{1}H NMR of pbdc-8a-u$_{2800}$.. 42

Figure 2S.12. ^{1}H NMR of pbdc-8a-u$_{7800}$.. 42

Figure 2S.13. ^{1}H NMR of pbdc-8a-u$_{42000}$... 43

Figure 2S.14. MALDI-TOF MS of a) pbdc-8e-u$_{2800}$, b) pbdc-8e-u$_{7800}$, and c) pbdc-8e-u$_{42000}$. No signal was obtained for the largest polymer.... 44

Figure 2S.15. PXRD data was obtained for polyUiO-66 prepared from pbdc-*x*a ligands... 45

Figure 2S.16. ^{1}H NMR of digested polyUiO-66 prepared from broad pbdc-6a-u.... 46

Figure 2S.17. ^{1}H NMR of digested polyUiO-66 prepared from broad pbdc-8a-u.... 46

Figure 2S.18. ^{1}H NMR of digested polyUiO-66 prepared from broad pbdc-10a-u 47

Figure 2S.19. ^{1}H NMR of digested UiO-66 polyMOF prepared from narrow molecular weight pbdc-8a-u..... 47

Figure 2S.20. (a) TGA and (b) (DSC) traces of polyUiO-66 prepared from narrow pbdc-8a-u 48

Figure 2S.21. (a) TGA and (b) (DSC) traces of narrow molecular weight pbdc-8a-u ligands..... 48

Figure 2S.22. PXRD data of pbdc-8a-u_{42000} after being stored for six months in air under ambient conditions..... 49

Figure 2S.23. SEM image of polyUiO-66 prepared from pbdc-6a-u 49

Figure 2S.24. SEM Images for polyUiO-66 prepared from a) pbdc-7a; b) pbdc-8a..... 50

Figure 2S.25. Pore-size distribution of polyUiO-66 prepared from a) pbdc-6a-u and b) pbdc-8a-u 50

Figure 2S.26. Pore-size distribution of polyUiO-66 prepared from narrow molecular weight pbdc-8a-u ligands 51

Figure 2S.27. N_2-Isotherm of polyUiO-66 prepared from pbdc-8a. 51

Figure 3.1. Illustrative representation of reticular (net-like) and isoreticular (same-net) chemistry in MOFs. Reticular MOFs can be prepared using the same ligand (H_2bdc) with different metal precursors to yield the Zn-IRMOF structure (top), or the Zr-UiO structure (bottom). For IRMOF-1 (top-left), replacing H_2bdc with H_2bdc-NH_2 or H_2pbdc yields.... 57

Figure 3.2. Illustration of polymer ligands used to prepare isoreticular polyMOFs in Chapter 3. The notation '*x*' represents the number of methylene spacers between each monomer unit, 'a' denotes 'acid', and 'u' signifies unsaturation in the alkyl spacers..... 58

Figure 3.3. Illustration demonstrating the isoreticular expansion of UiO-type polyMOFs. Figure adapted from reference..... 59

Figure 3.4. Comparison between *para*-substituted (left) and *ortho*-substituted (right) polymer ligands. Figure adapted from reference 59

Figure 3.5. Calculated and experimental PXRD patterns for isoreticular polyMOFs..... 63

Figure 3.6. SXRD structure of polyUiO-68-10a-u. a) The basic building unit of polyUiO-68-10a-u containing terphenyl and $Zr_6(\mu_3\text{-}O)_4(\mu_3\text{-}OH)_4$ SBU. The central phenyl ring of the terphenyl ligand is disordered, but the oxygen atom (red) and first carbon atom (green) of the polymer spacer were refined. b) The extended lattice structure of polyUiO-68-10a-u..... 64

Figure 3.7. SEM images of: (a) polyUiO-67-8a-u; (b) polyUiO-68-8a-u; (c) polyUiO-68-10a-u; (d) polyUiO-68-10a-u single crystal 65

Figure 3.8. Gas sorption isotherms of UiO polyMOFs (N_2, 77 K)..... 67

Figure 3.9. PXRD patterns for *o*-polyMOFs synthesized with two polymer ligands, *o*-pbdc-8a-u in red, *o*-pbdc-10a-u in blue, and calculated IRMOF-1 in black 70

Figure 3.10. SEM images of *o*-polyMOFs synthesized with: a) *o*-pbdc-8a-u, and b) *o*-pbdc-10a-u 71

Figure 3.11. N_2 sorption isotherms for *o*-polyIRMOF synthesized with two polymer-ligands: *o*-pbdc-8a-u in red and *o*-pbdc-10a-u in blue 72

Figure 3S.1. ^{1}H NMR of compound 1 86

Figure 3S.2. ^{1}H NMR of compound 2 86

Figure 3S.3. ^{1}H NMR of compound 3 87

Figure 3S.4. ^{1}H NMR of pbpdc-8e-u. End-group analysis was used to determine number of repeat units and M_n 87

Figure 3S.5. ^{1}H NMR of pbpdc-8a-u..... 88

Figure 3S.6. ^{1}H NMR of compound 4 88

Figure 3S.7. ^{1}H NMR of compound 5 89

Figure 3S.8. ^{1}H NMR of compound 6 89

Figure 3S.9. ^{1}H NMR of compound tpdc-10e-u, compound 7..... 90

Figure 3S.10. ^{1}H NMR of ptpdc-8e-u. End-group analysis was used to determine number of repeat units and M_n 90

Figure 3S.11. ^{1}H NMR of ptpdc-10e-u. End-group analysis was used to determine number of repeat units and M_n 91

Figure 3S.12. ^{1}H NMR of ptpdc-8a-u..... 91

Figure 3S.13. ^{1}H NMR of ptpdc-10a-u..... 92

Figure 3S.14. GPC traces of polymer ester ligands pbpdc-*x*e-u and ptpdc-*x*e-u..... 92

Figure 3S.15. ^{1}H NMR of digested polyUiO-67-8a-u 93

Figure 3S.16. ^{1}H NMR of digested polyUiO-68-8a-u 93

Figure 3S.17. ^{1}H NMR of digested polyUiO-68-10a-u 94

Figure 3S.18. Optical image of single crystals of polyUiO-68-10a-u used for ^{1}H NMR ... 94

Figure 3S.19. The ^{1}HNMR of the digested crystals (black trace) is compared to the 1H NMR of the ptpdc-10a-u (red trace) 95

Figure 3S.20. TGA curves of UiO-67, UiO-68, polyUiO-67-8a-u and polyUiO-68-*x*a-u, where x = 8 or 10..... 95

Figure 3S.21. Stability test of: a) native UiO-67 after 20 h; b) polyUiO-67 after 3 d; c) allyloxy-functionalized UiO-68 after 1.5h; d) polyUiO-68 after 5 h. Both polyUiO-67 and polyUiO-68 exhibit high crystallinity for extended times, when compared to their native counterparts, UiO-67 and allyloxy-functionalized UiO-68, respectively 96

Figure 3S.22. Chemical stability test for: a) allyloxy-functionalized UiO-68 and b) polyUiO-68-8a-u after being submerged in water for 12 h and allowed to dry over time 97

Figure 3S.23. a) Rouquerol plot for polyUiO-67-8a-u. Only points below $P/P_0 = 0.046$ satisfy the criteria for applying the BET theory. b) Plot of the linear region for the BET equation for polyUiO-67-8a-u 97

Figure 3S.24. a) Rouquerol plot for polyUiO-68-8a-u. Only points below $P/P_0 = 0.050$ satisfy the criteria for applying the BET theory. b) Plot of the linear region for the BET equation for polyUiO-68-8a-u 98

Figure 3S.25. a) Rouquerol plot for polyUiO-68-10a-u. Only points below $P/P_0 = 0.050$ satisfy the criteria for applying the BET theory. b) Plot of the linear region for the BET equation for polyUiO-68-10a-u 98

Figure 3S.26. The pore size distributions of a) UiO-67 and polyUiO-67-8a-u, and b) polyUiO-68-*x*a-u are presented..... 99

Figure 3S.27. PXRD patterns for polyIRMOF-10-8a-u and polyIRMOF-16-*x*a-u (x = 8, 10) 99

Figure 3S.28. ^{1}H NMR of digested polyIRMOF-10-8a-u 100

Figure 3S.29. ^{1}H NMR of digested polyIRMOF-16-8a-u 100

Figure 3S.30. ^{1}H NMR of digested polyIRMOF-16-10a-u 101

Figure 3S.31. SEM images of polyIRMOF-10-8a-u prepared from pbpdc-8a-u 102

Figure 3S.32. SEM images of polyIRMOF-16-8a-u prepared from ptpdc-8a-u 102

Figure 3S.33. SEM images of polyIRMOF-16-8a-u prepared from ptpdc-10a-u 102

Figure 3S.34. N_2-Isotherm of polyIRMOF-16-10a-u 103

Figure 3S.35. ^{1}H NMR of *o*-pbdc-8e-u 103

Figure 3S.36. ^{1}H NMR of *o*-pbdc-10e-u 104

Figure 3S.37. GPC traces of polymer esters in THF 104

Figure 3S.38. GPC traces of fractionated *o*-pbdc-8e-u in THF 105

Figure 3S.39. ^{1}H NMR of *o*-pbdc-8a-u 105

Figure 3S.40. ^{1}H NMR of *o*-pbdc-10a-u. 106

Figure 3S.41. ^{1}H NMR of digested *o*-polyIRMOF-1-8a-u 106

Figure 3S.42. ^{1}H NMR of digested *o*-polyIRMOF-1-10a-u 107

Figure 3S.43. PXRD of fractionated *o*-polyIRMOF-1-8a-u 107

Figure 3S.44. SEM images of polyIRMOF-1 synthesized with o-pbdc-8a-u: fraction 1 (left) and fraction 2 (right) 108

Figure 3S.45. PXRD of failed attempts at synthesis of *o*-polyUiO-66 with two polymer ligands, *o*-pbdc-8a-u in red, *o*-pbdc-10a-u in blue, and calculated UiO-66 in black 108

Figure 4.1. Representative Illustration of preparing a block co-polyMOF prepared from a block copolymer ligand that contains an H_2bdc tetramer coupled to a polystyrene chain. Figure was adapted from reference 115

Figure 4.2. Representative Illustration of preparing a polyMOF using a block copolymer ligand. In this example, the block copolymer ligand contains a MOF-forming block (pbdc-8a-u) and a morphology directing block (PEG) 116

Figure 4.3. PXRD patterns of polyUiO-66 prepared from pbdc-8a-PEG_{Mn}-x% block copolymers 121

Figure 4.4. SEM images of polyUiO-66 prepared from block copolymer ligands: (a) pbdc-8a-PEG_{2000}-2%; (b) pbdc-8a-PEG_{4000}-1%; (c) pbdc-8a-PEG_{2000}-20%; (d) pbdc-8a-PEG_{4000}-10%. 123

Figure 4.5. (a) PXRD patterns of polyUiO-66 prepared from purified pbdc-8a-PEG_{Mn}OMe. SEM images of polyUiO-66 prepared from: (b) pbdc-8a-PEG_{2000}OMe and (c) pbdc-8a-PEG_{5000}OMe 125

Figure 4.6. Representative N_2 isotherms of block-polyUiO-66 prepared from various block copolymer ligands that result in intergrown octahedra. The BET surface areas are included in parentheses. PolyUiO-66 prepared from homopolymer pbdc-8a is included for comparison. Closed and open symbols represent the adsorption and desorption processes, respectively. 128

Figure 4.7. PXRD patterns of polyIRMOF-1prepared from pbdc-8a-PEG_{Mn}-x% block copolymers 129

Figure 4.8. SEM images of polyIRMOF-1 prepared from polymer ligands: (a) pbdc-8a; (b) pbdc-8a-PEG_{2000}-2%; (c) pbdc-8a-PEG_{4000}-1%; (d) pbdc-8a-PEG_{2000}-20%; (e and f) pbdc-8a-PEG_{4000}-10%..... 131

Figure 4.9. N_2 isotherms of block-polyIRMOF-1 prepared from pbdc-8a-PEG_{Mn}-x% polymers 133

Figure 4S.1. ^{1}H NMR of 1,2-bis(pent-4-en-1-yloxy)PEG_{2000} 148

Figure 4S.2. ^{1}H NMR of 1,2-bis(pent-4-en-1-yloxy)PEG_{4000} 148

Figure 4S.3. ^{1}H NMR of 5-MeOPEG_{2000}-1-pentene 149

Figure 4S.4. ^{1}H NMR of 5-MeOPEG_{5000}-1-pentene 149

Figure 4S.5. ^{1}H NMR of pbdc-8e-PEG_{2000}-2% 150

Figure 4S.6. ^{1}H NMR of pbdc-8e-PEG_{2000}-20% 150

Figure 4S.7. ^{1}H NMR of pbdc-8e-PEG_{4000}-1% 151

Figure 4S.8. ^{1}H NMR of pbdc-8e-PEG_{4000}-10% 151

Figure 4S.9. ^{1}H NMR of crude pbdc-8e-PEG_{2000}OMe..... 152

Figure 4S.10. ^{1}H NMR of pbdc-8e-PEG_{2000}OMe. End-group analysis was used to determine the purity of the AB_2 copolymer 152

Figure 4S.11. ^{1}H NMR of crude pbdc-8e-PEG_{5000}OMe..... 153

Figure 4S.12. ^{1}H NMR of pbdc-8e-PEG$_{5000}$OMe. End-group analysis was used to determine the purity of the AB$_2$ copolymer 153

Figure 4S.13. ^{1}H NMR of pbdc-8e-COD$_{10:1}$..... 154

Figure 4S.14. ^{1}H NMR of pbdc-8e-COD$_{2:1}$..... 154

Figure 4S.15. ^{1}H NMR of pbdc-8e-COD$_{1:1}$..... 155

Figure 4S.16. ^{1}H NMR of pbdc-8a-PEG$_{2000}$-2%. 155

Figure 4S.17. ^{1}H NMR of pbdc-8a-PEG$_{2000}$-20% 156

Figure 4S.18. ^{1}H NMR of pbdc-8a-PEG$_{4000}$-1% 156

Figure 4S.19. ^{1}H NMR of pbdc-8a-PEG$_{4000}$-10% 157

Figure 4S.20. ^{1}H NMR of crude pbdc-8a-PEG$_{2000}$OMe..... 157

Figure 4S.21. ^{1}H NMR of pbdc-8a-PEG$_{2000}$OMe..... 158

Figure 4S.22. ^{1}H NMR of crude pbdc-8a-PEG$_{5000}$OMe..... 158

Figure 4S.23. ^{1}H NMR of pbdc-8a-PEG$_{5000}$OMe..... 159

Figure 4S.24. ^{1}H NMR of pbdc-8a-COD$_{1:1}$..... 159

Figure 4S.25. ^{1}H NMR of pbdc-8a-COD$_{2:1}$..... 160

Figure 4S.26. ^{1}H NMR of pbdc-8a-COD$_{10:1}$..... 160

Figure 4S.27. GPC traces obtained for polymers: a) pbdc-8e-PEG$_{Mn}$-x%; b) pbdc-8e-PEG$_{Mn}$OMe; c) pbdc-8e-COD$_{m:n}$; d) alkene-functionalized PEG macromonomers 161

Figure 4S.28. a) ^{1}H NMR and b) GPC trace of representative fractionated sample pbdc-8e-PEG$_{4000}$-1% is presented..... 162

Figure 4S.29. a) ^{1}H NMR and b) GPC trace of representative fractionated sample pbdc-8e-PEG$_{4000}$-10% is presented..... 163

Figure 4S.30. a) ^{1}H NMR and b) GPC trace of representative fractionated sample pbdc-8e-PEG$_{2000}$OMe is presented 164

Figure 4S.31. a) ^{1}H NMR and b) GPC trace of representative fractionated sample pbdc-8e-$COD_{1:1}$ is presented..... 165

Figure 4S.32. ^{1}H NMR of digested polyUiO-66 prepared from pbdc-8a-PEG_{2000}-2%..... 166

Figure 4S.33. ^{1}H NMR of digested polyUiO-66 prepared from pbdc-8a-PEG_{2000}-20%..... 166

Figure 4S.34. ^{1}H NMR of digested polyUiO-66 prepared from pbdc-8a-PEG_{4000}-1%..... 167

Figure 4S.35. ^{1}H NMR of digested polyUiO-66 prepared from pbdc-8a-PEG_{4000}-10%..... 167

Figure 4S.36. ^{1}H NMR of digested polyUiO-66 prepared from crude pbdc-8a-PEG_{2000}OMe. 168

Figure 4S.37. ^{1}H NMR of digested polyUiO-66 prepared from pbdc-8a-PEG_{2000}OMe 168

Figure 4S.38. ^{1}H NMR of digested polyUiO-66 prepared from crude pbdc-8a-PEG_{5000}OMe. 169

Figure 4S.39. ^{1}H NMR of digested polyUiO-66 prepared from pbdc-8a-PEG_{5000}OMe 169

Figure 4S.40. ^{1}H NMR of digested polyUiO-66 prepared from pbdc-8a-$COD_{1:1}$ 170

Figure 4S.41. ^{1}H NMR of digested polyUiO-66 prepared from pbdc-8a-$COD_{2:1}$ 170

Figure 4S.42. ^{1}H NMR of digested polyUiO-66 prepared from pbdc-8a-$COD_{10:1}$ 171

Figure 4S.43. SEM images for polyUiO-66 prepared from pbdc-8a and physically mixed PEG_{4000} at a) 1% loading and b) 10% loading..... 173

Figure 4S.44. Correlation functions, distribution fits, and number-average size distributions (inset) at 90° (a) and 13° (b) scattering angle for pbdc-8a-PEG_{2000}-20% 174

Figure 4S.45. Correlation functions, distribution fits, and number-average size distributions (inset) at 90° (a) and 13° (b) scattering angle for pbdc-8a-PEG_{4000}-10% 174

Figure 4S.46. Correlation functions, distribution fits, and number-average size distributions (inset) at 90° (a) and 13° (b) scattering angle for pbdc-8a-PEG_{2000}-2% 175

Figure 4S.47. Correlation functions, distribution fits, and number-average size distributions (inset) at 90° (a) and 13° (b) scattering angle for pbdc-8a-PEG_{4000}-1% 175

Figure 4S.48. PXRD data was obtained for polyUiO-66 prepared from crude pbdc-8a-PEG_{Mn}OMe..... 176

Figure 4S.49. SEM images for polyUiO-66 prepared from crude: a) pbdc-8a-PEG_{2000}OMe; b) pbdc-8a-PEG_{5000}OMe 176

Figure 4S.50. Correlation functions, distribution fits, and number-average size distributions (inset) at 90° (a) and 13° (b) scattering angle for pbdc-8a-PEG_{2000}OMe..... 177

Figure 4S.51. Correlation functions, distribution fits, and number-average size distributions (inset) at 90° (a) and 13° (b) scattering angle for pbdc-8a-PEG_{5000}OMe..... 177

Figure 4S.52. PXRD data was obtained for polyUiO-66 prepared from pbdc-8a-$COD_{m:n}$. 178

Figure 4S.53. SEM images of polyUiO-66 prepared from: a) pbdc-8a-$COD_{2:1}$; b) pbdc-8a-$COD_{1:1}$ 178

Figure 4S.54. SEM images of two different morphologies for polyUiO-66 prepared from pbdc-8a-$COD_{10:1}$..... 179

Figure 4S.55. Correlation functions, distribution fits, and number-average size distributions (inset) at 90° (a) and 13° (b) scattering angle for pbdc-8a-$COD_{1:1}$..... 179

Figure 4S.56. Correlation functions, distribution fits, and number-average size distributions (inset) at 90° (a) and 13° (b) scattering angle for pbdc-8a-$COD_{2:1}$..... 180

Figure 4S.57. Correlation functions, distribution fits, and number-average size distributions (inset) at 90° (a) and 13° (b) scattering angle for pbdc-8a-$COD_{10:1}$..... 180

Figure 4S.58. N_2 adsorption isotherms for all block-polyUiO-66 with an interlaced morphology..... 181

Figure 4S.59. N_2 adsorption isotherm for block-polyUiO-66 prepared from pbdc-8a-$COD_{2:1}$ is presented..... 181

Figure 4S.60. a) N_2 adsorption isotherms and b) CO_2 adsorption for block-polyUiO-66 prepared from pbdc-8a-PEG_{2000}-2%..... 182

Figure 4S.61. Pore-size distribution for block-polyUiO-66 with a(n): a) octahedral morphology; b) interlaced morphology..... 182

Figure 4S.62. PXRD data was obtained for polyIRMOF-1 prepared from pbdc-8a-PEG_{Mn}OMe..... 183

Figure 4S.63. PXRD data was obtained for polyIRMOF-1 prepared from pbdc-8a-$COD_{m:n}$.. 183

Figure 4S.64. ^{1}H NMR of digested polyIRMOF-1 prepared from pbdc-8a-PEG_{2000}-2%... 184

Figure 4S.65. ^{1}H NMR of digested polyIRMOF-1 prepared from pbdc-8a-PEG$_{2000}$-20%. 184

Figure 4S.66. ^{1}H NMR of digested polyIRMOF-1 prepared from pbdc-8a-PEG$_{4000}$-1%... 185

Figure 4S.67. ^{1}H NMR of digested polyIRMOF-1 prepared from pbdc-8a-PEG$_{4000}$-10%. 185

Figure 4S.68. ^{1}H NMR of digested polyIRMOF-1 prepared from pbdc-8a-PEG$_{2000}$OMe . 186

Figure 4S.69. ^{1}H NMR of digested polyIRMOF-1 prepared from pbdc-8a-PEG$_{5000}$OMe . 186

Figure 4S.70. ^{1}H NMR of digested polyIRMOF-1 prepared from pbdc-8a-COD$_{1:1}$..... 187

Figure 4S.71. ^{1}H NMR of digested polyIRMOF-1 prepared from pbdc-8a-COD$_{2:1}$..... 187

Figure 4S.72. ^{1}H NMR of digested polyIRMOF-1 prepared from pbdc-8a-COD$_{10:1}$ 188

Figure 4S.73. PXRD data was obtained for polyIRMOF-1 prepared from pbdc-8a-PEG$_{Mn}$-x% after activation 188

Figure 4S.74. PXRD data was obtained for polyIRMOF-1 prepared from pbdc-8a-PEG$_{Mn}$OMe after activation 189

Figure 4S.75. PXRD data was obtained for polyIRMOF-1 prepared from pbdc-8a-COD$_{m:n}$ after activation 189

Figure 4S.76. Representative PXRD data was obtained for polyIRMOF-1 prepared from pbdc-8a-PEG$_{4000}$-10% and shown here as synthesized, after activation, and after immersion in DMF at 60 °C for 1 h 190

Figure 4S.77. SEM images for polyIRMOF-1 prepared from a) pbdc-8a-PEG$_{2000}$OMe and b) pbdc-8a-PEG$_{5000}$OMe..... 190

Figure 4S.78. SEM images for polyIRMOF-1 prepared from a) pbdc-8a-COD$_{10:1}$, b) pbdc-8a-COD$_{2:1}$ and c) pbdc-8a-COD$_{1:1}$..... 191

Figure 4S.79. SEM images for polyIRMOF-1 prepared from pbdc-8a and physically mixed PEG$_{4000}$ at a)1% loading and b) 10% loading 191

Figure 4S.80. Correlation functions, distribution fits, and number-average size distributions (inset) at 90° (a) and 13° (b) scattering angle for polyIRMOF-1 prepared from pbdc-8a-PEG$_{4000}$-10%..... 192

Figure 4S.81. N_2 adsorption isotherm for polyIRMOF-1 prepared from pbdc-8a-PEG$_{2000}$OMe is presented 192

Figure 4S.82. N_2 adsorption isotherm for polyIRMOF-1 prepared from pbdc-8a-$COD_{m:n}$ is presented..... 193

Figure 5.1. Illustrative representation of multivariate MOFs (MTV-MOFs). Ditopic H_2bdc linkers with several different functional groups can be introduced into a single MOF crystal.199

Figure 5.2. *Top*: Illustration of preparing MTV-MOFs with incremental pore expansion. Whereas H_2bdc forms UiO-67 (top left), both H_2bpdc and H_2abpdc are similar in size and can fit into a single Zr-MTV-MOF with incrementally larger pores (top right). *Bottom*: The concept of core-shell MOFs is demonstrated, wherein the core of HKUST-1 is used as a..... 201

Figure 5.3. Illustrative representation of a multivariate polymer ligand used to synthesize MTV-polyMOFs..... 202

Figure 5.4. *Left*: Three possible arrangements are illustrated, wherein bdc-8e can be coupled to bdc-8e, bdc-8e can be coupled to tpdc-10e, and tpdc-10e can be coupled to tpdc-10e. *Right*: ^{1}H NMR analysis in the alkene region of MTVP-$1_{m:n}$ reveals these three combinations can be adjusted by changing the ratio of the starting precursors before polymerization..... 205

Figure 5.5. PXRD patterns of calculated UiO-66, UiO-68, and experimental Zr-polyMOFs prepared from (a) MTVP-$1_{m:n}$ and (b) physical mixtures of pbdc-8a-u and ptpdc-10a-u.... 207

Figure 5.6. SEM images of Zr-polyMOFs prepared from homopolymer and MTVP polymer ligands: (a) polyUiO-66-8a-u; (b) polyUiO-68-10a-u; (c) Zr-MTVP-$1_{3:1}$; (d) Zr-MTVP-$1_{1:1}$; (e) Zr-MTVP-$1_{1:3}$; (f) 3:1 ratio of polyUiO-66-8a-u and polyUiO-68-10a-u; (g) 1:1 ratio of polyUiO-66-8a-u and polyUiO-68-10a-u; (h) 1:3 ratio of polyUiO-66-8a-u and..... 208

Figure 5.7. PXRD patterns of calculated IRMOF-type patterns and experimental Zn-MTVP-$1_{m:n}$..... 210

Figure 5.8. SEM images of Zn-polyMOFs prepared from homopolymer and MTVP polymer ligands: (a) polyIRMOF-1-8a-u; (b) polyIRMOF-16-10a-u; (c) Zn-MTVP-$1_{1:1}$; (d) 1:1 ratio of polyIRMOF-1-8a and polyIRMOF-16-10a-u..... 211

Figure 5.9. A general strategy for the synthesis of MTV-polyMOFs using block copolymers is presented, using pbdc-8e-u and ptpdc-10e-u as examples. Exclusive end-functionalized polymers can be coupled by alkyne-azide copper "click" chemistry to yield block copolymer ligands. These new ligands may have the potential to yield polyMOFs with 213

Figure 5S.1. ^{1}H NMR of $(CH_3)_2$-MTVP-$1_{3:1}$. End-group analysis was used to quantify the repeating units of bdc-8a and tpdc-10e 218

Figure 5S.2. ^{1}H NMR of $(CH_3)_2$-MTVP-$1_{1:1}$..... 218

Figure 5S.3. ^{1}H NMR of $(CH_3)_2$-MTVP-$1_{1:3}$ 219

Figure 5S.4. GCP traces of $(CH_3)_2$-MTVP-$1_{m:n}$, pbdc-8e-u and ptpdc-10e-u 219

Figure 5S.5. ^{1}H NMR of MTVP-$1_{3:1}$ 220

Figure 5S.6. ^{1}H NMR of MTVP-$1_{1:1}$ 220

Figure 5S.7. ^{1}H NMR of MTVP-$1_{1:3}$ 221

Figure 5S.8. ^{1}H NMR of digested Zr-MTVP-$1_{3:1}$ 221

Figure 5S.9. ^{1}H NMR of digested Zr-MTVP-$1_{1:1}$ 222

Figure 5S.10. ^{1}H NMR of digested Zr-MTVP-$1_{1:3}$ 222

Figure 5S.11. PXRD patterns of Zn-polyMOFs prepared from a mixture of homopolymers pbdc-8a-u and ptpdc-10a-u in three different ratios 223

LIST OF SCHEMES

Scheme 2.1. Synthesis of polymer ligand and preparation of a UiO-66 polyMOF. 25

Scheme 3.1. General method for preparation of laterally extended polyMOF ligands, using pbpdc-8a-u as a representative example 61

Scheme 3S.1. Synthetic scheme of ptpdc-*x*a-u synthesis, where *x* = 8 or 10 77

Scheme 3S.2. Synthetic scheme of ptpdc-*x*a-u synthesis, where *x* = 8 or 10 80

Scheme 4.1. Synthesis of three types of polymer ligands used in this work: (i) Random AB PEG block copolymer ligand (pbdc-8a-PEG$_{Mn}$-x%); (ii) capped AB$_2$ PEG block copolymer ligand (pbdc-8a-PEG$_{Mn}$OMe); (iii) random AB COD block copolymer ligand (pbdc-8a-COD$_{m:n}$) 118

Scheme 4S.1. Synthesis of PEG macromonomers 135

Scheme 4S.2. Synthesis of pbdc-8a-PEG$_{Mn}$-x% 137

Scheme 4S.3. Synthesis of pbdc-8a-PEG$_{Mn}$OMe 139

Scheme 4S.4. Synthesis of pbdc-8a-COD$_{m:n}$ 143

Scheme 5.1. General method for the preparation of MTV-polyMOFs is presented 143

LIST OF TABLES

Table 2.1. Molecular weight determinations of pbdc-*x*e-u polymer ligands 25

Table 3.1. GPC and ^{1}H NMR characterization of axially-extended polymer esters 62

Table 3.2. GPC characterization of the *o*-pbdc-*x*e-u 69

Table 3S.1. ^{1}H NMR end-group analysis of the polymer acid ligands pbpdc-*x*a-u and ptpdc-*x*a-u 108

Table 3S.2. Crystal data and structure refinement for polyUiO-68-10a-u 109

Table 3S.3. GPC characterization of fractionated *o*-pbdc-*x*e-u 109

Table 4.1. Composition and Molecular Weight Determinations of Block copolymer Ligands. 120

Table 4S.1. Ratio of bdc-8e to co-monomer 161

Table 4S.2. Yields, compositions, and molecular weight of fractionated 8e-PEG$_{4000}$-1%.. 162

Table 4S.3. Yields, compositions, and molecular weight of fractionated 8e-PEG$_{4000}$-10%. 163

Table 4S.4. Yields, compositions, and molecular weight of fractionated 8e-PEG$_{2000}$OMe. 164

Table 4S.5. Yields, compositions, and molecular weight of fractionated 8e-COD$_{1:1}$. 165

Table 4S.6. Ratios of H_2bdc to co-monomer before and after digestion 172

Table 4S.7. Hydrodynamic radii at 90° and 13° scattering angle for polymer ligands, and polyIRMOF-1 derived from pbdc-8a-PEG$_{4000}$-10% 173

Table 5.1. GPC and ^{1}H NMR characterization of the multivariate polymer esters 205

ACKNOWLEDGEMENTS

I would first like to acknowledge Professor Seth Cohen for his support as my committee chair, advisor, and as a friend. His guidance and encouragements were instrumental to my development as a scientist, and I appreciate him for never letting me settle for anything less than my best. Also, Seth is one of the most organized, diligent people I have had the pleasure of working with, and I hope I have acquired some of those skills from him so that I can use them in my life. From the productive discussions in monthly meetings, to our casual conversations about the next best television series, I will always be grateful to have been part of your group.

I would also like to acknowledge all the members of the Cohen lab, past and present, who supported me as colleagues and as friends during this journey. I want to give a big thanks to those who worked on the 'polyMOFs' project with me, Professor Zhenjie Zhang, Professor Teng-Hao Chen, Dr. Kyle Bentz, Joey Palomba, Pablo Quijano Velasco, Giulia Schukraft, Yuta Otsubo, Kyle Barcus, and Renee Luo, because they all were part of the work presented in this dissertation, and I could not have done it without them. I want to thank many of the MOF-subgroup lab members, Dr. Mike Denny, Dr. Jessie Moreton, Dr. Xiao Yu, Dr. Le Wang, Dr. Jin Yeong Kim, and Mark Kalaj, for their helpful discussions, critical analysis of my work, and being overall great friends during this difficult journey. I also want to acknowledge Dr. Cy Credille, Dr. Christian Perez, Dr. Allie Chen, Ben Dick, and Rebecca Adamek of the for their help when the organic chemistry got tough, and for being great colleagues. You all have been my team, and my family in San Diego for the past six years.

I would like to acknowledge my external collaborators, particularly the groups of Professor Klaus Schmidt-Rohr and Professor Guillaume Maurin, for advancing my

understanding of the materials discussed in this work. I am grateful for their help and hope to see more fruitful publications in the upcoming years.

I would also like to thank Professor Zhibin Guan and Professor Davoud Mozhdehi because they gave me my start as a research chemist when I was just an undergrad at UC Irvine. Davoud was a graduate student in the Guan group when we first met at UC Irvine, and he dedicated a lot of his time to teach me the basics of a chemistry lab. His mentorship was what inspired me to go to graduate school in the first place, and so I appreciate him a lot for that. I wish for him the best in his career as a professor and independent researcher.

Finally, I want to thank my family for their unwavering love and support through this difficult journey. I want to thank my wife, Miriah Harris, for being a source of strength for me, even when the challenges ahead were daunting. I want to thank my son, Gavin Ayala, for being my motivation, and my reason to use my time in lab efficiently. I want to thank my sister, Crystal Ayala, for making me laugh and cheering me up those days when I was feeling gloomy. I want to give a special thanks to my parents, Sergio Ayala and Esther Ayala, for their unconditional support, and for all the sacrifices they made to put me through school. Lastly, I would like to thank my extended family, who always encouraged me to through this journey. Thank you all.

Chapter 1, in part, is an adaptation of the following materials listed: "MOF-Polymer Hybrid Materials: From Simple Composites to Tailored Architectures" *Chem. Rev.* **2020**, accepted for publication; PolyMOFs: Molecular Level Integration of MOFs and Polymers. In *Hybrid Metal-Organic Framework and Covalent Organic Framework Polymers*, Wang, B., Ed. The Royal Society of Chemistry: In Preparation. The dissertation author was an author of the review and the primary author of the book chapter. The dissertation author gratefully

acknowledges the contributions of coauthors Mark Kalaj, Kyle C. Bentz, Joseph M. Palomba, Kyle S. Barcus, Yuji Katayama, and Seth M. Cohen in the review titled, "MOF-Polymer Hybrid Materials: From Simple Composites to Tailored Architectures". The dissertation author also acknowledges the contributions of coauthor Seth M. Cohen in the book Chapter titled, "PolyMOFs: Molecular Level Integration of MOFs and Polymers".

Chapter 2, in part, is a reprint of the material, "Hierarchical structure and porosity in UiO-66 polyMOFs" *Chem. Commun.* **2017**, *53*, 3058-3061. The dissertation author was the primary author of this manuscripts and gratefully acknowledges the contributions of coauthors Zhenjie Zhang and Seth M. Cohen.

Chapter 3, in part, is a reprint of the following materials as listed: "Isoreticular expansion of polyMOFs achieves high surface area materials" *Chem. Commun.,* **2017,** *53*, 10684-10687; "polyMOF Formation from Kinked Polymer Ligands via ortho-Substitution" *Isr. J. Chem.*, **2018,** *58*, 1123-1126. The dissertation author was a coauthor of both these manuscripts. The dissertation author gratefully acknowledges the contributions of coauthors Giulia E. M. Schukraft, Benjamin L. Dick and Seth M. Cohen in the manuscript titled, "Isoreticular expansion of polyMOFs achieves high surface area materials". The disseration author also gratefully acknowledges Joseph M. Palomba and Seth M. Cohen for the manuscript titled, "polyMOF Formation from Kinked Polymer Ligands via ortho-Substitution".

Chapter 4, in part, is a reprint of the material, "Block co-polyMOFs: morphology control of polymer–MOF hybrid materials", *Chem. Sci.* **2019**, *10*, 1746-1753. The dissertation author was the primary author of this manuscript and gratefully acknowledges the contributions of coauthors Kyle C. Bentz and Seth M. Cohen.

The dissertation author gratefully acknowledges the MOF subgroup, and Seth M. Cohen for their helpful discussions regarding the project presented in Chapter 5.

VITA

Education

2014	Bachelor of Chemistry, University of California, Irvine
2016	Master of Science, University of California San Diego
2020	Doctor of Philosophy, University of California San Diego

Honors and Awards

2015-2017	Dept. of Education GAANN Fellowship Recipient
2017	Inamori Fellowship Recipient

Publications

Mark Kalaj, Kyle C. Bentz, Sergio Ayala Jr., Joseph M. Palomba, Kyle S. Barcus, Yuji Katayama, and Seth M. Cohen, "MOF-Polymer Hybrid Materials: From Simple Composites to Tailored Architectures," *Chem. Rev.* **2020**, accepted for publication.

Kyle C. Bentz, Sergio Ayala Jr., Mark Kalaj, and Seth M. Cohen, "Polyacids as Modulators for the Synthesis of UiO-66," *Aust. J. Chem.* **2019**, *72*, 848-851.

Sergio Ayala Jr., Kyle C. Bentz, and Seth M. Cohen, "Block co-polyMOFs: Morphology Control of Polymer-MOF Hybrid Materials," *Chem. Sci.* **2019**, *10*, 1746-1753.

Joseph M. Palomba, Sergio Ayala Jr., and Seth M. Cohen, "polyMOF Formation from Kinked Polymer Ligands via ortho- Substitution," *Isr. J. Chem.* **2018**, *58*, 1123-1126.

Giulia E. M. Schukraft, Sergio Ayala Jr., Benjamin L. Dick, and Seth M. Cohen, "Isoreticular Expansion of polyMOFs Achieves High Surface Area Materials," *Chem. Commun.* **2017**, *53*, 10684-10687.

Sergio Ayala Jr., Zhenjie Zhang and Seth M. Cohen, "Hierarchical Structure and Porosity in UiO-66 polyMOFs," *Chem. Commun.* **2017**, *53*, 3058-3061.

Davoud Mozhdehi, James A. Neal, Scott C. Grindy, Yves Cordeau, Sergio Ayala, Niels Holten-Andersen, and Zhibin Guan, "Tuning Dynamic Mechanical Response in Metallopolymer Networks through Simultaneous Control of Structural and Temporal Properties of the Networks," *Macromolecules* **2016**, *49*, 6310–632.

Davoud Mozhdehi, Sergio Ayala, Olivia R. Cromwell, and Zhibin Guan, "Self-Healing Multiphase Polymers via Dynamic Metal–Ligand Interactions," *J. Am. Chem. Soc.* **2014**, *136*, 16128–16131.

ABSTRACT OF THE DISSERTATION

PolyMOFs: A Novel Class of Polymer-Metal-Organic Framework Hybrid Materials

by

Sergio Ayala Jr.

Doctor of Philosophy in Chemistry

University of California San Diego, 2020

Professor Seth M. Cohen, Chair

The hybridization of crystalline, porous metal-organic frameworks (MOFs) with synthetic polymers has led to the development of unique composite materials that surpass the properties of the individual MOF and polymer components. To achieve molecular-level integration between these disparate materials, synthetic polymers containing organic linkers have been combined with inorganic building blocks for the preparation of a novel class of MOF-polymer composites, termed polyMOFs. These so-called polyMOFs merge the backbone of polymers with the lattice of the MOF to yield new materials with interesting characteristics. To promote the development of polyMOFs, the molecular arrangement of the polymers and the

lattice constraints of the MOF must both be satisfied. This dissertation describes how the compatibility between MOF-architecture and polymer architecture dictate the ability to synthesize polyMOFs, and describes the emergent properties of these novel MOF-polymer materials.

Chapter 2 describes the preparation of a Zr-polyMOF (UiO-66) using 1-dimensional, amorphous polymers of various alkyl-spacers, molecular weights, and dispersities. Under the appropriate conditions, a Zr-polyMOF with a unique, interlaced morphology, and hierarchical porosity was achieved.

The concept of isoreticular (same-net) chemistry is applied to polyMOFs in Chapter 3. Linear polymers with laterally extended organic linkers afford isoreticular polyMOFs with larger pores and surface areas than described in previous works. Furthermore, it was determined that changing the position of polymer backbone connectors prevents the formation of Zr-polyMOFs, signifying the importance of polymer architecture for polyMOF formation.

In Chapter 4, block copolymers containing MOF-forming linkers and morphology directing blocks were used to synthesize block co-polyMOFs (BCPMOFs) with controlled morphologies. The morphology of Zr-BCPMOFs could be manipulated by changing the weight fraction, connectivity, and the composition of the block co-polymer ligands. Moreover, the strategy of using block copolymers to direct morphology could be applied to Zn-polyMOFs, yielding materials with narrow sizes and uniform cubic shapes.

Chapter 5 describes preliminary results for the preparation of multivariate (MTV) polyMOFs. Random copolymers containing two linkers of different axials length were used to synthesize MTV polyMOFs. Preparation of novel MTV-polyMOFs may have the potential to yield materials with controlled hierarchical porosity.

Chapter 1: Metal-Organic Frameworks and MOF-Polymer Hybrids

1.1 Metal-Organic Frameworks

Metal-organic frameworks (MOFs) are a class of crystalline, porous coordination materials synthesized from multitopic organic ligands and inorganic secondary building units (SBUs).[1] These materials are highly porous, and to date hold the world record as the materials with the highest internal surface area (7100 m^2/g).[2] MOFs have been investigated for a variety of functions including gas-storage,[3-4] separation,[5-6] catalysis,[7-9] templating,[10-12] and other applications.[13-15] Recently, several companies have commercialized MOFs for applications including delayed ripening of fruit (developed by MOF Technologies), and for the safe storage of toxic gases (developed by NuMat Technologies).

Methodical choice of linker and SBU can lead to an infinite combination of reticular (net-like) MOFs that make these materials highly tunable in their topology, porosity, and chemical functionality (Figure 1.1). In fact, thousands of different MOFs have been reported[16-17] since the time they were first described in 1990 by Robson and co-workers.[18] For instance, combination of 1,4-benzenedicarboxylic acid (H_2bdc) with Zn_4O SBUs yields the cubic framework IRMOF-1 (also referred to as MOF-5), wherein the inorganic nodes are connected 6-fold by the linker (Figure 1.1a).[1, 19] Combining H_2bdc with a zirconium-oxo SBU instead yields UiO-66 (UiO = University of Oslo), a MOF in which the nodes are interconnected by twelve deprotonated H_2bdc linkers (Figure 1.1 b).[20] Both examples described so far produce framework materials with two different types of connectivity. Isoreticular (same-net) MOFs with functional group or extended pores can also be achieved, by using a ligand with a functional group like H_2bdc-NH_2 to yield IRMOF-3 or laterally expanding the organic linker to biphenyl-4,4′-dicarboxylic acid (H_2bpdc) to yield IRMOF-10 (Figure 1.1 c and d).[19-20]

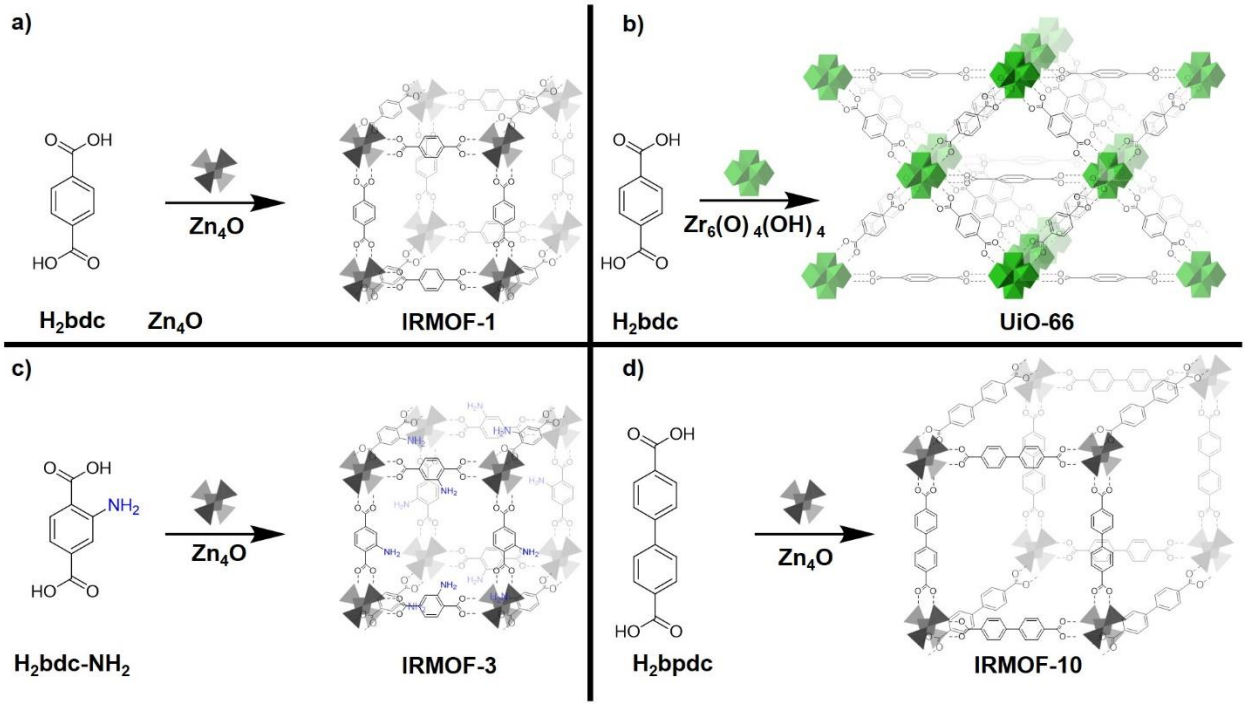

Figure 1.1. A representation of how different organic linkers and inorganic SBUs can be used to prepare several MOF topologies. (a) H_2bdc and Zn_4O clusters can be combined to produce cubic IRMOF-1 (also referred to as MOF-5) architecture. (b) H_2bdc and $Zr_6(O)_4(OH)_4$ clusters yield a highly interconnected framework, UiO-66. Isoreticular MOFs are achieved by using (c) a modified linker like H_2bdc-NH_2 or (d) expansion using laterally extended H_2pbdc with Zn_4Oclusters to yield IRMOF-3 and IRMOF-10, respectively.

The chemical functionality of MOFs can be fine-tuned using both presynthetic and postsynthetic methods. For presynthetic methods, a one-pot approach is employed where both the functionalized ligand(s) and the metal source are directly used as precursors to produce a MOF with a chemical functional group (Figure 1.1c). Several MOFs have been successfully prepared in this way, including IRMOF-3, UiO-66-NH_2, UMCM-1 (UMCM = University of Michigan Crystalline Material), and other multicomponent or multivariate (MTV) MOFs.[21-23] The presynthetic approach is typically limited to organic ligands that are isoreticular to the MOF being prepared, organic ligands that are stable under solvothermal conditions, or organic ligands that do

not interfere with formation of the framework (either by sterics or through competing coordination groups).[24-26]

To expand the possibilities of chemical functionality, MOFs can be modified after they have been synthesized, through postsynthetic modification (PSM) or postsynthetic exchange (PSE) (Figure 1.2.).[24-26] Both PSM and PSE have become routine methods to increase the diversity of MOFs because the two methods avoid the constraints of traditional MOF synthesis described earlier. For PSM, a preinstalled chemical handle within the MOF can be modified by traditional organic synthesis. For instance, the Cohen group performed amidations on IRMOF-3 and UiO-66-NH_2, as they bear a derivatizable amine.[27-31] There are several other examples of PSM in the literature, with MOFs that contain functional groups like azides,[32] alkynes,[33] aldehydes,[34] and halides and other functionalities.[35-36]

In comparison, PSE arises from the dynamic character of labile ligands and metals in coordination chemistry. The nature of displacement of both the metals and the ligands depends largely on the strength and lability of the coordination bonds within the MOF (Figure 1.2). For instance, several systematic studies have shown that Zn^{2+} ions in SBUs of IRMOF-1 can be partially exchanged with Ni^{2+},[37] Co^{2+},[38] and other transition metals. Similarly, successful ligand exchange has also been achieved for both IRMOF-1 and UiO-66 using H_2bdc-NH_2 to yield IRMOF-3 and UiO-66-NH_2, respectively.[24-25] Taken together, PSM and PSE make MOFs as a class of highly tunable materials for a variety of applications.

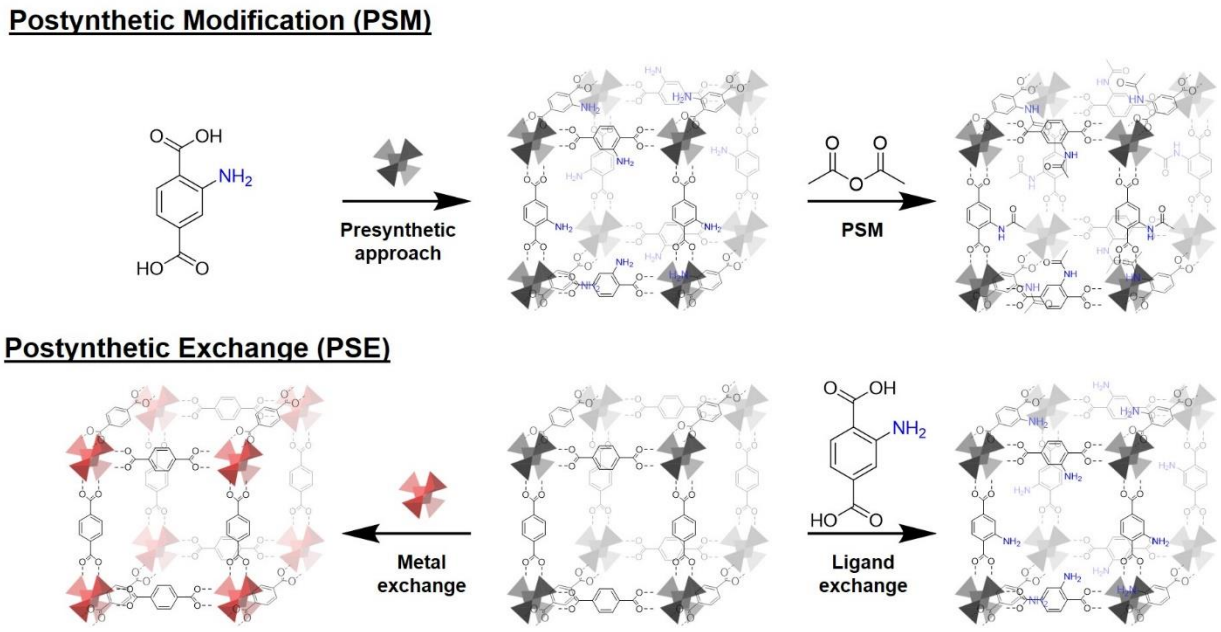

Figure 1.2. Schematic representation of postsynthetic modification (PSM) and postsynthetic exchange (PSE). PSM (top) can be achieved on a pre-installed chemical handle. PSE can be achieved by exchanging the metal (bottom left) or the organic linker (bottom right) after MOF formation.

1.2 MOF-Polymer Hybrid Materials

The high chemical tunability, long-range order, and porous nature of MOFs has made these materials attractive for the development of novel and interesting MOF-polymer hybrids.[7, 39-43] In contrast to MOFs, organic polymers are generally amorphous, but they are also processable materials with desirable properties like conductivity,[44] viscoelasticity,[45] self-healing ability,[46] and other valuable characteristics.[47] Combining MOFs with polymers has led to a continuum of unique materials including processable MOF composites,[48] MOFs with polymers grafted on their surfaces, MOFs with polymers within their pores,[11, 49-50] and MOFs templated by synthetic polymers.[51-53] A brief summary of the several types of MOF-polymer hybrid materials, and the methods used to devise them is described below.

MOF-Based Mixed-Matrix Membranes. Perhaps the major driver to prepare polymer-MOF hybrids is the production of processable, handleable MOF materials. MOFs are typically brittle, microcrystalline powders that are difficult to handle in their native form, but they can be embedded into synthetic polymers to produce composites called mixed-matrix membranes (MMMs).[48] MOF-based MMMs have proven to be promising materials for several applications including gas-separation,[54-55] separation of impurities from solvents,[56] degradation of chemical warfare agents,[57-58] and other applications. To prepare MMMs, MOFs are dispersed in a solution of polymer to produce a MOF 'ink', which can then be drop-casted on a substrate, spin coated on a surface, or drawdown coated to produce thin films; these methodologies provide simple, effective strategies to produce handleable MOF composites (Figure 1.3.).[59]

Figure 1.3. An illustrative representation of MOF mixed-matrix membranes (MMMs).

Traditionally, processable MOF MMMs have been prepared through noncovalent, physical mixing MOFs and polymers, but obtaining favorable interactions between the surface of the MOF and the polymer matrix are necessary to produce continuous materials without holes or macro voids. Cohen and co-workers demonstrated the production of MOF-based MMMs by combining several types of MOFs with polyvinylidene difluoride (PVDF) to afford MMMs with up to 67% loading of UiO-66 in the membrane.[56] These materials contained more MOF embedded in the polymer matrix than previously reported MOF MMMs, largely due to favorable interactions between the MOF surfaces and PVDF. Moreover, the composites retained complete accessible

surface area of the MOFs, the MOFs could undergo PSM while in the MMM and could be used for the separation of dyes in aqueous conditions. In an alternative strategy, the surface of MOFs can also be modified to improve MOF-polymer interface in MOF MMMs. Vankelecom and co-workers used PSM to modify MOFs with silyl groups, improving their interactions on a polydimethylsiloxane (PDMS) membrane, and as a result enhancing separation of dyes from isopropanol in comparison to unfunctionalized MOFs.[60]

MOFs with Polymer-Grafted on their Surfaces. The grafting of polymers onto the surfaces of MOFs can also yield hybrid materials with attractive properties like enhanced processability, but also dispersibility and other capacities. There are three general methods to attaching polymers on surfaces (an example of each approach is described below): grafting "through" the MOF surface, grafting "from" the MOF surface and grafting "to" the MOF surface (Figure 1.4.). To graft a polymer "through" the surface of the MOF, Wang and co-workers used acrylate-modified UiO-66-NH_2 nanoparticles to produce free-standing MMMs by photoinduced postsynthetic polymerization (PSP) with butyl methacrylate; no solvent or external polymer matrix was required to make a membrane.[61] The MOFs were well-dispersed within the composite material and could successfully separate Cr^{6+} better than the noncovalent, physically mixed MMM of UiO-66-NH_2 with butyl methacrylate polymer. In a different example, Webley and co-workers grafted a polymer "from" the surface of a MOF by using UiO-66-BiBB (BiBB = (bromoisobutyryl bromide) to grow poly(ethylene glycol) methyl ether methacrylate (PEGMA) directly from the MOF-surface using a controlled radical polymerization method.[62] The polymer-coated MOFs displayed appreciable dispersity when suspended in aqueous conditions. To graft a polymer "to" a MOF, Sada and co-workers synthesized a thermally responsive polymer poly(*N*-isopropylacrylamide) (PNIPAM), and attached to the surface of UiO-66-NH_2 using PSM.[63]

Controlled release of small molecules like caffeine could be achieved on a loaded UiO-66-PNIPAM by switching the pores from "open" to "closed through change of the temperature in which the MOF was suspended.

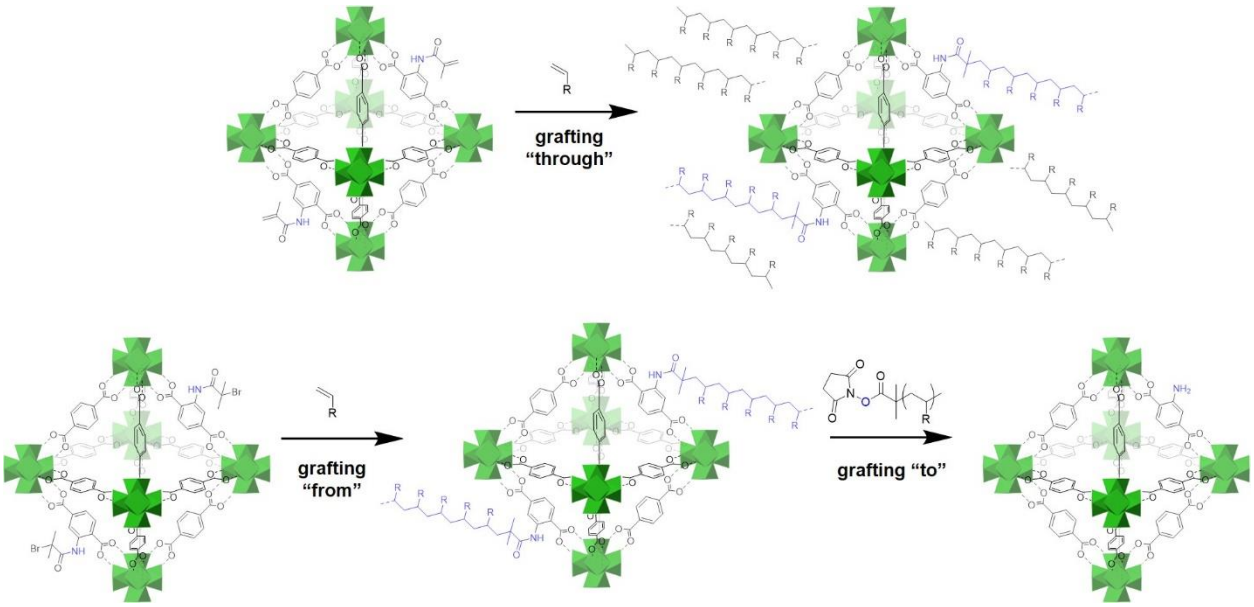

Figure 1.4. The three methods used to graft a polymer onto the surface of a MOF are presented. In a grafting "through" approach (top), the MOF is functionalized with a chemical handle to be copolymerized with a monomer and produce a polymer matrix. In a grafting "from" approach (bottom left), the MOF is functionalized with an initiator to grow polymers directly from the surface of a MOF. In a grafting "to" approach (bottom right), the presynthesized polymer is attached to the polymer by PSM.

Polymers Through the Pores of MOFs. Confining small-molecule monomers within the pores of MOFs to produce MOF-templated polymers has also been thoroughly investigated. Uemura and co-workers pioneered the first successful radical polymerization within the pores of the MOF.[64] In their report, styrene molecules were adsorbed into the pores of $[Zn_2(bdc)_2(DABCO)]_n$ (DABCO = 1,4- diazabicyclo[2.2.2]octane), followed by removing excess monomer under reduced pressure, and polymerization of the styrene within the confined pores. Traditionally, free radical polymerization in bulk yields polymers with broad dispersities, but

Uemura and co-workers demonstrated that the dispersity of resultant polystyrene was significantly reduced when confined within the pores of the MOF (Figure 1.5.). These results were propagated to other vinyl monomers, including PMMA, poly(vinyl acetate), polyacrylonitrile (PAN), and others.[49, 65] Moreover, Uemura and co-workers demonstrated the capability of confining monomers in the pores of MOFs to yield sequence-controlled polymers. This was done by adsorbing acrylonitrile into $[Cu(styrene\text{-}3,5\text{-}dicarboxylate)]_n$, a MOF with 1-D nanochannels containing a vinyl group on the organic linker for radical polymerization.[66] Interestingly, a total of exactly three acrylonitrile molecules fit between each sequential styrene-3,5-dicarboxylate; copolymerization of the acrylonitrile followed by subsequent digestion of the MOF yielded $(AB_3)_n$ sequence-controlled polymers (A = styrene-3,5-dicarboxylate; B = acrylonitrile).

Covalent crosslinking within the pores of MOFs with the organic linkers has also been achieved to produce free-standing polymer monoliths.[10-11, 67] For instance, Uemura and co-workers were able to partially replace bdc^{2-} with 2,5-divinyl-terephthalic acid in $[Cu_2(bdc)_2(DABCO)]_n$, adsorb styrene molecules that could be polymerized the organic linkers, and digest the MOF to obtain crosslinked polystyrene monoliths.[10] The crosslinked materials retained the shape of the original MOF structure, demonstrated high crystallinity as shown by powder X-ray diffraction (PXRD), and could retain long-range order even after treatment with various solvents and heat. In a related report, Sada and co-workers crosslinked azide difunctionalized linkers within the pores of MOFs with host tetrafunctional alkynes to produce MOF-templated polymer gels (Figure 1.5.).[11] The resultant polymer gels displayed no crystallinity, but they retained the shape of the MOFs and could be swelled under various solvents and pH ranges. Subsequent reports have also applied this method to produce anisotropic swelling gels, or gels that swell along one axis.[67]

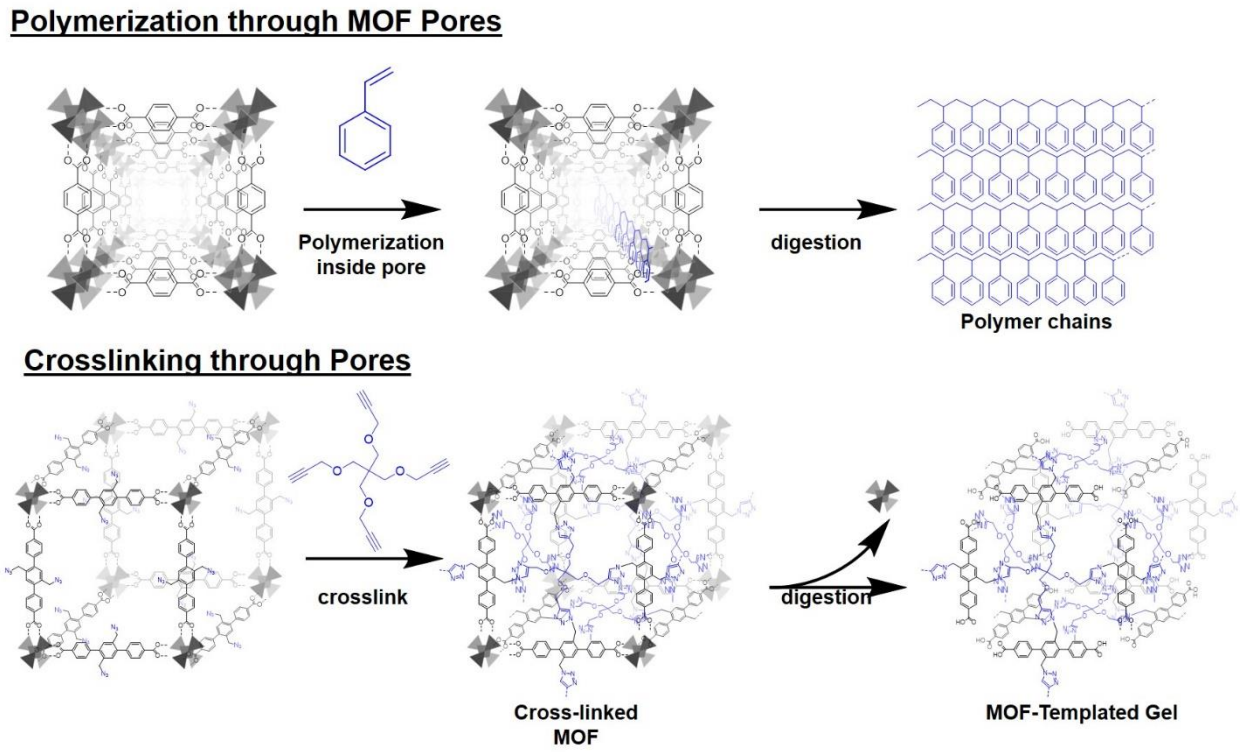

Figure 1.5. Schematic representation of polymerization through the pores of MOFs. In one approach (top), small molecule monomers like styrene are confined within the pore of a MOF, followed by subsequent polymerization and digestion, to afford polymers with narrow dispersity. Conversely, the MOF can be crosslinked through the pores (bottom), followed by subsequent digestion to produce MOF-templated gels.

MOFs Templated by Polymers. Synthetic polymers are promising tools to control size, shape, porosity and phase of MOF crystals, as polymers benefit from the ability to spontaneously self-assemble in solution, provide various coordination-sites for MOF-growth, and can be tuned to introduce new properties into MOFs. Three different types of polymers have been used to template the properties of MOFs: nonionic polymers, polymers with coordinating groups (ionic polymers), and block copolymers (Figure 1.6.).[59] Nonionic polymers like polyvinylpyrrolidone (PVP) have shown the ability to dictate the shape of square octahedral (soc) MOFs.[51, 53, 68] PVP can achieve shape-control of the MOFs through electrostatic interactions between the amide bonds

in the polymer and metal ions in solution. By combining the properties of PVP with small-molecule modulators like tetrabutylammonium nitrate, Eddaoudi and co-workers were able to control both the shape and size of socMOFs.[68] In comparison, introducing ionic polymers has proven to be an effective way to control the size of MOFs because of the competitive coordination of metals between the ionic polymers and the organic linkers. Kitagawa and co-workers introduced poly(vinylsulfonic acid) salts into the synthesis of $[Cu_2pzdc_2(pyz)_n]$ (pzdc = pyrazine-2,3-dicarboxylate; pyz = pyrazine) to increase the size of MOF crystallites from 2 μm to 70 μm.[69] Combining nonionic and ionic polymers, coordinative block copolymers have also shown to dictate the size and shape of MOFs. In a noteworthy example, a double-hydrophilic block copolymer (DHBC), poly(ethylene oxide)-*block*-poly(methacrylic acid) was used to control the topology of a MOF that exhibits two different crystalline structures.[52] Through a combination of electrostatic interactions and competitive coordination, the DHBC could be used to selectively grow hexagonal mesotructures of $[M_2(bdc)_2dabco]_n$ (M = Zn^{2+} or Cu^{2+}) over the thermodynamically favorable cubic phase of the MOF.

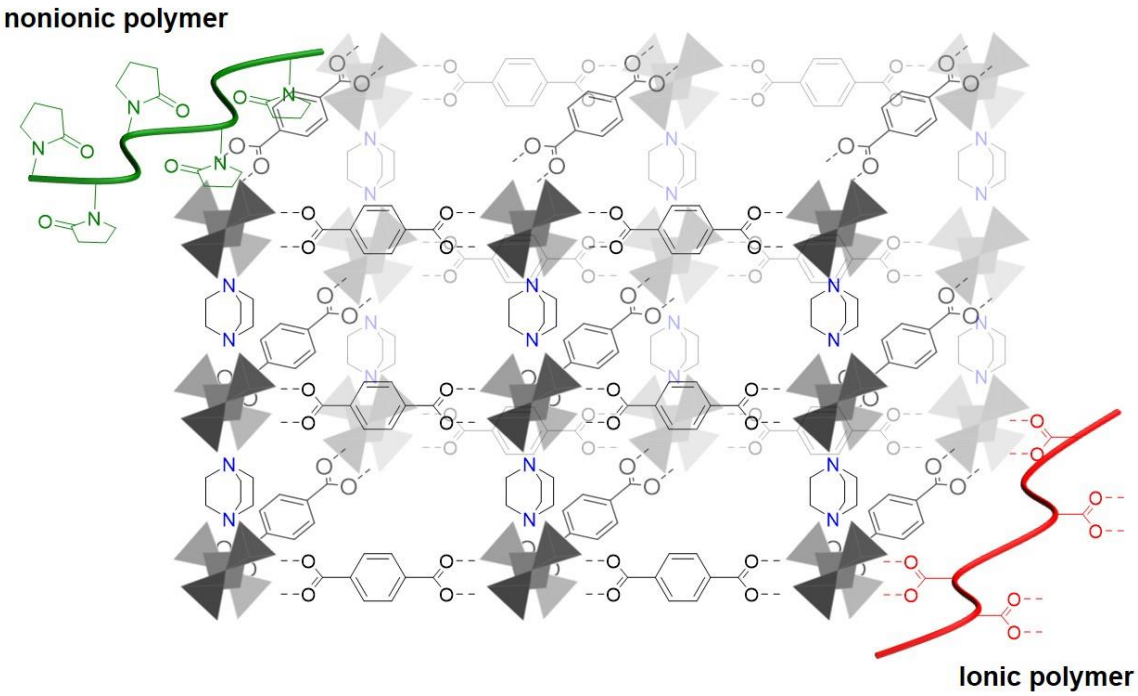

Figure 1.6. An illustrative representation of polymers being used to template the MOF. The synthetic polymer can control the shape of the MOF either through electrostatic interactions (green) or control the size by competitive coordination (red).

1.3 PolyMOFs

In contrast to the MOF-polymer hybrids just described, the Cohen group integrated MOFs and polymers at the molecular level to produce a new class of materials, coined as polyMOFs. In these materials, the framework is directly prepared from a synthetic polymer that contains multitopic metal-coordinating linkers, and the polymer is transformed in to a highly crystalline, 3-dimensional porous framework (Figure 1.7).[70-76] Using a polymer-ligand has led to MOFs with enhanced stability,[70-72] selective gas-separation,[71] hierarchical porosity,[72] and control of morphologies.[75-76] These materials exhibit several form-factors, including films, powders, and single-crystals, making them an integral part of the MOF-polymer hybrid families.

In order to successfully afford polyMOFs, the molecular arrangement of the polymer and the architecture of the MOF must both be satisfied; that is, the structure of the polymer must fit within the MOF, and the MOF must tolerate the connectivity of the polymer. In the first report of polyMOFs, Cohen and co-workers used Williamson ether polycondensation to synthesize various linear polymer-ligands of poly(1,4-benzenedicarboxylic acid) (referred to as 'pbdc-xa') connected by O-$(CH_2)_x$-O spacers.[70] Combining the pbdc-xa polymers with Zn^{2+} salts yielded a polyMOF with the well-known IRMOF lattice (**Error! Reference source not found.**.7.). Using a polymer ligand to prepare the IRMOF-1 architecture improved the hydrolytic stability of the framework, could be regenerated by addition of minimal solvent with mild heating, and produced microcrystalline films under the appropriate conditions.[70] Since then, two additional MOF structures (UiO-66,[72] and a pillaring-ligand MOF[71]), and features of an amorphous, 1-dimensional linear polymer architecture (e.g. varying the alkyl spacer-length, applying isoreticular chemistry[72, 74], using block co-polymers[73, 75]) have been varied to generate the several interesting properties of polyMOFs. Moreover, understanding how polymers dictate the properties of the resultant polyMOFs provides access to materials with functional properties for various applications.

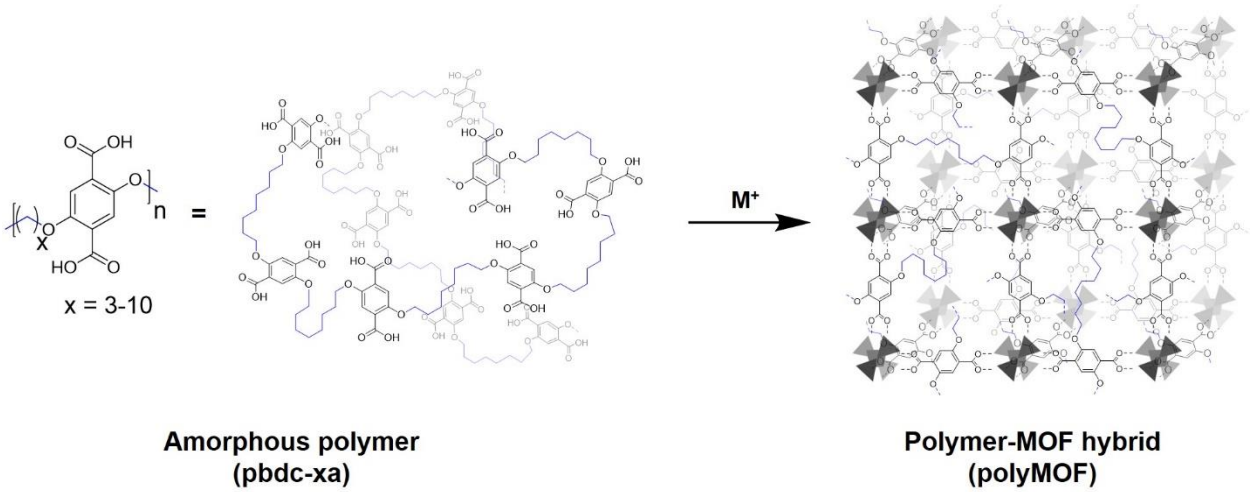

Figure 1.7. Illustrative example of an amorphous polymer ligand (pbdc-xa) transformed into a polymer-MOF (polyMOF) hybrid material.

1.4 Scope of the Dissertation

This dissertation will discuss efforts to understand how polymer structure and MOF architecture can dictate the capacity to form polyMOFs. Chapter 2 describes the first report of a polyMOF from a UiO-66 architecture using 1-dimensional, linear, amorphous polymers of various alkyl-spacers, molecular weights, and dispersities. Under the appropriate conditions, a UiO-66 polyMOF with a unique, interlaced morphology, and hierarchical porosity was achieved.

Chapter 3 describes the effects of applying the concept of isoreticular chemistry to polyMOFs. By synthesizing linear, amorphous polymers with laterally extended organic linkers, isoreticular polyMOFs with larger pores and surface areas could be achieved. Furthermore, it was determined that changing the position of the alkyl spacer from *para* to *ortho* prevented formation of UiO-66-type polyMOFs, signifying the importance of polymer architecture for polyMOF formation.

Chapter 4 describes the preparation of innovative block co-polyMOFs (BCPMOFs) with controlled morphologies using block copolymers containing poly(1,4-benzenedicarboxylic acid, H_2bdc) and morphology directing poly(ethylene glycol) (PEG) or poly(cyclooctadiene) (poly(COD)). By varying the connectivity, the weight fraction, and the composition of the block co-polymer ligands, the morphology of UiO-66 BCPMOFs could be controlled. Moreover, block co-polymer analogues of IRMOF-1 could be produced with narrow sizes and uniform cubic shapes.

Chapter 5 describes efforts to prepare multivariate (MTV) polyMOFs using random copolymers to produce materials with controlled hierarchical porosity. Random polymers containing various ratios H_2bdc and *p*-terphenyl-4,4″-dicarboxylic acid (H_2tpdc) were prepared and used to synthesize and characterize MTV polyMOFs.

1.5 Acknowledgements

Chapter 1, in part, is an adaptation of the following materials listed: "MOF-Polymer Hybrid Materials: From Simple Composites to Tailored Architectures" *Chem. Rev.* **2020**, accepted for publication; PolyMOFs: Molecular Level Integration of MOFs and Polymers. In *Hybrid Metal-Organic Framework and Covalent Organic Framework Polymers*, Wang, B., Ed. The Royal Society of Chemistry: In Preparation. The dissertation author was an author of the review and the primary author of the book chapter. The dissertation author gratefully acknowledges the contributions of coauthors Mark Kalaj, Kyle C. Bentz, Joseph M. Palomba, Kyle S. Barcus, Yuji Katayama, and Seth M. Cohen in the review titled, "MOF-Polymer Hybrid Materials: From Simple Composites to Tailored Architectures". The dissertation author also acknowledges the contributions of coauthor Seth M. Cohen in the book Chapter titled, "PolyMOFs: Molecular Level Integration of MOFs and Polymers".

1.6 References

1. Li, H.; Eddaoudi, M.; O'Keeffe, M.; Yaghi, O. M., Design and synthesis of an exceptionally stable and highly porous metal-organic framework. *Nature* **1999,** *402*, 276-279.

2. Farha, O. K.; Eryazici, I.; Jeong, N. C.; Hauser, B. G.; Wilmer, C. E.; Sarjeant, A. A.; Snurr, R. Q.; Nguyen, S. T.; Yazaydın, A. Ö.; Hupp, J. T., Metal–Organic Framework Materials with Ultrahigh Surface Areas: Is the Sky the Limit? *J. Am. Chem. Soc.* **2012,** *134*, 15016-15021.

3. Li, H.; Wang, K.; Sun, Y.; Lollar, C. T.; Li, J.; Zhou, H.-C., Recent advances in gas storage and separation using metal–organic frameworks. *Mater. Today* **2018,** *21*, 108-121.

4. Murray, L. J.; Dincă, M.; Long, J. R., Hydrogen storage in metal–organic frameworks. *Chem. Soc. Rev.* **2009,** *38*, 1294-1314.

5. Adil, K.; Belmabkhout, Y.; Pillai, R. S.; Cadiau, A.; Bhatt, P. M.; Assen, A. H.; Maurin, G.; Eddaoudi, M., Gas/vapour separation using ultra-microporous metal–organic frameworks: insights into the structure/separation relationship. *Chem. Soc. Rev.* **2017,** *46*, 3402-3430.

6. Li, J.-R.; Kuppler, R. J.; Zhou, H.-C., Selective gas adsorption and separation in metal–organic frameworks. *Chem. Soc. Rev.* **2009,** *38*, 1477-1504.

7. Bobbitt, N. S.; Mendonca, M. L.; Howarth, A. J.; Islamoglu, T.; Hupp, J. T.; Farha, O. K.; Snurr, R. Q., Metal–organic frameworks for the removal of toxic industrial chemicals and chemical warfare agents. *Chem. Soc. Rev.* **2017,** *46*, 3357-3385.

8. Lee, J.; Farha, O. K.; Roberts, J.; Scheidt, K. A.; Nguyen, S. T.; Hupp, J. T., Metal–organic framework materials as catalysts. *Chem. Soc. Rev.* **2009,** *38*, 1450-1459.

9. Yu, X.; Wang, L.; Cohen, S. M., Photocatalytic metal–organic frameworks for organic transformations. *CrystEngComm* **2017,** *19*, 4126-4136.

10. Distefano, G.; Suzuki, H.; Tsujimoto, M.; Isoda, S.; Bracco, S.; Comotti, A.; Sozzani, P.; Uemura, T.; Kitagawa, S., Highly ordered alignment of a vinyl polymer by host–guest cross-polymerization. *Nat. Chem.* **2013,** *5*, 335-341.

11. Ishiwata, T.; Furukawa, Y.; Sugikawa, K.; Kokado, K.; Sada, K., Transformation of Metal–Organic Framework to Polymer Gel by Cross-Linking the Organic Ligands Preorganized in Metal–Organic Framework. *J. Am. Chem. Soc.* **2013,** *135*, 5427–5432.

12. Yanai, N.; Uemura, T.; Ohba, M.; Kadowaki, Y.; Maesato, M.; Takenaka, M.; Nishitsuji, S.; Hasegawa, H.; Kitagawa, S., Fabrication of Two-Dimensional Polymer Arrays: Template Synthesis of Polypyrrole between Redox-Active Coordination Nanoslits. *Angew. Chem. Int. Ed.* **2008,** *47*, 9883-9886.

13. Lian, X.; Fang, Y.; Joseph, E.; Wang, Q.; Li, J.; Banerjee, S.; Lollar, C.; Wang, X.; Zhou, H.-C., Enzyme–MOF (metal–organic framework) composites. *Chem. Soc. Rev.* **2017,** *46*, 3386-3401.

14. Rubio-Martinez, M.; Avci-Camur, C.; Thornton, A. W.; Imaz, I.; Maspoch, D.; Hill, M. R., New synthetic routes towards MOF production at scale. *Chem. Soc. Rev.* **2017,** *46*, 3453-3480.

15. Stassen, I.; Burtch, N.; Talin, A.; Falcaro, P.; Allendorf, M.; Ameloot, R., An updated roadmap for the integration of metal–organic frameworks with electronic devices and chemical sensors. *Chem. Soc. Rev.* **2017,** *46*, 3185-3241.

16. Altintas, C.; Avci, G.; Daglar, H.; Nemati Vesali Azar, A.; Erucar, I.; Velioglu, S.; Keskin, S., An extensive comparative analysis of two MOF databases: high-throughput screening of computation-ready MOFs for CH4 and H2 adsorption. *J. Chem. Mater. Chem.* **2019,** *7*, 9593-9608.

17. Moghadam, P. Z.; Li, A.; Wiggin, S. B.; Tao, A.; Maloney, A. G. P.; Wood, P. A.; Ward, S. C.; Fairen-Jimenez, D., Development of a Cambridge Structural Database Subset: A Collection of Metal–Organic Frameworks for Past, Present, and Future. *Chem. Mater.* **2017,** *29*, 2618-2625.

18. Hoskins, B. F.; Robson, R., Design and construction of a new class of scaffolding-like materials comprising infinite polymeric frameworks of 3D-linked molecular rods. A reappraisal of the zinc cyanide and cadmium cyanide structures and the synthesis and structure of the diamond-related frameworks [N(CH3)4][CuIZnII(CN)4] and CuI[4,4',4",4"'-tetracyanotetraphenylmethane]BF4.xC6H5NO2. *J. Am. Chem. Soc.* **1990,** *112*, 1546-1554.

19. Eddaoudi, M.; Kim, J.; Rosi, N.; Vodak, D.; Wachter, J.; O'Keeffe, M.; Yaghi, O. M., Systematic Design of Pore Size and Functionality in Isoreticular MOFs and Their Application in Methane Storage. *Science* **2002,** *295*, 469-472.

20. Cavka, J. H.; Jakobsen, S.; Olsbye, U.; Guillou, N.; Lamberti, C.; Bordiga, S.; Lillerud, K. P., A New Zirconium Inorganic Building Brick Forming Metal Organic Frameworks with Exceptional Stability. *J. Am. Chem. Soc.* **2008,** *130*, 13850-13851.

21. Deng, H.; Doonan, C. J.; Furukawa, H.; Ferreira, R. B.; Towne, J.; Knobler, C. B.; Wang, B.; Yaghi, O. M., Multiple Functional Groups of Varying Ratios in Metal-Organic Frameworks. *Science* **2010,** *327*, 846-850.

22. Koh, K.; Wong-Foy, A. G.; Matzger, A. J., A Crystalline Mesoporous Coordination Copolymer with High Microporosity. *Angew. Chem. Int. Ed.* **2008,** *47*, 677-680.

23. Luo, T.-Y.; Liu, C.; Gan, X. Y.; Muldoon, P. F.; Diemler, N. A.; Millstone, J. E.; Rosi, N. L., Multivariate Stratified Metal–Organic Frameworks: Diversification Using Domain Building Blocks. *J. Am. Chem. Soc.* **2019,** *141*, 2161-2168.

24. Cohen, S. M., Postsynthetic Methods for the Functionalization of Metal–Organic Frameworks. *Chem. Rev.* **2012,** *112*, 970-1000.

25. Cohen, S. M., The Postsynthetic Renaissance in Porous Solids. *J. Am. Chem. Soc.* **2017,** *139*, 2855-2863.

26. Wang, Z.; Cohen, S. M., Postsynthetic modification of metal–organic frameworks. *Chem. Soc. Rev.* **2009,** *38*, 1315-1329.

27. Wang, Z.; Cohen, S. M., Postsynthetic Covalent Modification of a Neutral Metal−Organic Framework. *J. Am. Chem. Soc.* **2007,** *129*, 12368-12369.

28. Tanabe, K. K.; Wang, Z.; Cohen, S. M., Systematic Functionalization of a Metal−Organic Framework via a Postsynthetic Modification Approach. *J. Am. Chem. Soc.* **2008,** *130*, 8508-8517.

29. Wang, Z.; Cohen, S. M., Tandem Modification of Metal–Organic Frameworks by a Postsynthetic Approach. *Angew. Chem. Int. Ed.* **2008,** *47*, 4699-4702.

30. Nguyen, J. G.; Cohen, S. M., Moisture-Resistant and Superhydrophobic Metal−Organic Frameworks Obtained via Postsynthetic Modification. *J. Am. Chem. Soc.* **2010,** *132*, 4560-4561.

31. Garibay, S. J.; Cohen, S. M., Isoreticular synthesis and modification of frameworks with the UiO-66 topology. *Chem. Commun.* **2010,** *46*, 7700-7702.

32. Goto, Y.; Sato, H.; Shinkai, S.; Sada, K., "Clickable" Metal−Organic Framework. *J. Am. Chem. Soc.* **2008,** *130*, 14354-14355.

33. Gadzikwa, T.; Lu, G.; Stern, C. L.; Wilson, S. R.; Hupp, J. T.; Nguyen, S. T., Covalent surface modification of a metal–organic framework: selective surface engineering via CuI-catalyzed Huisgen cycloaddition. *Chem. Commun.* **2008**, 5493-5495.

34. Burrows, A. D.; Frost, C. G.; Mahon, M. F.; Richardson, C., Post-Synthetic Modification of Tagged Metal–Organic Frameworks. *Angew. Chem. Int. Ed.* **2008,** *47*, 8482-8486.

35. Dugan, E.; Wang, Z.; Okamura, M.; Medina, A.; Cohen, S. M., Covalent modification of a metal–organic framework with isocyanates: probing substrate scope and reactivity. *Chem. Commun.* **2008**, 3366-3368.

36. Volkringer, C.; Cohen, S. M., Generating Reactive MILs: Isocyanate- and Isothiocyanate-Bearing MILs through Postsynthetic Modification. *Angew. Chem. Int. Ed.* **2010,** *49*, 4644-4648.

37. Brozek, C. K.; Dincă, M., Lattice-imposed geometry in metal–organic frameworks: lacunary Zn4O clusters in MOF-5 serve as tripodal chelating ligands for Ni2+. *Chem. Sci.* **2012,** *3*, 2110-2113.

38. Botas, J. A.; Calleja, G.; Sánchez-Sánchez, M.; Orcajo, M. G., Cobalt Doping of the MOF-5 Framework and Its Effect on Gas-Adsorption Properties. *Langmuir* **2010,** *26*, 5300-5303.

39. Fathieh, F.; Kalmutzki, M. J.; Kapustin, E. A.; Waller, P. J.; Yang, J.; Yaghi, O. M., Practical water production from desert air. *Sci. Adv.* **2018,** *4*.

40. Lustig, W. P.; Mukherjee, S.; Rudd, N. D.; Desai, A. V.; Li, J.; Ghosh, S. K., Metal–organic frameworks: functional luminescent and photonic materials for sensing applications. *Chem. Soc. Rev.* **2017,** *46*, 3242-3285.

41. Palomba, J. M.; Credille, C. V.; Kalaj, M.; DeCoste, J. B.; Peterson, G. W.; Tovar, T. M.; Cohen, S. M., High-throughput screening of solid-state catalysts for nerve agent degradation. *Chem. Commun.* **2018,** *54*, 5768-5771.

42. Shivanna, M.; Yang, Q.-Y.; Bajpai, A.; Patyk-Kazmierczak, E.; Zaworotko, M. J., A dynamic and multi-responsive porous flexible metal–organic material. *Nat. Commun.* **2018,** *9*, 3080.

43. Tan, L.; Tan, B., Hypercrosslinked porous polymer materials: design, synthesis, and applications. *Chem. Soc. Rev.* **2017,** *46*, 3322-3356.

44. Kang, H. A.; Bronstein, H. E.; Swager, T. M., Conductive Block Copolymers Integrated into Polynorbornene-Derived Scaffolds. *Macromolecules* **2008,** *41*, 5540-5547.

45. Wang, Y.; Zhong, M.; Park, J. V.; Zhukhovitskiy, A. V.; Shi, W.; Johnson, J. A., Block Co-PolyMOCs by Stepwise Self-Assembly. *J. Am. Chem. Soc.* **2016,** *138*, 10708-10715.

46. Mozhdehi, D.; Neal, J. A.; Grindy, S. C.; Cordeau, Y.; Ayala, S.; Holten-Andersen, N.; Guan, Z., Tuning Dynamic Mechanical Response in Metallopolymer Networks through Simultaneous Control of Structural and Temporal Properties of the Networks. *Macromolecules* **2016,** *49*, 6310-6321.

47. Berda, E. B.; Lande, R. E.; Wagener, K. B., Precisely Defined Amphiphilic Graft Copolymers. *Macromolecules* **2007,** *40*, 8547-8552.

48. Denny Jr, M. S.; Moreton, J. C.; Benz, L.; Cohen, S. M., Metal–organic frameworks for membrane-based separations. *Nat. Rev. Mater.* **2016,** *1*, 16078.

49. Uemura, T.; Yanai, N.; Kitagawa, S., Polymerization reactions in porous coordination polymers. *Chem. Soc. Rev.* **2009,** *38*, 1228-1236.

50. Uemura, T.; Kaseda, T.; Sasaki, Y.; Inukai, M.; Toriyama, T.; Takahara, A.; Jinnai, H.; Kitagawa, S., Mixing of immiscible polymers using nanoporous coordination templates. *Nat. Commun.* **2015,** *6*, 7473.

51. Cai, X.; Deng, X.; Xie, Z.; Bao, S.; Shi, Y.; Lin, J.; Pang, M.; Eddaoudi, M., Synthesis of highly monodispersed Ga-soc-MOF hollow cubes, colloidosomes and nanocomposites. *Chem. Commun.* **2016,** *52*, 9901-9904.

52. Hwang, J.; Heil, T.; Antonietti, M.; Schmidt, B. V. K. J., Morphogenesis of Metal–Organic Mesocrystals Mediated by Double Hydrophilic Block Copolymers. *J. Am. Chem. Soc.* **2018,** *140*, 2947-2956.

53. Pang, M.; Cairns, A. J.; Liu, Y.; Belmabkhout, Y.; Zeng, H. C.; Eddaoudi, M., Synthesis and Integration of Fe-soc-MOF Cubes into Colloidosomes via a Single-Step Emulsion-Based Approach. *J. Am. Chem. Soc.* **2013,** *135*, 10234-10237.

54. Rezakazemi, M.; Ebadi Amooghin, A.; Montazer-Rahmati, M. M.; Ismail, A. F.; Matsuura, T., State-of-the-art membrane based CO2 separation using mixed matrix membranes (MMMs): An overview on current status and future directions. *Prog. Polym. Sci.* **2014,** *39*, 817-861.

55. Katayama, Y.; Bentz, K. C.; Cohen, S. M., Defect-Free MOF-Based Mixed-Matrix Membranes Obtained by Corona Cross-Linking. *ACS Appl. Mater. Interfaces* **2019,** *11*, 13029-13037.

56. Denny Jr., M. S.; Cohen, S. M., In Situ Modification of Metal–Organic Frameworks in Mixed-Matrix Membranes. *Angew. Chem. Int. Ed.* **2015,** *54*, 9029-9032.

57. DeCoste, J. B.; Denny, J. M. S.; Peterson, G. W.; Mahle, J. J.; Cohen, S. M., Enhanced aging properties of HKUST-1 in hydrophobic mixed-matrix membranes for ammonia adsorption. *Chem. Sci.* **2016,** *7*, 2711-2716.

58. Peterson, G. W.; Browe, M. A.; Durke, E. M.; Epps, T. H., Flexible SIS/HKUST-1 Mixed Matrix Composites as Protective Barriers against Chemical Warfare Agent Simulants. *ACS Appl. Mater. Interfaces* **2018,** *10*, 43080-43087.

59. Kalaj, M.; Bentz, K. C.; Ayala, S.; Palomba, J. M.; Barcus, K. S.; Katayama, Y.; Cohen, S. M., MOF-Polymer Hybrid Materials: From Simple Composites to Tailored Architectures. *Chem. Rev.* **2020**.

60. Basu, S.; Maes, M.; Cano-Odena, A.; Alaerts, L.; De Vos, D. E.; Vankelecom, I. F. J., Solvent resistant nanofiltration (SRNF) membranes based on metal-organic frameworks. *J. Membr. Sci.* **2009,** *344*, 190-198.

61. Zhang, Y.; Feng, X.; Li, H.; Chen, Y.; Zhao, J.; Wang, S.; Wang, L.; Wang, B., Photoinduced Postsynthetic Polymerization of a Metal–Organic Framework toward a Flexible Stand-Alone Membrane. *Angew. Chem. Int. Ed.* **2015,** *54*, 4259-4263.

62. Xie, K.; Fu, Q.; He, Y.; Kim, J.; Goh, S. J.; Nam, E.; Qiao, G. G.; Webley, P. A., Synthesis of well dispersed polymer grafted metal–organic framework nanoparticles. *Chem. Commun.* **2015,** *51*, 15566-15569.

63. Nagata, S.; Kokado, K.; Sada, K., Metal–organic framework tethering PNIPAM for ON–OFF controlled release in solution. *Chem. Commun.* **2015,** *51*, 8614-8617.

64. Uemura, T.; Kitagawa, K.; Horike, S.; Kawamura, T.; Kitagawa, S.; Mizuno, M.; Endo, K., Radical polymerisation of styrene in porous coordination polymers. *Chem. Commun.* **2005**, 5968-5970.

65. Kitao, T.; Zhang, Y.; Kitagawa, S.; Wang, B.; Uemura, T., Hybridization of MOFs and polymers. *Chem. Soc. Rev.* **2017,** *46*, 3108-3133.

66. Mochizuki, S.; Ogiwara, N.; Takayanagi, M.; Nagaoka, M.; Kitagawa, S.; Uemura, T., Sequence-regulated copolymerization based on periodic covalent positioning of monomers along one-dimensional nanochannels. *Nat. Commun.* **2018,** *9*, 329.

67. Ishiwata, T.; Kokado, K.; Sada, K., Anisotropically Swelling Gels Attained through Axis-Dependent Crosslinking of MOF Crystals. *Angew. Chem. Int. Ed.* **2017,** *56*, 2608-2612.

68. Pang, M.; Cairns, A. J.; Liu, Y.; Belmabkhout, Y.; Zeng, H. C.; Eddaoudi, M., Highly Monodisperse MIII-Based soc-MOFs (M = In and Ga) with Cubic and Truncated Cubic Morphologies. *J. Am. Chem. Soc.* **2012,** *134*, 13176-13179.

69. Uemura, T.; Hoshino, Y.; Kitagawa, S.; Yoshida, K.; Isoda, S., Effect of Organic Polymer Additive on Crystallization of Porous Coordination Polymer. *Chem. Mater.* **2006,** *18*, 992-995.

70. Zhang, Z.; Nguyen, H. T. H.; Miller, S. A.; Cohen, S. M., polyMOFs: A Class of Interconvertible Polymer-Metal-Organic-Framework Hybrid Materials. *Angew. Chem. Int. Ed.* **2015,** *54*, 6152-6157.

71. Zhang, Z.; Nguyen, H. T. H.; Miller, S. A.; Ploskonka, A. M.; DeCoste, J. B.; Cohen, S. M., Polymer–Metal–Organic Frameworks (polyMOFs) as Water Tolerant Materials for Selective Carbon Dioxide Separations. *J. Am. Chem. Soc.* **2016,** *138*, 920-925.

72. Schukraft, G. E. M.; Ayala, S.; Dick, B. L.; Cohen, S. M., Isoreticular expansion of polyMOFs achieves high surface area materials. *Chem. Commun.* **2017,** *53*, 10684-10687.

73. MacLeod, M. J.; Johnson, J. A., Block co-polyMOFs: assembly of polymer–polyMOF hybrids via iterative exponential growth and "click" chemistry. *Polym. Chem.* **2017,** *8*, 4488-4493.

74. Palomba, J. M.; Ayala Jr., S.; Cohen, S. M., polyMOF Formation from Kinked Polymer Ligands via ortho-Substitution. *Isr. J. Chem.* **2018,** *58*, 1123-1126.

75. Ayala, S.; Bentz, K. C.; Cohen, S. M., Block co-polyMOFs: morphology control of polymer–MOF hybrid materials. *Chem. Sci.* **2019,** *10*, 1746-1753.

76. Gu, Y.; Huang, M.; Zhang, W.; Pearson, M. A.; Johnson, J. A., PolyMOF Nanoparticles: Dual Roles of a Multivalent polyMOF Ligand in Size Control and Surface Functionalization. *Angew. Chem. Int. Ed.* **2019,** *58*, 16676-16681.

Chapter 2: UiO-66 polyMOFs with Hierarchical Structure and Porosity

2.1 Introduction

The successful preparation of polyMOFs in an IRMOF-1 architecture,[1] as discussed in Chapter 1, prompted the investigation of other MOF lattices that could accommodate a linear, 1-dimensional polymer-ligand. Cohen and co-workers used a 4,4′-bipyridine to afford new pillaring-ligand polyMOFs.[2] As with IRMOF-1, the hydrophobic nature of the polymer-ligand improved the hydrolytic stability of the pillaring-ligand polyMOFs, and the gas adsorption of these materials revealed that the new frameworks preferably adsorb CO_2 over N_2, making them promising materials for flue gas separation. These hybrid materials served as proof-of-concept that additional MOF architectures might be achievable under specific conditions.

Zirconium-based MOFs, such as UiO-66,[3] are of particular interest because of their high chemical stability and rich tunability, making them promising for a variety of applications.[4] As described in Chapter 1, UiO-66 is composed of $Zr_6O_4(OH)_4$ metal-oxo clusters connected by twelve 1,4-benzenedicarboxylate (bdc^{2-}) units that act as struts for the framework, forming both tetrahedral and octahedral cages. Several reports have demonstrated that the use of monotopic acid modulators can produce defect sites in the framework,[5] as H_2bdc units can be replaced with modulators thereby providing access to mesoporous MOFs.[6-8] UiO-66 crystals typically display octahedral, truncated octahedral, or cubic morphologies depending on synthetic conditions.[9-10]

In Chapter 2 the preparation of a UiO-66 polyMOF is described using polymer ligands prepared using acyclic diene metathesis (ADMET) polymerization (Scheme 2.1), which possess improved, higher molecular weight compared to earlier polymer ligands.[11] Importantly, it is observed that under certain conditions, an unprecedented, mesoporous crystalline morphology is produced that is completely distinct from any known form of UiO-66 and which shows hierarchical (micro- and meso-porous) gas sorption properties.

2.2 Synthesis and Characterization of Polymer Ligands

New polymer ligands were prepared using ADMET polymerization to obtain larger, more uniform polymers than previous reports.[1-2] Polymer ligands were prepared through a three-step synthesis (Scheme 2.1). Suitable monomers were prepared via Williamson ether synthesis using dimethyl 2,5-dihydroxyterephthalate and bromoalkenes ($Br(CH_2)_yCHCH_2$, y = 2-4) that would allow for variations in the distance between H_2bdc units in the final polymer. The monomers were polymerized using Grubbs 2nd generation metathesis catalyst to afford the polymer ligand ester precursors (indicated as pbdc-*x*e-u or pbdc-*x*e-u$_{Mn}$, where *x* represents the number of methylene spacers between each H_2bdc unit, 'e' denotes 'ester', 'u' signifies unsaturation in the alkyl spacers, and M_n indicates the number-average molecular weight for fractionated, narrow dispersity polymers, Figure 2S.1-7). It is well established that ADMET polymerization produces broad molecular weight polymers.[12-13] Therefore, to narrow polymer dispersity, automated silica gel column chromatography was used to fractionate the polymer esters (Figure 2S.4-7). The polymer ester precursors were hydrolyzed to afford the polymer acid ligands (pbdc-*x*a-u, where, 'a' indicates 'acid', Figure 2S.8-13).

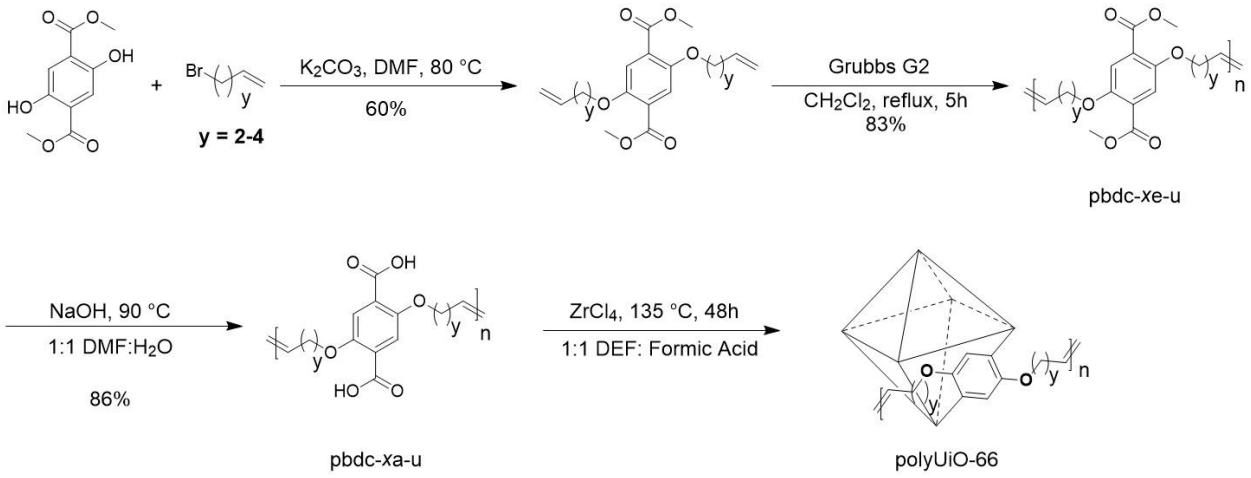

Scheme 2.1. Synthesis of polymer ligand and preparation of a UiO-66 polyMOF.

To determine the molecular weight of the polymer ligands, the polymer ester precursors were analyzed using ^{1}HNMR end-group analysis and gel permeation chromatography (GPC, Table 2.1). Both ^{1}HNMR and GPC yield similar M_n values and degrees of polymerization (DP). Some deviation in M_n values between the two analytical methods was observed (for example, pbdc-8e-u and pbdc-8e-u$_{7800}$), which can be attributed to a limit of detection when analyzing polymer molecular weights via end-group analysis using ^{1}HNMR, and because poly(methyl methacrylate) (PMMA) was used as a GPC standard to obtain relative M_n values. For the narrow dispersity polymers of pbdc-8e-u (fractionated by column chromatography), MALDI-TOF mass spectrometry data was also collected (Figure 2S.14). MALDI-TOF MS gave well resolved spectra only for the smallest molecular weight fraction (pbdc-8e-u$_{2800}$). Larger polymers (pbdc-8e-u$_{7800}$, pbdc-8e-u$_{42000}$) provided poor resolution MALDI-TOF data (Figure 2S.14). The hydrolyzed polymer ligands (e.g. acid form, pbdc-8a-u) were not characterized by GPC as they are excluded from the column due to their high polarity. MALDI-TOF MS of the hydrolyzed ligands could not be resolved because the ligands were insoluble in low-boiling point solvents. However, ^{1}HNMR end-group analysis could still be performed to obtain reasonable M_n values for pbdc-*x*a-u polymer ligands (see Supporting Information).

Table 2.1. Molecular weight determinations of pbdc-*x*e-u polymer ligands.

Ligand	M_n (^{1}HNMR) [a]	M_n (GPC)	M_w/M_n	DP (^{1}HNMR) [b]	DP (GPC) [b]
pbdc-6e-u	20,500	20,500	2.1	67	61
pbdc-8e-u	33,400	19,600	2.9	100	59
pbdc-10e-u	12,000	10,800	3.1	33	30
pbdc-8e-u$_{2800}$	2,360	2,760	1.2	7	8
pbdc-8e-u$_{7800}$	16,700	7,780	1.5	50	23
pbdc-8e-u$_{42000}$	33,400	42,200	1.3	100	126

[a] Number average molecular weight was determined using end-group analysis by ^{1}HNMR. [b] The number of repeat units of the polymers were determined using the following formula: DP = (M_n-MW$_{ethylene}$)/(MW$_{monomer}$-MW$_{ethylene}$).

2.3 Synthesis and Characterization of PolyUiO-66

To prepare polyUiO-66, a procedure was adapted using excess formic acid modulator (1:1 formic acid:DEF); it was found that the use of modulator was critical for formation of the polyMOF.[5] Using either pbdc-6a-u or pbdc-8a-u polymer ligands resulted in formation of the desired polyMOF (e.g. polyUiO-66) as confirmed by powder X-ray diffraction (PXRD) (Figure 2.1). However, pbdc-10a-u only formed amorphous materials (in the form of films) under several different reaction conditions, suggesting an upper limit on linker spacing (Figure 2.1).[1-2] The ADMET polymerization techniques used here can only produce polymers with even numbers of methylene groups in the alkyl spacers and contain unsaturation in the middle of the spacer (see Scheme 1). To examine more systems, polymer ligands (pbdc-*x*a)[1-2] were used to verify the effect of spacer length on polyUiO-66 formation. Indeed, PXRD confirmed that polyUiO-66 only formed with polymers of a certain linker spacing (pbdc-*x*a, x = 3-8, Figure 2S.15). For pbdc-9a and pbdc-10a, only amorphous materials were obtained (Figure 2S.15, ESI†).

To study polymer size and dispersity effects on polyMOF formation, pbdc-8a-u was purified into different fractions containing different molecular weights and narrower dispersities (see Table 2.1). Surprisingly, it was noted that small chain oligomers of pbdc-8a-u_{2800} (DP = 7) yielded less crystalline polyUiO-66 than larger-chain polymers as gauged by PXRD (Figure 2.1). For higher molecular weight polymers (pbdc-8a-u_{7800}, pbdc-8a-u_{42000}), an additional reflection is observed in the PXRD as a shoulder at $2\theta = 7.05°$. This feature may be due to a distortion in polyUiO-66 lattice to accomodate the spacer restrictions between bdc^{2-} linkers. This hypothesis is consistent with reports of modified UiO-66 that show lower symmetry.[12, 14] A reflection observed at $2\theta = 12.1°$ corresponds to a hydrated SBU of polyUiO-66, and has been observed in UiO-66 in the literature.[15]

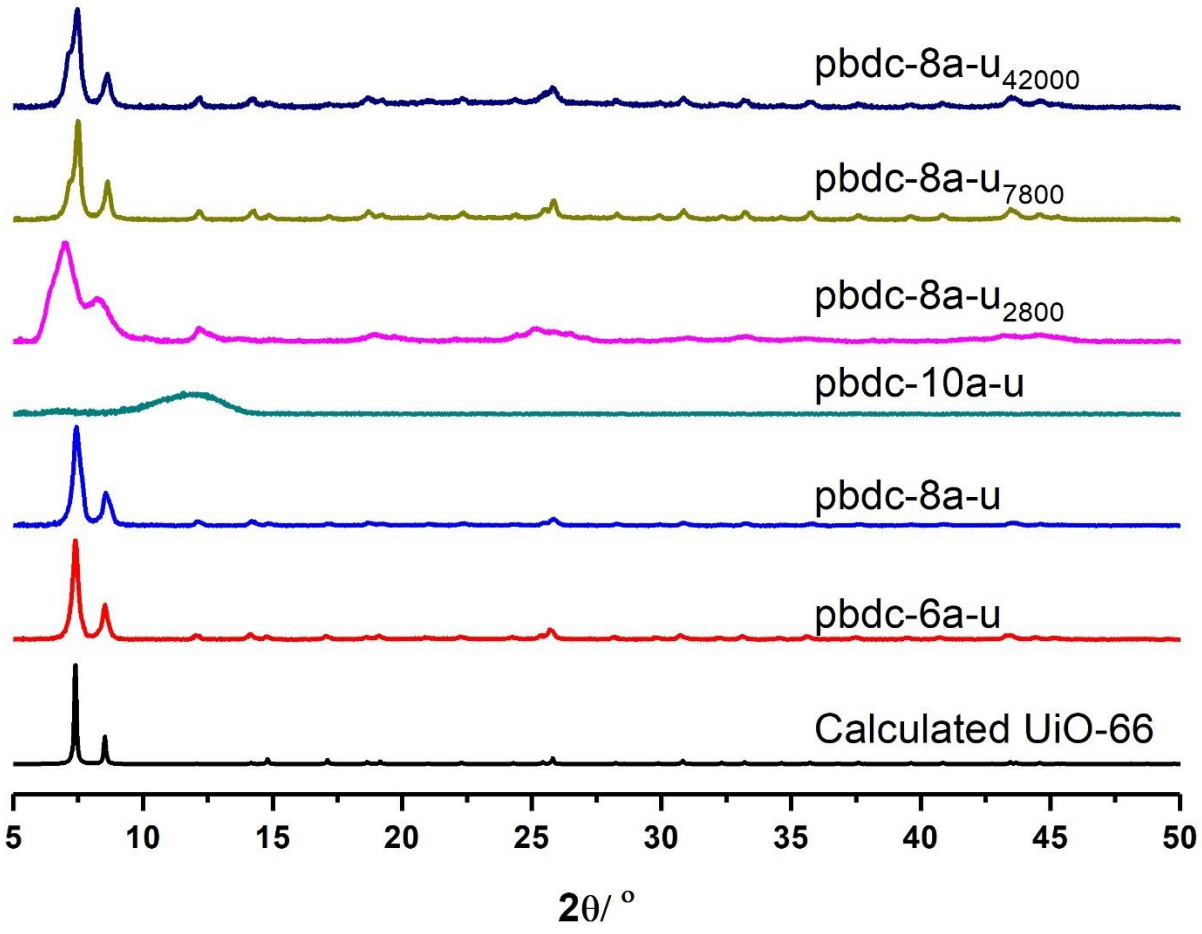

Figure 2.1. PXRD patterns for UiO-66 polyMOFs prepared from pbdc-*x*a-u ligands.

The polyUiO-66 materials were analyzed to confirm retention of polymer ligand integrity. Upon dissolution of the materials, ^{1}HNMR established that the polymer ligands did not decompose after polyMOF synthesis (Figures 2S.16-18). ^{1}HNMR end-group analysis of the fractionated, narrow-dispersity polymer ligands confirmed that the polymers did not change molecular weight (Figure 2S.19). From the ^{1}H NMR digestions, it is noted that formic acid modulator remains in the sample, which may contribute to additional defects in the metal-oxo clusters of the framework. The thermal stability of the UiO-66 polyMOFs was examined with thermogravimetric analysis (TGA), which showed polyUiO-66 materials degraded at significantly lower temperatures (330 -

350 °C, Figure 2S.20) compared to native UiO-66 (400 - 450 °C).[4, 16-17] Degradation of the polymer ligand alone occurs at 340 - 390 °C (Figure 2S.21). No degradation of polyUiO-66 was observed after storage in air for six months (Figure 2S.22) .

Although both pbdc-6a-u and pbdc-8a-u formed polyUiO-66 materials, different morphologies of polyUiO-66 were obtained with these two polymer ligands. Morphology and particle size of polyUiO-66 were investigated using scanning electron microscopy (SEM) (Figure 2.2). For pbdc-6a-u, a microcrystalline powder was obtained composed of very small, crystalline nanostructures (Figure 2.2a, Figure 2S.23). Using pbdc-8a-u, a thin, brittle crystalline polyMOF film was produced. Unlike native UiO-66, which manifests as octahedral, truncated octahedral, or cubic morphologies, polyUiO-66 from pbdc-8a-u yielded an interlaced, morphology (Figure 2.2b). To evaluate the polymer features that produce the interlaced polyMOFs, other polymer ligands were studied. Polymer size and dispersity were examined using fractionated pbdc-8a-u polymer ligands and all of these polymer ligands gave the same interlaced morphology (Figures 2.2d-f). Interestingly, the saturated polymer ligands, pbdc-7a and pbdc-8a,[1-2] both produced polyMOF films; however only pbdc-8a yielded the interlaced morphology observed with pbdc-8a-u (Figure 2S.24). To date, only the pbdc-8a and pbdc-8a-u polymer ligands produce this unique morphology, suggesting spacer-length plays an important role in control of the crystallization of these materials.

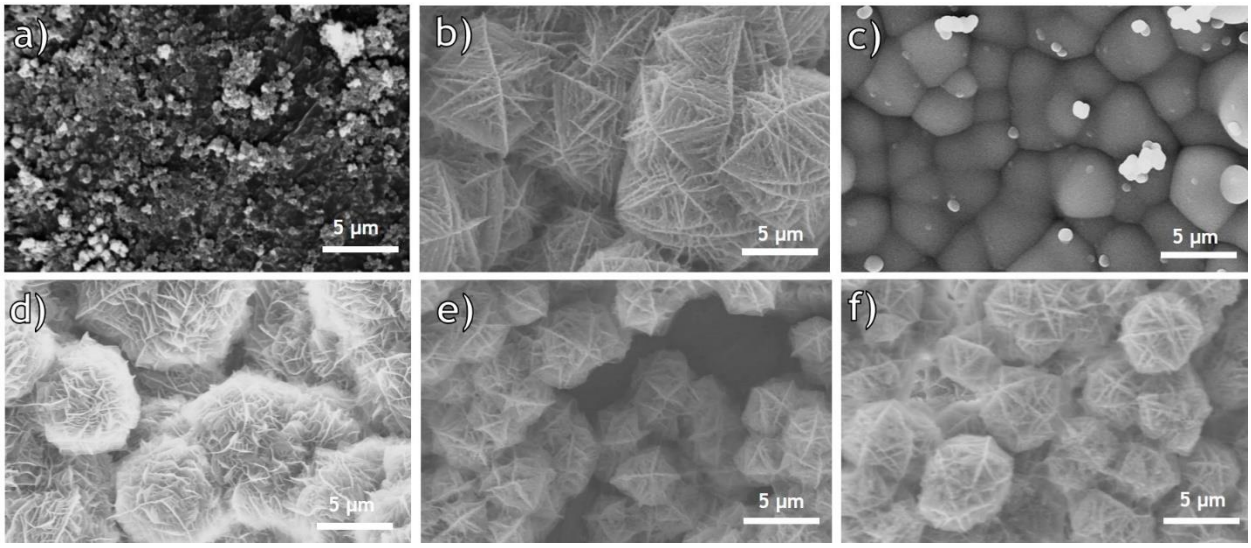

Figure 2.2. SEM images of polyUiO-66 prepared from different polymer ligands: a) pbdc-6a-u; b) pbdc-8a-u; c) pbdc-10a (does not form polyUiO-66, only amorphous material). The interlaced morphology found with pbdc-8a-u was also found using fractionated polymer ligands of different M_n: d) pbdc-8a-u_{2800}; e) pbdc-8a-u_{7800}; and f) pbdc-8a-u_{42000}.

Nitrogen gas adsorption provided insight into the sorption behavior of polyUiO-66 (Figure 2.3). The Brunauer-Emmett-Teller (BET) surface area of polyUiO-66 materials are lower (200-400 m^2/g) than that of the parent UiO-66 (1000-1500 m^2/g), which is attributed pore filling by the methylene spacers in the polymer ligands.[8] polyUiO-66 generated from pbdc-6a-u produces a type-1 isotherm, which is indicative of a typical microporous material (Figure 2.3a). The amorphous material generated from pbdc-10a-u is essentially nonporous (Figure 2.3a). Similarly, the BET surface area of pbdc-8a-u_{2800} polyUiO-66 is lower compared to the other pbdc-8a-u polyMOFs (Figure 2.3b), the latter of which show better crystallinity as gauged by PXRD (see Figure 2.1). More significantly, when using pbdc-8a-u as the polymer ligand, hysteresis in the gas sorption behavior is observed (Figure 2.3), indicative of a hierarchal mesoporous-microporous material. Previous reports by Cai and coworkers demonstrate that hydrophobic acid modulators can be used to introduce lattice defects and the formation of mesopores.[6] A hysteresis loop and mesoporosity is observed for all polyUiO-66 that display the interlaced morphology, regardless of

the polymer size or dispersity of the pbdc-8a-u polymer ligand (Figure 2.3b). It can be suggested that the interlaced morphology produces imperfections at the surface of the film that can act as mesopores during N_2-sorption. A similar result was observed by Yan and coworkers with mesoporous zirconium oxide substrates,[18] and is referred to as an "ink-bottle" effect.[19-20] As expected, polyUiO-66 prepared from the saturated pbdc-8a ligand also produces the same hysteric gas sorption behavior (Figure 2.S26, ESI†). For the polyMOFs from pbdc-6a-u and pbdc-8a-u, pore size analysis showed two populations, centered at 8-11 Å and 25-30 Å (Figures 2S.24-25). These differ from UiO-66, which typically exhibits pores of 8.5-11.5 Å.[9, 16]

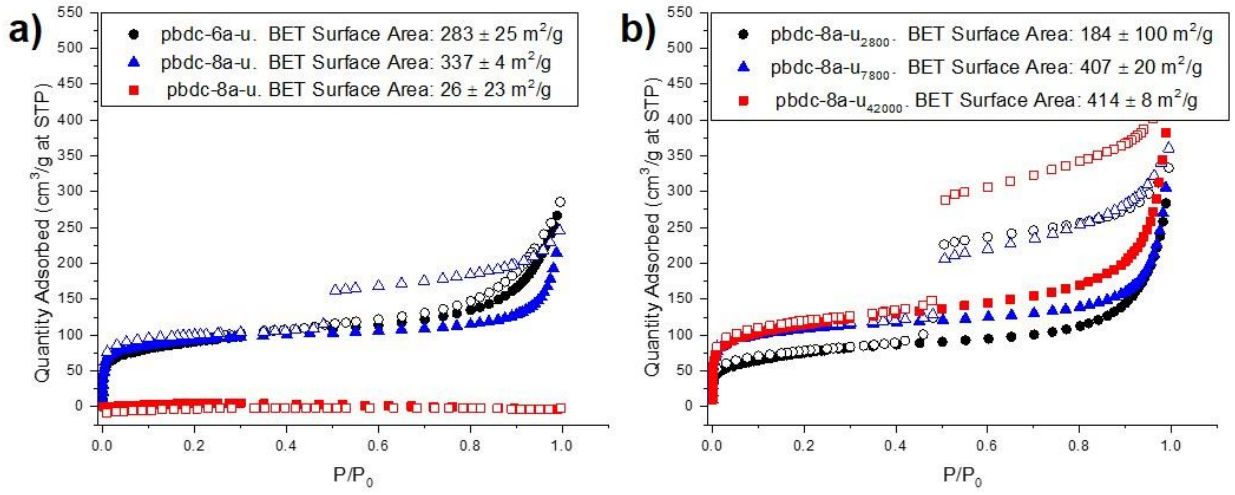

Figure 2.3. N_2 sorption isotherms for polyUiO-66 generated from different polymer ligands. A hysteresis loop was observed for polyMOFs from both: disperse pbdc-8a-u (a), and more uniform, fractionated pbdc-8a-u polymers (b). The hysteric behavior found with all pbdc-8a-u derived samples is indicative of a hierarchal micro- and meso-porous material.

2.4 Conclusions

In summary, polyMOFs of the UiO-66 architecture were prepared for the first time, showing high crystallinity and a unique morphology resulting in hierarchical porosity. Compared to the previously published polymer ligands, using ADMET polymerization provides for better-defined polymers, with higher molecular weight and improved dispersity, which can be further improved by fractionation. These findings show an important new feature of polyMOFs, namely ability of polymer ligands to generate and direct new polyMOF morphologies, resulting in unprecedented MOF materials with hierarchal pore structures and distinctive gas sorption behavior.

2.5 Appendix: Supporting Information

Experimental

General Materials and Methods. Starting materials were purchased and used from commercially available suppliers (Sigma-Aldrich, Acros Organics, Matrix Scientific, and others) without further purification. Chromatography was performed using a CombiFlash R_f 200 automated system from Teledyne Isco. ^{1}H and ^{13}C nuclear magnetic resonance (NMR) spectra were collected using a Varian spectrometer running at 400 MHz.

General Procedure for Synthesis of Monomers. To a 250 mL round bottom flask was added ester-protected 2,5-dihydroxyterephthalate (5.0 g, 7.9 mmol, 1 eq), the appropriate bromoalkene (79 mmol, 4 eq), and potassium carbonate (5.4 g, 39.3 mmol, 5 eq) in 60mL DMF. The suspension was stirred and heated at 80 °C overnight, and monitored by TLC using 20% ethyl acetate (EtOAc) in hexanes. Once completed, potassium carbonate was removed by filtration, and DMF was

removed via evaporation. The tar produced by the reaction was removed by silica gel chromatography eluting 20% ethyl acetate (EtOAc) in hexanes, affording the desired monomers.

Dimethyl 2,5-bis(but-3-en-1-yloxy)terephthalate (bdc-6e): Physical state: solid crystals. Yield: 46% (3.4 g, 8.1 mmol). ^{1}H NMR (400 MHz, DMSO-d_6) δ 7.32 (s, 2H), 6.20 – 5.80 (m, 2H), 5.42 (ddd, *J* = 17.2, 3.5, 1.7 Hz, 2H), 5.23 (q, *J* = 10.6, 1.6 Hz, 2H), 4.68 – 4.54 (m, 4H), 4.27 (q, *J* = 7.1 Hz, 4H), 1.28 (t, *J* = 7.1 Hz, 6H).

Dimethyl 2,5-bis(pent-4-en-1-yloxy)terephthalate (bdc-8e): Physical state: solid crystals. Yield: 58% (5.7 g, 13 mmol). ^{1}H NMR (400 MHz, $CDCl_3$) δ 7.35 (s, 2H), 5.85 (ddt, *J* = 16.9, 10.1, 6.7 Hz, 2H), 5.05 (dd, *J* = 17.1, 1.6 Hz, 2H), 4.99 (d, *J* = 10.2 Hz, 2H), 4.02 (t, *J* = 6.3 Hz, 4H), 3.90 (s, 6H), 2.31 – 2.20 (m, 4H), 1.95 – 1.85 (m, 4H).

Dimethyl 2,5-bis(hex-5-en-1-yloxy)terephthalate (bdc-10e): Physical state: yellow-amber liquid. Yield: 89% (7.7 g, 4.2 mmol). ^{1}H NMR (400 MHz, $CDCl_3$): δ= 7.35 (s, 2H), 5.91 – 5.75 (m, 2H), 5.06 – 4.99 (m, 2H), 4.96 (ddd, *J* = 10.2, 2.0, 1.1 Hz, 2H), 4.01 (t, *J* = 6.4 Hz, 4H), 3.89 (s, 6H), 2.12 (td, *J* = 7.6, 1.1 Hz, 4H), 1.86 – 1.77 (m, 4H), 1.63 – 1.53 (m, 4H).

General Polymerization Procedure for Synthesis of pbdc-*x*e-u. To a 25 mL round bottom flask was added monomer (3.00 mmol, 1.00 eq), and dissolved in 5 mL of DCM. The solution was degassed for 2 min. Grubbs second-generation catalyst was loaded neat (25 mg, 0.030 mmol, 0.01 eq). The reaction was set at mild reflux (45 °C) under mild nitrogen for 5 h. After the solution was cooled to room temperature, ethyl vinyl ether (2 mL) was added to quench the catalyst, and the solution was stirred for 30 min. The polymer was precipitated in methanol, followed by centrifugation at 7000 rpm for 10 min. at room temperature. The supernatant was decanted and the polymer was dissolved in DCM and precipitated four more times in methanol. After the final wash, the polymer was transferred to a vial, and dried under vacuum for 2 h.

For narrow dispersity polymers: The procedure was followed as before, but the catalyst loading was varied to 0.003 mmol to obtain small oligomers. The polymer was precipitated in methanol, followed by centrifugation at 7000 rpm for 10 min at room temperature. The supernatant was decanted and the polymer was dissolved in DCM and precipitated one more time in methanol. The polymer was purified using silica gel chromatography at gradient from 0% to 3% methanol in dichloromethane, affording the desired polymers.

Poly-dimethyl 2,5-bis(but-3-en-1-yloxy)terephthalate (pbdc-6e-u): Yield: 74% (740 mg, 2.2 mmol) ^{1}H NMR (400 MHz, $CDCl_3$) δ 7.36 (s, 1H), 6.06 – 5.79 (m, 1H), 5.75 – 5.59 (m, 1H), 5.16 (d, J = 17.1 Hz, 1H), 5.10 (d, J = 10.4 Hz, 1H), 4.03 (t, J = 6.7 Hz, 3H), 3.88 (s, 4H), 2.66 – 2.47 (m, 2H). M_n: 20,500 g/mol, M_w/M_n: 2.1, DP: 67 repeat units.

Poly-dimethyl 2,5-bis(pent-4-en-1-yloxy)terephthalate (pbdc-8e-u): Yield: 75% (820 mg, 2.3 mmol). ^{1}H NMR (400 MHz, $CDCl_3$) δ= 7.34 (s, 1H), 5.72 – 5.34 (m, 1H), 4.00 (t, J = 6.0 Hz, 2H), 3.89 (s, 2H), 2.32 – 2.10 (m, 2H), 1.86 (dd, J = 22.9, 16.1 Hz, 2H). M_n: 19,600 g/mol, M_w/M_n: 2.9, DP: 58 repeat units.

Poly-dimethyl 2,5-bis(hex-5-en-1-yloxy)terephthalate (pbdc-10e-u): Yield: 40% (470 mg, 0.48 mmol). ^{1}H NMR (400 MHz, $CDCl_3$): δ= 7.35 (s, 1H), 5.43 (m, J = 14.0 Hz, 1H), 4.00 (t, J = 5.9 Hz, 2H), 3.89 (s, 3H), 2.05 (bs, 2H), 1.90 – 1.71 (m, 2H), 1.62 – 1.47 (m, 2H). M_n: 10,800, M_w/M_n: 3.1, DP: 30 repeat units.

General Polymer Hydrolysis Procedure for pbdc-*x*a-u synthesis. The polymer ester (300mg-800 mg) was added to a 250 mL round-bottom flask, along with sodium hydroxide (15 equivalents), and placed in 60 mL a 1:1 of n,n-dimethylformamide (DMF): water solution. The mixture was heated at 90 °C for 24 h, or until the solution became clear. The solvent was reduced by evaporation. The solution was acidified to a pH value of ~1 using a 2M HCl solution. The

resultant solid was collected by vacuum filtration. The solid was washed with copious amounts of 2M HCl solution, and water to remove any salts.

Poly-2,5-bis(but-3-en-1-yloxy)terephthalic acid (pbdc-6a-u): Yield: 97% (630 mg, 2.0 mmol), ^{1}H NMR (400 MHz, DMSO-d_6) δ 7.22 (s, 1H), 5.97 – 5.71 (m, 1H), 5.72 – 5.40 (m, 1H), 5.13 (d, *J* = 17.4 Hz, 1H), 5.04 (d, *J* = 10.1 Hz, 1H), 3.97 (s, 2H), 2.38 (s, 2H).

Poly-2,5-bis(pent-4-en-1-yloxy)terephthalic acid (pbdc-8a-u): Yield: 94% (670 mg, 2.0 mmol) ^{1}H NMR (400 MHz, DMSO-d_6) δ 7.25 (s, 1H), 5.47 (m, 1H), 3.96 (t, *J* = 5.8 Hz, 2H), 2.12 (m, 2H), 1.86 – 1.60 (m, 2H).

Poly-2,5-bis(hex-5-en-1-yloxy)terephthalic acid (pbdc-10a-u): Yield: 97% (360 mg, 0.99 mmol) ^{1}H NMR (400 MHz, DMSO-d_6) δ 7.23 (s, 1H), 5.79 (m, 1H), 5.61 – 5.21 (m, 1H), 5.01 (d, *J* = 18.4 Hz, 1H), 4.94 (d, *J* = 9.9 Hz, 1H), 3.95 (t, *J* = 5.7 Hz, 2H), 2.05 (m, 2H), 1.65 (m, 2H), 1.53 – 1.36 (m, 2H).

General procedure for Zr-polyMOF synthesis. Procedure was adapted and modified from a previously published report.[5] Briefly, polymer-ligand (0.03 mmol) and zirconium (IV) chloride ($ZrCl_4$) (0.037 mmol) were dissolved in 20 mL scintillation vials using 2 mL of *N*,*N*-diethylformamide (DEF). After dissolving, 2 mL of formic acid was added to the vial. The reaction was set in a pre-heated oven at 135 °C for 2 d. A powder or brittle film was obtained at the bottom of the vial. The resultant materials were washed by exchanging the solvent with copious amounts of DMF.

Analytical Characterization

Gel-permeation chromatography (GPC) conditions for pbdc-*x*e-u. Gel-permeation chromatography was performed in DMF (0.7 mL/min) using a Malvern GPC equipped with D4000 single-pore column and D-6000M general-purpose mixed-bed weight divinylbenzene column connected in series to determine molecular weights and molecular weight distributions, M_w/M_n, of our polymers. The solutions were filtered through 0.4 μm PTFE membrane before being injected into either GPC instrument. Narrow poly (methyl methacrylate) (PMMA) was used as the calibration standard.

PXRD Analysis. The synthesized polyMOFs were collected by filtration, washed with copious amounts of methanol to remove DEF, and dried for ~20 min before data collection. PXRD data were collected at ambient temperature on a Bruker D8 Advance diffractometer at 40 kV and 40 mA for Cu Kα (λ = 1.5418 Å), with a scan speed of 1 s/step, a step size of 0.02° in 2θ, and a 2θ range of 5−50°.

^{1}H NMR Digestions. Samples were filtered and washed with copious amounts of DMF, methanol, and acetone to remove any impurities. About 10 mg of material was dissolved in 600 μL DMSO-d_6 using 10 μL of 50% HF in water to digest the polyMOF.

Scanning Electron Microscopy (SEM). polyUiO-66 samples were transferred to conductive carbon tape on a sample holder, and coated using a Ir-sputter coating for 7 sec. A Philips XL ESEM instrument was used for acquiring images using a 10 kV energy source under vacuum at a working distance at 10 mm.

N_2-Sorption Measurements. Prior to analysis, the materials were washed by exchanging the solvent with DMF three times for one day, then with methanol twice a day for 2 d. About 40-50 mg of the samples were transferred to pre-weighed sample tubes, and the samples were evacuated

in a vacuum line for 2 h. The crystals were activated using an ASAP 2020 Adsorption analyzer under vacuum at 105 °C for 10 h. After degassing, the sample tube was reweighed to obtain an accurate mass measurement for the degassed sample. All measurements were obtained at 77K using a liquid nitrogen bath.

TGA/DSC Measurements. Between 5−10 mg of dried material weighed for thermogravimetric analysis (TGA) measurements. Samples were analyzed under a stream of dried N_2 gas at a flow rate of 80 mL/min using a Mettler Toledo TGA/DSC 1 STAR System running from 35 to 800 °C with a ramping rate of 10 °C/min.

Supplemental Figures

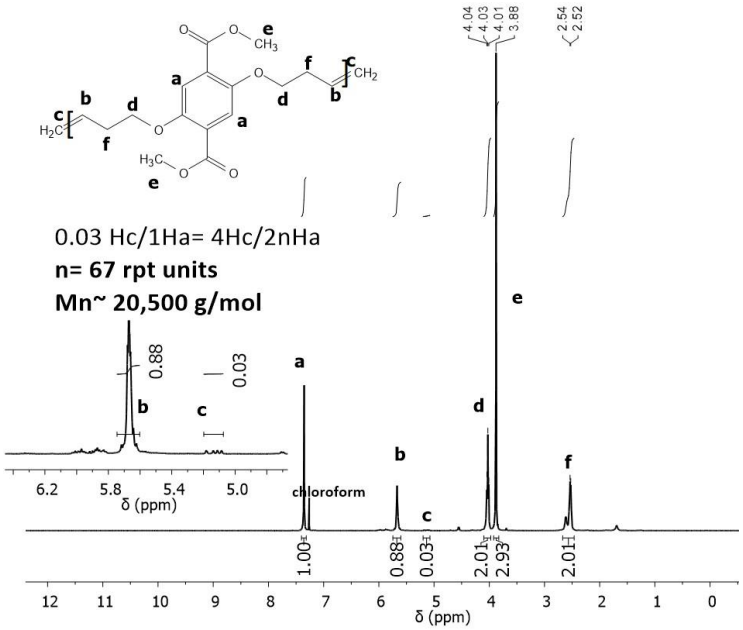

Figure 2S.1. ^{1}H NMR of pbdc-6e-u. End-group analysis was used to determine number of repeat units and M_n.

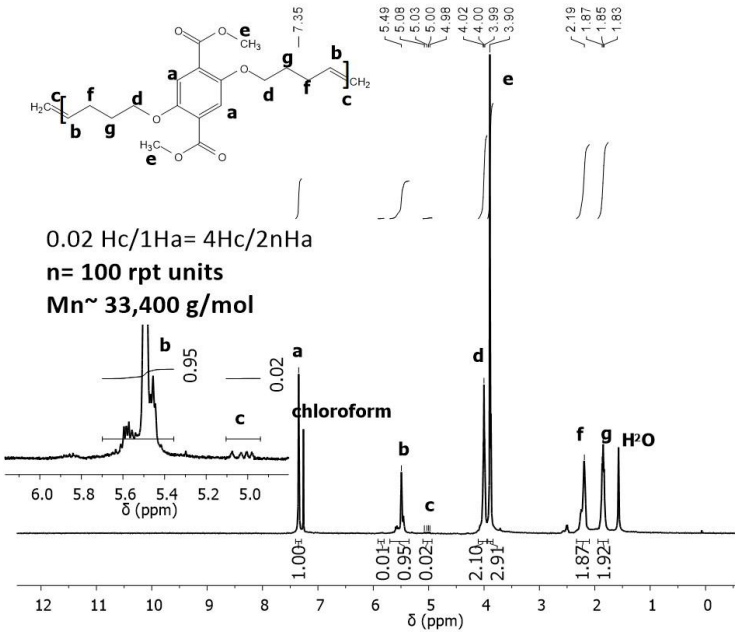

Figure 2S.2. ^{1}H NMR of pbdc-8e-u. End-group analysis was used to determine number of repeat units and M_n.

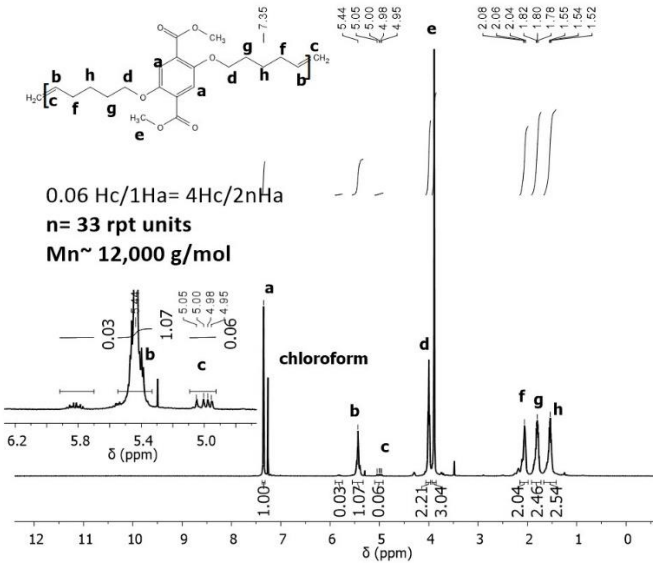

Figure 2S.3. ^{1}H NMR of pbdc-10e-u. End-group analysis was used to determine number of repeat units and M_n.

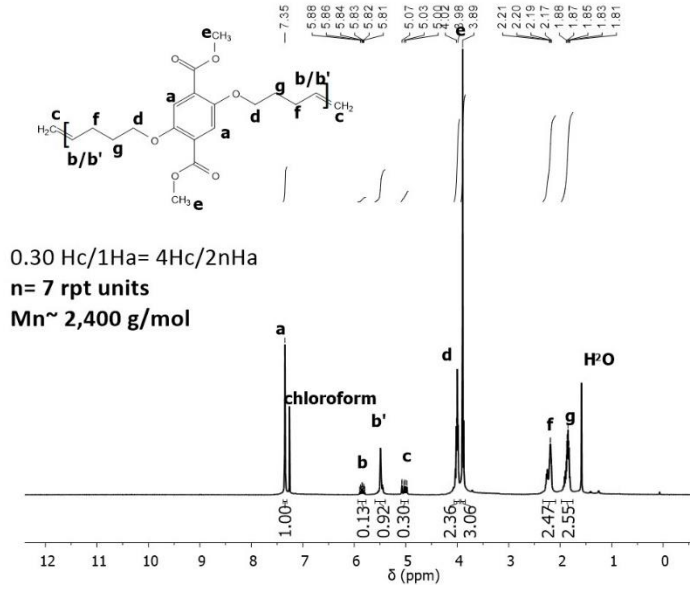

Figure 2S.4. ^{1}H NMR of pbdc-8e-u$_{2700}$. End-group analysis was used to determine number of repeat units and M_n.

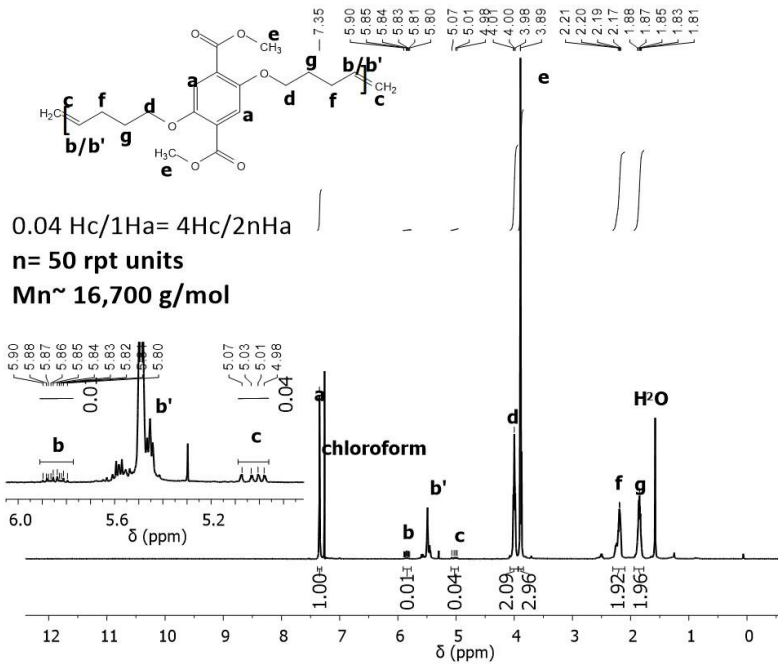

Figure 2S.5. ^{1}H NMR of pbdc-8e-u$_{7800}$. End-group analysis was used to determine number of repeat units and M_n after column chromatography.

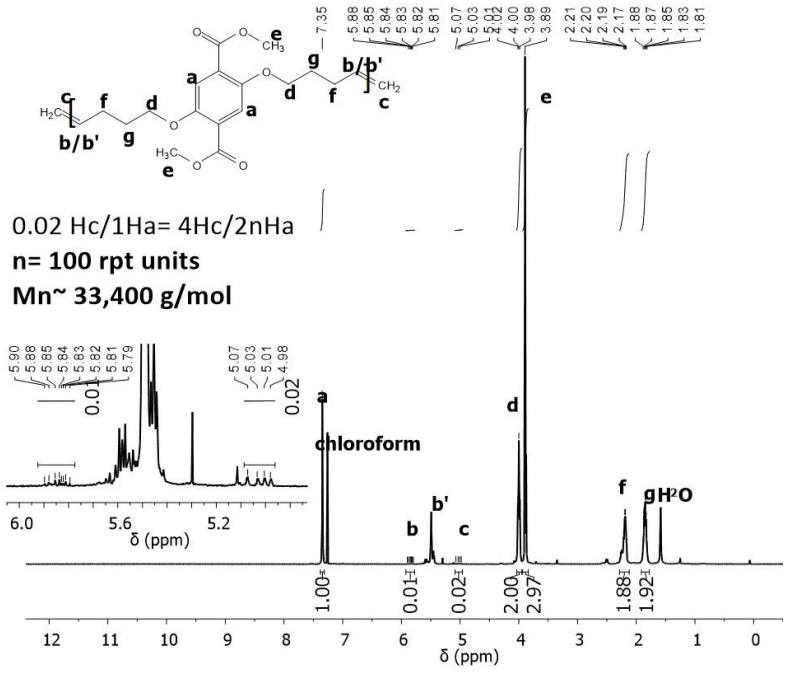

Figure 2S.6. ^{1}H NMR of pbdc-8e-u$_{42000}$. End-group analysis was used to determine number of repeat units and M_n after column chromatography.

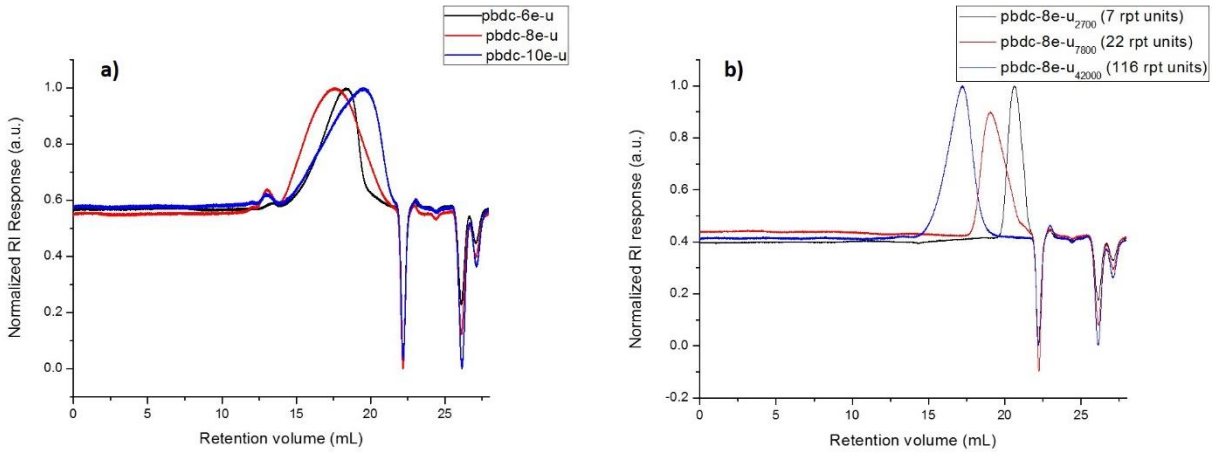

Figure 2S.7. GPC traces obtained for **a)** broad molecular weight pbdc-*x*e-u ligands and **b)** narrow molecular weight pbdc-8e-u ligands. Negative refraction are solvent markers.

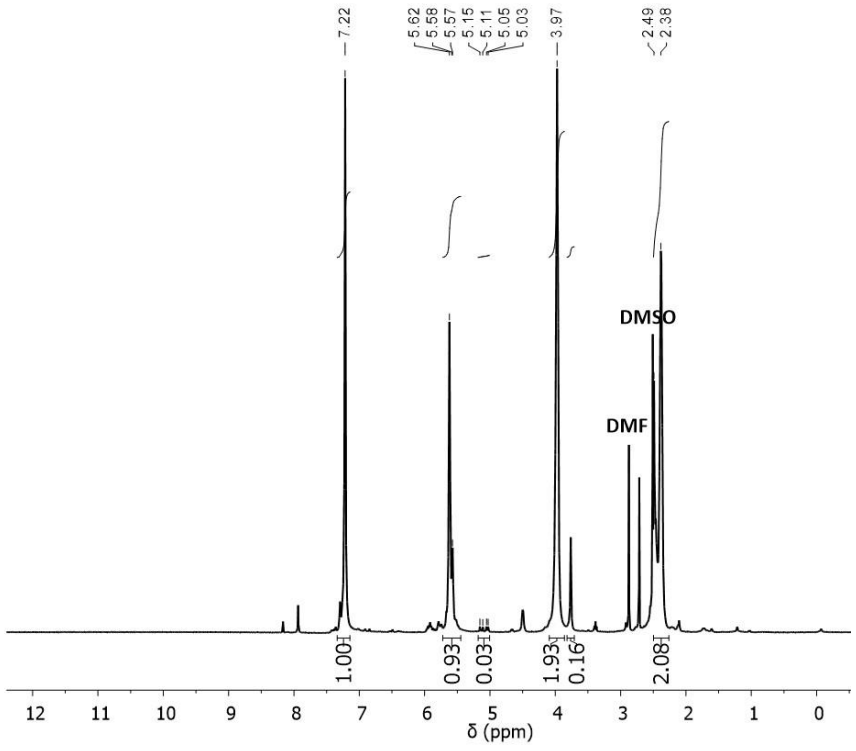

Figure 2S.8. ^{1}H NMR of pbdc-6a-u.

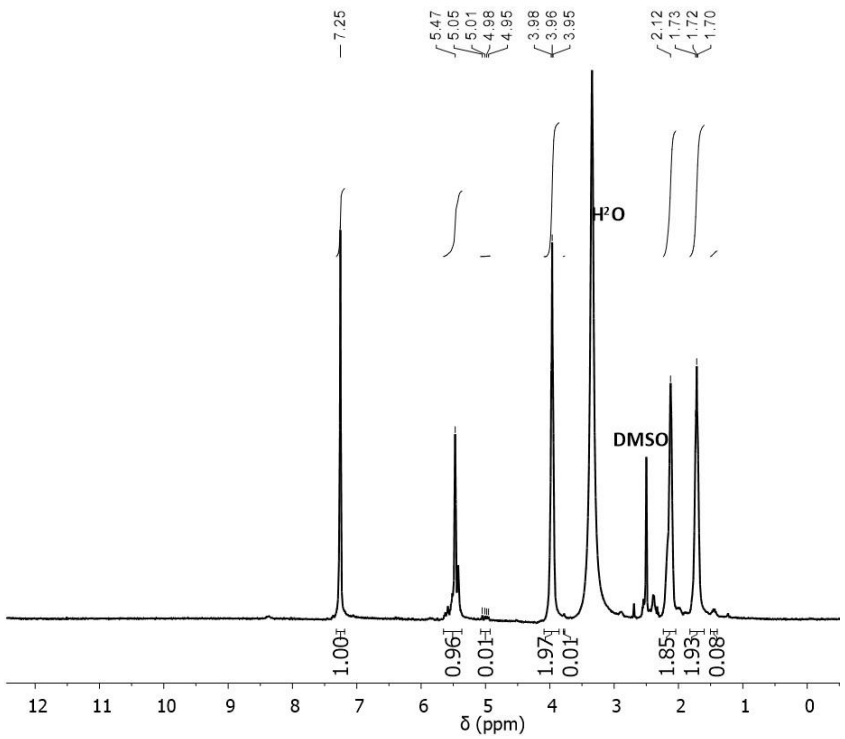

Figure 2S.9. [1]H NMR of pbdc-8a-u.

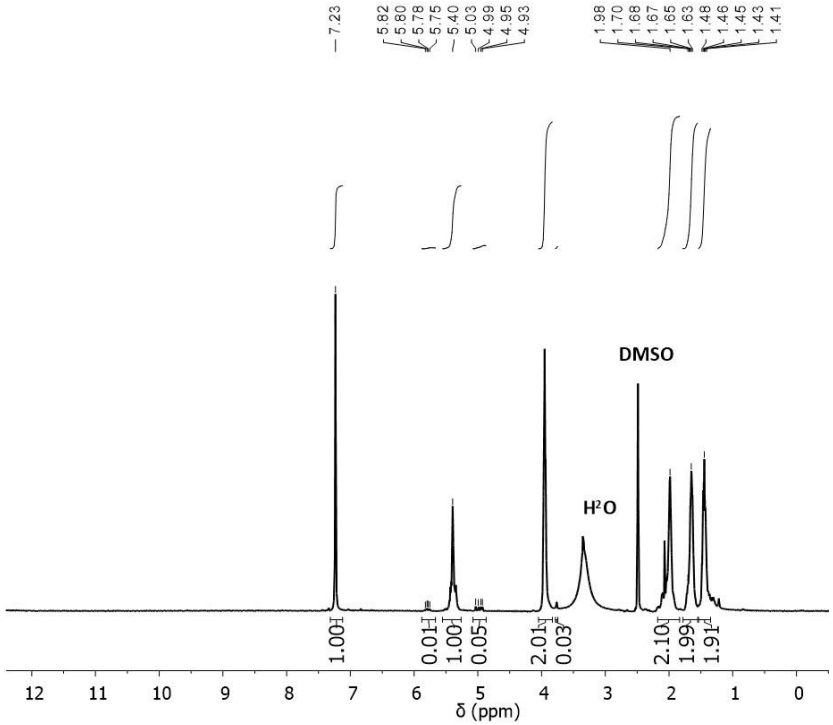

Figure 2S.10. [1]H NMR of pbdc-10a-u.

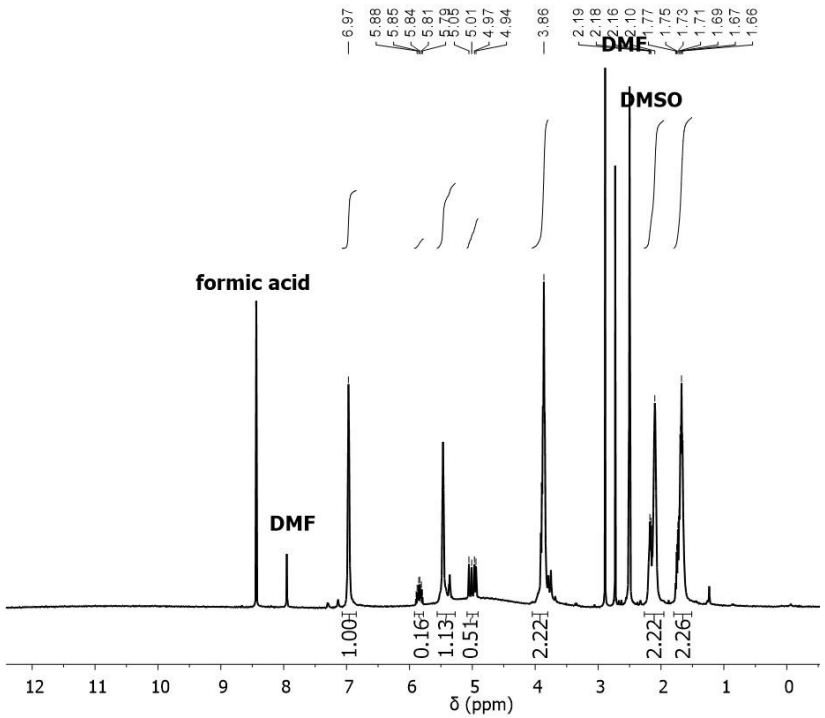

Figure 2S.11. ^{1}H NMR of pbdc-8a-u$_{2800}$.

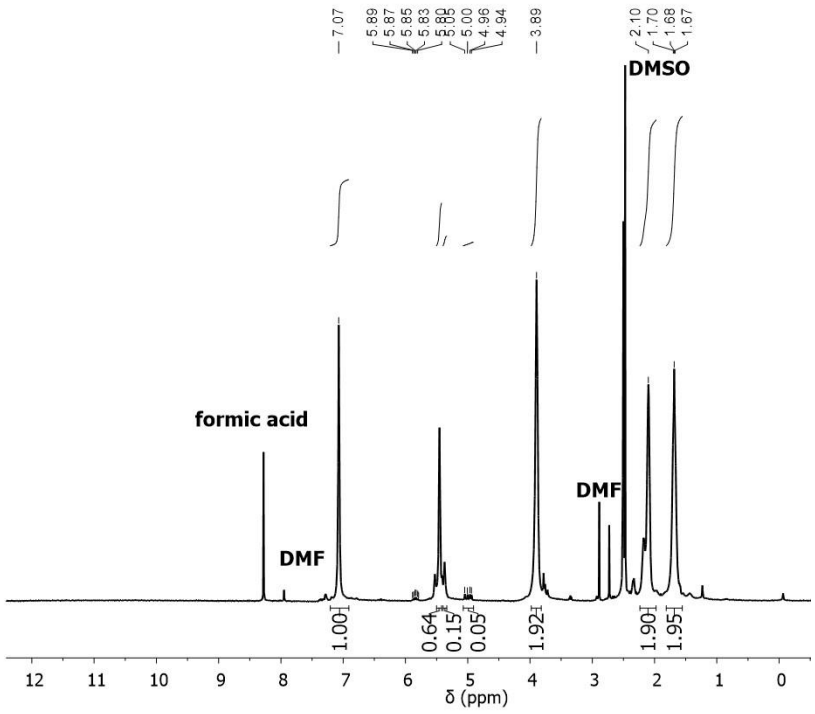

Figure 2S.12. ^{1}H NMR of pbdc-8a-u$_{7800}$.

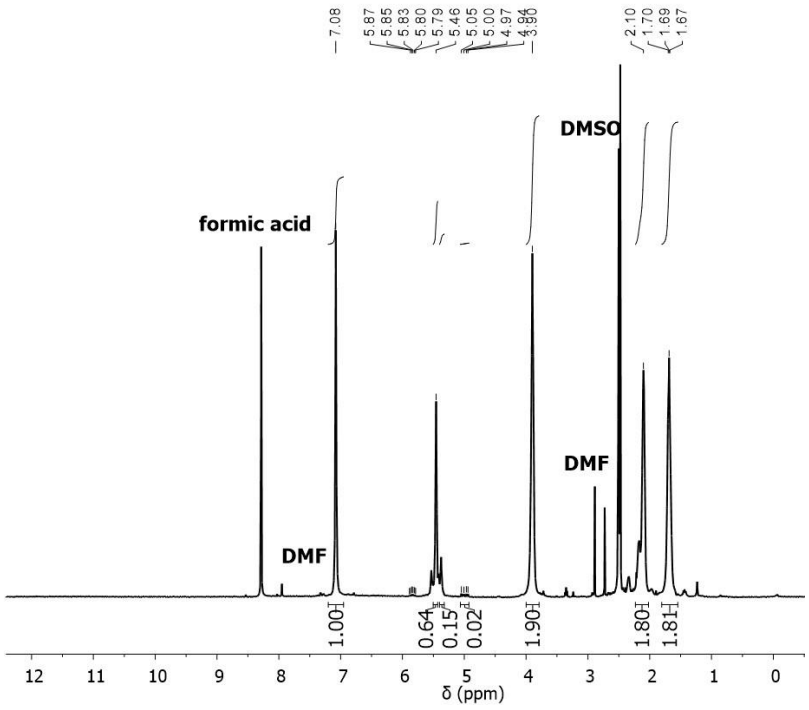

Figure 2S.13. ^{1}H NMR of pbdc-8a-u$_{42000}$.

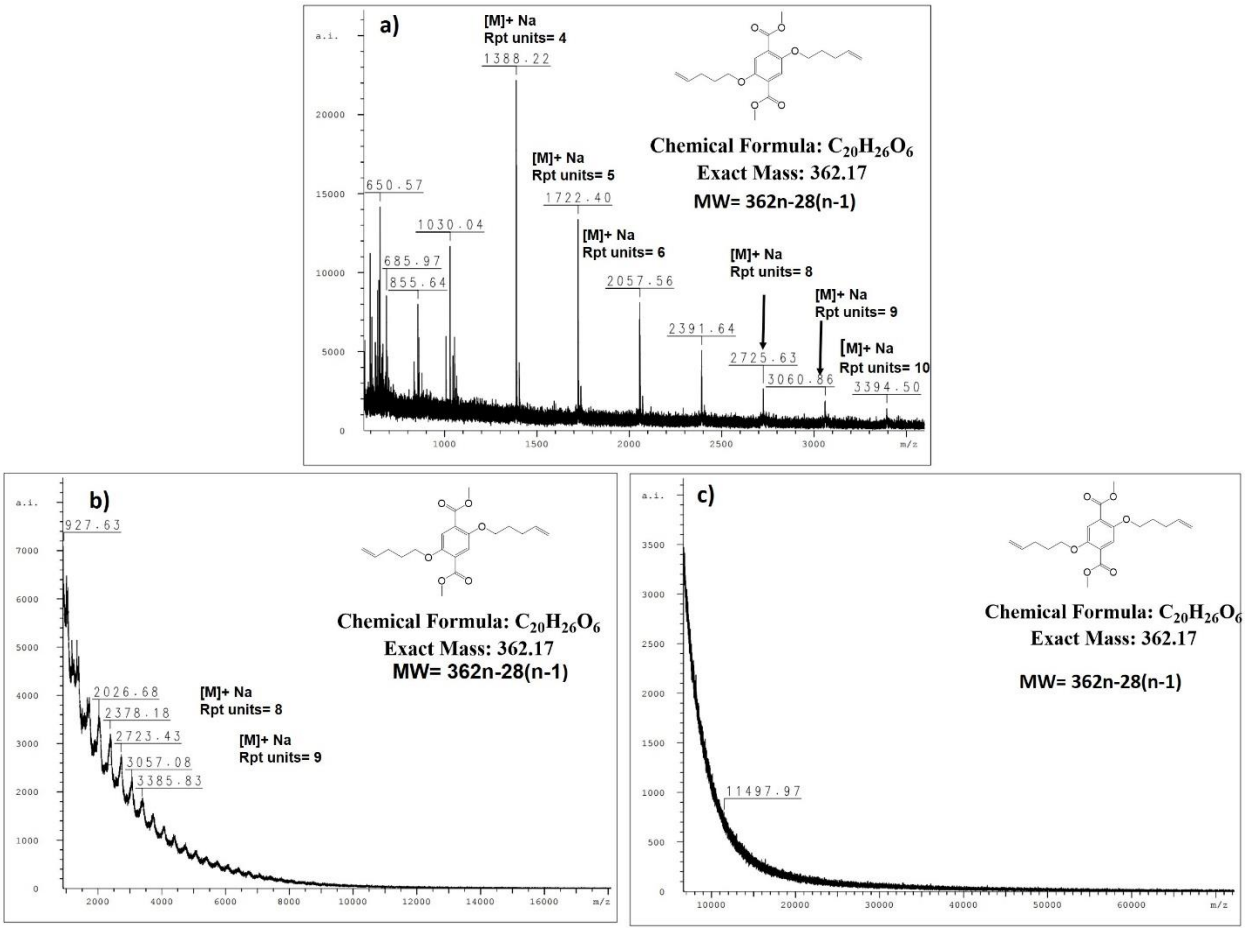

Figure 2S.14. MALDI-TOF MS of **a)** pbdc-8e-u$_{2800}$, **b)** pbdc-8e-u$_{7800}$, and **c)** pbdc-8e-u$_{42000}$. No signal was obtained for the largest polymer.

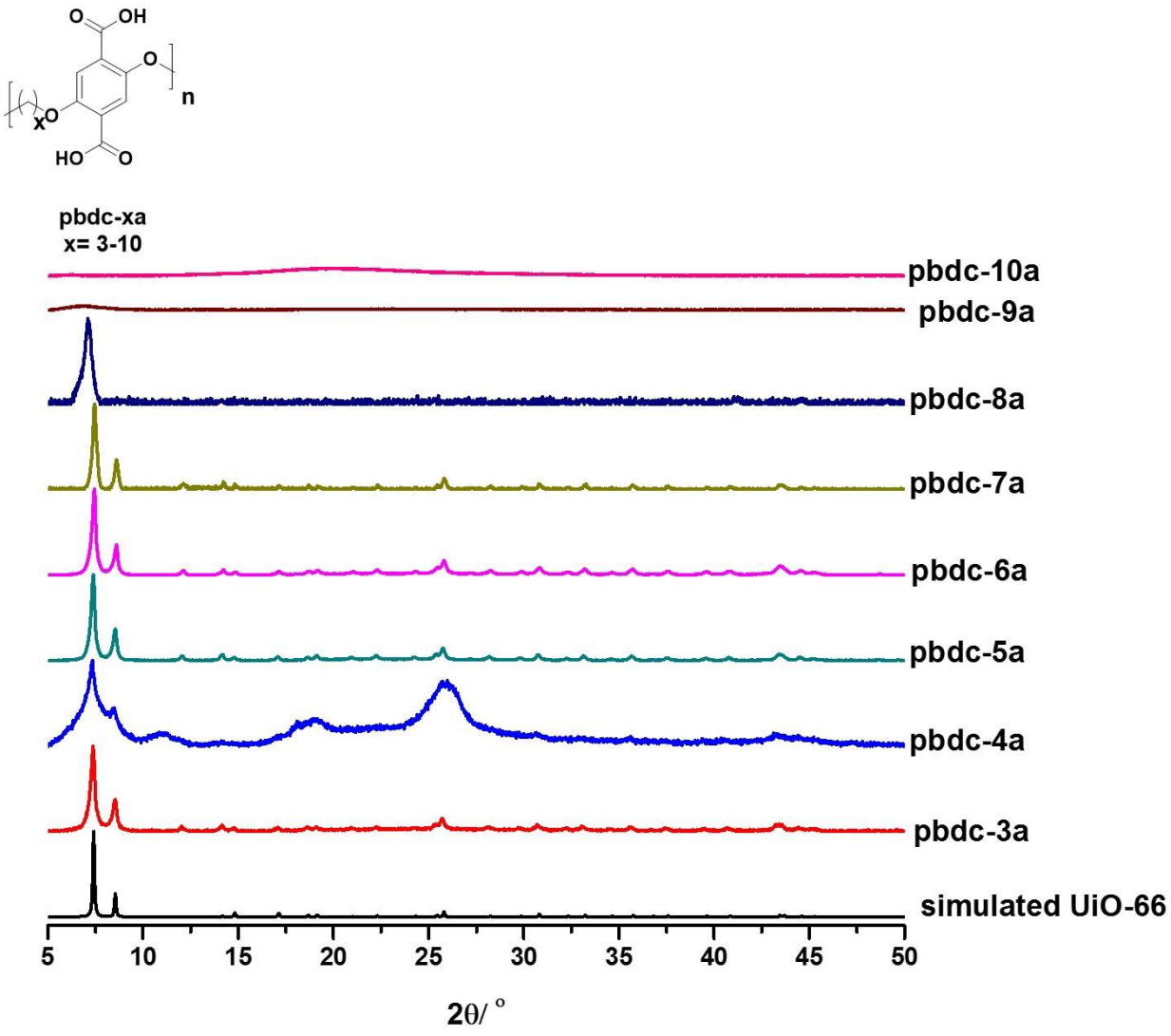

Figure 2S.15. PXRD data was obtained for polyUiO-66 prepared from pbdc-*x*a ligands.[1-2]

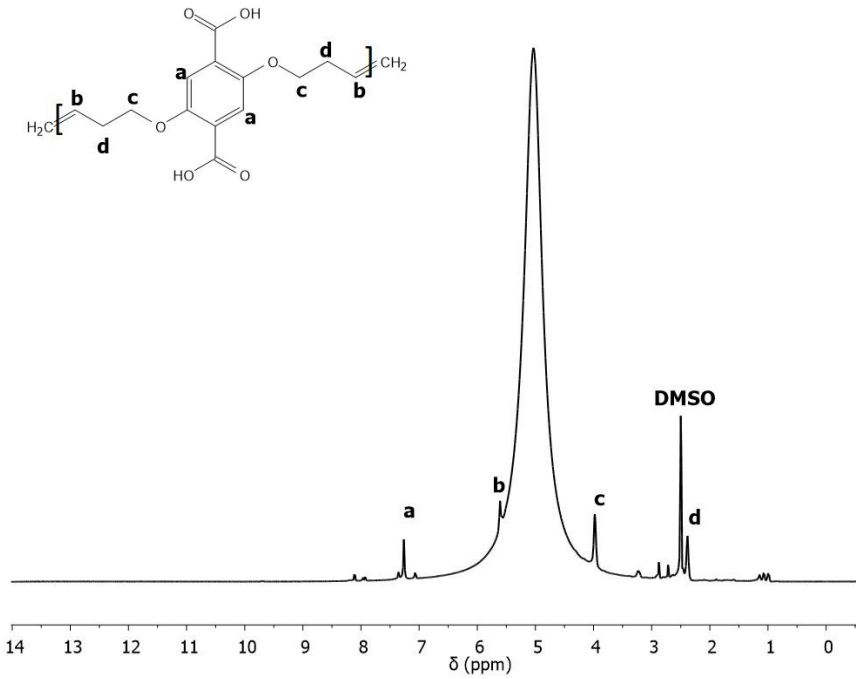

Figure 2S.16. ^{1}H NMR of digested polyUiO-66 prepared from broad pbdc-6a-u.

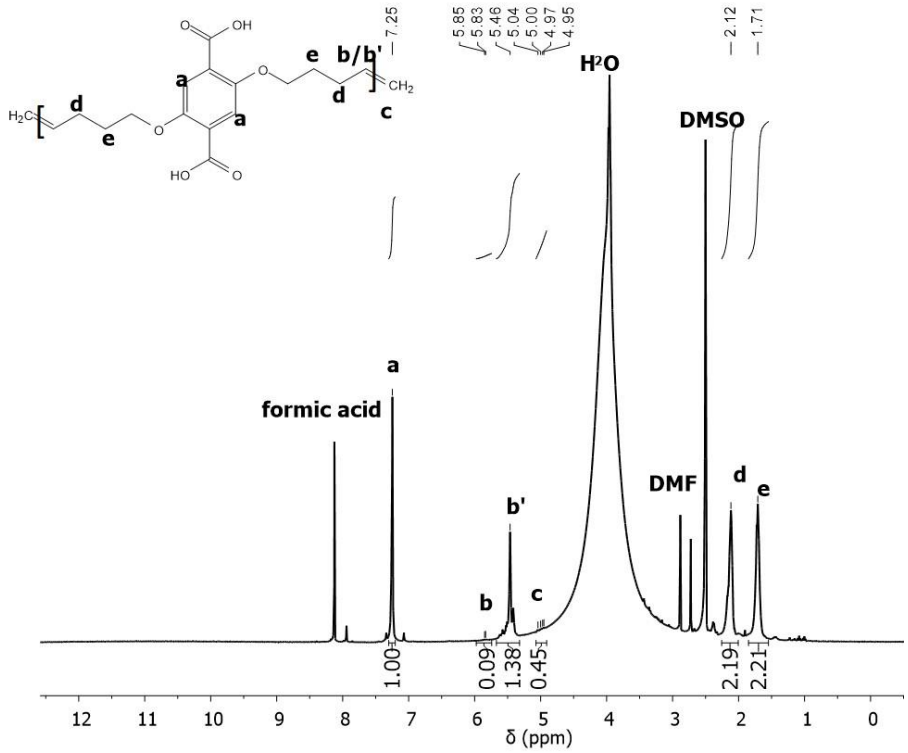

Figure 2S.17. ^{1}H NMR of digested polyUiO-66 prepared from broad pbdc-8a-u.

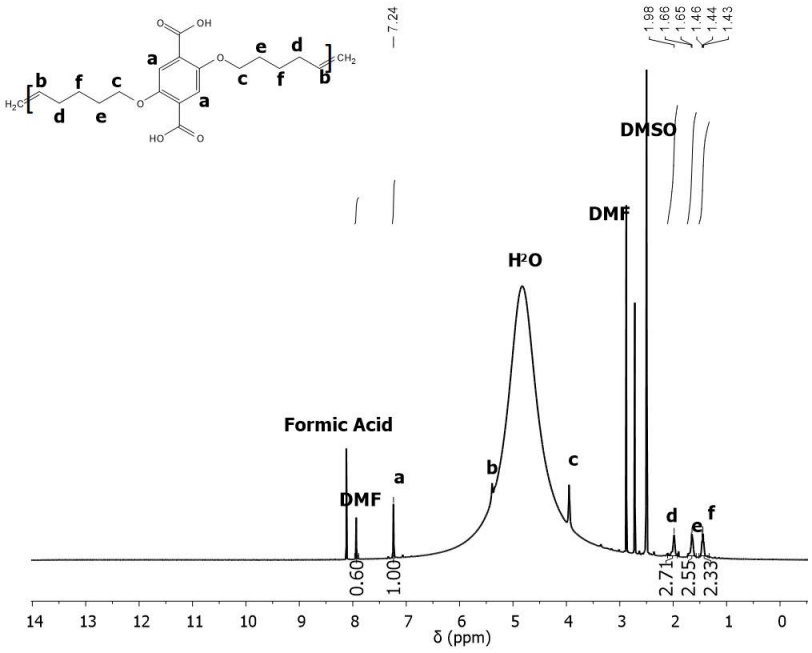

Figure 2S.18. [1]H NMR of digested polyUiO-66 prepared from broad pbdc-10a-u.

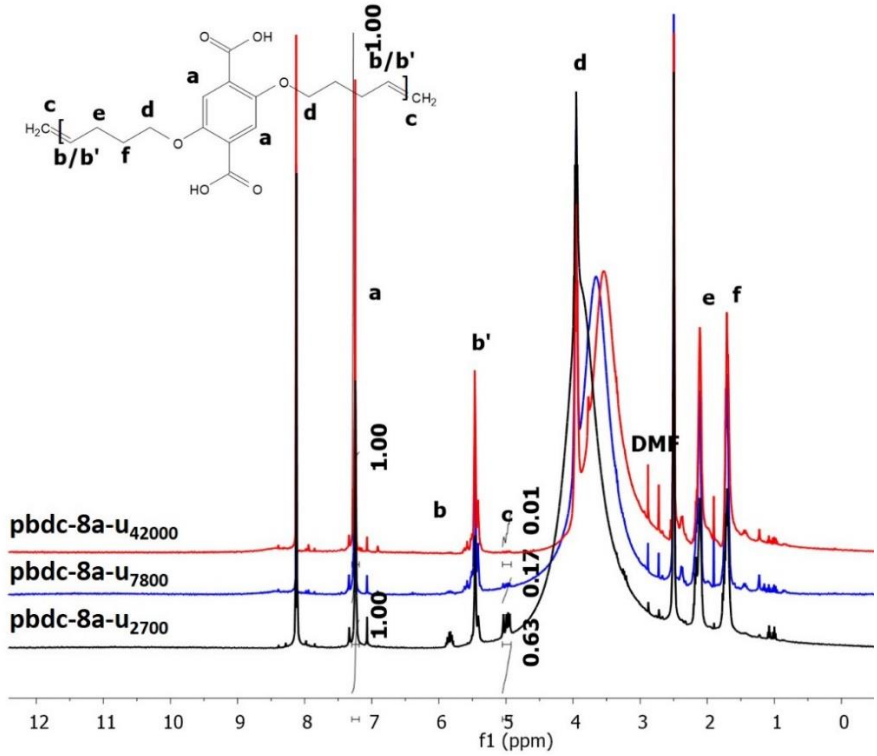

Figure 2S.19. [1]H NMR of digested UiO-66 polyMOF prepared from narrow molecular weight pbdc-8a-u.

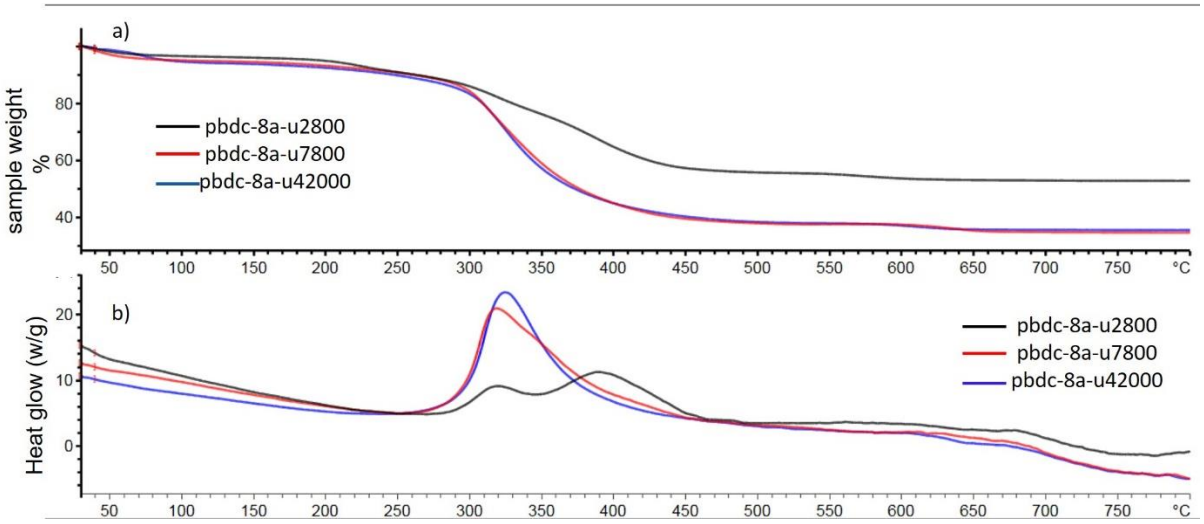

Figure 2S.20. (a) TGA and (b) (DSC) traces of polyUiO-66 prepared from narrow pbdc-8a-u.

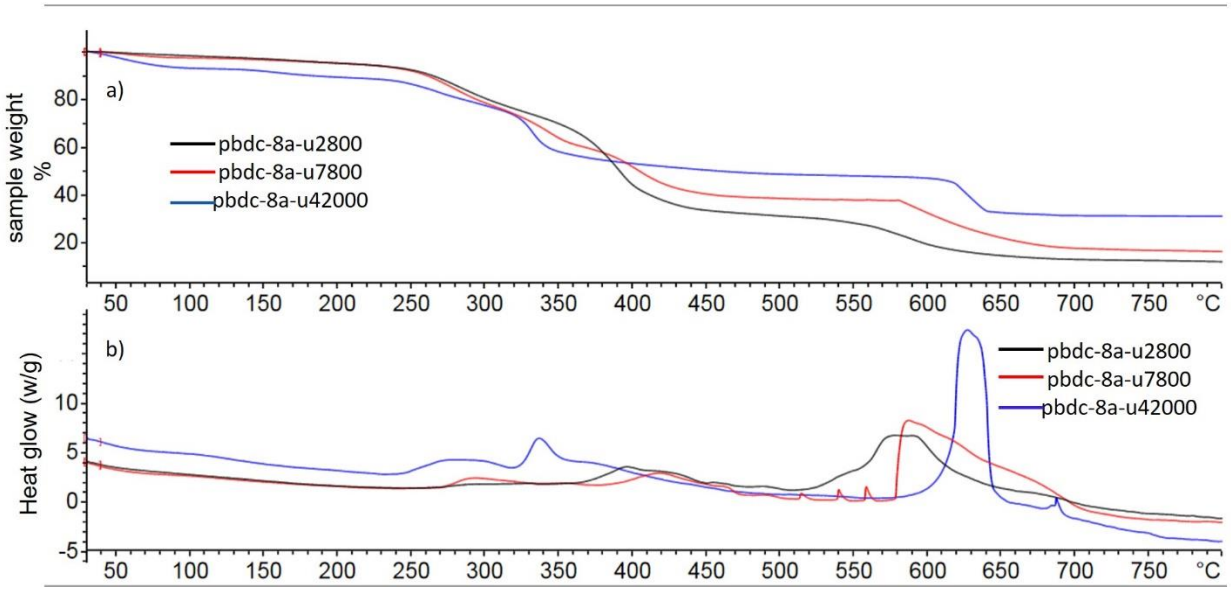

Figure 2S.21. (a) TGA and (b) (DSC) traces of narrow molecular weight pbdc-8a-u ligands.

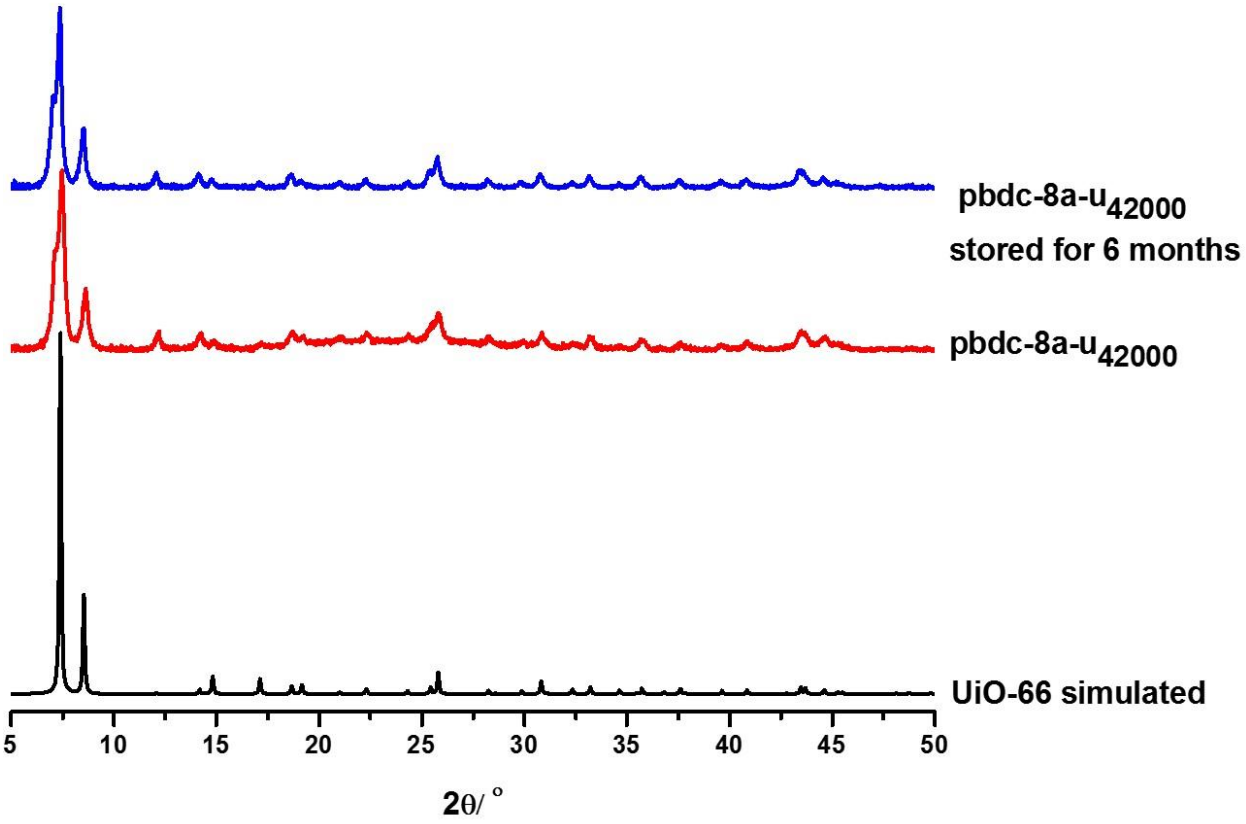

Figure 2S.22. PXRD data of pbdc-8a-u$_{42000}$ after being stored for six months in air under ambient conditions.

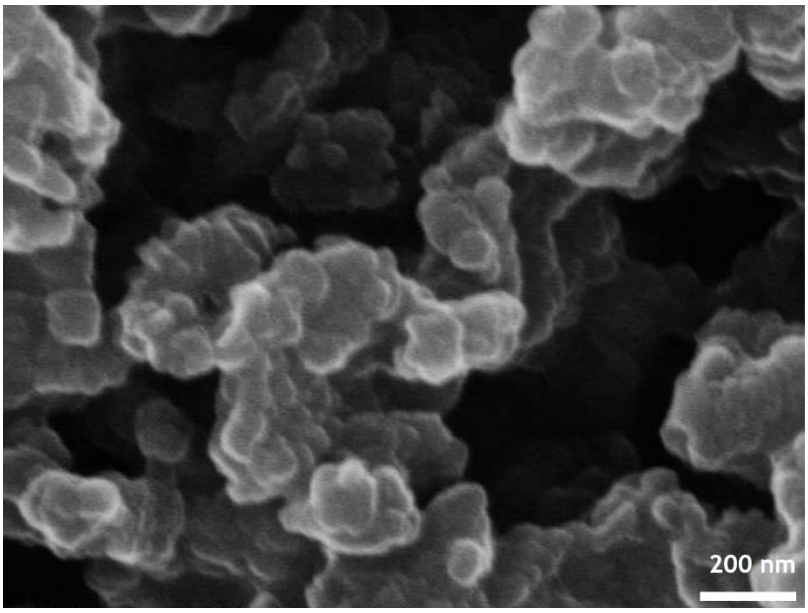

Figure 2S.23. SEM image of polyUiO-66 prepared from pbdc-6a-u.

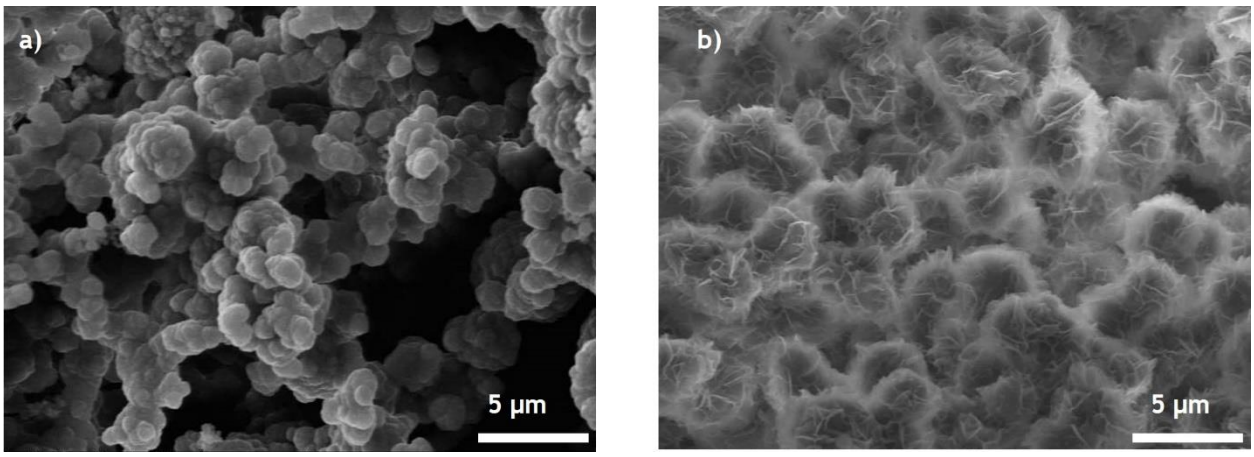

Figure 2S.24. SEM Images for polyUiO-66 prepared from **a)** pbdc-7a; **b)** pbdc-8a.

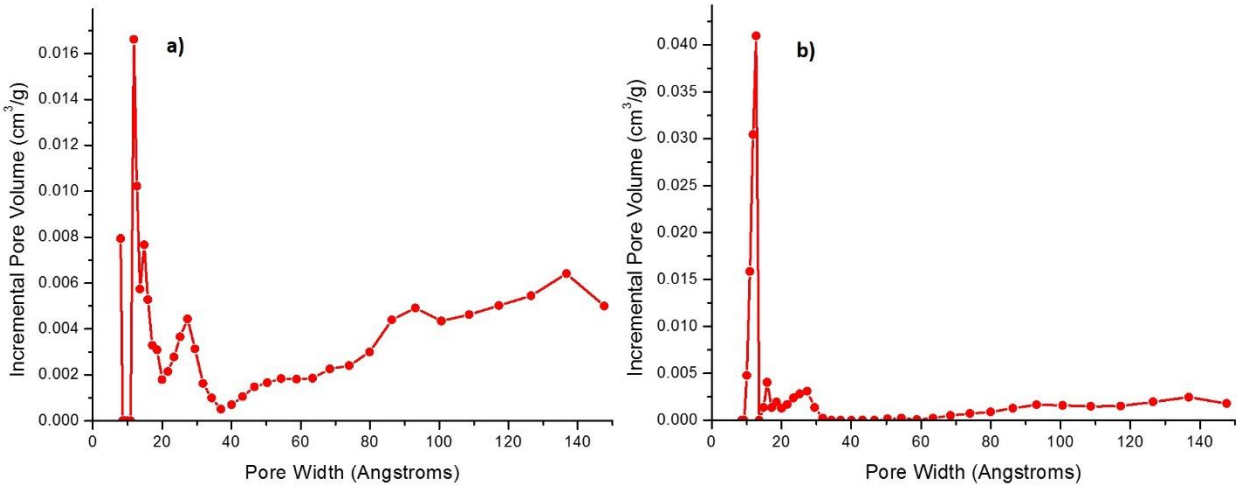

Figure 2S.25. Pore-size distribution of polyUiO-66 prepared from **a)** pbdc-6a-u and **b)** pbdc-8a-u.

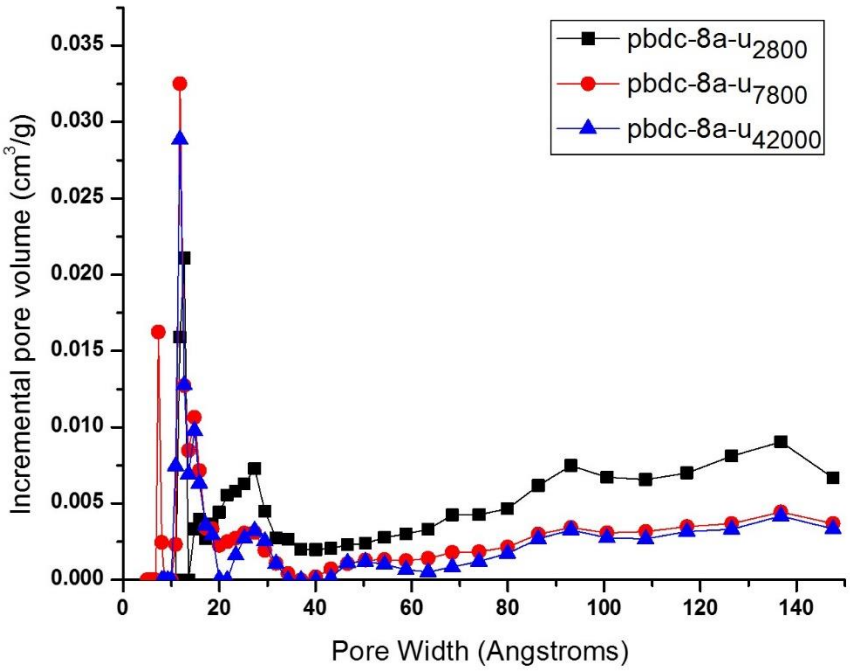

Figure 2S.26. Pore-size distribution of polyUiO-66 prepared from narrow molecular weight pbdc-8a-u ligands.

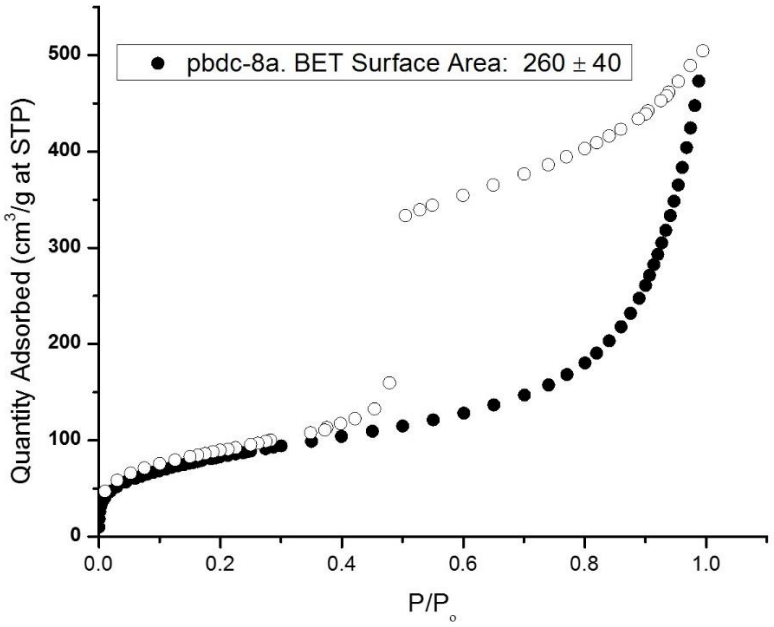

Figure 2S.27. N_2-Isotherm of polyUiO-66 prepared from pbdc-8a.

2.6 Acknowledgements

Chapter 2, in part, is a reprint of the material, "Hierarchical structure and porosity in UiO-66 polyMOFs" *Chem. Commun.* **2017**, *53*, 3058-3061. The dissertation author was the primary author of this manuscripts and gratefully acknowledges the contributions of coauthors Zhenjie Zhang and Seth M. Cohen.

2.7 References

1. Zhang, Z.; Nguyen, H. T. H.; Miller, S. A.; Cohen, S. M., polyMOFs: A Class of Interconvertible Polymer-Metal-Organic-Framework Hybrid Materials. *Angew. Chem. Int. Ed.* **2015,** *54*, 6152-6157.

2. Zhang, Z. J.; Nguyen, H. T. H.; Miller, S. A.; Ploskonka, A. M.; DeCoste, J. B.; Cohen, S. M., Polymer-Metal-Organic Frameworks (polyMOFs) as Water Tolerant Materials for Selective Carbon Dioxide Separations. *J. Am. Chem. Soc.* **2016,** *138*, 920-925.

3. Cavka, J. H.; Jakobsen, S.; Olsbye, U.; Guillou, N.; Lamberti, C.; Bordiga, S.; Lillerud, K. P., A new zirconium inorganic building brick forming metal organic frameworks with exceptional stability. *J. Am. Chem. Soc.* **2008,** *130*, 13850-13851.

4. Mathieu Bosch, S. Y., and Hong-Cai Zhou, Group 4 Metals as Secondary Building Units: Ti, Zr, and Hf-Based MOFs. In *The Chemistry of Metal-Organic Frameworks: Synthesis, Characterization and Applications*, 1 ed.; Kaskel, S., Ed. Wiley-VCH Verlag & Co. KGaA: 2016; pp 144-159.

5. Trickett, C. A.; Gagnon, K. J.; Lee, S.; Gandara, F.; Burgi, H. B.; Yaghi, O. M., Definitive Molecular Level Characterization of Defects in UiO-66 Crystals. *Angew. Chem. Int. Ed.* **2015,** *54*, 11162-11167.

6. Cai, G.; Jiang, H.-L., A Modulator-Induced Defect-Formation Strategy to Hierarchically Porous Metal–Organic Frameworks with High Stability. *Angew. Chem. Int. Ed.* **2016,** *129*, 578-582.

7. Hu, Z. G.; Faucher, S.; Zhuo, Y. Y.; Sun, Y.; Wang, S. N.; Zhao, D., Combination of Optimization and Metalated-Ligand Exchange: An Effective Approach to Functionalize UiO-66(Zr) MOFs for CO2 Separation. *Chem. Eur. J.* **2015,** *21*, 17245-17255.

8. Wu, H.; Chua, Y. S.; Krungleviciute, V.; Tyagi, M.; Chen, P.; Yildirim, T.; Zhou, W., Unusual and Highly Tunable Missing-Linker Defects in Zirconium Metal-Organic Framework

UiO-66 and Their Important Effects on Gas Adsorption. *J. Am. Chem. Soc.* **2013,** *135*, 10525-10532.

9. Han, Y. T.; Liu, M.; Li, K. Y.; Zuo, Y.; Wei, Y. X.; Xu, S. T.; Zhang, G. L.; Song, C. S.; Zhang, Z. C.; Guo, X. W., Facile synthesis of morphology and size-controlled zirconium metal-organic framework UiO-66: the role of hydrofluoric acid in crystallization. *CrystEngComm* **2015,** *17*, 6434-6440.

10. Zhu, X. Y.; Gu, J. L.; Wang, Y.; Li, B.; Li, Y. S.; Zhao, W. R.; Shi, J. L., Inherent anchorages in UiO-66 nanoparticles for efficient capture of alendronate and its mediated release. *Chem. Commun.* **2014,** *50*, 8779-8782.

11. Li, H.; Caire da Silva, L.; Schulz, M. D.; Rojas, G.; Wagener, K. B., A review of how to do an acyclic diene metathesis reaction. *Polym. Int.* **2016,** *66*, 7-12.

12. Bueken, B.; Vermoortele, F.; Cliffe, M. J.; Wharmby, M. T.; Foucher, D.; Wieme, J.; Vanduyfhuys, L.; Martineau, C.; Stock, N.; Taulelle, F.; Van Speybroeck, V.; Goodwin, A. L.; De Vos, D., A Breathing Zirconium Metal-Organic Framework with Reversible Loss of Crystallinity by Correlated Nanodomain Formation. *Chem. Eur. J.* **2016,** *22*, 3264-3267.

13. Mutlu, H.; de Espinosa, L. M.; Meier, M. A. R., Acyclic diene metathesis: a versatile tool for the construction of defined polymer architectures. *Chem. Soc. Rev.* **2011,** *40*, 1404-1445.

14. Reinsch, H.; Bueken, B.; Vermoortele, F.; Stassen, I.; Lieb, A.; Lillerud, K. P.; De Vos, D., Green synthesis of zirconium-MOFs. *CrystEngComm* **2015,** *17*, 4070-4074.

15. Valenzano, L.; Civalleri, B.; Chavan, S.; Bordiga, S.; Nilsen, M. H.; Jakobsen, S.; Lillerud, K. P.; Lamberti, C., Disclosing the Complex Structure of UiO-66 Metal Organic Framework: A Synergic Combination of Experiment and Theory. *Chem. Mater.* **2011,** *23*, 1700-1718.

16. Katz, M. J.; Brown, Z. J.; Colon, Y. J.; Siu, P. W.; Scheidt, K. A.; Snurr, R. Q.; Hupp, J. T.; Farha, O. K., A facile synthesis of UiO-66, UiO-67 and their derivatives. *Chem. Commun.* **2013,** *49*, 9449-9451.

17. Shearer, G. C.; Chavan, S.; Ethiraj, J.; Vitillo, J. G.; Svelle, S.; Olsbye, U.; Lamberti, C.; Bordiga, S.; Lillerud, K. P., Tuned to Perfection: Ironing Out the Defects in Metal-Organic Framework UiO-66. *Chem. Mater.* **2014,** *26*, 4068-4071.

18. Yan, X. L.; Lu, N. Y.; Fan, B. B.; Bao, J. H.; Pan, D. H.; Wang, M. J.; Li, R. F., Synthesis of mesoporous and tetragonal zirconia with inherited morphology from metal-organic frameworks. *CrystEngComm* **2015,** *17*, 6426-6433.

19. De Lange, M. F.; Vlugt, T. J. H.; Gascon, J.; Kapteijn, F., Adsorptive characterization of porous solids: Error analysis guides the way. *Micropor Mesoporou Mater.* **2014,** *200*, 199-215.

20. Duan, G. R.; Zhang, C. X.; Li, A. M.; Yang, X.; Lu, L.; Wang, X., Preparation and characterization of mesoporous zirconia made by using a poly (methyl methacrylate) template. *Nanoscale Res. Lett* **2008,** *3,* 118-122.

Chapter 3: Applying Isoreticular Chemistry to polyMOFs

3.1 Introduction

As described in Chapter 1, MOFs are often categorized as reticular, or net-like, because of their diverse, open networks and can often be isoreticular, or same net, structures. Using reticular chemistry, the SBUs and ligands of MOFs are easily modified, opening numerous possibilities for interesting, crystallographically ordered chemical environments with isostructural topologies. Yaghi and co-workers synthesized the first isoreticular metal-organic frameworks (IRMOFs) from octahedral Zn-O SBUs combined with ditopic linkers of the same linear geometry, but with various functional groups and different lengths including H_2bdc (IRMOF-1), H_2bdc-NH_2 (IRMOF-3), H_2bpdc (IRMOF-10), and others (Figure 3.1).[1] Similarly, Lillerud and co-workers synthesized an isoreticular series of Zr-based MOFs prepared from H_2bdc, H_2bpdc and H_2tpdc, to make UiO-66, -67, and -68, respectively.[2-3] The concept of isoreticular chemistry has become a core principle for the development of these materials,[4-5] and several series of isoreticular MOFs have been reported (Figure 3.1).[6-7]

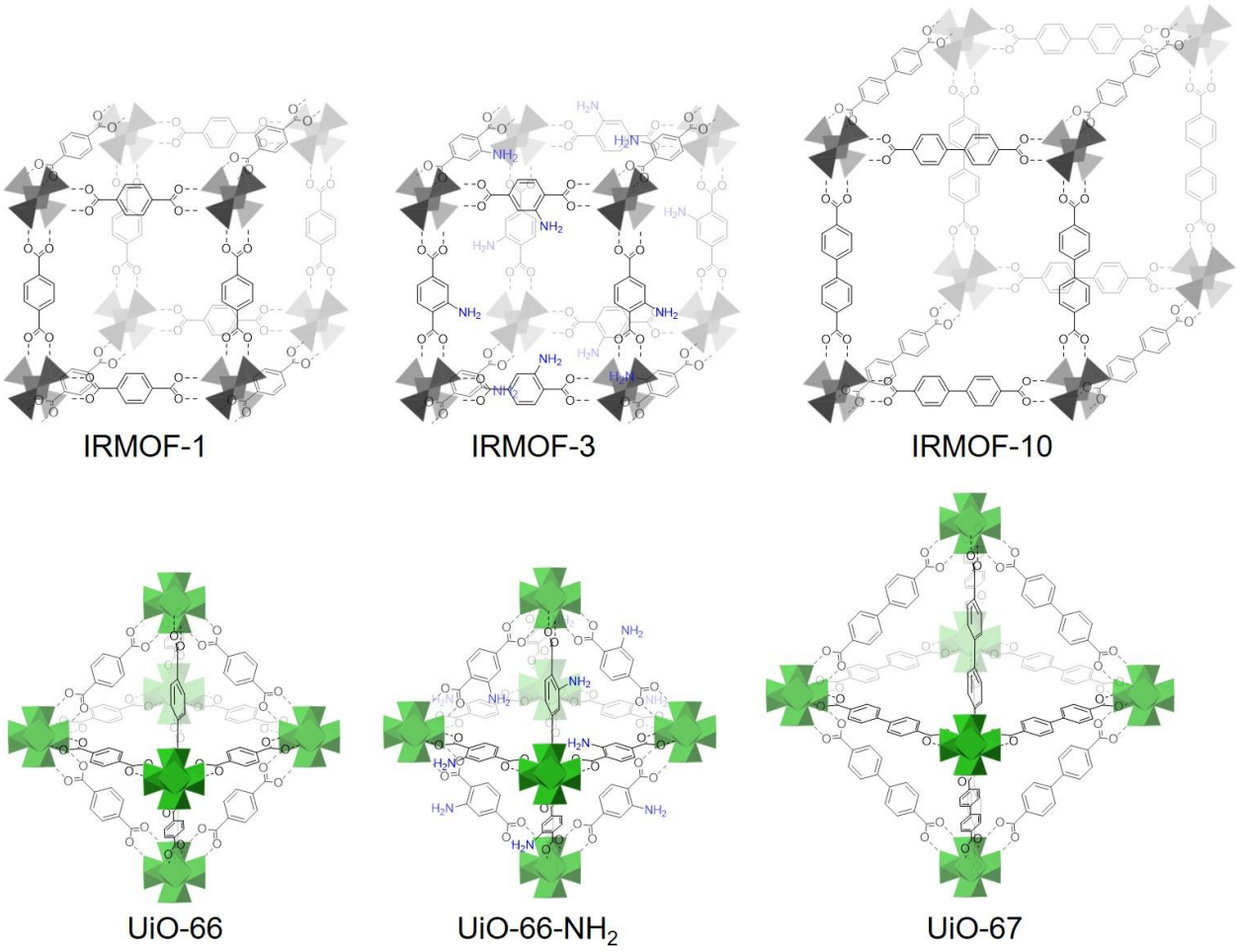

Figure 3.1. Illustrative representation of reticular (net-like) and isoreticular (same-net) chemistry in MOFs. Reticular MOFs can be prepared using the same ligand (H_2bdc) with different metal precursors to yield the Zn-IRMOF structure (top), or the Zr-UiO structure (bottom). For IRMOF-1 (top-left), replacing H_2bdc with H_2bdc-NH_2 or H_2pbdc yields IRMOF-3 (top-middle) or IRMOF-10 (top-right), respectively. For UiO-66 (bottom-left), replacing H_2bdc with H_2bdc-NH_2 or H_2pbdc yields isoreticular UiO-66-NH_2 (bottom-middle) or UiO-67 (bottom-right), respectively.

To prepare crystalline polyMOFs, molecular restraints of the MOF lattice and the structural connectivity of the polymer-ligand must both be considered concurrently. For this reason, polymer-MOF relationships in polyMOFs have been investigated by varying the alkoxy spacer in the backbone of 1-dimensional, amorphous polymer ligands (Figure 3.2), and utilizing these polymer ligands on three different MOF structures.[8-10] In this regard, applying isoreticular chemistry provides a systematic understanding of how manipulations in the polymer ligand affect

the properties of polyMOF materials.[11-12] In Chapter 3, the principle of isoreticular chemistry is used to explore the scope of linear, 1-dimensional, amorphous polymer ligands that can make polyMOFs (Figure 3.2).

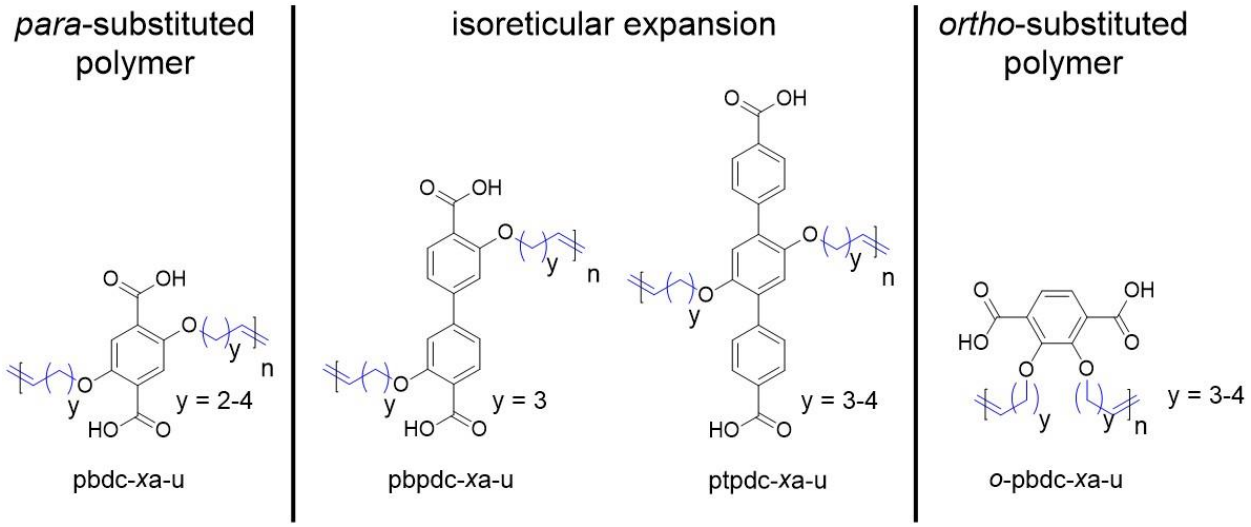

Figure 3.2. Illustration of polymer ligands used to prepare isoreticular polyMOFs in Chapter 3. The notation '*x*' represents the number of methylene spacers between each monomer unit, 'a' denotes 'acid', and 'u' signifies unsaturation in the alkyl spacers.

For the first part of Chapter 3, polyMOFs are expanded, using laterally extended polymer ligands to obtain isoreticular polyMOFs with a UiO architecture (Figure 3.3) and an IRMOF architecture.[12] As described in previous chapters, the surface area of polyMOFs is reduced substantially when compared to their parent MOFs because of the polymer alkyl spacer filling the pore. The isoreticular expansion described here provides access to materials with substantially increased surface areas and larger pore volumes in contrast to previously reported polyMOFs.[8-10] In addition, a single-crystal X-ray diffraction (SXRD) study was achieved with a UiO-68 polyMOF, unequivocally proving that a metal-coordinating organic polymer was transformed into the desired crystalline, 3-dimensional, porous MOF architecture.

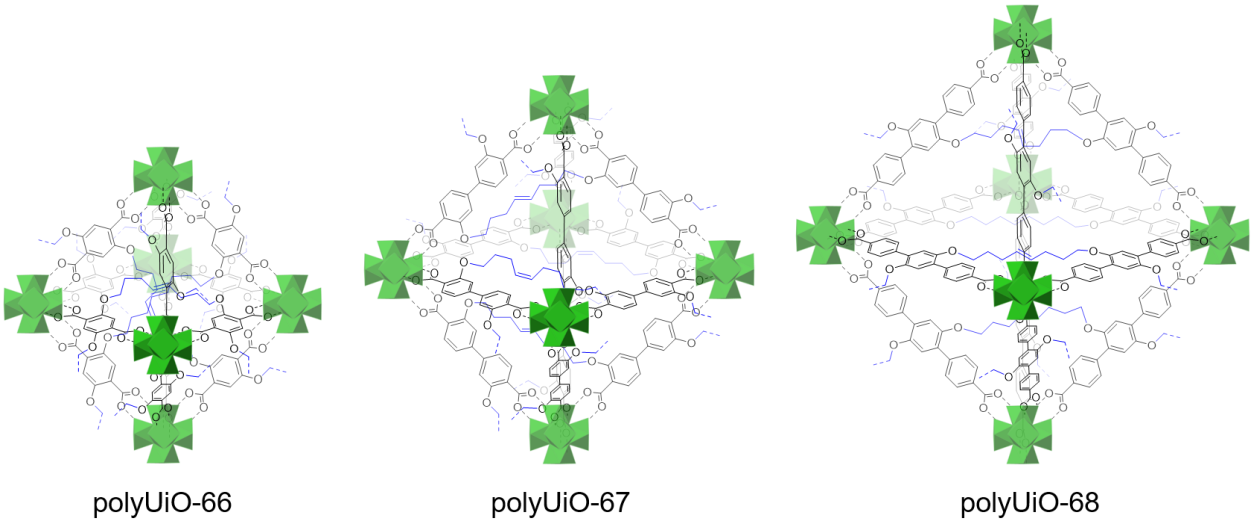

Figure 3.3. Illustration demonstrating the isoreticular expansion of UiO-type polyMOFs. Figure adapted from reference.[13]

For the second part of Chapter 3, the importance of the position of H_2bdc on the polymer-backbone was explored next. The successful preparation of polyMOFs had only been achieved from *para*-substituted ditopic polymer ligands connected through alkoxy backbone segments. In Section 3.3, *ortho*-substituted polymer ligands were used to determine the tolerance of polyMOFs towards change in the polymer structure (Figure 3.4).[11] Changing the position of the alkoxy linkers reveals that while a polyIRMOF-1 lattice can be achieved, the polyUiO-66 lattice does not readily form, signifying the importance of polymer structure for polyMOF formation.

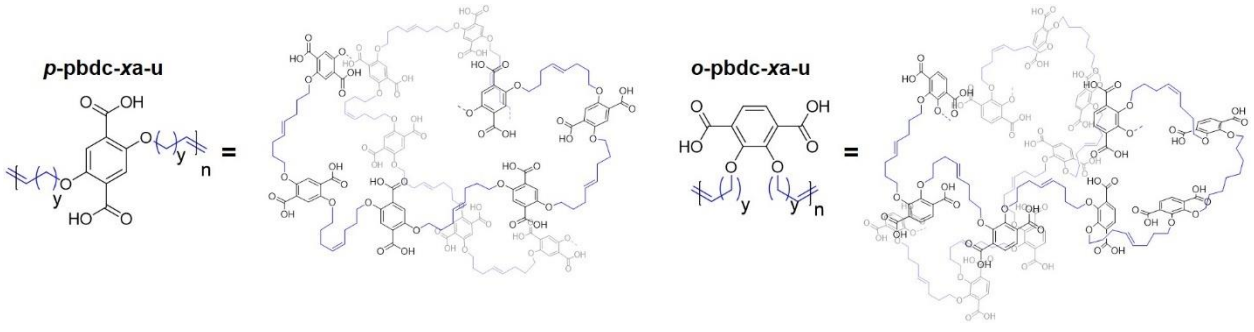

Figure 3.4. Comparison between *para*-substituted (left) and *ortho*-substituted (right) polymer ligands. Figure adapted from reference.[13]

3.2 Results and Discussion – Isoreticular Expansion of polyMOFs

Monomers for the polymer ligands needed to prepare isoreticular polyMOFs were prepared according to the following procedure (Schemes 3.1 and 3S.1). Suzuki coupling of a methoxycarbonyl phenyl boronic acid and bromobenzene derivatives afforded methyl ether-protected precursors. These precursors were then deprotected using boron tribromide to produce dimethyl-3,3'-dihydroxy-[1,1'-biphenyl]-4,4'-dicarboxylate (for polyUiO-67) and dimethyl-2',5'-dihydroxy-[1,1':4',1''-terphenyl]-4,4''-dicarboxylate (for polyUiO-68). Finally, the laterally-extended monomers were completed via Williamson ether synthesis using bromo alkenes ($Br(CH_2)_yCHCH_2$, y = 3 or 4). Polymer ligands were prepared through a modified procedure described in Chapter 2.[8] The monomers were polymerized using Hoveyda-Grubbs 2nd-generation metathesis catalyst to afford the linear, high molecular weight polymers pbpdc-8e-u (for UiO-67, x = 8) and ptpdc-xe-u (for UiO-68, x = 8, 10). It should be noted that Hoveyda-Grubbs 2nd-generation catalyst was used because Grubbs 2nd-generation catalyst only afforded small oligomers, rather than the desired polymers. The resulting polymer ligands were then hydrolyzed to yield pbpdc-8a-u and ptpdc-xa-u (x = 8, 10; where ‘a’ denotes the ‘acid’ form of the polymer) (Figure 3S.1-13).

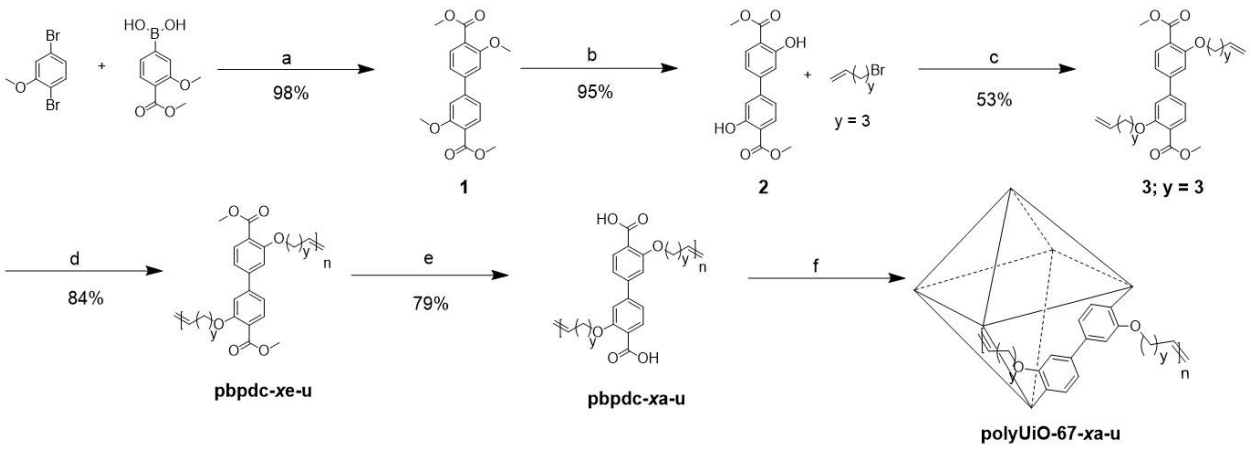

Scheme 3.1. General method for preparation of laterally extended polyMOF ligands, using pbpdc-8a-u as a representative example. a-f) Reagents and conditions: a) $Pd(dppf)Cl_2$, K_2CO_3, 2:1 dioxane/H_2O, 80 °C, 12 h; b) BBr_3, CH_2Cl_2, reflux, 48 h; c) K_2CO_3, DMF, 80 °C 12 h; d) Hoveyda-Grubbs 2nd-generation catalyst, $CHCl_3$, 80 °C, 5 h; e) KOH , 1:1 THF/H_2O, 60 °C, 12 h; f) $ZrCl_4$, 1:1 DEF/formic acid, 135 °C, 48 h.

To characterize and determine the molecular weight of the polymer ligands, the polymer esters were analyzed using ^{1}HNMR end-group analysis and GPC (Table 3.1). ^{1}HNMR and GPC analysis yield different M_n values and degrees of polymerization (DP), in part, because PMMA was used as a molecular weight standard for the GPC measurements. Because PMMA is structurally dissimilar to the polymer ligands reported here the M_n values obtained with this standard must be interpreted with care (Figure 3S.14). For these polymers, ^{1}HNMR end-group is considered a more reliable method for polymer characterization than GPC because with the shortcomings of the PMMA standard. Polymer acid ligands were not characterized by GPC as they are size-excluded due to their high polarity. However, ^{1}HNMR end-group analysis was performed on the final carboxylic acid-containing polymer ligands and gave reasonable M_n values (Table 3S.1).

Table 3.1. GPC and ^{1}H NMR characterization of axially-extended polymer esters.

Ligand	M_n (^{1}HNMR) [a]	M_n (GPC)	M_w/M_n	DP (^{1}HNMR) [b]	DP (GPC) [b]
pbpdc-8e-u	17,560	12,710	2.9	40	31
ptpdc-8e-u	16,480	5,980	3.8	29	12
ptpdc-10e-u	17,376	4,090	4.2	22	8

[a] Number average molecular weight was determined using end-group analysis by ^{1}HNMR. [b] The number of repeat units of the polymers were determined using the following formula: DP = (M_n-$MW_{ethylene}$)/($MW_{monomer}$-$MW_{ethylene}$).

The isoreticular Zr-based polyMOFs were prepared under the same solvothermal conditions as discussed for polyUiO-66.[8] An excess of formic acid was used (1700 eq of formic acid to 1 eq of monomer repeat unit), as it was demonstrated that modulators are critical for UiO-66 polyMOF formation.[8] The formation of polyUiO-67 and polyUiO-68 were confirmed by PXRD (Figure 3.5). The polyMOFs were digested to confirm presence of polymer ligand by ^{1}HNMR (Figure 3S.15-17).

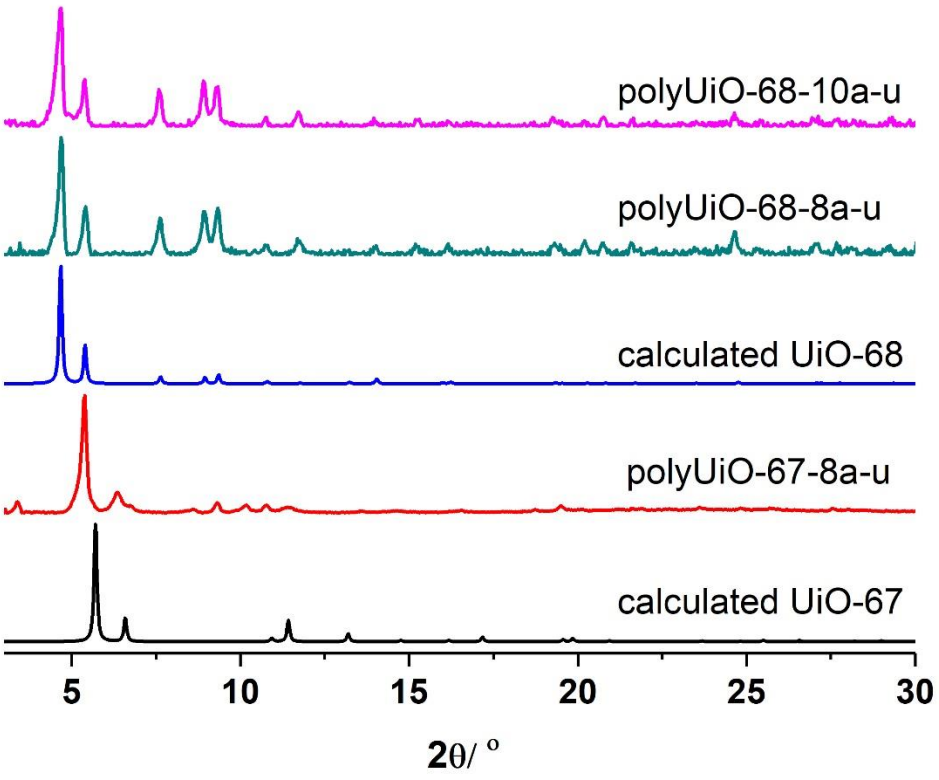

Figure 3.5. Calculated and experimental PXRD patterns for isoreticular polyMOFs.

In addition to PXRD analysis, a single crystal X-ray diffraction (SXRD) study was achieved with polyUiO-68-10a-u (Table 3S.2 and Figure 3S.18). Single crystals were obtained using the reported solvothermal synthesis conditions (see supporting information for experimental details). The SXRD structure (Figure 3.6) shows that the solvothermal reaction results in the formation of the expected $Zr_6(\mu_3\text{-}O)_4(\mu_3\text{-}OH)_4$ cluster producing a UiO-68 lattice type.[2] The unit cell dimensions of polyUiO-68-10a-u agree with those reported for other UiO-68 derivatives (Table 3S.2).[3] The central phenyl ring of the terphenyl ligand is disordered, but the oxygen atom and first carbon atom of the polymer spacer could be refined. While no other carbon atoms of the methylene spacer could be refined (Figure 3.6), residual electron density within the pore suggests

the presence of the polymer ligand in the framework. To provide evidence of the presence of the polymer ligand in polyUiO-68-10a-u, single crystals were dissolved using a solution of NaOD, DMSO-d_6, and D_2O, and the resulting mixture was analyzed by ^{1}HNMR, which shows that the polymer from the polyMOF is intact (Figure 3S.18-19).

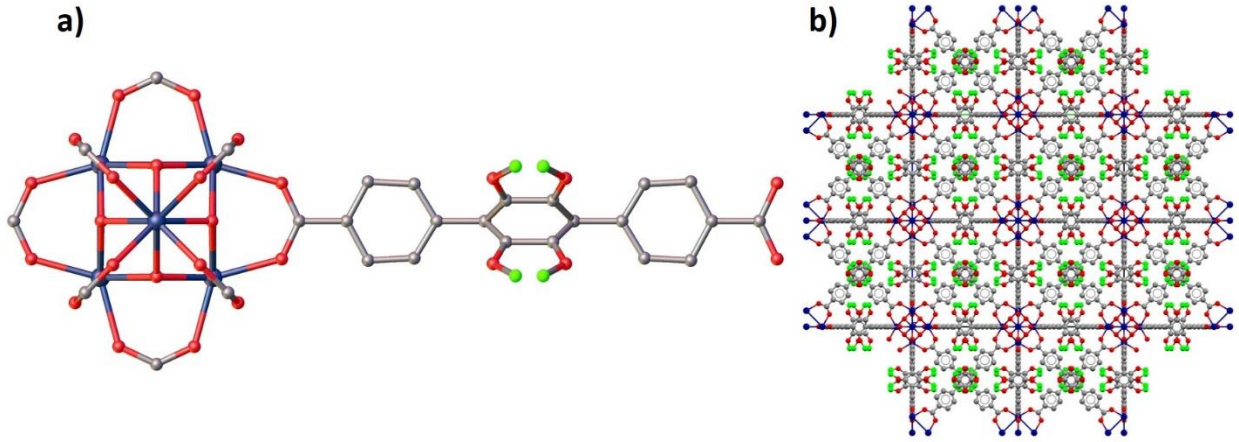

Figure 3.6. SXRD structure of polyUiO-68-10a-u. a) The basic building unit of polyUiO-68-10a-u containing terphenyl and $Zr_6(\mu_3\text{-}O)_4(\mu_3\text{-}OH)_4$ SBU. The central phenyl ring of the terphenyl ligand is disordered, but the oxygen atom (red) and first carbon atom (green) of the polymer spacer were refined. b) The extended lattice structure of polyUiO-68-10a-u. Zirconium, oxygen, and carbon are blue, red, and grey, respectively.

The morphology and size of the polyMOF particles were also investigated using SEM (Figure 3.7). SEM images of polyUiO-67 suggest the presence of a hexagonal, plate-like morphology. SEM images of polyUiO-68-8a-u indicate the more typical octahedral morphology associated with UiO MOFs. SEM images of polyUiO-68-10a-u showed the existence of an uncommon crosshatched morphology.[14] These results confirm earlier findings that indicate polyMOFs can generate atypical crystal morphologies.

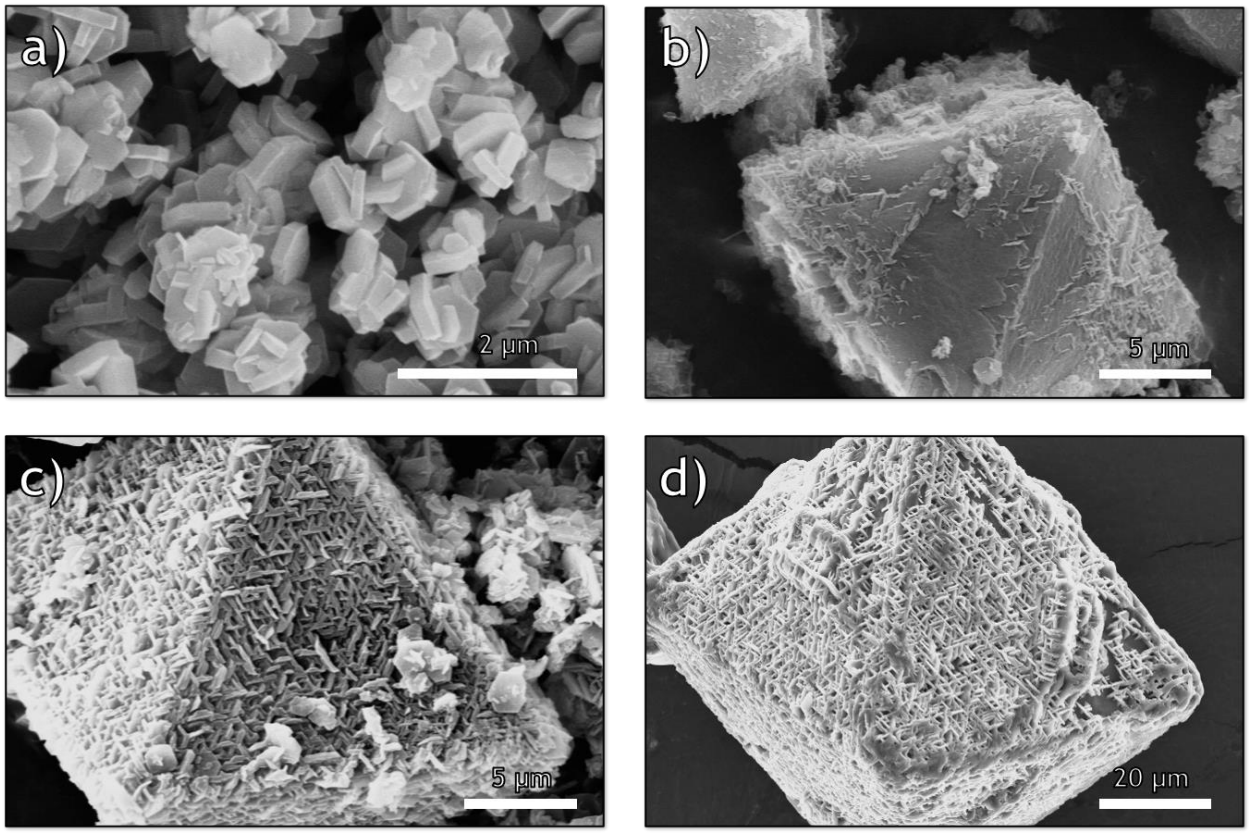

Figure 3.7. SEM images of: (a) polyUiO-67-8a-u; (b) polyUiO-68-8a-u; (c) polyUiO-68-10a-u; (d) polyUiO-68-10a-u single crystal.

As shown in the pillaring-ligand polyMOFs,[10] using a polymer ligand to construct a polyMOF enhances the stability of the framework when compared to the native MOF material. To evaluate the stability of the polyMOFs, TGA and ambient stability tests were performed. The isoreticular polyUiO-67 and polyUiO-68 materials reported here exhibit a high thermal stability by TGA (340° C and 400 °C, respectively; Figure 3S.20). Pore collapse and chemical stability were evaluated by comparing polyUiO-67-8a-u and both polyUiO-68-*x*a-u materials to polymer-free counterparts (i.e. native UiO-67 and UiO-68 functionalized with allyloxy groups, Figure 3S.21).[15] polyUiO-67-8a-u exhibits good stability after 3 d of exposure to ambient air as gauged by PXRD, while native UiO-67 degrades after 1 d (Figure 3S.21). Allyloxy-functionalized UiO-68 and both polyUiO-68-*x*a-u samples were loaded wet with DMF on a PXRD sample holder

because of their low stability under ambient conditions (see supporting information). A decrease in diffraction intensities were observed as the materials began to degrade, but both polyUiO-68-*x*a-u samples exhibited crystallinity after 5 h of exposure to ambient air, when compared to only 1.5 h for the allyloxy-substituted UiO-68, which may be due to longer solvent retention within the voids of the polyMOF framework. Allyloxy-functionalized UiO-68 and polyUiO-68-*x*a-u samples were also submerged in water for 12 h and loaded wet on a PXRD sample holder to evaluate hydrolytic stability (Figure 3S.22). Both samples retained their crystallinity after immediate removal from water, but polyUiO-68-8a-u remained crystalline for 5.5 h after removal, while the allyloxy-functionalized UiO-68 degraded after 30 min after removal from water. From this it can be concluded that polyUiO-68-*x*a-u is more resilient to capillary-force driven pore collapse, as observed in other MOFs containing Zr_6 metal-oxo clusters.[16] These observations corroborate the idea that polyMOFs have the ability to increase stability relative to the parent MOFs.[10]

The surface area of these isoreticular polyMOFs was examined by collecting gas adsorption data using dinitrogen gas (Figure 3.8). The BET surface areas obtained for polyUiO-67-8a-u, polyUiO-68-8a-u, and polyUiO-68-10a-u were 618±180, 1626±190, and 1342±100 m^2/g, respectively (Fig. 3S.23-25). The polyMOF surface areas obtained here are significantly higher than those reported for polyUiO-66[8] (414±8 m^2/g), showing that isoreticular expansion provides access to polyMOFs with much larger surface areas than previously reported polyMOFs. The surface areas of the polyMOFs are lower than for native UiO-67 and allyloxy-functionalized UiO-68[15] (2600-3000 and 2800 m^2/g, respectively), which can be attributed to the pore filling by the polymer ligands. However, the pore-size distribution of these materials does not change significantly when compared to the parent MOFs (Fig. 3S.26). This result can be attributed to retention of the framework despite pore filling by the polymer ligands; a similar result has been

observed by Wang and co-workers using click chemistry to quantitatively functionalize alkyne-tagged UiO-68.[17] Overall, the polyMOFs have the advantage of being more stable materials (as described above).

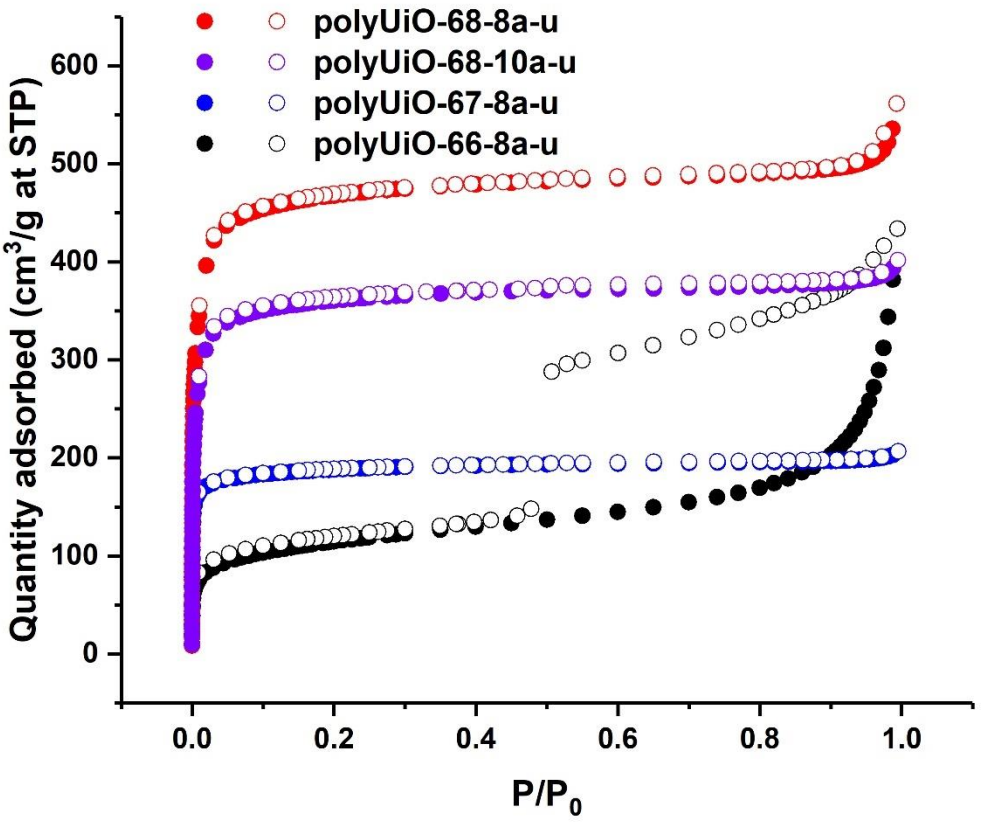

Figure 3.8. Gas sorption isotherms of UiO polyMOFs (N_2, 77 K).

Finally, to demonstrate that of isoreticular expansion could be applied to other polyMOF systems, Zn-based polyIRMOF-10 and polyIRMOF-16 were also successfully synthesized. Using $Zn(NO_3)_2 \cdot 6H_2O$ and the extended polymer ligands, polyIRMOF-10 and polyIRMOF-16 were obtained as confirmed by PXRD (Fig. 3S.27). Interestingly, PXRD revealed that the IRMOFs grew with a preferred orientation, as gauged by the relative intensities of the reflections. This

result was also observed by Yaghi and co-workers in the original report of the IRMOF architecture.[1] The polyIRMOFs were digested in DCl/DMSO-d_6 solution, which confirmed the presence of polymer ligands in the polyIRMOFs (Figures 3S.28-30). SEM images of the polyIRMOF crystals revealed a cubic morphology (Figures 3S.31-33), which is typical for IRMOF crystals. The BET surface area of polyIRMOF16-10a-u was determined to be 541±69 m^2/g. These results correlate with the reported surface area of IRMOF-16 (472-1912 m^2/g), which can vary greatly depending on activation conditions (Fig. 3S.34).[18] These experiments confirm that the principal of isoreticular expansion in polyMOFs can be applied to both IRMOF and UiO scaffolds, suggesting the possibility of a wide variety of high surface area polyMOFs.

3.3 Results and Discussion – PolyMOF Formation from ortho-Substituted Polymer Ligands

Monomer synthesis was achieved as described in Chapter 2, in one step by Williamson ether synthesis with two equivalents of bromo-alkene ($Br(CH_2)_yCHCH_2$, y = 3–4) and dimethyl 2,3-dihydroxyterephathalate (Scheme 3S.2). ADMET polymerization was employed in a concentrated solution of monomer (>1.5 M) with Grubbs' 2nd generation metathesis catalyst, resulting in ester-protected polymer ligands (*o*-pbdc-*x*e-u, where "*o*" denotes the H_2bdc is in the 'ortho position' within the polymer). Polymer esters were hydrolyzed to produce polymer acid ligands (*o*-pbdc-*x*a-u) which were used for polyMOF synthesis.

Analysis of *o*-pbdc-*x*e-u by ^{1}H NMR (Figure 3S.35-36) and GPC (Table 3.3, Figure 3S.37) reveals that polymerization yielded reasonably high molecular weight polymers. Polymer ester ligands were analyzed by GPC, as opposed to polymer acid ligands, due to the better solubility of the polyesters. Despite their high dispersity (Table 3.2) the polymers used throughout were free of any monomer and small-chain oligomers. Although *o*-pbdc-8e-u polymer products were

fractionated into narrower dispersity populations (Table 3S.3, Figure 3S.38), it was shown in Chapter 2 that polyMOF formation is also possible using high dispersity polymers.[8] Therefore, complete hydrolysis of polymer esters was confirmed by ^{1}H NMR (Figure 3S.39-40) and subsequent polyMOF formation was performed using high dispersity polymers.

Table 3.2. GPC characterization of the *o*-pbdc-*x*e-u.

Ligand	M_n (GPC)	M_w/M_n	DP (GPC)
o-pbdc-8e-u	16,100	2.9	44
o-pbdc-10e-u	12,200	3.8	31

o-polyIRMOF-1 was synthesized from zinc nitrate and the corresponding polymer acids (*o*-pbdc-8e-u or *o*-pbdc-10e-u) under the same solvothermal conditions reported for *p*-polyIRMOF.[19] PolyMOF formation was confirmed using PXRD (Figure 3.9). The relative intensities of *o*-polyIRMOF reflections match closely to an IRMOF-1 calculated pattern, indicating that a highly crystalline material is synthesized from the amorphous *o*-pbdc polymer. Digestion of the *o*-polyIRMOF using deuterium chloride dissolves the MOF structure, yielding intact polymer ligand as confirmed by ^{1}H NMR (Figure 3S.41-42). This confirms that *o*-pbdc polymer acts as the sole ligand source in polyMOF formation.

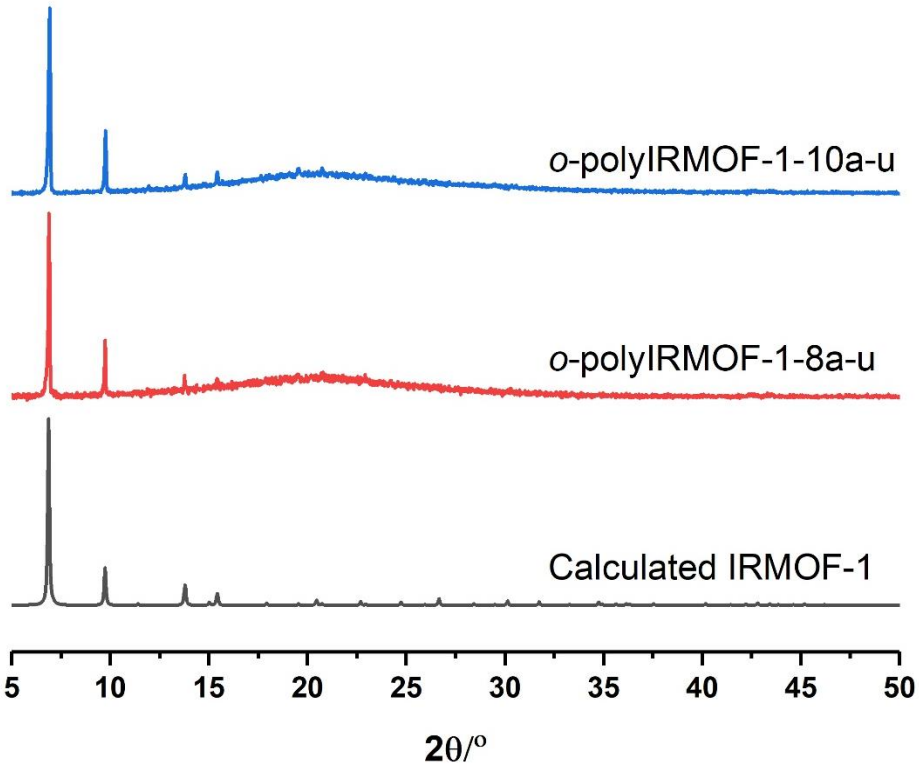

Figure 3.9. PXRD patterns for *o*-polyMOFs synthesized with two polymer ligands, *o*-pbdc-8a-u in red, *o*-pbdc-10a-u in blue, and calculated IRMOF-1 in black.

The particle morphology of *o*-polyIRMOF was compared to that reported for *p*-polyIRMOF by SEM. The crystal morphology of *o*-polyIRMOF synthesized with *o*-pbdc-8a-u shows mixtures of cubes and intergrown crystallites (Figure 3.10) consistent with *p*-polyIRMOF.[19] The morphology for the *o*-pbdc-10a-u polyMOF is similar to *o*-pbdc-8a-u, but with fewer intergrown crystallites, and rather a greater number of solitary cubic crystals that possessed softened, curved edges (Figure 3.10). This new morphology is distinct from any seen in *p*-polyIRMOFs. These results suggest that the increase in methylene spacer length affects the *o*-polyIRMOF-1 growth without affecting the crystallinity. Formation ofo-polyIRMOF-1 with fractionated *o*-pbdc-8a-u gave materials that were essentially the same as those obtained with

unfractionated *o*-pbdc-8a-u (Figure 3S.43-44). Because no notable differences were observed, no attempts to investigate fractionated *o*-pbdc-10a-u were attempted.

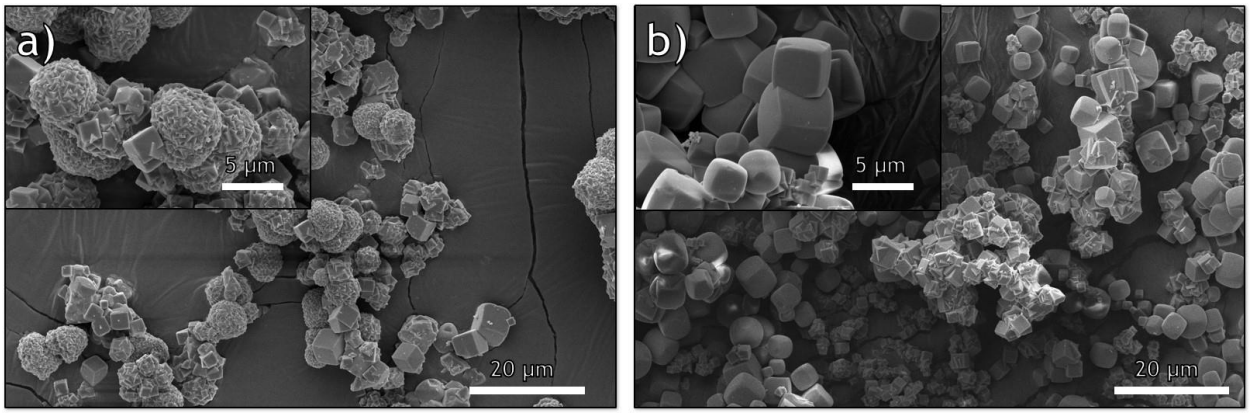

Figure 3.10. SEM images of *o*-polyMOFs synthesized with: a) *o*-pbdc-8a-u, and b) *o*-pbdc-10a-u.

Nitrogen gas adsorption measurements were used to investigate the sorption properties of *o*-polyIRMOF. These materials produce a type I isotherm,[20] revealing the microporous nature of these materials (Figure 3.11). The calculated BET surface areas[21] are 1090 m^2/g and 960 m^2/g for the *o*-pbdc-8a-u and *o*-pbdc-10a-u generated polyIRMOFs, respectively. The surface areas of both *o*-polyIRMOFs are nearly two-thirds lower than the BET surface area of the parent IRMOF-1 (2960±30 m^2/g),[19] but still demonstrate that these materials have a high degree of microporosity. The lower surface area of the *o*-pbdc-10a-u derived *o*-polyIRMOF when compared to the *o*-pbdc-8e-u derived *o*-polyIRMOF logically follows due to increased pore blockage by the larger alkyl spacers in pbdc-10a-u.

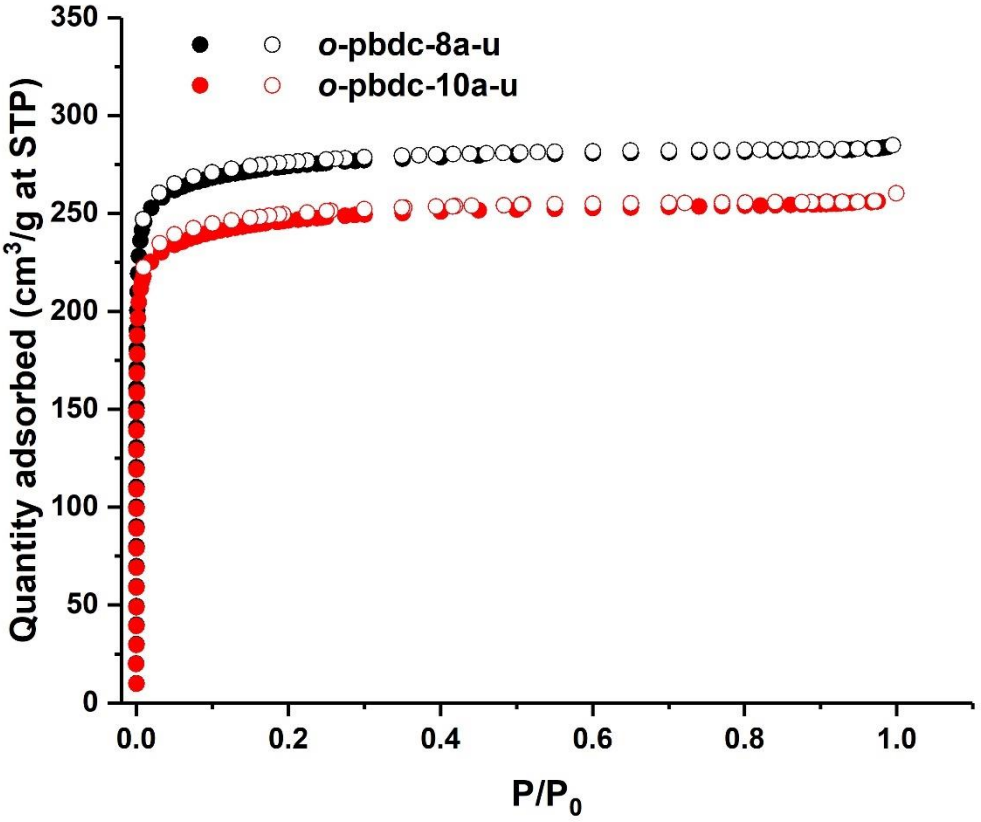

Figure 3.11. N_2 sorption isotherms for *o*-polyIRMOF synthesized with two polymer-ligands: *o*-pbdc-8a-u in red and *o*-pbdc-10a-u in blue.

The two *o*-pbdc ligands were also used for the syntheses of *o*-polyUiO-66 materials using previously-reported polyMOF conditions.[8] However, all *o*-pbdc-*x*a-u ligands (unfractionated and fractionated) were unsuccessful in producing polyUiO-66 formation under the same reaction conditions. In addition, *o*-pbdc-8a-u was employed under two other reported UiO-66 synthesis conditions[22-23] , but did not produce the desired *o*-polyUiO-66 (see Supporting Information for details). Precipitates were obtained from these reaction solutions, indicating a Zr(IV)-coordination compound is formed, but these precipitated were not crystalline as gauged by PXRD analysis (Figure 3S.45). The failure of *o*-pbdc polymer ligands to form the UiO-66 topology in these

conditions may indicate that the polymer is incapable of fitting into this structure type, but more exhaustive testing would be required to confirm this hypothesis.

3.4 Conclusions

In summary, the principle of isoreticular chemistry was successfully demonstrated in polyMOFs for the first time on UiO and IRMOF scaffolds. The highest surface area reported for a polyMOF was achieved using laterally extended polyUiO-68-8a-u. A SXRD study was also successful with polyUiO-68-10a-u, unequivocally proving that a metal-coordinating organic polymer was transformed into the desired crystalline, 3-dimensional, porous MOF architecture. The enhanced stability of polyUiO-67 and polyUiO-68 relative to the parent MOFs and their unique crystal morphologies suggest potential advantages of the polyMOFs materials. These results further establish polyMOFs as a new subclass of porous materials with unusual physical and chemical properties that result in emergent and unprecedented properties.

In addition, the importance of polymer structure was emphasized by making simple changes to polymer ligand architecture and observing polyMOF formation ability. There are many parallels of the *o*-pbdc polyMOFs discussed here to the isoreticular *p*-pbdc polyMOFs reported previously.[8, 19] Both systems are high molecular weight polymers with the ability to construct polyIRMOF without the aid of molecular (i.e., non-polymeric) ligands. These materials have similarly high BET surface areas (1090 and 860±16 m^2/g for *o*-pbdc-8a-u and *p*-pbdc-8a, respectively)[19] despite the presence of polymer chains in pores of the materials. However, there are also notable differences between the two polymer ligands and their ability to form polyMOFs, in that *o*-pbdc does not form polyUiO-66 under the same conditions used in the formation of polyUiO-66 with *p*-pbdc. These results strongly suggest that ligand architecture influences

polyMOF formation. As the investigation of polyMOFs continues, designing and investigating polymer architecture will be critical to expanding the limits of these hybrid materials. Efforts to improve the polymer-like properties of these hybrid materials will also be essential for their further development.[24]

3.5 Appendix: Supporting Information

General Materials and Methods. Starting materials were purchased and used from commercially available suppliers (Sigma-Aldrich, Acros Organics, Matrix Scientific, and others) without further purification. Chromatography was performed using a CombiFlash R_f 200 automated system from Teledyne Isco. Allyloxy-functionalized UiO-68 and UiO-67 were prepared using previous reports.[15, 25] ^{1}H and ^{13}C nuclear magnetic resonance (NMR) spectra were collected using a Varian spectrometer running at 400 MHz.

Experimental: Isoreticular Expansion of Polymer Ligands

[1,1'-Biphenyl]-4,4'-dicarboxylic acid-3,3'-dimethoxy-4,4'-dimethyl ester (1). Methyl 4-bromo-2-methoxybenzoate (1.00 g, 4.1 mmol, 1 eq), (3-methoxy-4- (methoxycarbonyl)phenyl boronic acid (1.04 g, 4.9 mmol, 1.2 eq), K_2CO_3 (3.46 g, 525 mmol, 6.3 eq), and $PdCl_2$(dppf) (175 mg, 0.70 mmol, 0.17 eq) were added to a round bottom flask with 10 mL of water and 25 mL of 1,4-dioxane. The solution was degassed for 5 minutes and heated at 80 °C under nitrogen atmosphere for 14h. After cooling to room temperature, 20 mL of water was added, and the solution was filtered. The product was then purified by recrystallization using a large excess of DMF and 2 mL of water. Compound **5** was isolated as white-gray crystals. Yield: 98% (1.31 g, .4.0 mmol). ^{1}H NMR (400 MHz, $CDCl_3$): δ 7.90 (d, J = 8.0 Hz, 2H), 7.20 (dd, J = 8.0, 1.6 Hz,

2H), 7.15 (d, *J* = 1.6 Hz, 2H), 3.99 (s, 6H), 3.92 (s, 6H). See Figure 3S.1 for ^{1}H NMR spectrum with assignments.

[1,1'-Biphenyl]-4,4'-dicarboxylic acid-3,3'-dihydroxy- 4,4'-dimethyl ester (2). Compound **1** (700 mg, 2.1 mmol, 1 eq), 1 M BBr_3 in heptane (22 mL, 22 mmol, 10 eq), and 15mL of CH_2Cl_2 were added to a flask and stirred at room temperature for 48h. After allowing the solution to cool, the reaction was quenched with excess methanol. The solution was co-evaporated with excess of methanol until a yellow solid precipitated. The solid was then added to 650 mL of MeOH, catalytic H_2SO_4 (4 drops using a glass pipette), and heated to reflux in MeOH for 4 d. The solution was concentrated by evaporation of MeOH, and water was added to yield an off-white solid. Yield: 95% (550 mg, 2.0 mmol). ^{1}H NMR (400 MHz, DMSO-d): δ 7.87 (d, *J* = 7.2 Hz, 2H), 7.30 (d, *J* = 6.9 Hz, 2H), 7.30 (d, *J* = 6.9 Hz, 2H), 3.91 (s, 3H). See Figure 3S.2 for ^{1}H NMR spectrum with assignments.

[1,1'-Biphenyl]-4,4'-dicarboxylic acid-3,3'-bis(pent-4-en-1-yloxy) 4,4'-dimethyl ester (3). Compound **2** (0.50 g, 1.6 mmol, 1 eq), 5-bromo-1pentene (2.48 g, 16.7 mmol, 9 eq), K_2CO_3 (1.53 g, 11.1 mmol, 6 eq) and 40 mL of DMF were added to a 250 mL round bottom flask. The solution was stirred and heated at 80 °C for 14 h and monitored by TLC using 20% of ethyl acetate and 80% hexane. Potassium carbonate was then removed by filtration and the DMF was removed by rotary evaporation and the resulting residue was subjected to column chromatography (hexane/ethyl acetate). The biphenyl monomer **3** was isolated as a white powder. Chromatography gradient: 0-5 min of 5% EtOAc, 5-10 min of 10% EtOAc, 10-20 min of 15% EtOAc. Yield: 53% (0.40 g, 0.90 mmol). ^{1}H NMR (400 MHz, $CDCl_3$): δ 7.88 (d, *J* = 8.0 Hz, 2H), 7.17 (d, *J* = 8.0 Hz, 2H), 7.11 (s, 2H), 5.95 – 5.80 (m, 2H), 5.08 (d, *J* = 17.1 Hz, 2H), 5.01 (d,

J = 10.2 Hz, 2H), 4.13 (t, *J* = 6.3 Hz, 4H), 3.91 (s, *J* = 2.3 Hz, 6H), 2.32 (q, *J* = 7.0 Hz, 4H), 1.97 (p, 4H). See Figure 3S.3 for ^{1}HNMR spectrum with assignments.

Poly-[1,1'-Biphenyl]-4,4'-dicarboxylic acid-3,3'-bis(pent-4-en-1-yloxy)-4,4'-dimethyl ester (pbpdc-8e-u). Compound **3** (0.39 mmol, 1 eq), Hoveyda-Grubbs 2nd-generation catalyst (11 mg, 0.017 mmol, 0.045 eq) and 0.8 mL of $CHCl_3$ were added into a flask and heated at 70 °C for 5 h. The reaction was then quenched with ethyl vinyl ether (0.29 mL, 3 mmol, 7.7 eq). After allowing the reaction to cool to room temperature, 15 mL of MeOH was added to the solution. The polymer was isolated by centrifugation (Beckman Coulter Allegra X-22R Centrifuge, fixed-angle rotor, 5300 rpm for 6 min) and washed three times with MeOH. The polymer was then dried by removing MeOH under high vacuum. Yield: 84% (135 mg, 0.31 mmol). ^{1}H NMR (400 MHz, $CDCl_3$): δ 7.83 (s, 2H), 7.12 (bs, 4H), 5.52 (s, 2H), 4.64 (s, 0.10H), 4.08 (s, 4H), 3.87 (s, 6H), 2.23 (bs, 4H), 1.88 (bs, 4H). See Figure 3S.4 for ^{1}H NMR spectrum with assignments.

Poly-[1,1'-Biphenyl] -3,3'-bis(pent-4-en-1-yloxy)- 4,4'-dicarboxylic acid (pbpdc-8a-u). To hydrolyze the protecting ester groups, pbpdc-8e-u (107 mg, 0.24 mmol, 1 eq) was placed in a 1:1 mixture of water and THF (15 mL total) with excess KOH (30 eq). The mixture was heated at 80 °C for 5 h. The solution was acidified with 1.0 M HCl. The resulting precipitate was collected by centrifugation and washed three times with MeOH. The isolated solid was dried by removing methanol under high vacuum. Yield: 79% (79 mg, 0.19 mmol). ^{1}H NMR (400 MHz, DMSO-d_6): δ 7.68 (bs, 2H), 7.31 (bs, 4H), 5.49 (bm, 2H), 4.69 (m, 0.10H), 4.12 (s, 4H), 2.16 (bs, 4H), 1.76 (bs, 4H). See Figure 3S.5 for ^{1}H NMR spectrum with assignments.

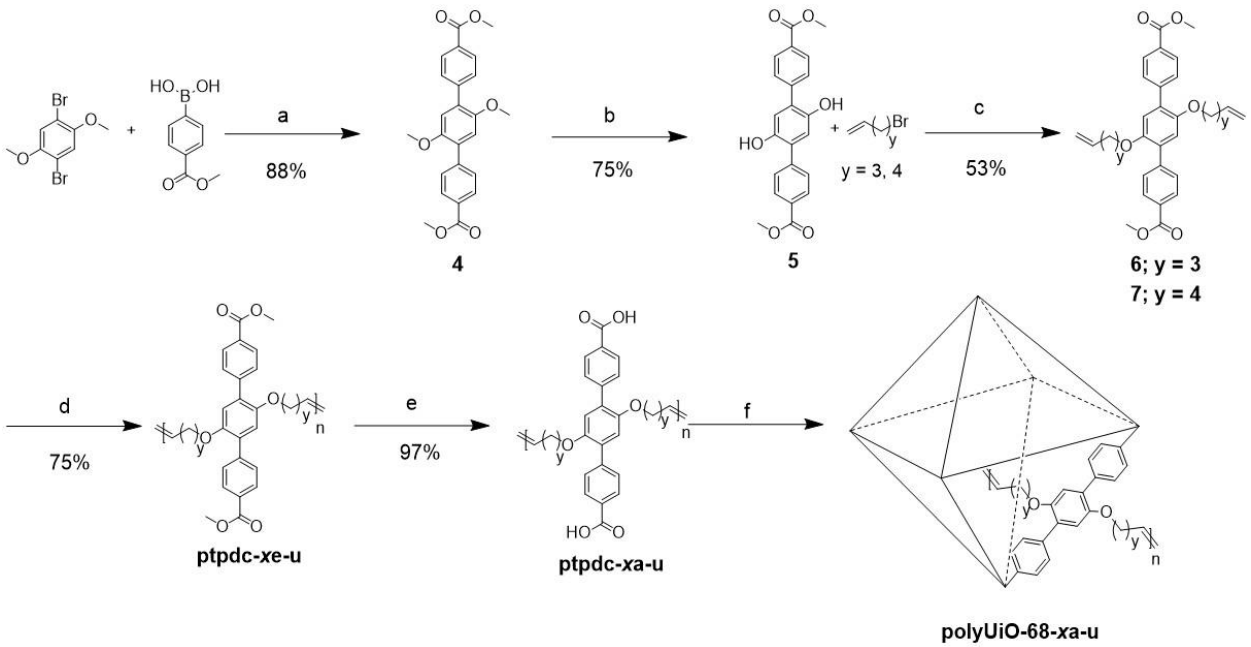

Scheme 3S.1. Synthetic scheme of ptpdc-*x*a-u synthesis, where x = 8 or 10. a-f) Reagents and conditions: a) $Pd(dppf)Cl_2$, K_2CO_3, 2:1 dioxane/H_2O, 80 °C, 12 h; b) BBr_3, CH_2Cl_2, reflux, 48 h; c) K_2CO_3, DMF, 80 °C 12 h; d) Hoveyda-Grubbs 2nd-generation catalyst, $CHCl_3$, 80 °C, 5 h; e) KOH , 1:1 THF/H_2O, 60 °C, 12 h; f) $ZrCl_4$, 1:1 DEF/formic acid, 135 °C, 48 h.

[1,1':4',1''-Terphenyl]-4,4''-dicarboxylic acid-2',5'-dimethoxy-4,4''-dimethyl ester (4). To a 250 mL round bottom flask was added methoxycarbonyl phenyl boronic acid (3.00 g, 16.7 mmol, 2.5 eq), bromobenzene (2 g, 7 mmol, 1 eq), K_2CO_3 (6.91 g, 50.0 mmol, 7.4 eq), and $PdCl_2(dppf)$ (275 mg, 1.1 mmol, 0.16 eq) in 25 mL of water and 50 mL of 1,4-dioxane. The solution was degassed for 5 min and heated at 80 °C under nitrogen atmosphere for 14 h. After cooling down, 50 mL of water was added to the solution followed by filtration. The product was then purified by recrystallization using DMF and a few drops of water. The desired product **4** was isolated as white gray crystals. Yield: 88% (2.42 g, 5.95 mmol). ^{1}H NMR (400 MHz, $CDCl_3$): δ 7.89 (dd, J = 176.6, 7.8 Hz, 8H), 6.99 (s, 1H), 3.95 (s, 6H), 3.81 (s, 6H). See Figure 3S.6 for NMR spectrum with assignments.

[1,1':4',1''-Terphenyl]-4,4''-dicarboxylic acid-2',5'-hydroxy-4,4''-dimethyl ester (5). Compound **4** (1.2 g, 3.0 mmol, 1 eq), 1 M BBr_3 (30 mL, 30 mmol, 10 eq), and 14 mL of CH_2Cl_2 were added to a 250 mL flask and the reaction mixture was heated at 50 °C for 48 h. After cooling down the solution, the reaction was quenched with 100 mL of MeOH. The product **5** was isolated as an orange powder. Yield: 75% (0.77 g, 2.0 mmol). ^{1}H NMR (400 MHz, DMSO-d_6): δ 9.26 (s, 2H), 8.05 – 7.68 (m, 8H), 6.94 (s, 2H), 3.87 (s, 6H). See Figure 3S.7 for ^{1}H NMR spectrum with assignments.

[1,1':4',1''-Terphenyl]-4,4''-dicarboxylic acid-2',5'-bis(pent-4-en-1-yloxy)-4,4''-dimethyl ester (6). The same procedure was applied as for compound **3**, using compound **5** and 5-bromo-1-pentene. ^{1}H NMR (400 MHz, $CDCl_3$): δ 7.88 (dd, J = 170.3, 8.2 Hz, 8H), 6.99 (s, 2H), 5.76 (ddt, J = 16.9, 10.2, 6.7 Hz, 2H), 5.00 – 4.92 (m, 4H), 3.95 (bs, J = 3.4 Hz, 10H), 2.17 – 2.06 (dt, 4H), 1.78 (dt, J = 13.5, 6.4 Hz, 4H). See Figure 3S.8 for ^{1}H NMR spectrum with assignments.

[1,1':4',1''-Terphenyl]-4,4''-dicarboxylic acid-2',5'-bis(hex-5-en-1-yloxy)-4,4''-dimethyl ester (7). The same procedure was applied as for compound **3**, using compound **5** and 6-bromo-1-hexene. Yield: 70% (0.65 g, 1.7 mmol). ^{1}H NMR (400 MHz, $CDCl_3$): δ 8.09 (d, J = 8.7 Hz, 4H), 7.67 (d, J = 8.1 Hz, 4H), 6.99 (s,2H), 5.76 (ddt, J = 16.9, 10.2, 6.6 Hz, 2H), 4.95 (s, 4H), 3.95 (s, 10H), 2.04 (q, J = 7.4 Hz, 4H), 1.77 – 1.63 (p, 4H), 1.46 (p, J = 7.5 Hz, 4H). See Figure 3S.9 for ^{1}H NMR spectrum with assignments.

Poly-[1,1':4',1''-Terphenyl]-4,4''-dicarboxylic acid-2',5'-bis(pent-4-en-1-yloxy) 4,4''-dimethyl ester (ptpdc-8e-u). The conditions used are identical to those used for the polymerization synthesis of pbpdc-8e-u, using compound **6.** Yield: 75% (150 mg, 0.29 mmol). ^{1}H NMR (400 MHz, $CDCl_3$): δ 8.05 (s, 4H), 7.64 (s, 4H), 6.96 (s, 2H), 5.31 (m, 2H), 4.52 (d, J =

99.5 Hz, 0.15H), 3.89 (bs, 2H), 2.35 (bs, 4H), 2.02 (dt, 4H). See Figure 3S.10 for ^{1}H NMR spectrum with assignments.

Poly-[1,1':4',1''-Terphenyl]-4,4''-dicarboxylic acid-2',5'-bis(hex-5-en-1-yloxy) 4,4''-dimethyl ester (ptpdc-10e-u). The conditions used are identical to those used for the polymerization synthesis of pbpdc-8e-u, using compound **7.** Yield: 98% (420 mg, 0.77 mmol). ^{1}H NMR (400 MHz, $CDCl_3$): δ 8.06 (s, 4H), 7.65 (s, 4H), 6.97 (s, 2H), 5.32 (m, 2H), 4.49 (s, 0.14H), 3.90 (s, 10H), 2.02 (bs,40H), 1.67 (bs, 4H), 1.31 (bs, 4H). See Figure 3S.11 for ^{1}H NMR spectrum with assignments.

Poly-[1,1':4',1''-Terphenyl]-2',5'-bis(pent-4-en-1-yloxy)4,4''-dicarboxylic acid (ptpdc-8a-u). The conditions used are identical to those used for the hydrolysis of pbpdc-8e-u, using ptpdc-8e-u. Yield: 97% (92 mg, 0.19 mmol). ^{1}H NMR (400 MHz, DMSO-d_6): δ 8.05 (s, 4H), 7.64 (s, 4H), 6.96 (s, 2H), 5.31 (m, 2H), 4.52 (d, J = 99.5 Hz, 0.15H), 3.89 (bs, 2H), 2.35 (bs, 4H), 2.02 (dt, 4H). See Figure 3S.12 for ^{1}H NMR spectrum with assignments.

Poly-[1,1':4',1''-Terphenyl]-2',5'-bis(hex-5-en-1-yloxy)4,4''-dicarboxylic acid (ptpdc-10a-u). The conditions used are identical to those used for the hydrolysis of pbpdc-8e-u, using ptpdc-10e-u. Yield: 90% (0.390 g, 0.79 mmol). ^{1}H NMR (400 MHz, DMSO-d_6): δ 8.04 (s, 4H), 7.66 (s, 4H), 7.05 (s, 0H), 5.25 (bs, 2H), 4.49 (s, 0.25H), 3.91 (s, 3H), 3.41 (s, 3H), 1.87 (bs, 4H), 1.56 (bs, 4H), 1.23 (bs, 4H). See Figure 3S.13 for ^{1}H NMR spectrum with assignments.

Experimental: Ortho-Substituted Polymer Ligands

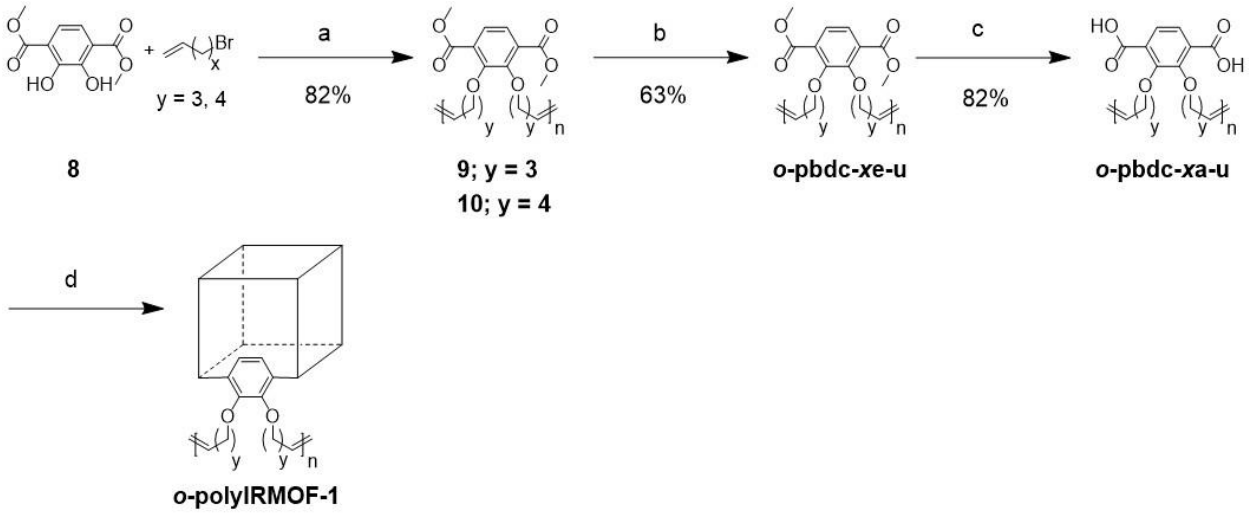

Scheme 3S.2. Synthesis of *o*-pbdc-*x*a-u and subsequent formation of polyIRMOF-1. Shown for *o*-pbdc-8a-u, where y = 3. Reagents and conditions: a) K_2CO_3, DMF, 80 °C, 12 h; b) Grubbs G2 catalyst, CH_2Cl_2, 50 °C, 5 h.; c) H_2O: THF 1:1, 45 °C, 12 h; d) $Zn(NO_3)_2$, DMF, 100 °C, 24 h.

Dimethyl 2,3-bis(pent-4-en-1-yloxy)terephthalate (9). The same procedure was applied as for compound **3**, using compound **8** and 5-bromo-1-pentene. Physical state: yellow oil. Yield: 70% (3.4 g, 9.3 mmol). ^{1}H NMR (400 MHz, $CDCl_3$): δ 7.48 (d, J = 5.7 Hz, 2H), 5.97 – 5.76 (m, 2H), 5.02 (ddd, J = 13.7, 11.3, 1.3 Hz, 4H), 4.07 (t, J = 6.7 Hz, 4H), 3.92 (s, 6H), 2.23 (dd, J = 14.6, 7.0 Hz, 4H), 1.96 – 1.85 (m, 4H).

Dimethyl 2,3-bis(hex-5-en-1-yloxy)terephthalate (10). The same procedure was applied as for compound **3**, using compound **8** and 6-bromo-1-hexene. Physical State: yellow oil. Yield: 80% (4.1 g, 10.5 mmol). ^{1}H NMR (400 MHz, $CDCl_3$): δ 7.48 (s, J = 6.2 Hz, 2H), 5.83 (ttd, J = 13.2, 6.7, 2.7 Hz, 2H), 5.00 (dd, J = 23.8, 13.6 Hz, 4H), 4.06 (td, J = 6.6, 2.7 Hz, 5H), 3.91 (s, J = 2.8 Hz, 7H), 2.12 (dd, J = 13.9, 6.4 Hz, 5H), 1.90 – 1.73 (m, 5H), 1.66 – 1.48 (m, 6H).

Synthesis of poly-dimethyl 2,3-bis(pent-4-en-1-yloxy)terephthalate (*o*-pbdc-8e-u). To a 10 mL round bottom flask **2** (1.09 g, 3.00 mmol, 1.00 eq) was added and dissolved in 1.8 mL of

CH_2Cl_2 (conc. of monomer 1.6 M). Grubbs second-generation catalyst was loaded neat (25.5 mg, 0.030 mmol, 0.01 eq). The reaction was heated to reflux (50 °C) under mild nitrogen for 5 h. After the solution was cooled to room temperature, ethyl vinyl ether (2 mL) was added to quench the catalyst, and the solution was stirred for 30 min. The polymer was precipitated in methanol (~30 mL), followed by centrifugation at 7000 rpm for 10 min. at room temperature. The supernatant was decanted and the polymer was dissolved in CH_2Cl_2 and precipitated four more times in methanol. After the final wash, the polymer was transferred to a vial, and dried under vacuum for 1 h. Yield: 63% (690 mg, 1.9 mmol). ^{1}H NMR (400 MHz, $CDCl_3$): δ 7.45 (s, J = 16.7 Hz, 2H), 5.80 – 5.34 (m, 2H), 5.09 – 4.95 (m, 1H), 4.04 (t, J = 5.9 Hz, 4H), 3.89 (s, J = 11.7 Hz, 7H), 2.08 (d, J = 40.6 Hz, 4H), 2.00 – 1.71 (m, 4H). See Figure 3S.35 for ^{1}H NMR spectrum with assignments.

For fractionated samples. The procedure was followed as before, but after the final wash the polymer was purified using silica gel chromatography at gradient from 0% to 10% methanol in CH_2Cl_2, yielding the desired polymers.

Poly-dimethyl 2,3-bis(pent-4-en-1-yloxy)terephthalate (*o*-pbdc-10e-u). The same procedure was applied as for *o*-pbdc-8e-u, using compound **10**. Yield: 59% (240 mg, 0.61 mmol). ^{1}H NMR (400 MHz, $CDCl_3$): δ 7.46 (s, 2H), 5.43 (d, J = 9.8 Hz, 2H), 4.04 (t, J = 6.5 Hz, 5H), 3.89 (s, 6H), 2.03 (s, 4H), 1.77 (s, 4H), 1.49 (s, 4H). See Figure 3S.36 for ^{1}H NMR spectrum with assignments.

Poly-2,3-bis(pent-4-en-1-yloxy)terephthalic acid (*o*-pbdc-8a-u). The conditions used are identical to those used for the hydrolysis of pbpdc-8e-u, using *o*-pbdc-8e-u. Yield: 82% (410 mg, 1.2 mmol). ^{1}H NMR (300 MHz, DMSO-d_6): δ 13.11 (s, 1H), 7.35 (d, J = 3.1 Hz, 1H), 5.44 (s,1H), 3.95 (s, 2H), 2.08 (s, 2H), 1.71 (s, 2H). See Figure 3S.39 for ^{1}H NMR spectrum with assignments.

Poly-2,3-bis(hex-5-en-1-yloxy)terephthalic acid (*o*-pbdc-10a-u). The conditions used are identical to those used for the hydrolysis of pbpdc-8e-u, using *o*-pbdc-10e-u. Yield: 62% (124 mg, 0.34 mmol). ^{1}H NMR (300 MHz, DMSO-d_6): δ 7.35 (s, 2H), 5.38 (s, 2H), 3.94 (s, 4H), 1.97 (s, 3H), 1.67 (s, 4H), 1.43 (s, 3H). See Figure 3S.40 for ^{1}H NMR spectrum with assignments.

Experimental: Procedures for polyMOF synthesis

General procedure for Zr-polyMOF synthesis. Procedure was adapted from the synthesis of polyUiO-66.[8] In a 20 mL scintillation vial, the polymer-acid ligand (0.03 mmol) and $ZrCl_4$ (0.037 mmol) were added to 2 mL of DEF. After the solution became clear, 2 mL of formic acid was added. The vial was heated at 135 °C for 48 h. *For Single crystal growth prepared from ptpdc-xa-u.* Single crystals of ptpdc-10a-u were prepared as described above. After removal from the oven, the 20 mL scintillation vial containing the polyMOF was sonicated to suspend microparticles of polyUiO-68-10a-u, allowing for large crystals to sink to the bottom of the vial. The supernatant and microparticles were removed, leaving the large crystals at the bottom of the vial.

Procedure for additional synthesis attempts of polyUiO-66 using *o*-pbdc-8a-u. First procedure was adapted from J.T. Hupp, O. K. Farha *et al.*[22] *o*-pbdc-8a-u (0.030 mmol) and zirconium (IV) chloride ($ZrCl_4$, 0.054 mmol) were combined in 1.5 mL of DMF in a 5 mL vial. To this mixture HCl (12M, 0.1 mL) was added as a modulator. The reaction was set in a pre-heated oven at 80 °C for 24 h. Resulting material was an amorphous, yellow gel. Second procedure was adapted from F. Hou *et al.*[23] *o*-pbdc-8a-u (0.052 mmol) and zirconium (IV) chloride ($ZrCl_4$, 0.052 mmol) were combined in 3.0 mL of DMF in a 5 mL vial. To this mixture acetic acid (glacial, 0.09 mL) was added as a modulator. The reaction was set in a pre-heated oven at 120 °C for 24 h. Resulting material was an amorphous, yellow gel**.**

General procedure for Zn-polyMOFs synthesis. The IRMOF-type polyMOFs were prepared by adapting a previously reported procedure.[9] To a 20 mL scintillation vial was added 0.05 mmol of the appropriate extended polymer ligand (pbpdc-*x*a-u or ptpdc-*x*a-u), $Zn(NO_3)_2 \cdot 6H_2O$ (0.30 mmol), and 2.5 mL of DMF. The vial was placed in a pre-heated oven at 100 °C for 24 h. The off-white crystals were cleaned by extensive washing and solvent-exchange of DMF (5x5 mL of DMF) and kept in solvent until further studies were performed.

Analytical methods

GPC conditions for pbpdc-8e-u and ptpdc-*x*e-u (*x* = 8 and 10). GPC was performed in DMF (0.7 mL/min) using a Malvern GPC equipped with D4000 single-pore column and D-6000M general-purpose mixed-bed weight divinylbenzene column connected in series. Before injection into the GPC instrument the solutions were filtered using a 0.4 μm PTFE membrane. Narrow PMMA was used as standard for the calibration curve. *For o-pbdc-xe-u*. The conditions were identical, except using THF as the solvent.

PXRD Analysis. The synthesized polyMOFs were filtered, washed with DEF, and PXRD data was collected at ambient temperature on a Bruker D8 Advance with a step size of 0.03° in 2θ, a scan speed of 0.5 s/step, and a 2θ range of 3° to 50°.

^{1}H NMR Digestions. To 10 mg of polyMOF was added a solution containing 440 μL of 6 M NaOD and 160 μL of DMSO-d_6. The mixture was sonicated at 50 °C for 24 h. The solvent was evaporated, and the mixture was re-suspended in a solution containing 500 μL of DMSO-d_6 and 100 μL of D_2O. The supernatant was collected by centrifugation for ^{1}H NMR analysis, leaving Zr-O byproducts behind. *For single-crystal digestion of polyUiO-68 prepared from ptpdc-10a-u.* Single crystals (<100 μg) were washed by exchanging the solvent with DMF (3x50 μL), and absolute ethanol (5x100 μL). The solvent was evaporated, and to the crystals was added a solution

containing 15 μL of 6 M NaOD and 5 μL of DMSO-d_6. The mixture sat at room temperature for 24 h. The mixture was evaporated, and resuspended in 40 μL of 1:1 DMSO-d_6:D_2O and the supernatant was collected by centrifugation for ^{1}H NMR. *For polyIRMOFs.* To 10 mg of polyMOF was added a solution containing 600 μL of DMSO-d_6 and 5 μL of DCl. The mixture was sonicated at room temperature for 1 h. The solution was used for ^{1}H NMR analysis.

SEM Measurements. The polyMOFs materials were filtered and transferred to conductive carbon tape on a sample holder and coated using a Ir-sputter coating for 7-14 sec. A Philips XL ESEM instrument was used for acquiring images. A 10 kV energy source under vacuum at a working distance at 10 mm was used during the measurements.

N_2 gas adsorption Measurements. Between 15-50 mg of sample was transferred to pre-weighed sample tubes. The samples were activated for 10 h at 105 °C using an ASAP 2020 Adsorption analyzer. After degassing, the sample tube was reweighed to obtain an accurate mass of the degassed sample. All measurements were obtained at 77 K using a liquid nitrogen bath. *Solvent-exchange for polyUiO-67.* polyUiO-67 was washed by exchanging the solvent with DMF overnight and then with MeOH three times a day over 3 d. The samples were transferred to a pre-weighed sample tube and evacuated in a vacuum line until no solvent was observed. *Solvent-exchange for polyUiO-68.* polyUiO-68 was washed by exchanging the solvent with EtOH three times a day over 3 d. The EtOH-exchanged samples were then soaked in liquid CO_2 in a Samdri-PVT-3D supercritical dryer for 6 h, purging the chamber with fresh liquid CO_2 every 30 min for the first 2 h, then purging every hour for 4 h. The temperature in the dryer was maintained between 0-10 °C during the solvent exchange with liquid CO_2. The temperature was then increased to 40 °C and maintained for 15 min. Finally, the supercritical CO_2 in the drying chamber was released over a period of 30 min. The samples were removed from the chamber and immediately

transferred to a dried, pre-weighed sample tube to prevent degradation. *Solvent-exchange and activation for polyIRMOFs.* polyIRMOFs were washed with $CHCl_3$ by soaking over 3 d with fresh $CHCl_3$ exchanged every 24 h. The crystals were transferred wet to a pre-weighed sample tube and evacuated in a vacuum line to remove residual solvent.

TGA/DSC Measurements. Between 5−10 mg of dried material was weighed for TGA measurements. The samples were analyzed under a stream of dried N_2 gas at a flow rate of 80 mL/min and heated from 35 to 800 °C with a ramping rate of 5 °C/min using a Mettler Toledo TGA/DSC 1 STAR System.

Single X-ray Diffraction Crystallography. A suitable crystal of polyUiO-68-10a-u was selected and placed on a Bruker APEX-II Ultra diffractometer, with a Mo-Kα Microfocus Rotating Anode and a APEX-II CCD area detector. The crystal was kept at 100 K during data collection. Using Olex2, the structure was solved with the ShelXT structure solution program using direct methods and refined with the XL refinement package using Least Squares minimisation.[25-27] Minor restraints, including bond distances restraints and planar restraints were applied along with occupancies <1, to the linker central phenyl ring and methylene spacer to allow for their refinement. The disordered alkyl spacer and solvent molecules within the framework were treated with the SQUEEZE protocol in PLATON to account for electron density.[28] The crystal data file of polyUiO-68-10a-u was deposited into the Cambridge Crystallographic Data Centre (CCDC) and assigned a number (1552853). Crystallographic data collection and refinement information is listed in Table 3S.2.

Supplemental Figures

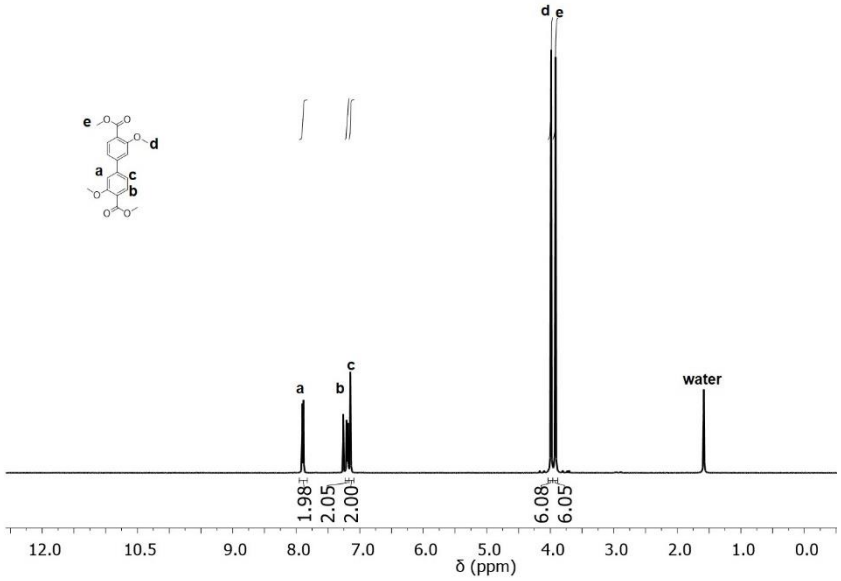

Figure 3S.1. [1]H NMR of compound **1**.

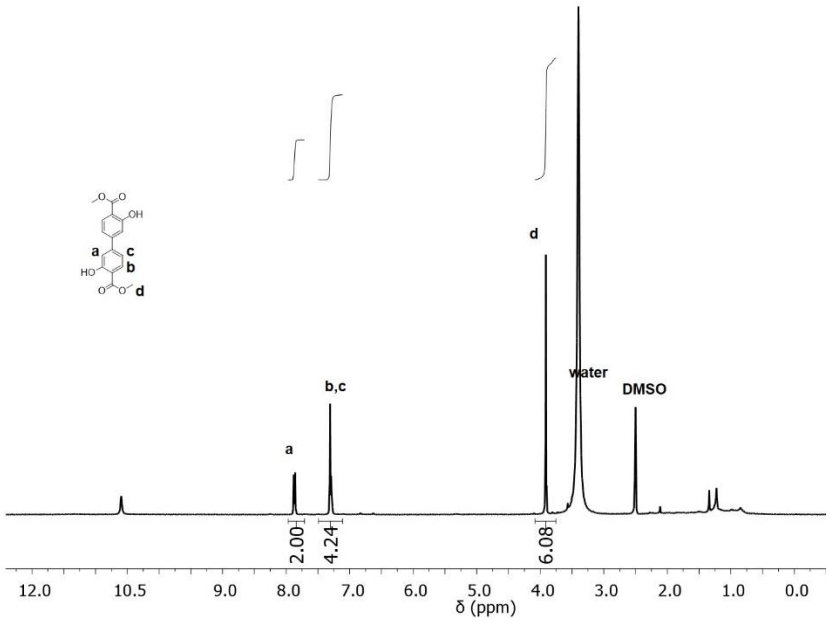

Figure 3S.2. [1]H NMR of compound **2**.

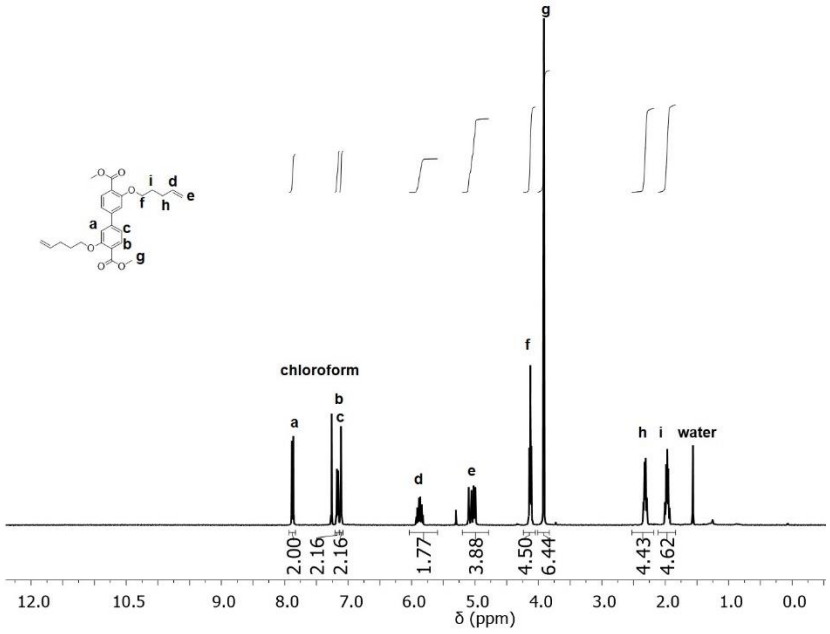

Figure 3S.3. [1]H NMR of compound **3**.

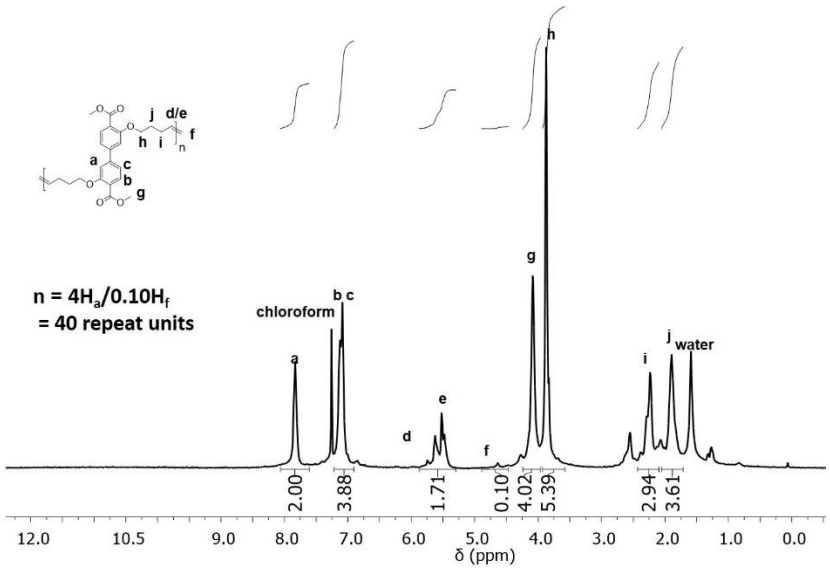

Figure 3S.4. [1]H NMR of pbpdc-8e-u. End-group analysis was used to determine number of repeat units and M_n.

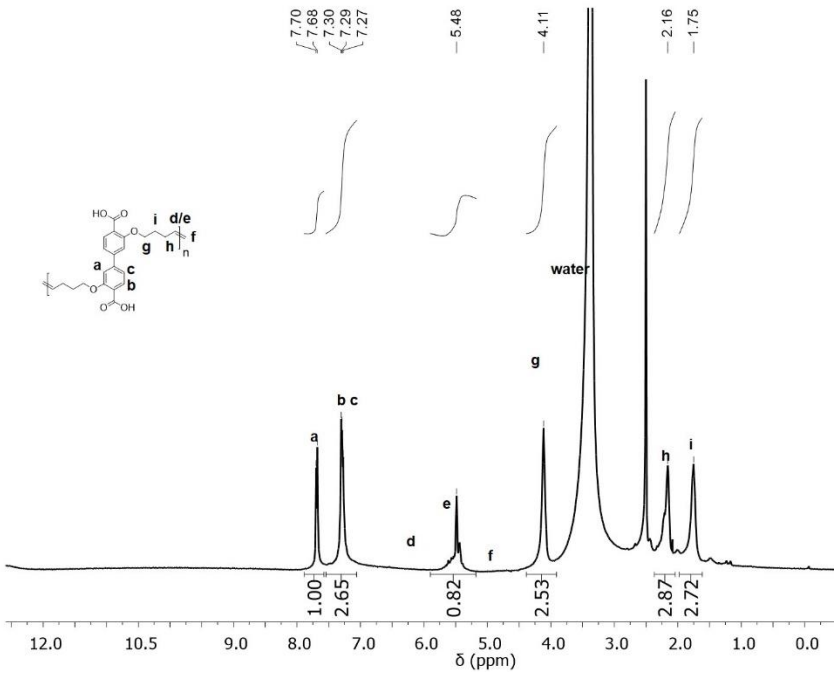

Figure 3S.5. [1]H NMR of pbpdc-8a-u.

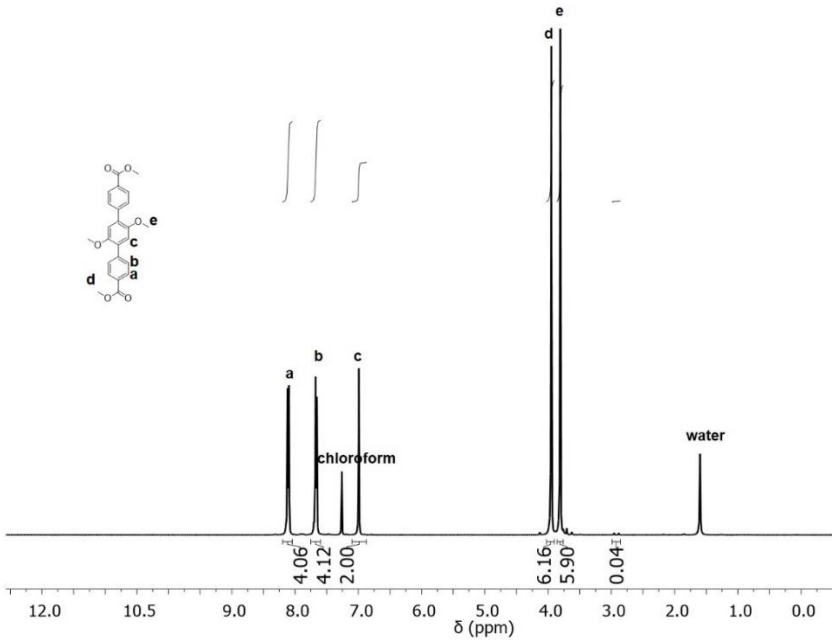

Figure 3S.6. [1]H NMR of compound **4.**

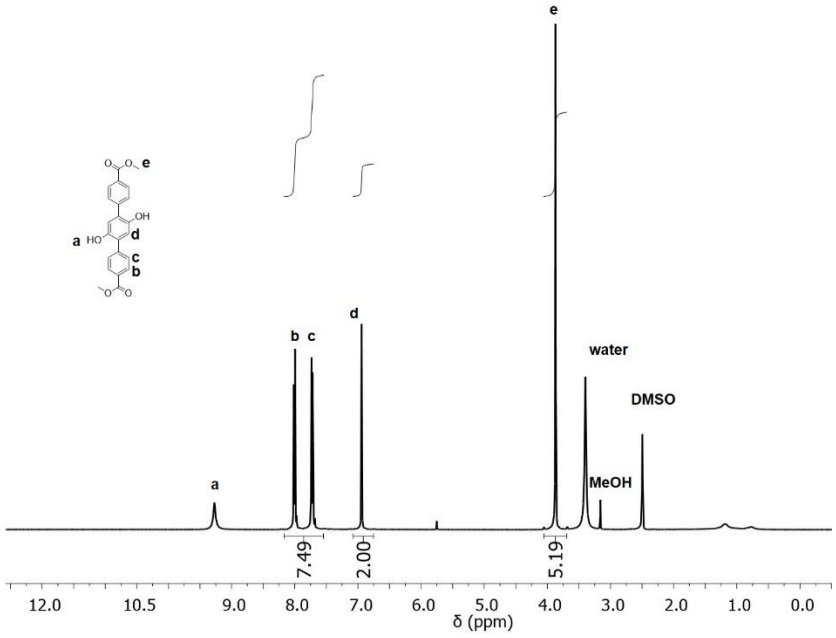

Figure 3S.7. ^{1}H NMR of compound **5.**

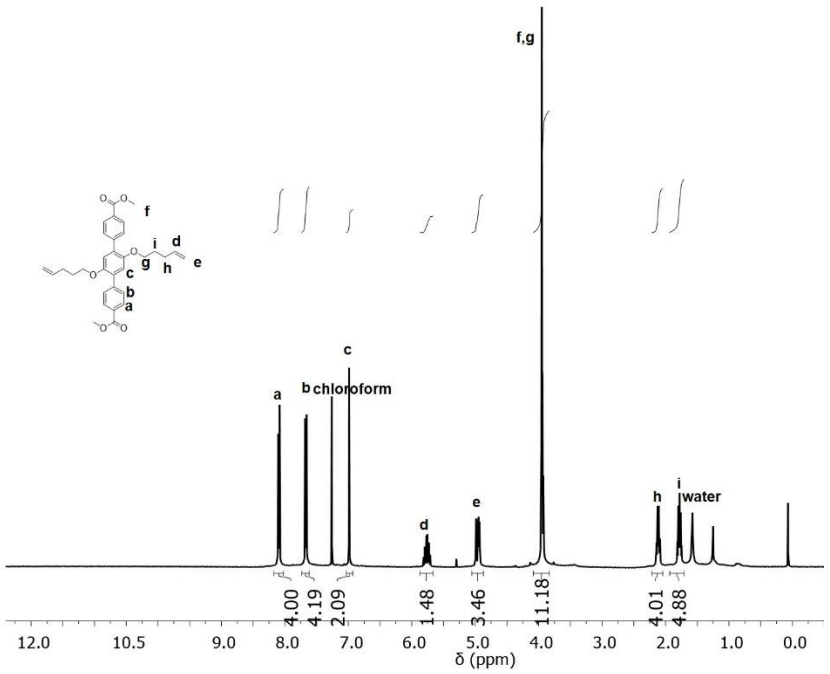

Figure 3S.8. ^{1}H NMR of tpdc-8e-u, compound **6.**

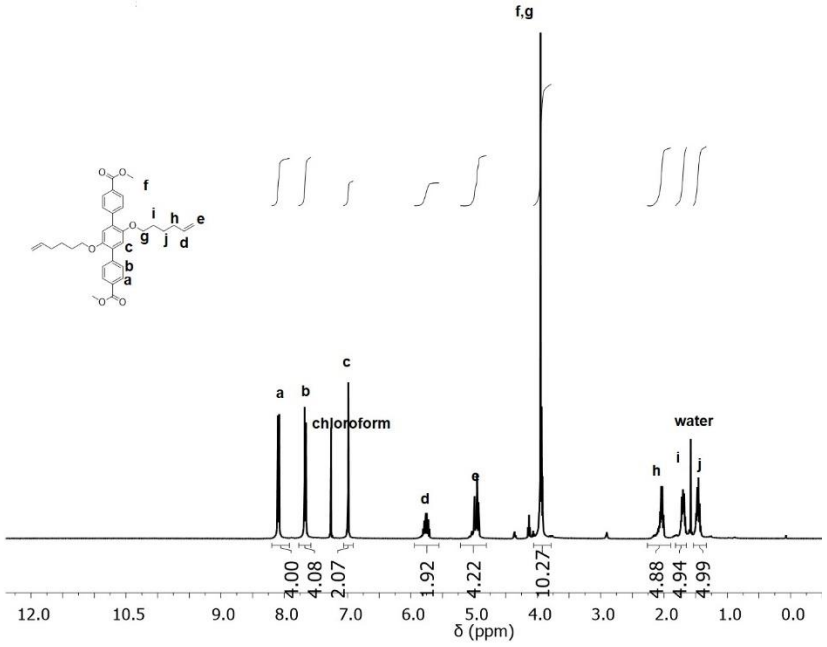

Figure 3S.9. [1]H NMR of compound tpdc-10e-u, compound **7**.

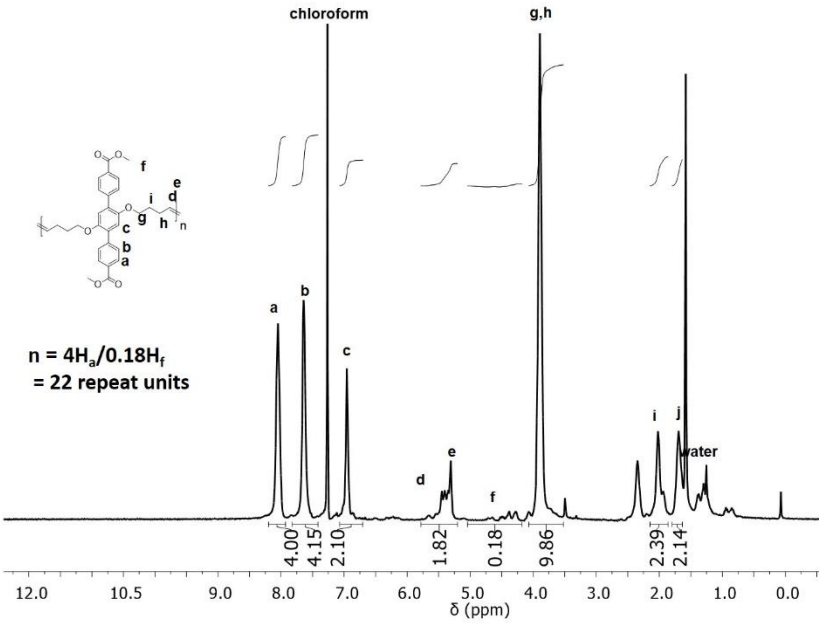

Figure 3S.10. [1]H NMR of ptpdc-8e-u. End-group analysis was used to determine number of repeat units and M_n.

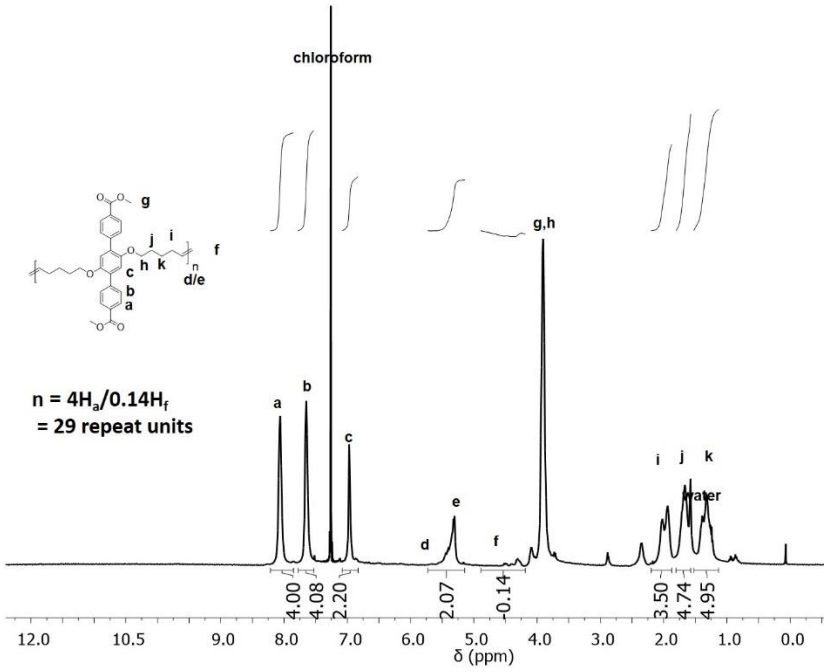

Figure 3S.11. [1]H NMR of ptpdc-10e-u. End-group analysis was used to determine number of repeat units and M_n.

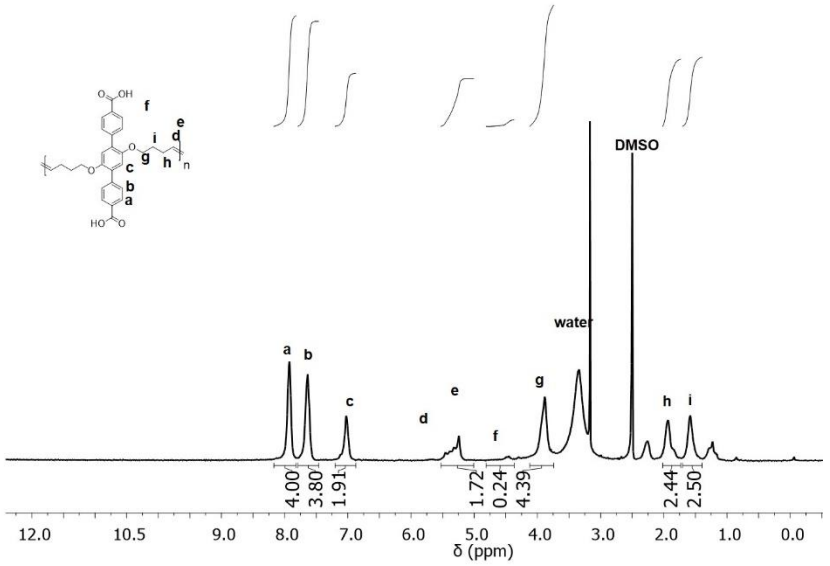

Figure 3S.12. [1]H NMR of ptpdc-8a-u.

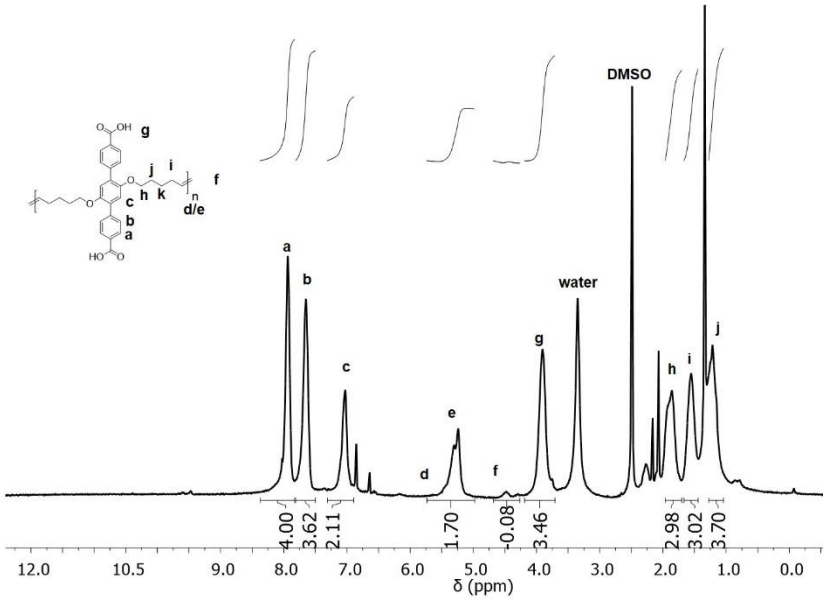

Figure 3S.13. [1]H NMR of ptpdc-10a-u.

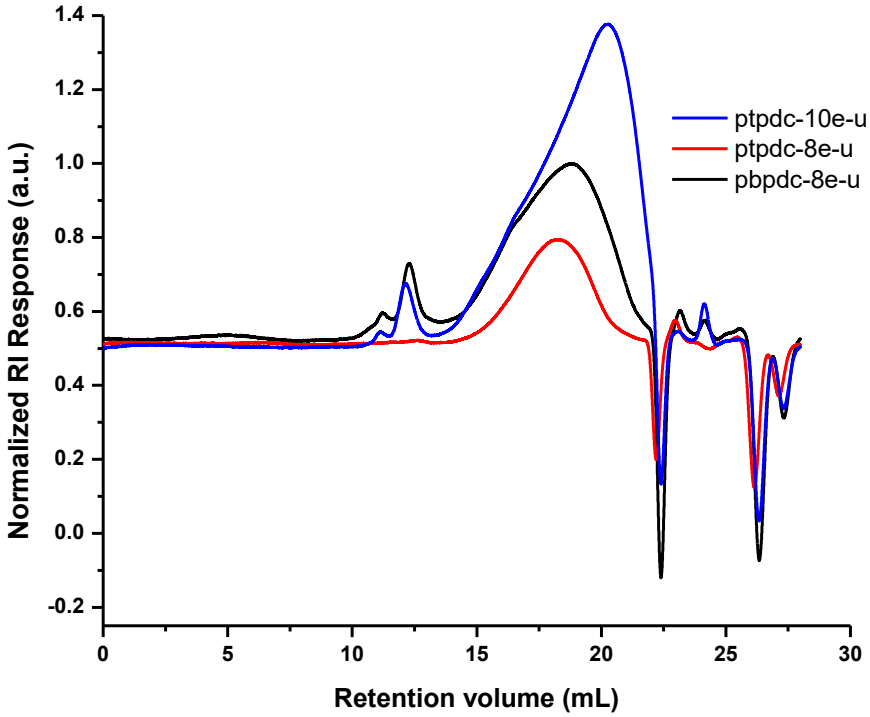

Figure 3S.14. GPC traces of polymer ester ligands pbpdc-*x*e-u and ptpdc-*x*e-u.

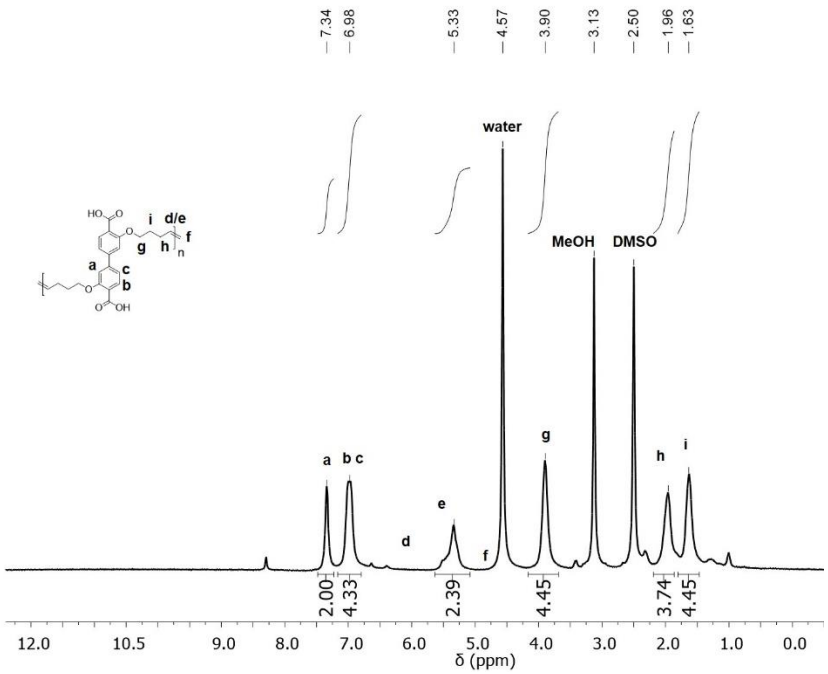

Figure 3S.15. [1]H NMR of digested polyUiO-67-8a-u.

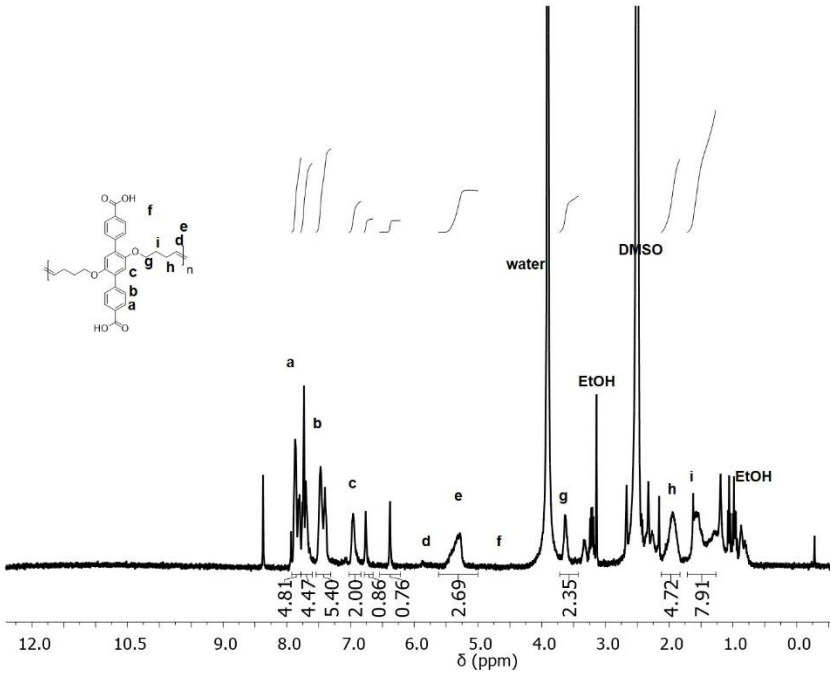

Figure 3S.16. [1]H NMR of digested polyUiO-68-8a-u.

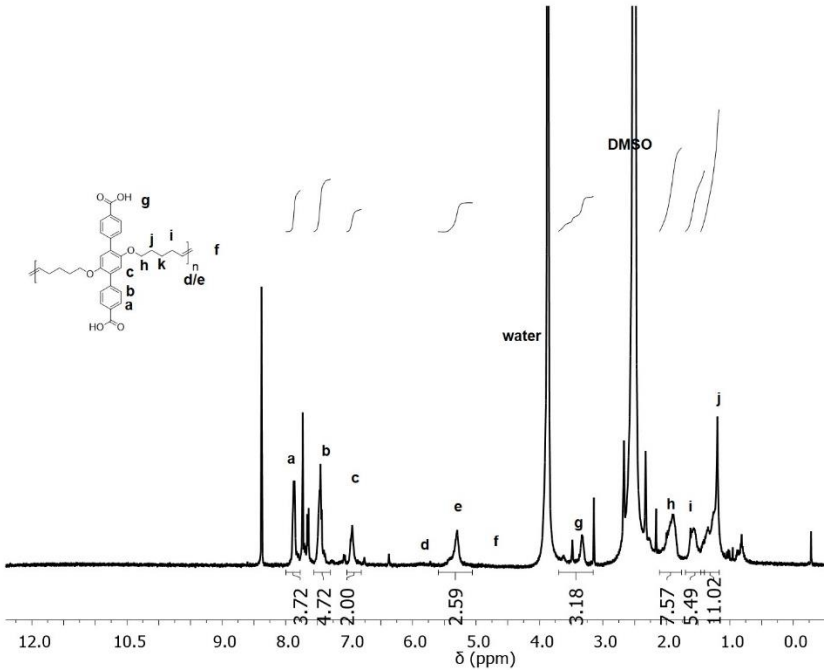

Figure 3S.17. [1]H NMR of digested polyUiO-68-10a-u.

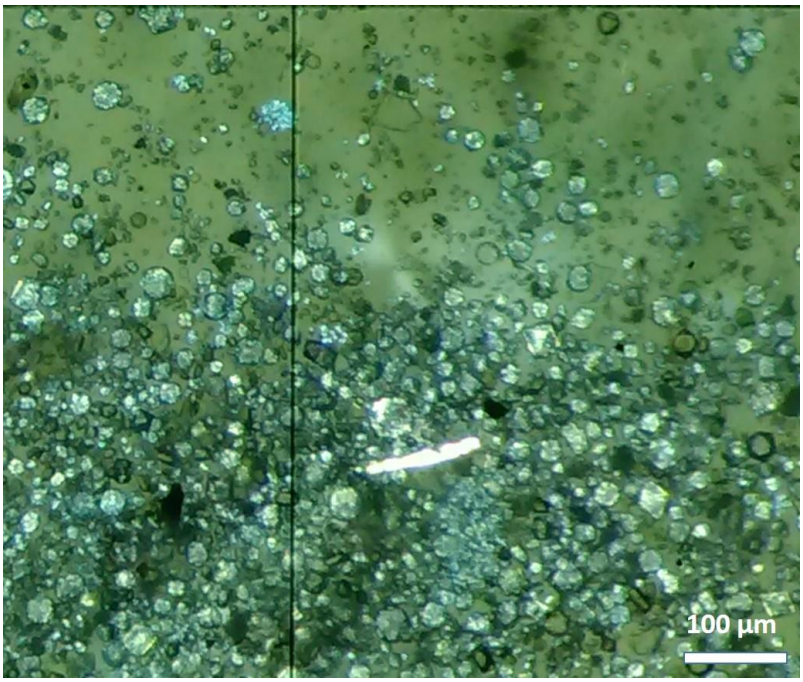

Figure 3S.18. Optical image of single crystals of polyUiO-68-10a-u used for [1]H NMR.

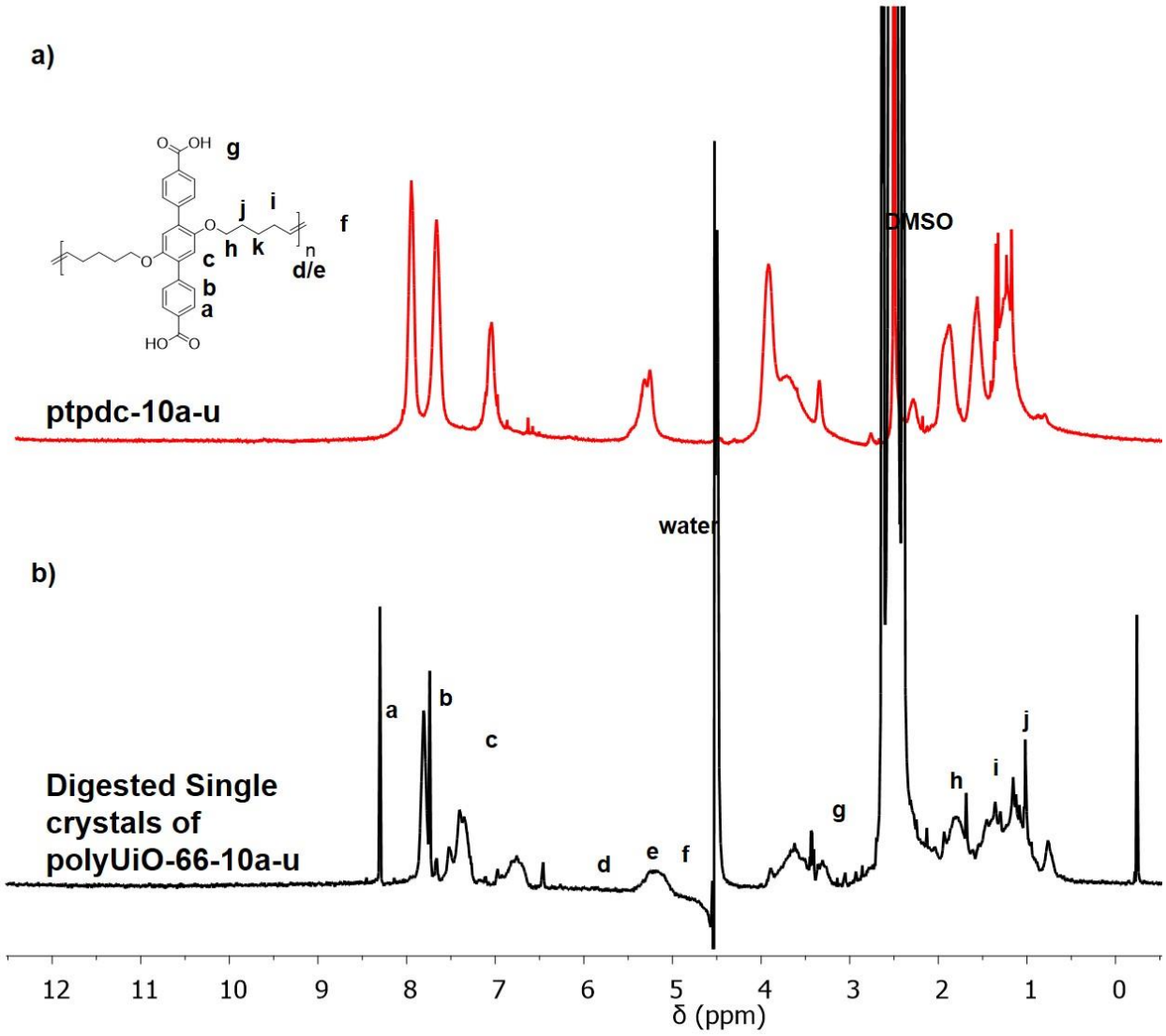

Figure 3S.19. The [1]HNMR of the digested crystals (black trace) is compared to the 1H NMR of the ptpdc-10a-u (red trace).

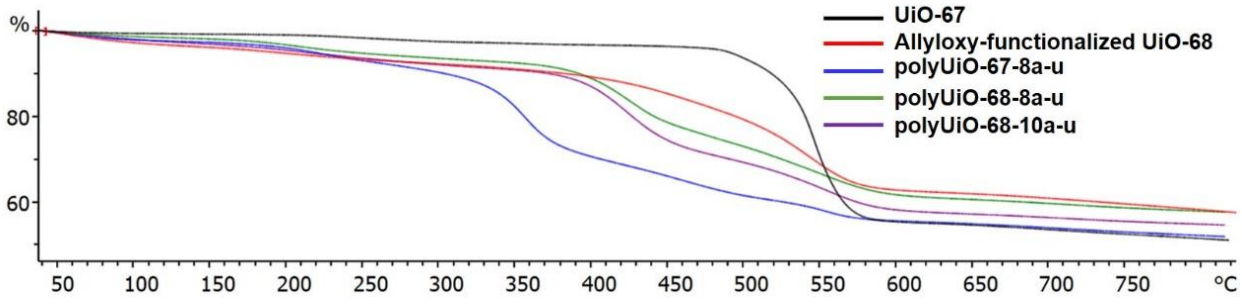

Figure 3S.20. TGA curves of UiO-67, UiO-68, polyUiO-67-8a-u and polyUiO-68-*x*a-u, where x = 8 or 10.

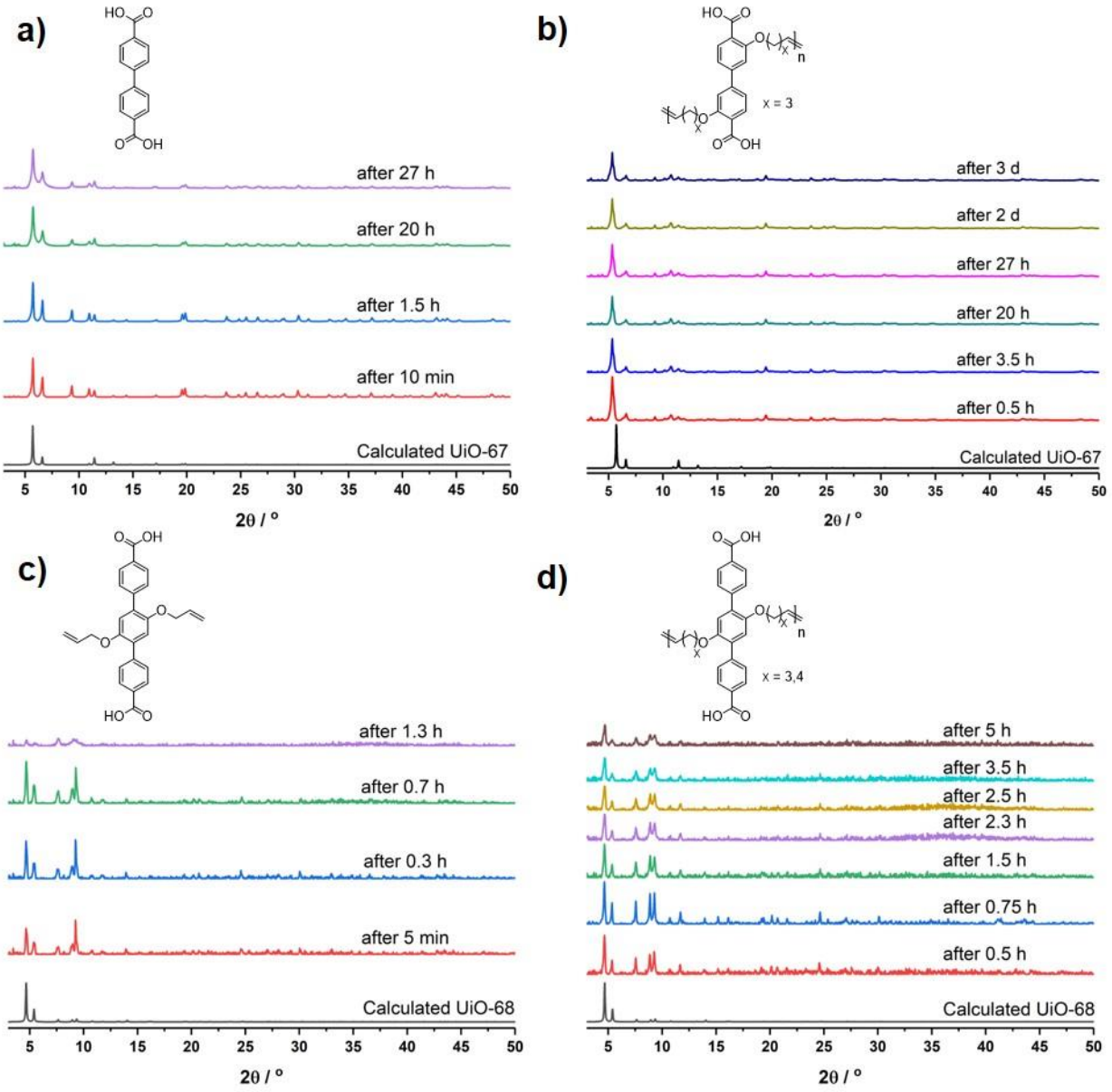

Figure 3S.21. Stability test of: a) native UiO-67 after 20 h; b) polyUiO-67 after 3 d; c) allyloxy-functionalized UiO-68 after 1.5h; d) polyUiO-68 after 5 h. Both polyUiO-67 and polyUiO-68 exhibit high crystallinity for extended times, when compared to their native counterparts, UiO-67 and allyloxy-functionalized UiO-68, respectively.

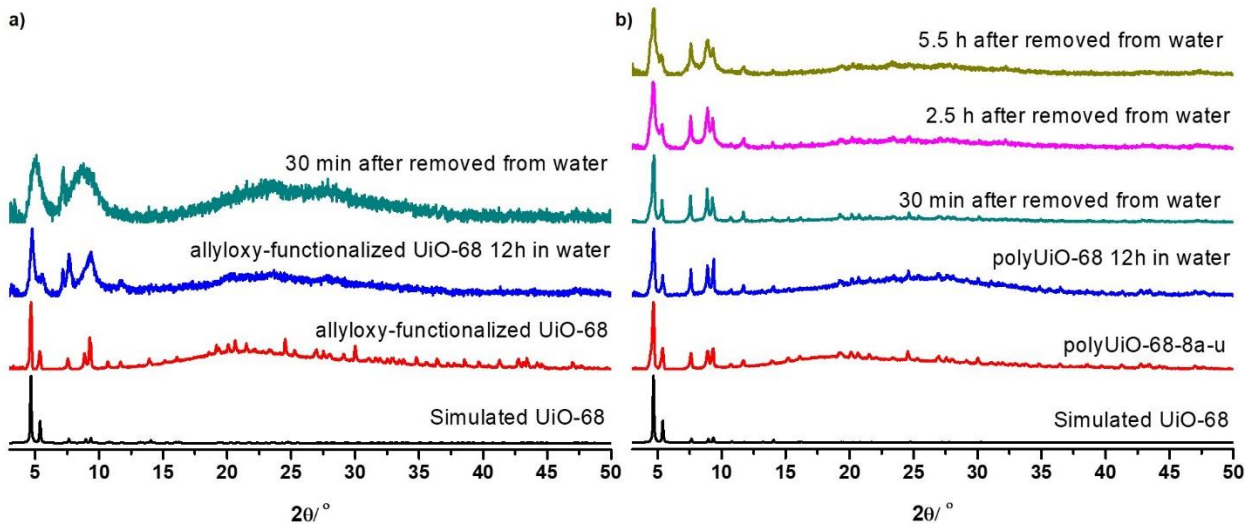

Figure 3S.22. Chemical stability test for: a) allyloxy-functionalized UiO-68 and b) polyUiO-68-8a-u after being submerged in water for 12 h and allowed to dry over time.

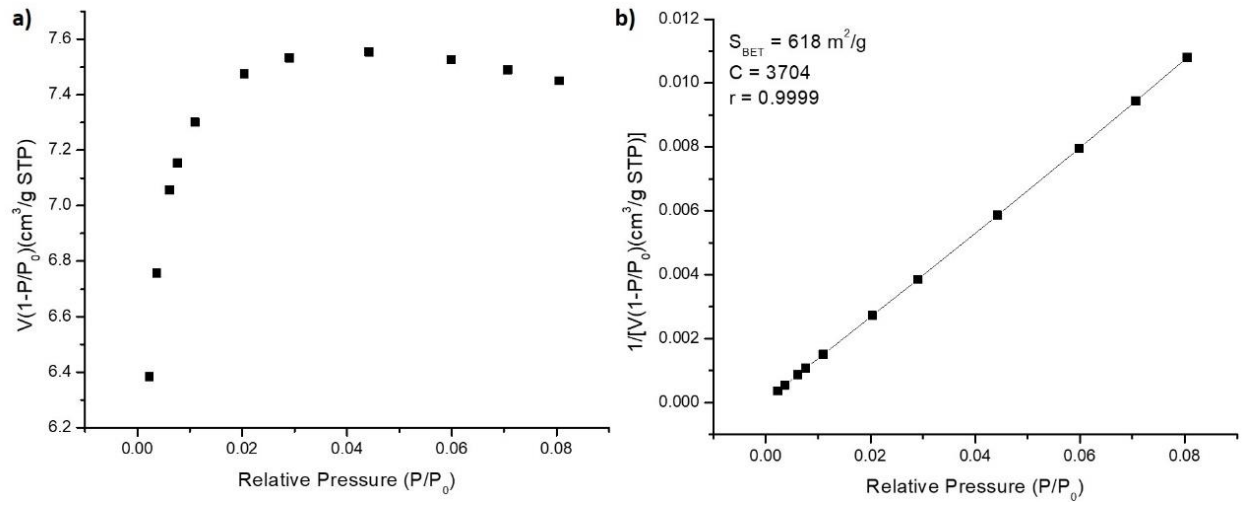

Figure 3S.23. a) Rouquerol plot for polyUiO-67-8a-u. Only points below $P/P_0 = 0.046$ satisfy the criteria for applying the BET theory. b) Plot of the linear region for the BET equation for polyUiO-67-8a-u.

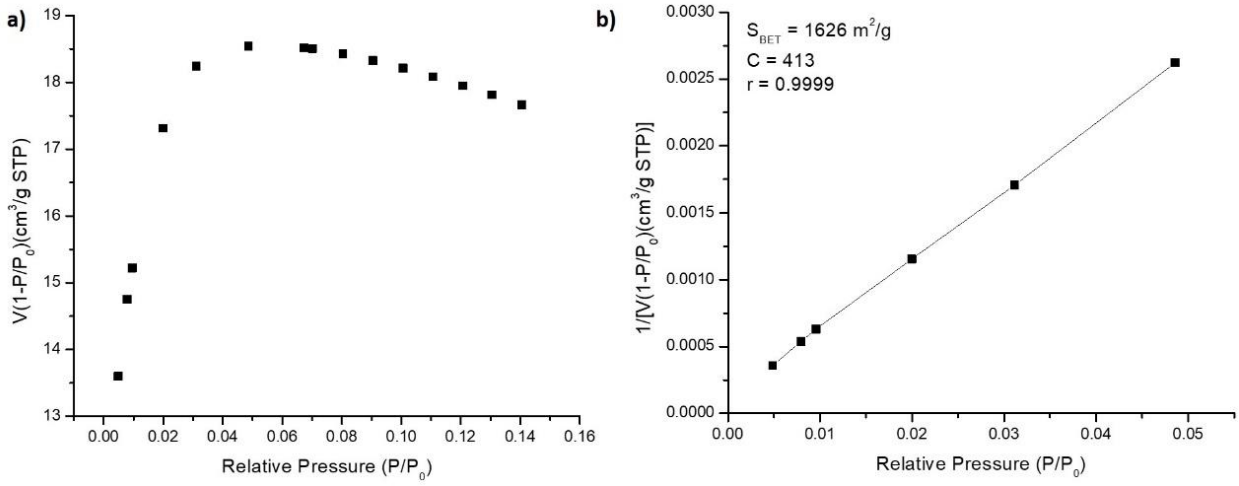

Figure 3S.24. a) Rouquerol plot for polyUiO-68-8a-u. Only points below $P/P_0 = 0.050$ satisfy the criteria for applying the BET theory. b) Plot of the linear region for the BET equation for polyUiO-68-8a-u.

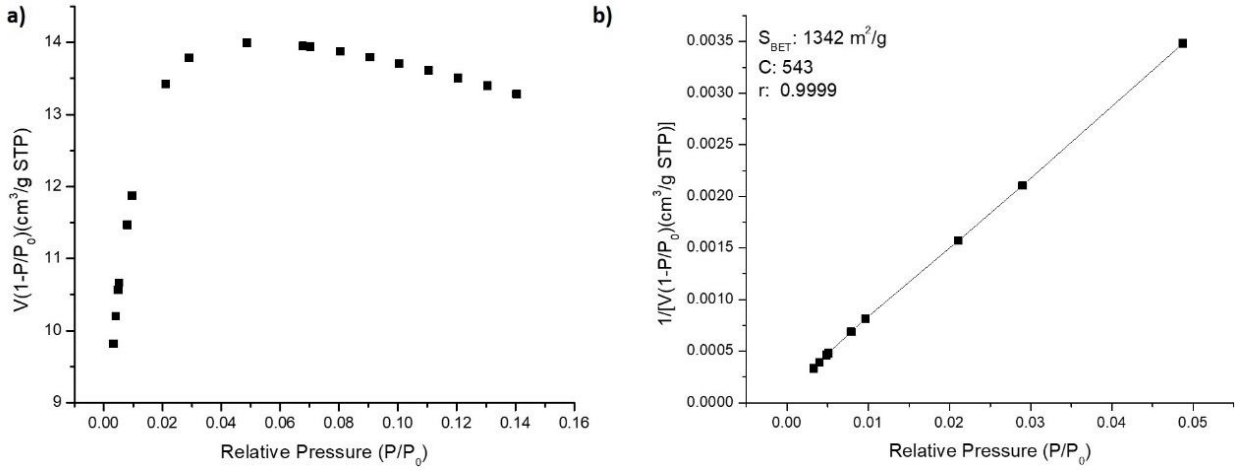

Figure 3S.25. a) Rouquerol plot for polyUiO-68-10a-u. Only points below $P/P_0 = 0.050$ satisfy the criteria for applying the BET theory. b) Plot of the linear region for the BET equation for polyUiO-68-10a-u.

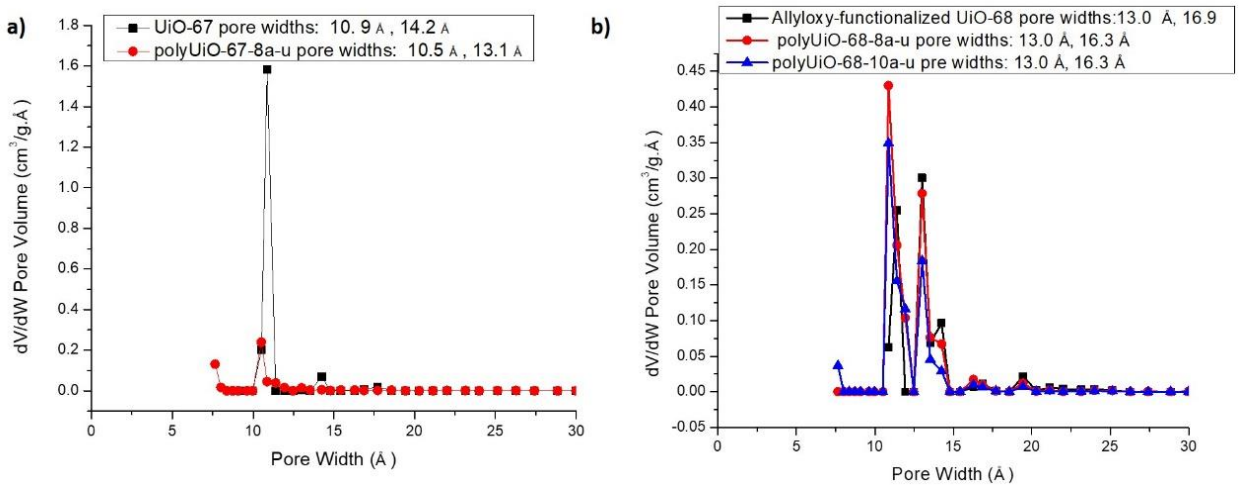

Figure 3S.26. The pore size distributions of a) UiO-67 and polyUiO-67-8a-u, and b) polyUiO-68-*x*a-u are presented.

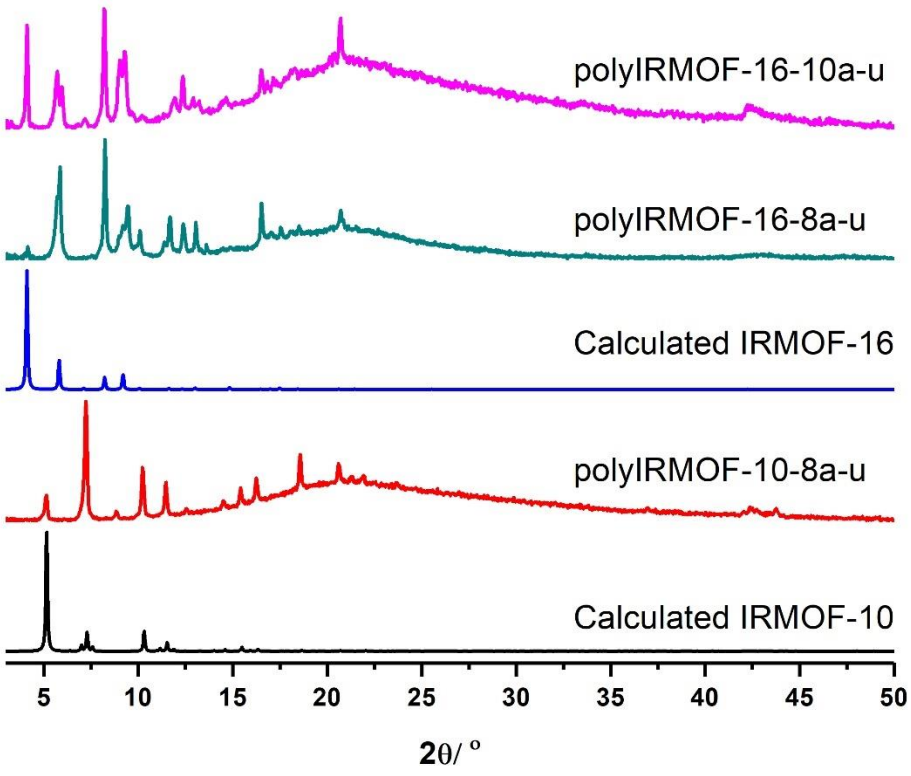

Figure 3S.27. PXRD patterns for polyIRMOF-10-8a-u and polyIRMOF-16-*x*a-u (*x* = 8, 10).

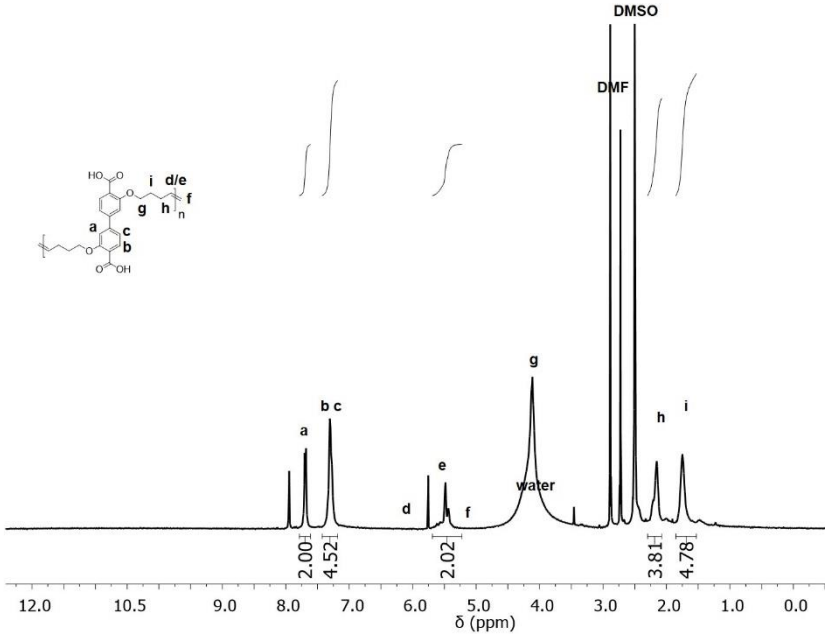

Figure 3S.28. [1]H NMR of digested polyIRMOF-10-8a-u.

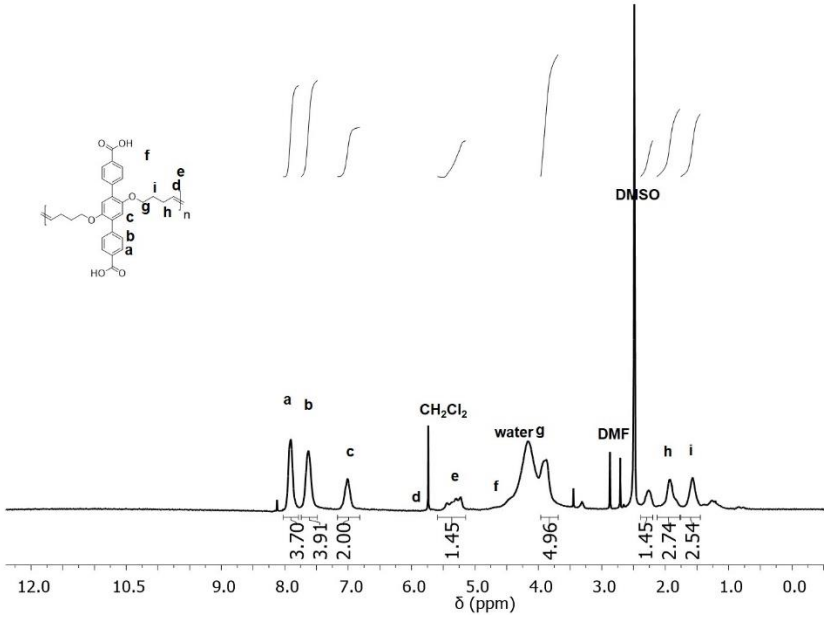

Figure 3S.29. [1]H NMR of digested polyIRMOF-16-8a-u.

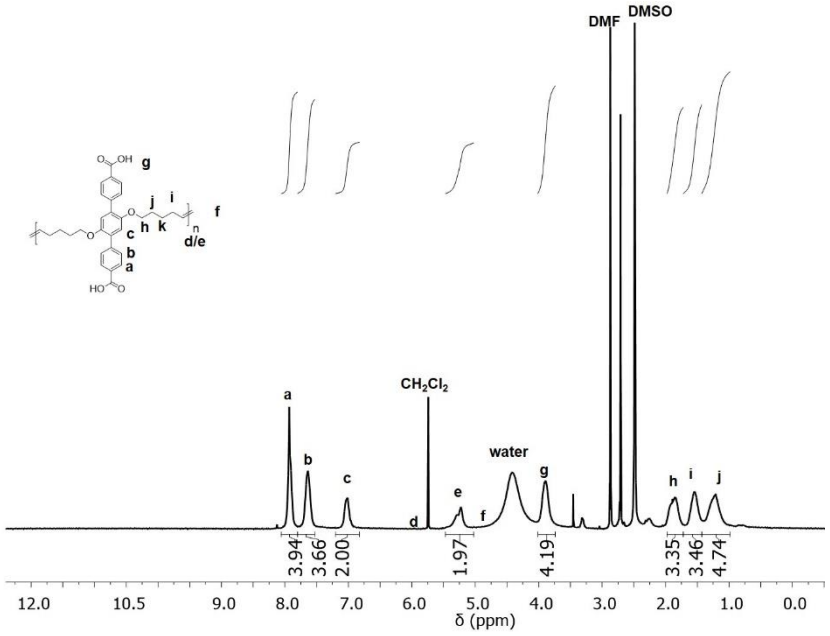

Figure 3S.30. [1]H NMR of digested polyIRMOF-16-10a-u.

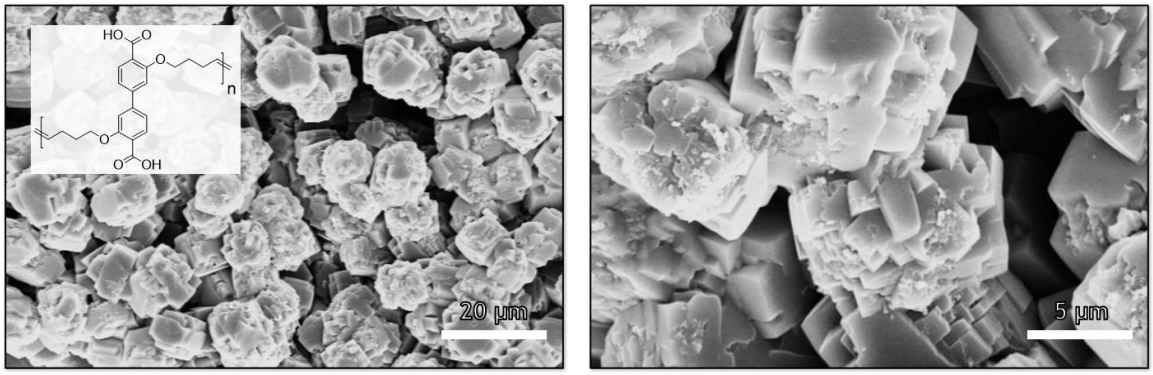

Figure 3S.31. SEM images of polyIRMOF-10-8a-u prepared from pbpdc-8a-u.

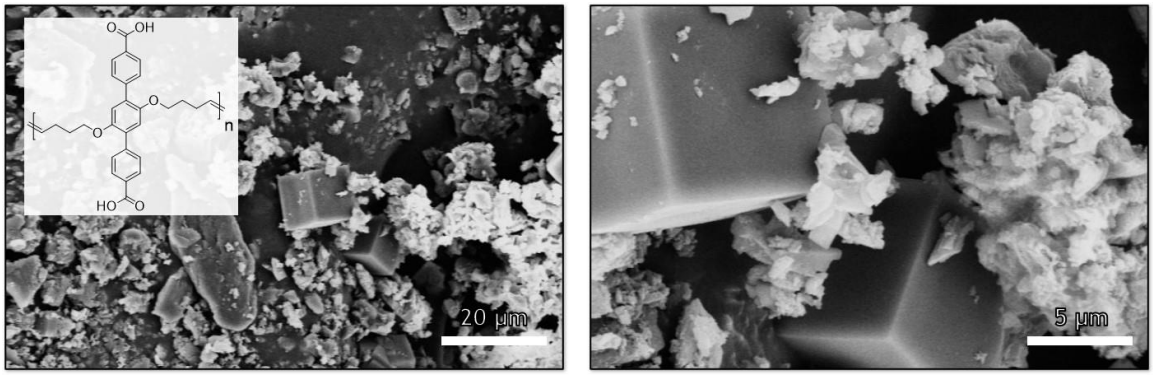

Figure 3S.32. SEM images of polyIRMOF-16-8a-u prepared from ptpdc-8a-u.

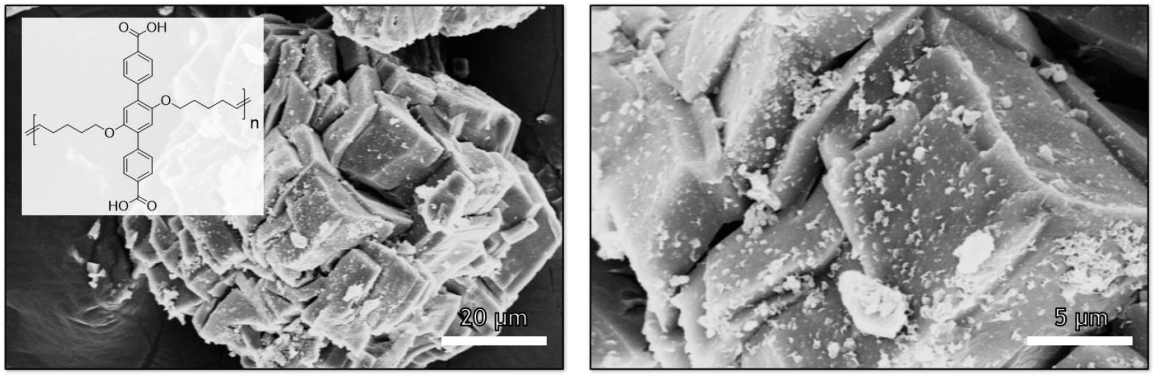

Figure 3S.33. SEM images of polyIRMOF-16-8a-u prepared from ptpdc-10a-u.

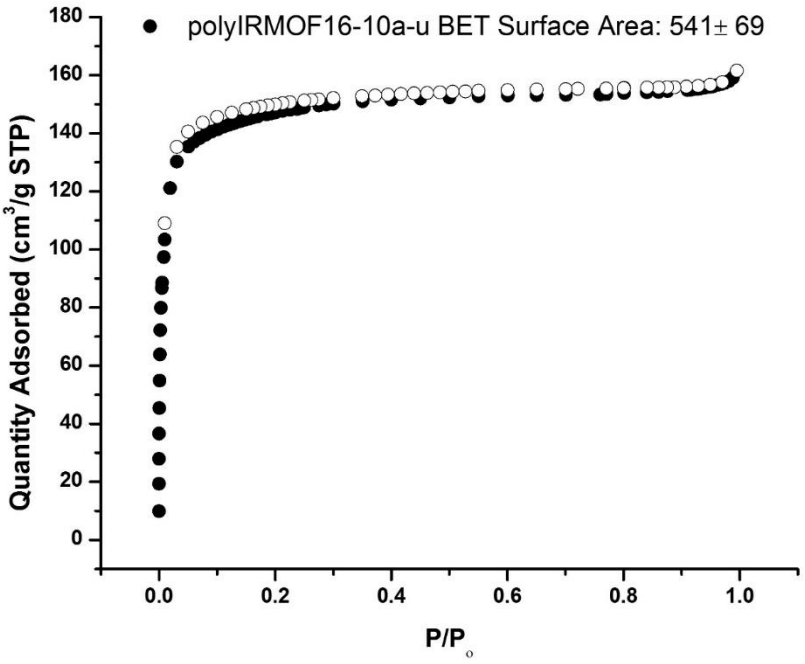

Figure 3S.34. N_2-Isotherm of polyIRMOF-16-10a-u.

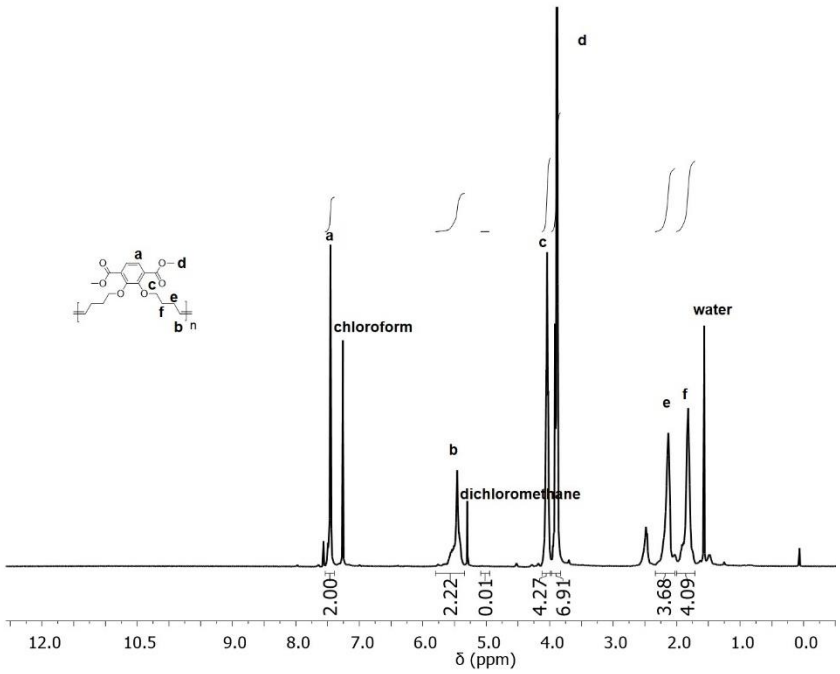

Figure 3S.35. ^{1}H NMR of *o*-pbdc-8e-u.

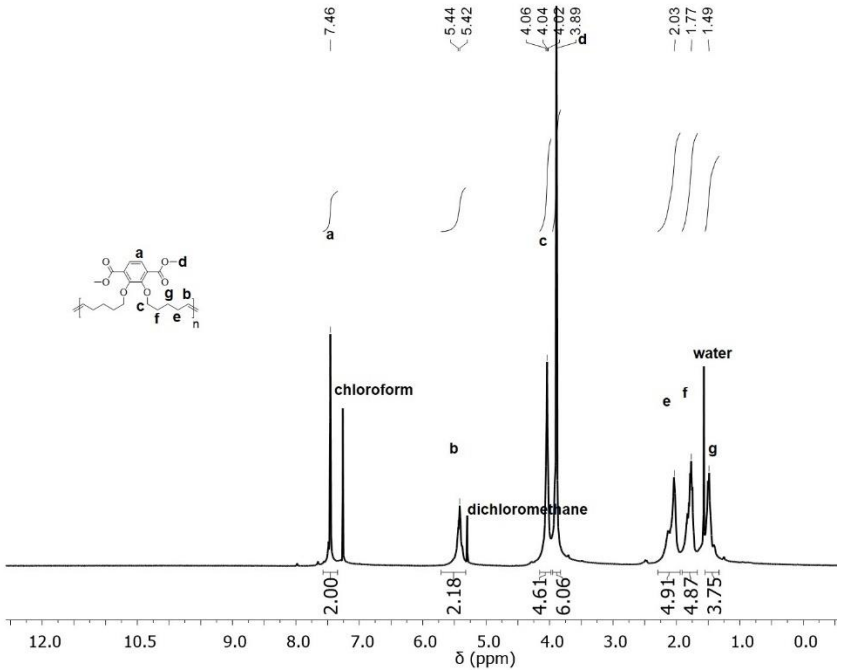

Figure 3S.36. ^{1}H NMR of *o*-pbdc-10e-u.

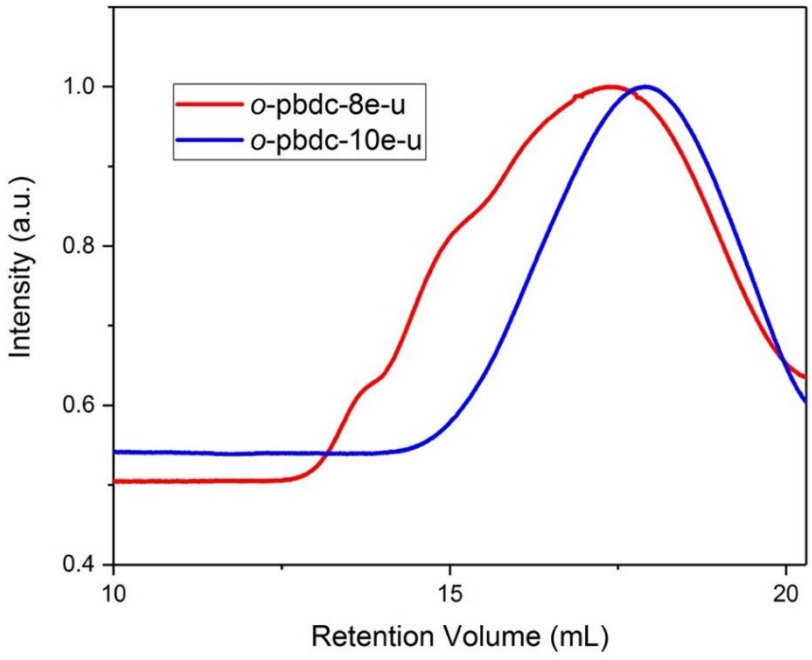

Figure 3S.37. GPC traces of polymer esters in THF.

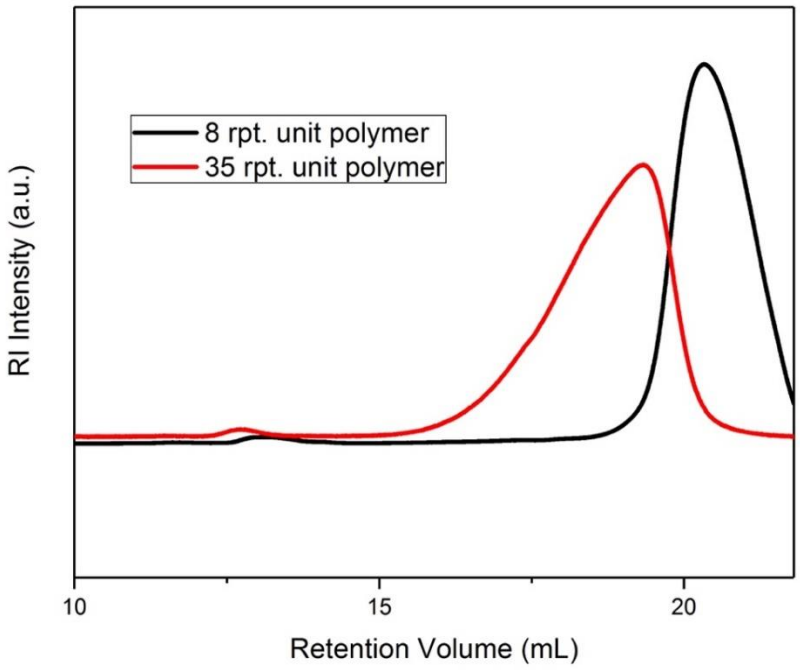

Figure 3S.38. GPC traces of fractionated *o*-pbdc-8e-u in THF.

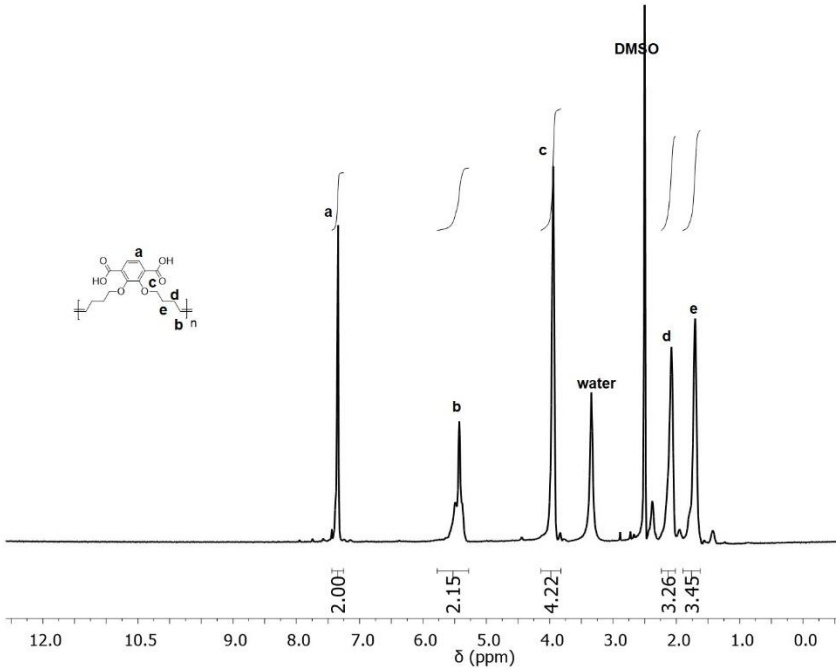

Figure 3S.39. ^{1}H NMR of *o*-pbdc-8a-u.

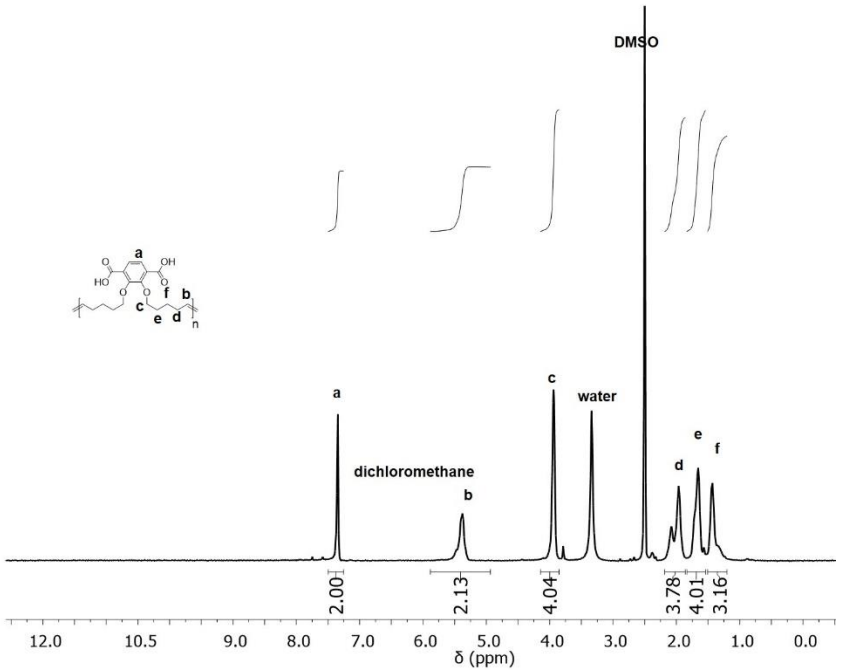

Figure 3S.40. ^{1}H NMR of *o*-pbdc-10a-u.

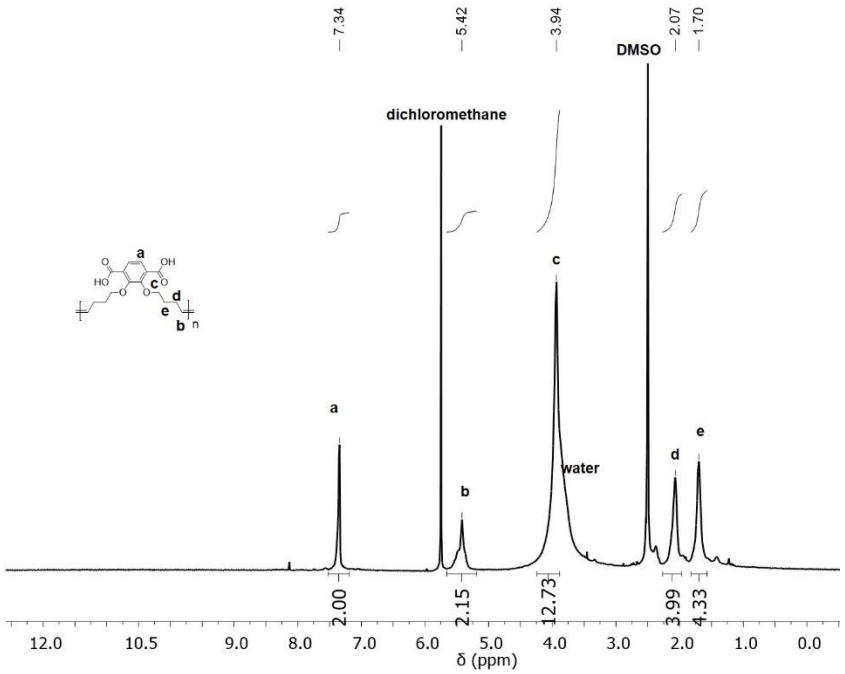

Figure 3S.41. ^{1}H NMR of digested *o*-polyIRMOF-1-8a-u.

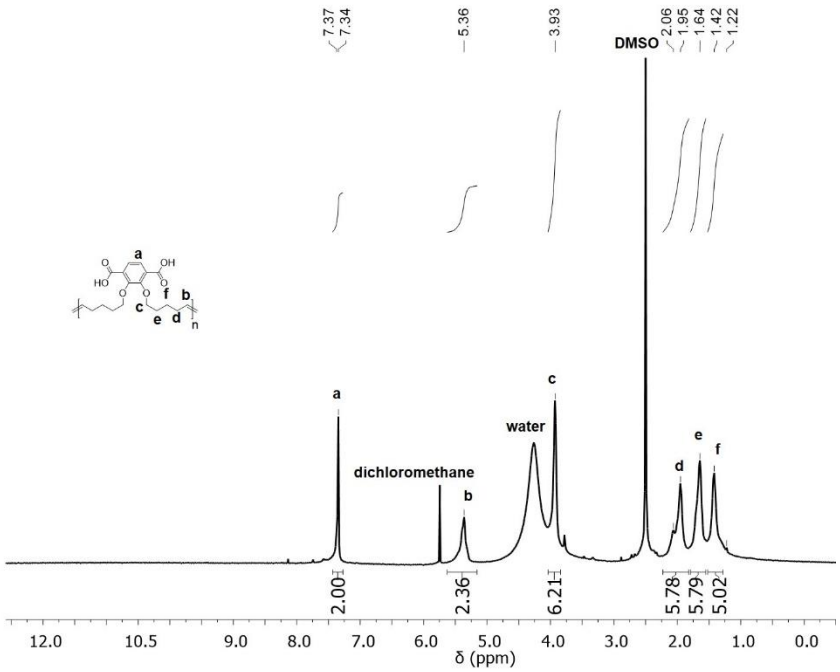

Figure 3S.42. [1]H NMR of digested *o*-polyIRMOF-1-10a-u.

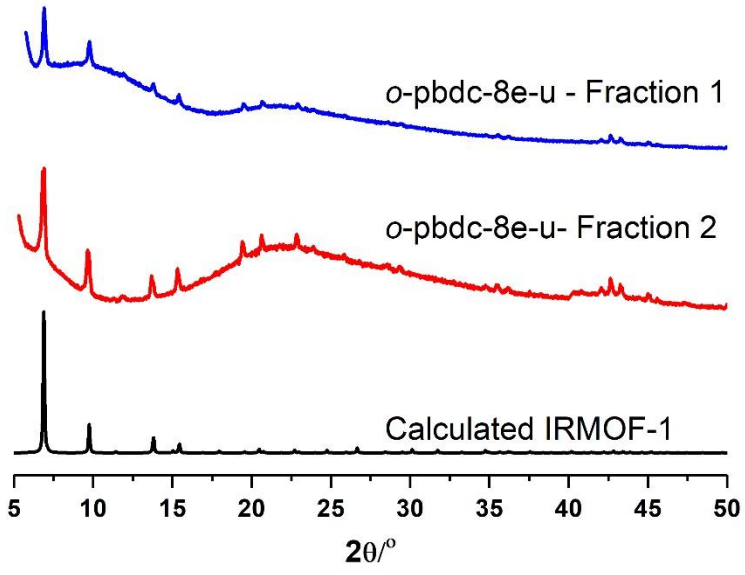

Figure 3S.43. PXRD of fractionated *o*-polyIRMOF-1-8a-u.

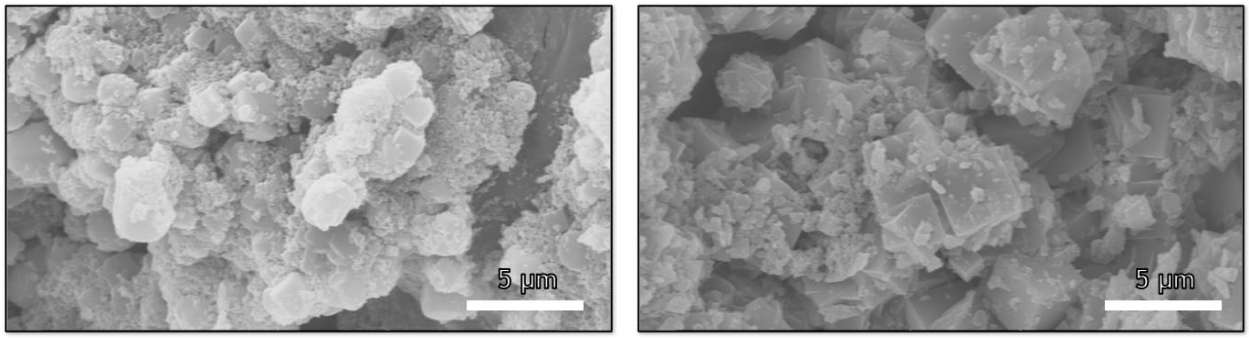

Figure 3S.44. SEM images of polyIRMOF-1 synthesized with o-pbdc-8a-u: fraction 1 (left) and fraction 2 (right).

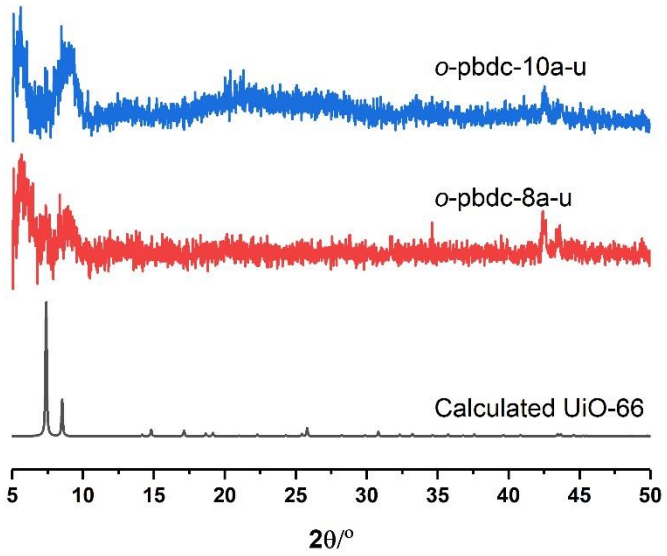

Figure 3S.45. PXRD of failed attempts at synthesis of *o*-polyUiO-66 with two polymer ligands, *o*-pbdc-8a-u in red, *o*-pbdc-10a-u in blue, and calculated UiO-66 in black.

Table 3S.1. ^{1}H NMR end-group analysis of the polymer acid ligands pbpdc-*x*a-u and ptpdc-*x*a-u.

Ligand	M_n	DP
pbpdc-8a-u	17,560	40
ptpdc-8a-u	9,270	18
ptpdc-10a-u	8,145	15

Table 3S.2. Crystal data and structure refinement for polyUiO-68-10a-u.

CCDC Identification code	1552853
Empirical formula	$C_{114}O_{38}Zr_6$
Formula weight	2524.46
Temperature/K	100.0
Crystal system	cubic
Space group	*F*m-3m
a/Å	32.6990(13)
b/Å	32.6990(13)
c/Å	32.6990(13)
α/°	90
β/°	90
γ/°	90
Volume/Å^3	34963(4)
Z	4
ρ_{calc}g/cm^3	0.480
μ/mm^{-1}	0.199
F(000)	4912.0
Crystal size/mm^3	0.1 × 0.075 × 0.075
Radiation	MoKα (λ = 0.71073)
2Θ range for data collection/°	2.49 to 50.066
Index ranges	-38 ≤ h ≤ 37, -38 ≤ k ≤ 34, -38 ≤ l ≤ 37
Reflections collected	70023
Independent reflections	1586 [R_{int} = 0.0862, R_{sigma} = 0.0190]
Data/restraints/parameters	1586/84/68
Goodness-of-fit on F^2	1.159
Final *R* indexes [I>=2σ (I)]	R_1 = 0.0597, wR_2 = 0.1709
Final *R* indexes [all data]	R_1 = 0.0702, wR_2 = 0.1801
Largest diff. peak/hole / e Å^{-3}	0.66/-0.68

Table 3S.3. GPC characterization of fractionated *o*-pbdc-*x*e-u.

Ligand	M_n (GPC)	M_w/M_n	DP (GPC)
o-pbdc-8e-u	2,700	1.45	8
o-pbdc-10e-u	11,700	1.63	35

3.6 Acknowledgements

Chapter 3, in part, is a reprint of the following materials as listed: "Isoreticular expansion of polyMOFs achieves high surface area materials" *Chem. Commun.*, **2017,** *53*, 10684-10687; "polyMOF Formation from Kinked Polymer Ligands via ortho-Substitution" *Isr. J. Chem.*, **2018,** *58*, 1123-1126. The dissertation author was a coauthor of both these manuscripts. The dissertation

author gratefully acknowledges the contributions of coauthors Giulia E. M. Schukraft, Benjamin L. Dick and Seth M. Cohen in the manuscript titled, “Isoreticular expansion of polyMOFs achieves high surface area materials”. The disseration author also gratefully acknowledges Joseph M. Palomba and Seth M. Cohen for the manuscript titled, “polyMOF Formation from Kinked Polymer Ligands via ortho-Substitution”.

3.7 References

1. Eddaoudi, M.; Kim, J.; Rosi, N.; Vodak, D.; Wachter, J.; O'Keeffe, M.; Yaghi, O. M., Systematic Design of Pore Size and Functionality in Isoreticular MOFs and Their Application in Methane Storage. *Science* **2002,** *295*, 469-472.

2. Cavka, J. H.; Jakobsen, S.; Olsbye, U.; Guillou, N.; Lamberti, C.; Bordiga, S.; Lillerud, K. P., A new zirconium inorganic building brick forming metal organic frameworks with exceptional stability. *J. Am. Chem. Soc.* **2008,** *130*, 13850-13851.

3. Schaate, A.; Roy, P.; Godt, A.; Lippke, J.; Waltz, F.; Wiebcke, M.; Behrens, P., Modulated Synthesis of Zr-Based Metal-Organic Frameworks: From Nano to Single Crystals. *Chem. Eur J.* **2011,** *17*, 6643-6651.

4. Furukawa, H.; Go, Y. B.; Ko, N.; Park, Y. K.; Uribe-Romo, F. J.; Kim, J.; O’Keeffe, M.; Yaghi, O. M., Isoreticular Expansion of Metal–Organic Frameworks with Triangular and Square Building Units and the Lowest Calculated Density for Porous Crystals. *Inorg. Chem.* **2011,** *50*, 9147-9152.

5. Liu, J.; Lukose, B.; Shekhah, O.; Arslan, H. K.; Weidler, P.; Gliemann, H.; Bräse, S.; Grosjean, S.; Godt, A.; Feng, X.; Müllen, K.; Magdau, I.-B.; Heine, T.; Wöll, C., A novel series of isoreticular metal organic frameworks: realizing metastable structures by liquid phase epitaxy. *Sci. rep.* **2012,** *2*, 921.

6. Surble, S.; Serre, C.; Mellot-Draznieks, C.; Millange, F.; Ferey, G., A new isoreticular class of metal-organic-frameworks with the MIL-88 topology. *Chem. Commun.* **2006**, 284-286.

7. Yuan, D. Q.; Zhao, D.; Sun, D. F.; Zhou, H. C., An Isoreticular Series of Metal-Organic Frameworks with Dendritic Hexacarboxylate Ligands and Exceptionally High Gas-Uptake Capacity. *Angew. Chem. Int. Ed.* **2010,** *49*, 5357-5361.

8. Ayala, S.; Zhang, Z.; Cohen, S. M., Hierarchical structure and porosity in UiO-66 polyMOFs. *Chem. Commun.* **2017,** *53*, 3058-3061.

9. Zhang, Z. J.; Nguyen, H. T. H.; Miller, S. A.; Cohen, S. M., polyMOFs: A Class of Interconvertible Polymer-Metal-Organic-Framework Hybrid Materials. *Angew. Chem. Int. Ed.* **2015,** *54*, 6152-6157.

10. Zhang, Z. J.; Nguyen, H. T. H.; Miller, S. A.; Ploskonka, A. M.; DeCoste, J. B.; Cohen, S. M., Polymer-Metal-Organic Frameworks (polyMOFs) as Water Tolerant Materials for Selective Carbon Dioxide Separations. *J. Am. Chem. Soc.* **2016,** *138*, 920-925.

11. Palomba, J. M.; Ayala Jr., S.; Cohen, S. M., polyMOF Formation from Kinked Polymer Ligands via ortho-Substitution. *Isr. J. Chem.* **2018,** *58*, 1123-1126.

12. Schukraft, G. E. M.; Ayala, S.; Dick, B. L.; Cohen, S. M., Isoreticular expansion of polyMOFs achieves high surface area materials. *Chem. Commun.* **2017,** *53*, 10684-10687.

13. Ayala Jr., S.; Cohen, S. M., PolyMOFs. In *Hybrid Metal-Organic Framework and Covalent Organic Framework Polymers*, Wang, B., Ed. The Royal Society of Chemistry: In Preparation.

14. Li, Y. A.; Yang, S.; Liu, Q. K.; Chen, G. J.; Ma, J. P.; Dong, Y. B., Pd(0)@UiO-68-AP: chelation-directed bifunctional heterogeneous catalyst for stepwise organic transformations. *Chem. Commun.* **2016,** *52*, 6517-6520.

15. Gui, B.; Hu, G. P.; Zhou, T. L.; Wang, C., Pore surface engineering in a zirconium metal-organic framework via thiol-ene reaction. *J Solid State Chem* **2015,** *223*, 79-83.

16. Mondloch, J. E.; Katz, M. J.; Planas, N.; Semrouni, D.; Gagliardi, L.; Hupp, J. T.; Farha, O. K., Are Zr6-based MOFs water stable? Linker hydrolysis vs. capillary-force-driven channel collapse. *Chem. Commun.* **2014,** *50*, 8944-8946.

17. Li, B.; Gui, B.; Hu, G.; Yuan, D.; Wang, C., Postsynthetic Modification of an Alkyne-Tagged Zirconium Metal–Organic Framework via a "Click" Reaction. *Inorg. Chem.* **2015,** *54*, 5139-5141.

18. Bae, Y.-S.; Dubbeldam, D.; Nelson, A.; Walton, K. S.; Hupp, J. T.; Snurr, R. Q., Strategies for Characterization of Large-Pore Metal-Organic Frameworks by Combined Experimental and Computational Methods. *Chem. Mater.* **2009,** *21*, 4768-4777.

19. Zhang, Z.; Nguyen, H. T. H.; Miller, S. A.; Cohen, S. M., polyMOFs: A Class of Interconvertible Polymer-Metal-Organic-Framework Hybrid Materials. *Angew. Chem. Int. Ed.* **2015,** *54*, 6152-6157.

20. Wu, H.; Chua, Y. S.; Krungleviciute, V.; Tyagi, M.; Chen, P.; Yildirim, T.; Zhou, W., Unusual and Highly Tunable Missing-Linker Defects in Zirconium Metal–Organic Framework UiO-66 and Their Important Effects on Gas Adsorption. *J. Am. Chem. Soc.* **2013,** *135*, 10525-10532.

21. Gómez-Gualdrón, D. A.; Moghadam, P. Z.; Hupp, J. T.; Farha, O. K.; Snurr, R. Q., Application of Consistency Criteria To Calculate BET Areas of Micro- And Mesoporous Metal–Organic Frameworks. *J. Am. Chem. Soc.* **2016,** *138*, 215-224.

22. Katz, M. J.; Brown, Z. J.; Colón, Y. J.; Siu, P. W.; Scheidt, K. A.; Snurr, R. Q.; Hupp, J. T.; Farha, O. K., A facile synthesis of UiO-66, UiO-67 and their derivatives. *Chem. Commun.* **2013,** *49*, 9449-9451.

23. Lu, G.; Cui, C.; Zhang, W.; Liu, Y.; Huo, F., Synthesis and Self-Assembly of Monodispersed Metal-Organic Framework Microcrystals. *Chemistry – An Asian Journal* **2013,** *8*, 69-72.

24. MacLeod, M. J.; Johnson, J. A., Block co-polyMOFs: assembly of polymer-polyMOF hybrids via iterative exponential growth and "click" chemistry. *Polym. Chem.* **2017,** *8*, 4488-4493.

25. Yu, X.; Cohen, S. M., Photocatalytic metal–organic frameworks for the aerobic oxidation of arylboronic acids. *Chem. Commun.* **2015,** *51*, 9880-9883.

26. Sheldrick, G. M., A short history of SHELX. *Acta Cryst. A* **2008,** *64*, 112-122.

27. Sheldrick, G. M., Crystal structure refinement with SHELXL. *Acta Cryst. C* **2015,** *71*, 3-8.

28. Vandersluis, P.; Spek, A. L., Bypass - an Effective Method for the Refinement of Crystal-Structures Containing Disordered Solvent Regions. *Acta Crystallographica Section A* **1990,** *46*, 194-201.

Chapter 4: Block co-PolyMOFs with Controlled Morphologies

4.1 Introduction

So far, the successful preparation of polyMOFs from UiO-66,[1] IRMOF-1,[2] pillared structures,[3] and isoreticular MOFs[4] have been described, but attempts to improve the polymer-like properties of these hybrid materials has not been discussed. The use of block copolymers has been an effective strategy to produce several new materials with self-healing capacities,[5-6] hierarchical self-assembly,[7-8] coordinative properties,[9] and many other features.[10] Therefore, a rational progression to polyMOFs is to introduce block copolymers that yield block co-polyMOFs (BCPMOFs) with emergent properties. Johnson and co-workers reported the first BCPMOF, synthesized from dimeric or tetrameric H_2bdc ligands coupled to a polystyrene (PS) block (Figure 4.1).[11] Using IRMOF-1 as a scaffold, Johnson's work demonstrated that diblock BCPMOFs formed hybrid materials with MOF domains surrounded by a PS matrix, which could potentially result in processable polyMOF materials. Moreover, Johnson's report suggests that additional polymer-like properties can be introduced to polyMOFs by using a block copolymer ligand.

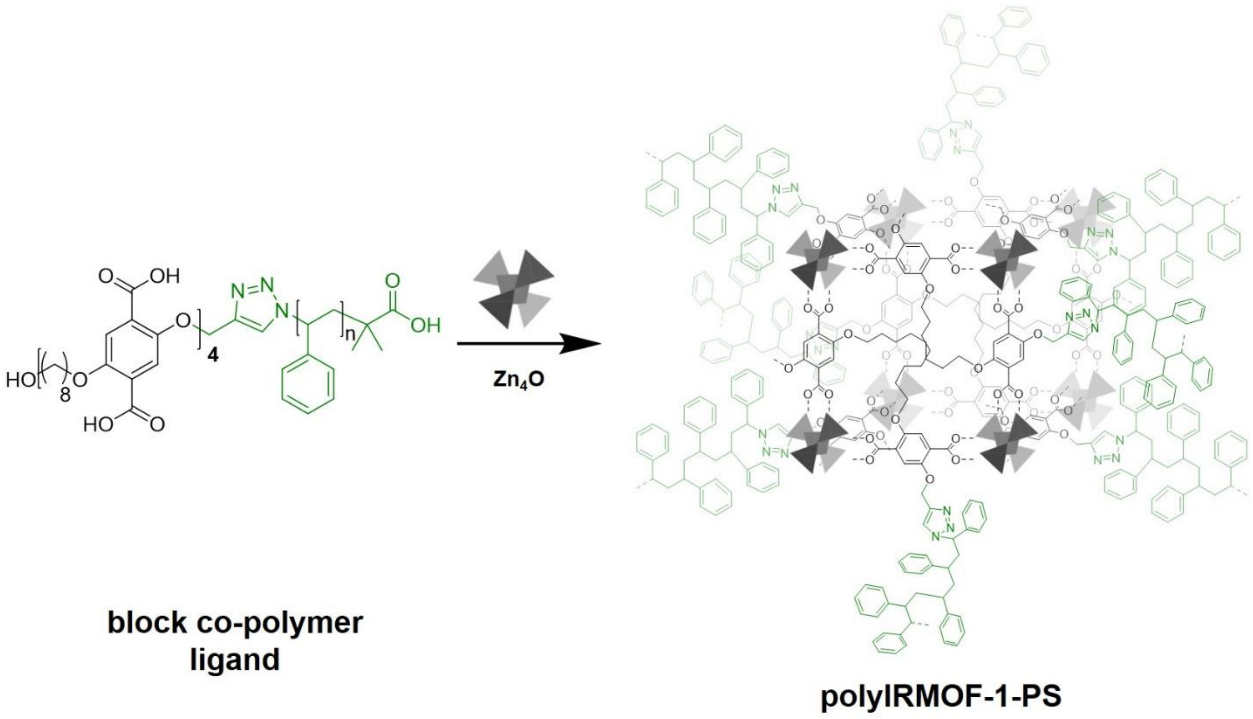

Figure 4.1. Representative Illustration of preparing a block co-polyMOF prepared from a block copolymer ligand that contains an H_2bdc tetramer coupled to a polystyrene chain. Figure was adapted from reference.[12]

As described in Chapter 1, synthetic polymers have the potential to modulate MOF growth by providing multiple binding sites and through electrostatic interactions during nucleation. There are several methods to control the shape, size, and morphologies of MOFs, such as varying solvothermal conditions,[13-14] templating,[15-17] and using small molecules as coordination modulators.[18-21] However, block copolymers provide opportunities for controlled self-assembly; [22-26] the size and morphology of the resulting polymer assemblies can be dictated by overall block copolymer molecular weight and the relative weight fractions of each block.[27] To date, polymer templating of MOFs has been achieved by combining small-molecule MOF precursors (multitopic ligands and metal salts) with polymers that promote particle stabilization (PVP, PVDF, polyvinylsulfonic acid, polyacrylic acid, and two types of block cpolymers).[28-35] In all of these

examples, small-molecule multitopic ligands serve as the precursors for MOF formation, while the polymers serve only to modulate growth, and do not become part of the final MOF.

In Chapter 4, it is demonstrated that block copolymers containing non-coordinating PEG or polyCOD blocks combined with pbdc-8a-u blocks can spontaneously assemble in solution, leading to distinct morphologies of the resulting polyMOFs.[36] In contrast to other synthetic strategies to control MOF morphologies, the polymers in this work act both as the *source* of multitopic ligands for MOF formation and as the *director* for shaping crystal habit of the MOF (Figure 4.2). Moreover, this work demonstrates that block copolymer composition can inherently affect the shapes the resulting materials take upon MOF formation, affecting properties such as porosity. Importantly, this is the first study to examine how block copolymer composition (architecture and identity of blocks) influence polyMOF morphology. The addition of a non-coordinating, morphology-directing or functional blocks hold promise as a means to create hybrid polyMOFs with a variety of functions and properties.

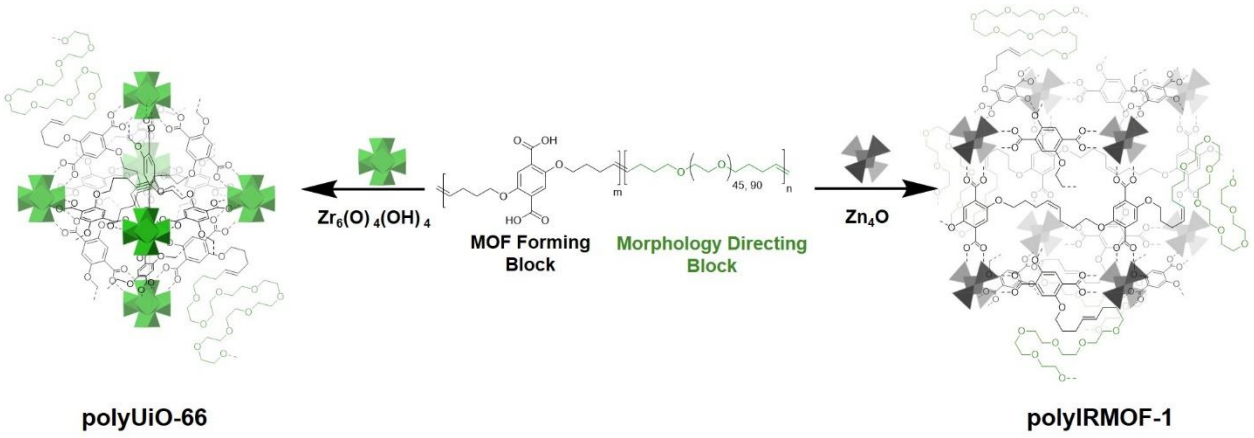

Figure 4.2. Representative Illustration of preparing a polyMOF using a block copolymer ligand. In this example, the block copolymer ligand contains a MOF-forming block (pbdc-8a-u) and a morphology directing block (PEG).

4.2 Synthesis and Characterization of pbdc-8a Block Copolymers

Monomers suitable for polymer formation were either purchased from commercially available sources or prepared via Williamson ether synthesis as described in Chapter 2 (Scheme 4S.1).[1] For this study, the MOF-forming block was synthesized from methyl ester protected monomer bdc-8e (Scheme 4.1). Monomer bdc-8e and alkene-modified PEG (diene or monoalkene) were copolymerized via ADMET polymerization using Grubbs 2nd generation catalyst to afford two different types of PEG block copolymer esters: (i) random AB block copolymers, or (ii) capped AB_2 triblock copolymers (wherein the "A" block is the bdc-8e block and the "B" block is the PEG block, Scheme 4.1). Random AB PEG block copolymers are designated as pbdc-8e-PEG$_{Mn}$-x% (where M_n indicates the molecular weight of PEG used in the synthesis, and "x%" indicates the mol% of reactive PEG diene in the reaction feed). AB_2 triblock copolymers are denoted as pbdc-8e-PEG$_{Mn}$OMe (where OMe denotes a capped pbdc-8e polymer). For polymers containing COD, monomer bdc-8e was polymerized via ADMET polymerization using Hoveyda-Grubbs 2nd-Generation catalyst, followed by ring-opening metathesis polymerization (ROMP, Scheme 4.1) of COD to afford random AB COD block copolymers pbdc-8e-COD$_{m:n}$, (where *m:n* indicates the molar ratio of bdc-8e:COD, Scheme 4S.4, Figures 4S.13-15). All of the aforementioned polymers were hydrolyzed to afford block copolymer acid ligands pbdc-8a-PEG$_{Mn}$-x%, pbdc-8a-PEG$_{Mn}$OMe, and pbdc-8a-COD$_{m:n,}$ where "a" indicates the block copolymer contains carboxylic acid groups (Scheme 4.1, Figures 4S.16-26).

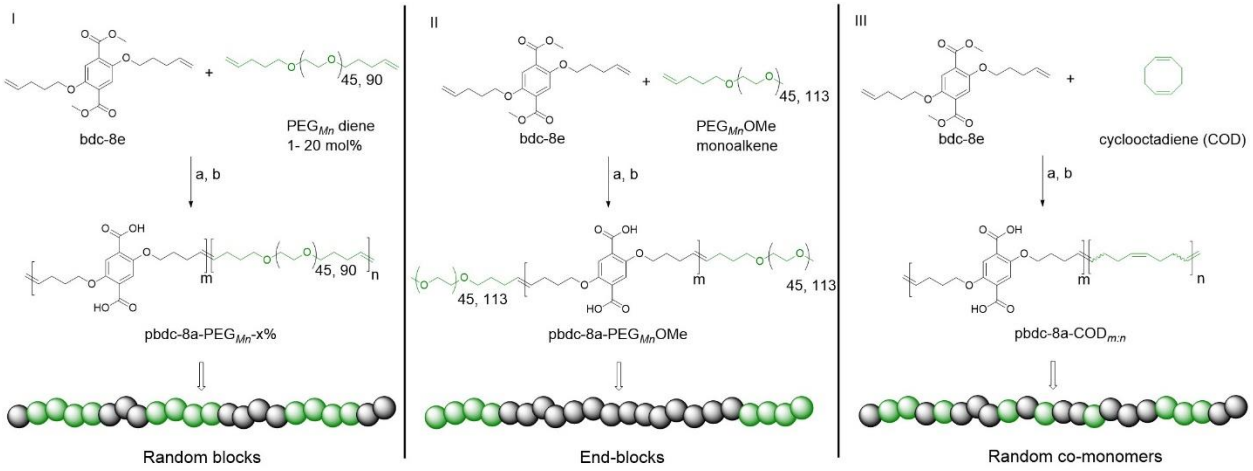

Scheme 4.1. Synthesis of three types of polymer ligands used in this work: (i) Random AB PEG block copolymer ligand (pbdc-8a-PEG$_{Mn}$-x%); (ii) capped AB_2 PEG block copolymer ligand (pbdc-8a-PEG$_{Mn}$OMe); (iii) random AB COD block copolymer ligand (pbdc-8a-COD$_{m:n}$). Reagents and conditions: (a) G2 catalyst, CH_2Cl_2, 50 °C, 5 h; (b) KOH, THF/H_2O, 40 °C, 12h.

A combination of ^{1}H NMR and GPC were used to characterize the block copolymer esters (Table 4.1). For all block copolymers, the relative weight percent of bdc-8e to co-monomers were calculated using ^{1}H NMR and ranged between 50-90%. ^{1}H NMR was also used to determine incorporation of PEG or COD to pbdc-8e by examining the ratios of small-molecule repeat units (ethylene glycol or COD) to bdc-8e present in the sample Table 4S.1, ESI). Relative molecular weights were determined via GPC for the polymer esters using PMMA as a calibration standard (Fig. 4S.27). Molecular weight distributions were narrow, as the molecular dispersity was <2.0 for polymers containing PEG (pbdc-8e-PEG$_{Mn}$-x% and pbdc-8e-PEG$_{Mn}$OMe); this is indicative of the narrow dispersity of the PEG block. In contrast, block copolymers prepared with COD have broader dispersities, which are reflective of ADMET being a step-growth polymerization (Table 4.1). Polymer acid ligands were too polar to evaluate by GPC, as described in previous chapters. However, ^{1}H NMR analysis was performed on the final carboxylic acid-containing polymer ligands, revealing that the ratios between H_2bdc units and the other polymer block are reflective of those determined for the ester polymer precursors (Fig. 4S.16-26).

Although ADMET polymerization is a useful technique for synthesizing MOF-forming polymers (because it produces large polymers with precise alkyl spacings between H_2bdc), the method lacks control over degree of polymerization and it is generally not ideal for making block copolymers.[37] Therefore, fractionation by automated silica gel column chromatography was used to characterize the components of the block copolymer ester ligands. Fractionation of pbdc-8e-PEG$_{Mn}$-x% revealed that block copolymers of pbdc-8e predominantly lacked the PEG block when low loadings of PEG (1-2 mol%) were used for the synthesis, whereas with larger loadings of PEG (10-20 mol%) resulted in block copolymers with PEG chains (as gauged by ^{1}H NMR, Figures 4S.28-29, Tables 4S.2-3). For pbdc-8e-PEG$_{Mn}$OMe polymers, fractionation revealed that the polymers contained a mixture of unfunctionalized (i.e., no PEG block) pbdc-8e, monofunctionalized (i.e., one PEG block) block copolymers, and bifunctionalized (i.e., two PEG blocks) pbdc-8e (as gauged by ^{1}H NMR end-group analysis, Figure 4S.30, Table 4S.4). Purified forms of bifunctionalized pbdc-8e-PEG$_{Mn}$OMe were obtained via column chromatography and were used for the synthesis of polyMOFs (Table 4.1). For block copolymers of pbdc-8e-COD$_{m:n}$, no noticeable fractionation could be achieved, suggesting an even distribution of COD throughout all polymer chains within pbdc-8e-COD$_{m:n}$ samples (Figure 4S.31, Table 4S.5).

Table 4.1. Composition and Molecular Weight Determinations of Block copolymer Ligands.

Ligand	wt% pbdc-8e(^{1}HNMR) [a]	M_n (GPC)	M_w/M_n
pbdc-8e-PEG$_{2000}$-2%	93	18,700	1.3
pbdc-8e-PEG$_{2000}$-20%	56	14,700	1.4
pbdc-8e-PEG$_{4000}$-1%	90	18,700	1.5
pbdc-8e-PEG$_{4000}$-10%	52	16,000	2.2
pbdc-8e-PEG$_{2000}$OMe [b]	84	20,300	1.6
pbdc-8e-PEG$_{5000}$OMe [b]	52	19,900	1.4
pbdc-8e-COD$_{1:1}$	85	17,200	2.8
pbdc-8e-COD$_{2:1}$	92	17,500	2.8
pbdc-8e-COD$_{10:1}$	98	26,500	3.5

[a] The weight percentages of bdc-8e in the block copolymers were calculated using the following formula: wt% pbdc-8e = (ratio of bdc-8e × M.W.$_{bdc\text{-}8e}$)/[(ratio of bdc-8e × M.W.$_{bdc\text{-}8e}$) + (ratio of co-monomer × M.W.$_{co\text{-}monomer}$)] × 100%. [b] Purified forms of bifunctionalized pbdc-8e-PEG$_{Mn}$OMe are represented.

4.3 Formation and Morphology Control of UiO-66 BCPMOFs

Zirconium-based UiO-66 was selected for BCPMOF formation because of the high chemical stability of this MOF and the large number of studies using it in the literature.[38] As described in Chapter 2, preparation of polyUiO-66 was achieved with $ZrCl_4$, the corresponding polymer ligand, and excess formic acid modulator under solvothermal conditions for 48 h.[1] The block-polyUiO-66 were dissolved and analysed to confirm the presence and integrity of the block copolymer ligands during the solvothermal synthesis (Table 4S.6, Figures 4S.32-42).

BCPMOFs were first prepared from pbdc-8a-PEG$_{Mn}$-x% to investigate how the molecular weight of PEG and the amount of incorporated PEG affect the morphology of polyUiO-66. All polyMOFs formed from the pbdc-8a-PEG$_{Mn}$-x% series resulted in UiO-66 as confirmed from PXRD (Figure 4.3). Polymers with low amounts of PEG (pbdc-8a-PEG$_{2000}$-2% or pbdc-8a-PEG$_{4000}$-1%) yielded polyMOFs with much sharper primary PXRD reflections than those with larger amounts of PEG (pbdc-8a-PEG$_{2000}$-20% or pbdc-8a-PEG$_{4000}$-10%) where broadening was

observed. Broadening of PXRD reflections is indicative of materials with reduced crystallinity. This may be simply due to the lower relative amount of MOF forming block in pbdc-8a-PEG$_{2000}$-20% and pbdc-8a-PEG$_{4000}$-10% (50% PEG by weight) when compared to pbdc-8a-PEG$_{2000}$-2% and pbdc-8a-PEG$_{4000}$-1% (10% PEG by weight) (Table 4.1). The molecular weight of the PEG block itself had an insignificant effect on the crystallinity of the polyMOFs, as gauged by PXRD (Figure 4.3).

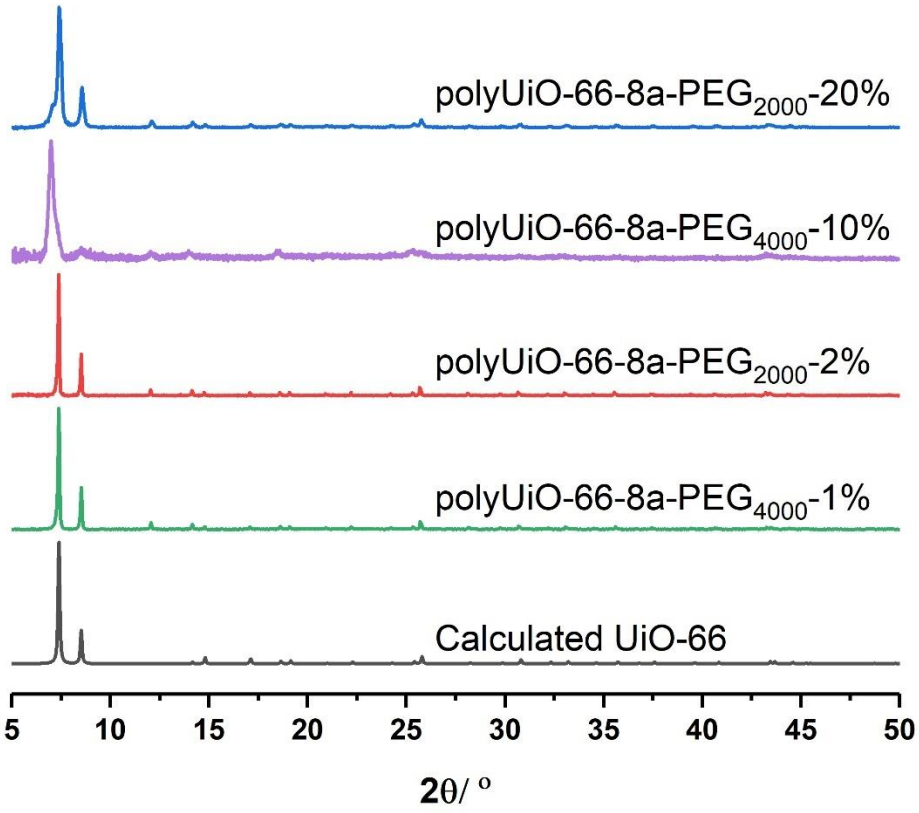

Figure 4.3. PXRD patterns of polyUiO-66 prepared from pbdc-8a-PEG$_{Mn}$-x% block copolymers.

SEM revealed that the amount of the PEG component in pbdc-8a-PEG$_{Mn}$-x% has a significant effect on the morphology of block-polyUiO-66. Using synthetic conditions discussed

in Chapter 2, UiO-66 prepared from H_2bdc typically forms highly symmetric octahedra[39] whereas using the homopolymer ligand pbdc-8a produces a crystalline film of polyUiO-66 with an "interlaced" morphology.[1] In contrast, the BCPMOFs are able to produce both observed morphologies for UiO-66, yielding rounded octahedral structures or polyMOFs with an interlaced morphology simply by changing the block copolymer composition. PolyUiO-66 films prepared from pbdc-8a-PEG_{2000}-2% and pbdc-8a-PEG_{4000}-1% consisted of microcrystalline, intergrown octahedra, but with rounded edges (Figures 4.4a, 4.4b). In contrast, polyUiO-66 prepared from pbdc-8a-PEG_{2000}-20% and pbdc-8a-PEG_{4000}-10% produced films with an interlaced morphology with interwoven facets (Figures 4.4c, 4.4d). The morphology of these materials correlates with the crystallinity observed by PXRD (Figure 4.3), for the sharper reflections in the pbdc-8a-PEG_{2000}-2% or pbdc-8a-PEG_{4000}-1% block polyMOFs correspond to the observed octahedra, whereas the broader reflections produced by 8a-PEG_{2000}-20% or pbdc-8a-PEG_{4000}-10% correspond to block-polyUiO-66 with an interlaced morphology. Using a mixture of PEG and pbdc-8a homopolymers only yields polyUiO-66 with an interlaced morphology,[1] showing that the presence of PEG alone did not allow for control of UiO-66 morphology (Figure 4S.43).

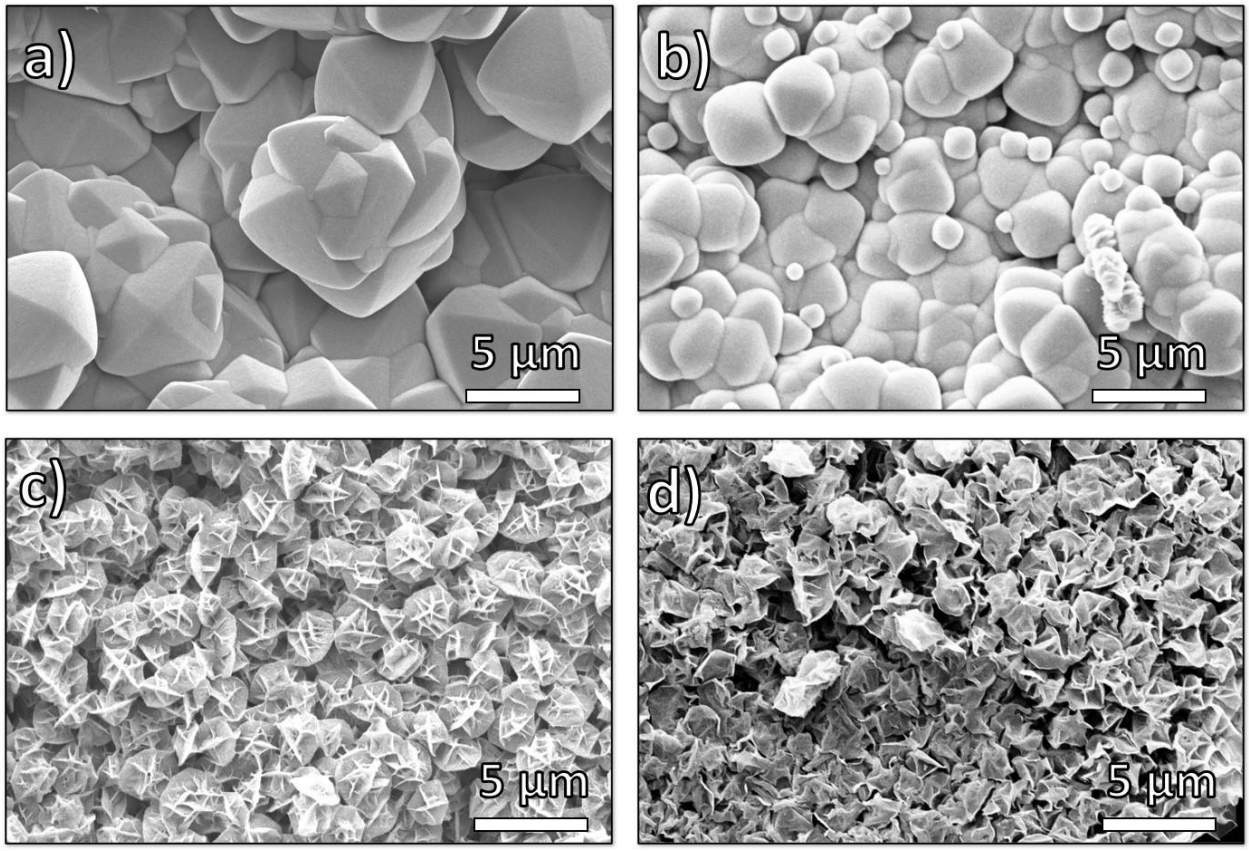

Figure 4.4. SEM images of polyUiO-66 prepared from block copolymer ligands: (a) pbdc-8a-PEG_{2000}-2%; (b) pbdc-8a-PEG_{4000}-1%; (c) pbdc-8a-PEG_{2000}-20%; (d) pbdc-8a-PEG_{4000}-10%.

Dynamic light scattering (DLS) revealed that all block copolymers used in this study aggregate to form assemblies in solution, which suggest a cause for the morphological differences in BCPMOFs (Table 4S.7). At 13° scattering angle, pbdc-8a-PEG_{2000}-20% and pbdc-8a-PEG_{4000}-10% formed large aggregates in solution, with hydrodynamic radii of 101 nm and 72 nm, respectively (Figures 4S.44-45). In contrast, pbdc-8a-PEG_{2000}-2% and pbdc-8a-PEG_{4000}-1% formed much smaller assemblies with hydrodynamic radii of 27 and 13 nm, respectively (Figures 4S.46-47). Polymers will form assemblies with particular curvatures in order to minimize various thermodynamic factors including core chain stretching, corona chain crowding, and interfacial surface tension.[40] When the weight fractions of two blocks are quite disparate, smaller assemblies

with high curvature are preferred. Conversely, similar block weight fractions typically give rise to larger assemblies with low curvature, as is observed in the pbdc-PEG block copolymers in this study.

The origin of the morphologies observed in Figure 4.3 is likely related to the accessibility of pbdc blocks to the growing crystal faces. During polyMOF growth, pbdc-8a-PEG_{2000}-2% and pbdc-8a-PEG_{4000}-1% generate controlled aggregation to yield octahedral morphology, but block copolymers with a large PEG content inhibit octahedra formation, reverting to the previously observed interlaced morphology for polyUiO-66.[23-25] Hwang and coworkers[31] observed similar behavior in MOF formation modulated by double hydrophilic block copolymers (DHBC) of PEG-*b*-poly(methacrylic acid) where higher proportions of polymer yielded smaller and more irregularly shaped morphologies compared to the native MOF. DHBCs have been commonly used to control the crystal morphologies of various hybrid materials.[23-25, 31] However, the pbdc-8a-PEG_{Mn}-x% polymers used in this study offer the unique advantage of providing both modulation of MOF crystal morphology and source of ligand for the framework itself.

To probe the effects of block copolymer architecture on polyUiO-66, pbdc-8a-PEG_{Mn}OMe ligands were used for polyUiO-66 synthesis. Following the same synthetic procedure described above, pure AB_2 co polymers pbdc-8a-PEG_{2000}OMe and pbdc-8a-PEG_{5000}OMe were used to successfully synthesize polyUiO-66 (Figure 4.5a). Block-polyUiO-66 prepared from crude (i.e., unfractionated) samples of pbdc-8a-PEG_{2000}OMe and pbdc-8a-PEG_{5000}OMe produced crystalline materials as assessed by PXRD (Figure 4S.48). SEM reveals that all polyUiO-66 prepared from pbdc-8a-PEG_{Mn}OMe have an interlaced morphology (Figures 4.5b, 4.5c, and Figure 4S.49). This result demonstrates that positioning of the PEG is important to control the shape of these materials; when PEG blocks are located within the backbone of the polymer ligand (e.g., pbdc-8a-PEG_{2000}-

2%) an octahedral morphology is observed (Figures 4.3a, b), but when PEG blocks are located only at the ends of the polymer ligand (e.g., pbdc-8a-PEG$_{2000}$OMe) the material retains the interlaced morphology (Figures 4.4b, c).

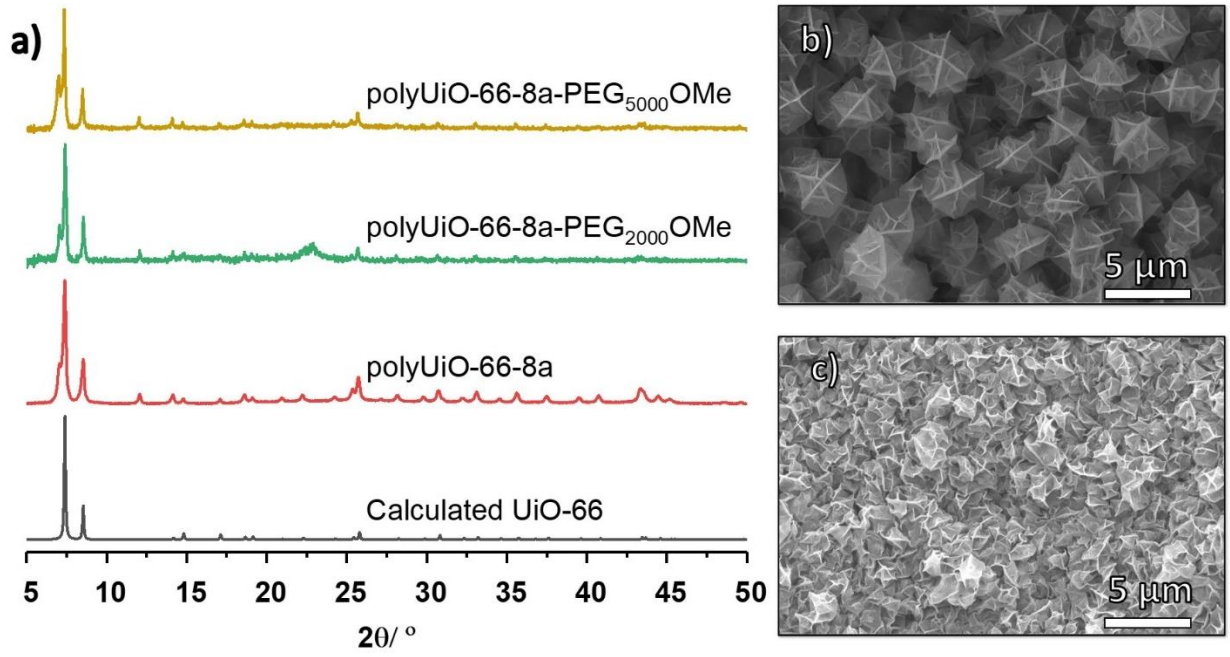

Figure 4.5. (a) PXRD patterns of polyUiO-66 prepared from purified pbdc-8a-PEG$_{Mn}$OMe. SEM images of polyUiO-66 prepared from: (b) pbdc-8a-PEG$_{2000}$OMe and (c) pbdc-8a-PEG$_{5000}$OMe.

An additional reflection in the PXRD pattern at 2θ = 7.06° was present in all samples of polyUiO-66 prepared from pbdc-8a-PEG$_{Mn}$OMe ligands (Figure 4.4a, Figure 4S.48). This may be due to a distortion of the polyUiO-66 lattice to accommodate filling of the pore.[1] Alternatively, this additional reflection may be the result of defects (e.g., missing clusters).[41]. Regardless of its origin, this additional reflection at 2θ = 7.06° is observed for all polyUiO-66 comprising the interlaced morphology (pbdc-8a-PEG$_{2000}$-20%, pbdc-8a-PEG$_{4000}$-10% and all pbdc-8a-PEG$_{Mn}$OMe), but not for polyUiO-66 materials with an octahedral morphology (pbdc-8a-PEG$_{2000}$-2%, pbdc-8a-PEG$_{4000}$-1%).

DLS was used to probe how aggregation of pbdc-8a-PEG$_{Mn}$OMe ligands affects the morphology of block-polyUiO-66. As in the pbdc-8a-PEG$_{Mn}$-x% series, small polymer assemblies yield larger polyMOF crystals. The hydrodynamic radii (13° scattering angle) of pbdc-8a-PEG$_{2000}$-OMe and pbdc-8a-PEG$_{5000}$-OMe were 129 nm and 33 nm, leading to polyMOFs with crystal sizes of approximately 3μm and 1μm, respectively (Figure 4S.50-51).

Block copolymer ligands pbdc-8a-COD$_{m:n}$ were investigated to determine the effects of polymer composition on polyUiO-66. In contrast to PEG-based block copolymers, the polyCOD block is significantly more hydrophobic, making it less likely to interact with growing MOF surfaces. All pbdc-8a-COD$_{m:n}$ produced polyUiO-66 with good crystallinity (Figure 4S.52). SEM imaging shows both pbdc-8a-COD$_{2:1}$ and pbdc-8a-COD$_{1:1}$ produced polyUiO-66 with intergrown octahedral morphologies that are different than those previously reported for polyUiO-66 (Figure 4S.53). Block-polyUiO-66 prepared from pbdc-8a-COD$_{10:1}$ produced an interlaced morphology and a new, but related morphology (Figure 4S.54). The variability in morphology control may be attributed to pbdc-8a-COD$_{10:1}$ containing broad polymer dispersities and the block copolymer containing a greater proportion of H_2bdc (98 % wt). All polymers containing COD showed the presence of large assemblies in solution based on DLS (R_h >50 nm, Table 4S.7, Figures 4S.55-57).

The morphology of the polyUiO-66 materials affected the porosity of the materials, as characterized by N_2 gas adsorption. PolyUiO-66 generated from pbdc-8a produces a polyMOF with a BET surface area of 340-420 m^2/g with the interlaced morphology resulting in a mesoporous material, as indicated by a type IV isotherm with a hysteresis loop.[1] Similarly, block-polyUiO-66 with an interlaced morphology (produced from pbdc-8a-PEG$_{2000}$-20%, pbdc-8a-PEG$_{4000}$-10%, and all pbdc-8a-PEG$_{Mn}$OMe polymer ligands) produced the expected type IV isotherms (Figure 4S.58). However, changing the morphology of block-polyUiO-66 to intergrown octahedron (from pbdc-

8a-PEG_{4000}-1%, pbdc-8a-$COD_{1:1}$, and pbdc-8a-$COD_{2:1}$ polymer ligands) yielded type I isotherms, which are indicative of a microporous material (Figure 4.6, Figure 4S.59). One exception was block-polyUiO-66 prepared from pbdc-8a-PEG_{2000}-2%, for which there was no accessible surface area, perhaps due to pore filling of the polyMOF by PEG (Figure 4S.60a). CO_2 adsorption at 195K was used to determine accessibility of the pores in pbdc-8a-PEG_{2000}-2%, which gave a surface area of 151±3 cm^3/g (Figure 4S.60b). Analysis of the pore width distribution of all block-polyUiO-66 showed two different populations, one centred at between 9-13 Å, and another population between 14-40 Å, consistent with previous reports on polyUiO-66 (Figure 4S.61). It should be noted that for block-polyUiO-66 with intergrown octahedron, the pore width distribution between 14-40 Å is significantly reduced when compared to the distribution of block-polyUiO-66 that yielded the interlaced morphology. Based on these results, it can be proposed that changing the morphology influences the formation of mesopores. As such, using block copolymer ligands may be a way to fine-tune the porosity of polyMOF materials.

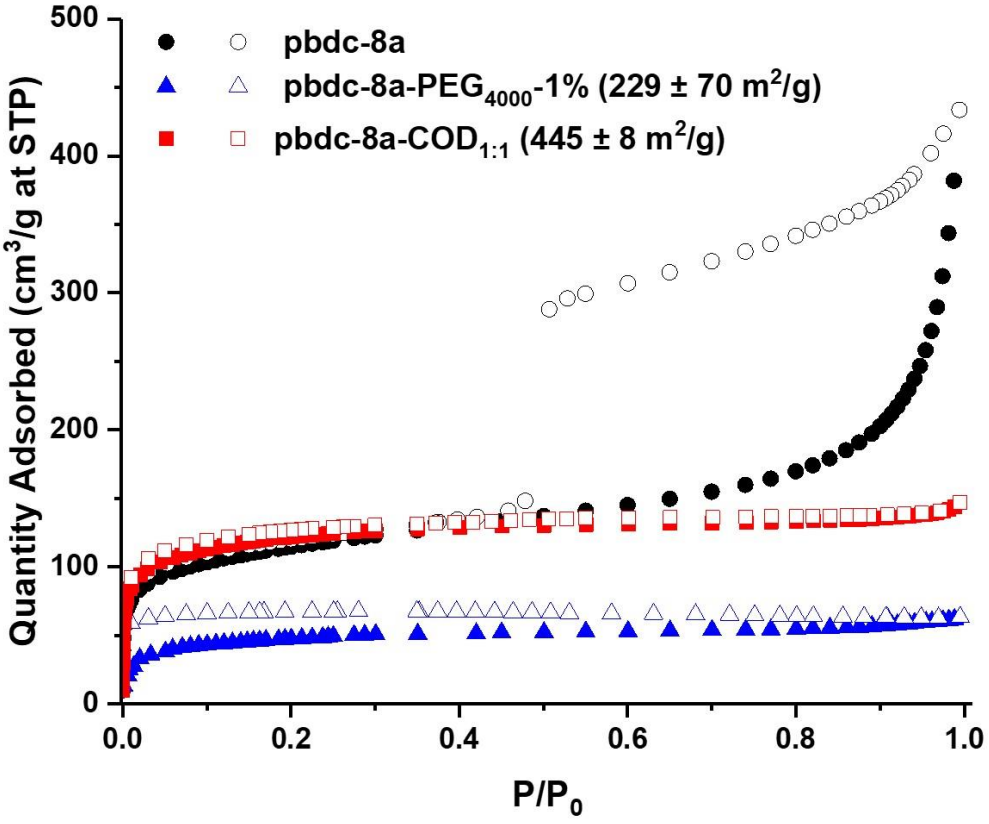

Figure 4.6. Representative N_2 isotherms of block-polyUiO-66 prepared from various block copolymer ligands that result in intergrown octahedra. The BET surface areas are included in parentheses. PolyUiO-66 prepared from homopolymer pbdc-8a is included for comparison. Closed and open symbols represent the adsorption and desorption processes, respectively.

4.4 Synthesis and Characterization of IRMOF-1 Type BCPMOFs

The successful preparation of block-polyUiO-66 prompted study of a different MOF architecture, namely Zn-based IRMOF-1. PolyIRMOF-1 was synthesized under solvothermal conditions at 100 °C for 24 h to yield off-white solids or an off-white suspension.[2] Analysis by PXRD confirmed the preparation of polyIRMOF-1 using all block copolymers prepared in this study (Figure 4.7, and Figures 4S.62-63). All block-polyIRMOF-1 displayed a broad amorphous phase, centred at 2θ ~22° that can be attributed uncoordinated block copolymer present in the

material (Figures 4S.62-63). To confirm the integrity of the copolymers, block-polyIRMOF-1 were digested and analysed by ^{1}H NMR (Figures 4S.64-72), which showed the polymer ligands were intact. Furthermore, the stability of all block-polyIRMOF-1 were tested by storing activated, dried samples under ambient conditions. In general, block-polyIRMOF-1 produced PXRD patterns with broad reflections after 10 min of exposure to air (Figures 4S.73-75), but the crystallinity of these materials could be regenerated by immersion of solids in DMF at 60 °C for 1 h (Figure 4S.76).[2] The ability to restore the crystallinity of block-polyIRMOF-1 under mild conditions could make these materials reusable.[2, 11]

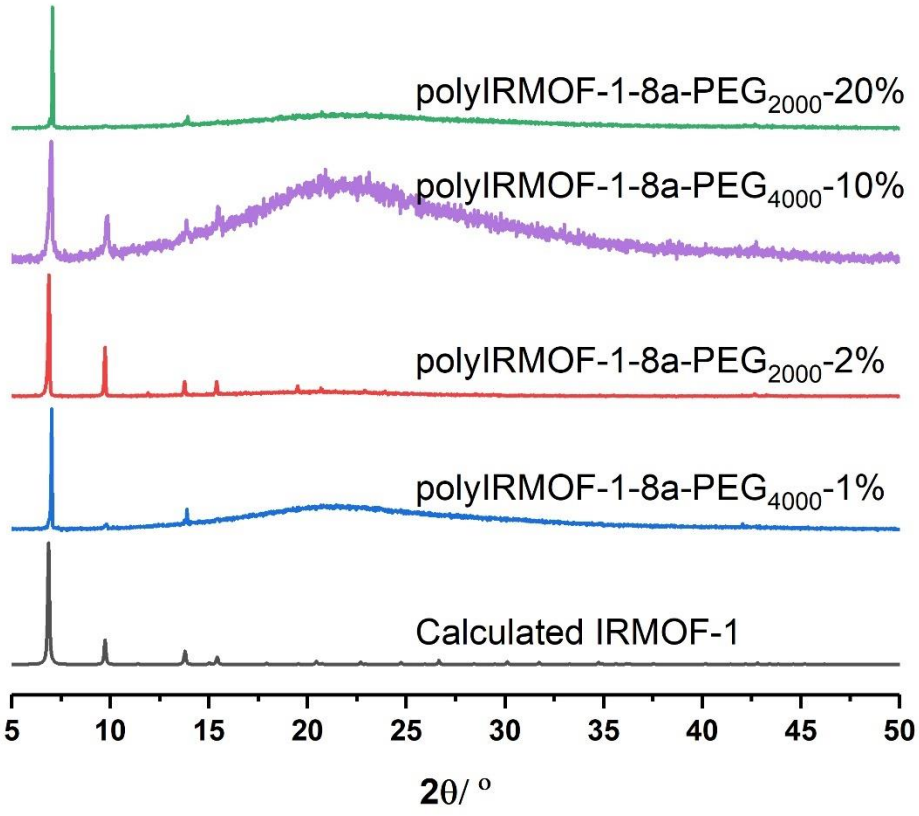

Figure 4.7. PXRD patterns of polyIRMOF-1prepared from pbdc-8a-PEG$_{Mn}$-x% block copolymers.

SEM images of block-polyIRMOF-1 revealed that block copolymer ligands notably affect the size and uniformity of these materials, with size control achieved through block copolymer composition and relative weight fractions. Homopolymer pbdc-8a used to synthesize polyIRMOF-1 produces microcrystalline cubes that are irregular in size and dimensionality (Figure 4.8a). By comparison, PEG block copolymers pbdc-8a-PEG_{2000}-2% and pbdc-8a-PEG_{4000}-1% produce microcrystalline cubes that are uniform in shape and size (Figures 4.8b, 4.8c), measuring at 1.8±0.3 μm for pbdc-8a-PEG_{2000}-2% (Figure 4.8b) and measuring at 1.0±0.3 μm for pbdc-8a-PEG_{4000}-1% (Figure 4.8c). At higher amounts of PEG, nanocrystallites of block-polyIRMOF-1 with a uniform cubic morphology and size were produced (Figures 4.8d-f), measuring at 540±200 nm for pbdc-8a-PEG_{2000}-20% and measuring at 320±90 nm for pbdc-8a-PEG_{4000}-10%. Block-polyIRMOF-1 prepared from ligands pbdc-8a-PEG_{Mn}OMe also resulted in distinct shape and size behaviour (Figure 4S.77). With increasing PEG molecular weight, the size of the particles significantly decreased, as gauged by SEM. In contrast, block-polyIRMOF-1 prepared from pbdc-8a-$COD_{m:n}$ ligands did not show good size and shape control, with the exception of pbdc-8a-$COD_{1:1}$, which also gave relatively monodisperse, rounded particles (Fig S.78). To ensure that PEG alone was not the result of morphology control, polyIRMOF-1 was synthesized using a physical mixture of homopolymer pbdc-8a and PEG (at 1 and 10 mol%), which was unable to provide uniform shape and size of these materials (Figure 4S.79). These results suggest that the PEG block copolymers play an important role generating metastable intermediates during MOF formation, similarly to those observed for DHBCs. Overall, using block copolymer ligands show a promising route to control the regularity of IRMOF-1 and related scaffolds.

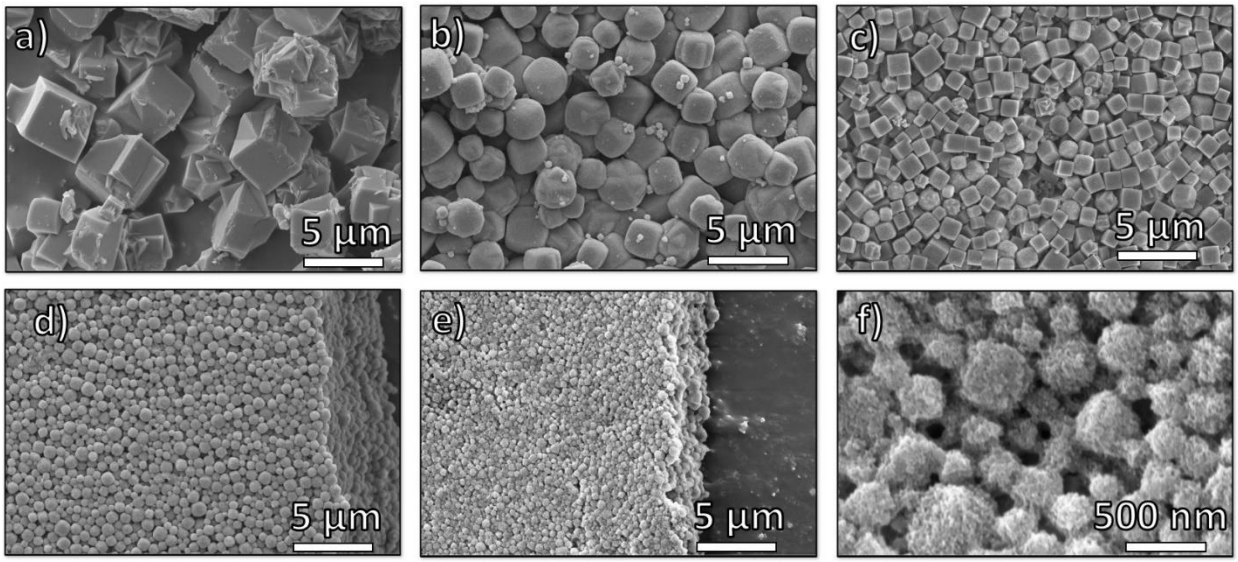

Figure 4.8. SEM images of polyIRMOF-1 prepared from polymer ligands: (a) pbdc-8a; (b) pbdc-8a-PEG_{2000}-2%; (c) pbdc-8a-PEG_{4000}-1%; (d) pbdc-8a-PEG_{2000}-20%; (e and f) pbdc-8a-PEG_{4000}-10%.

The ability to transform block copolymers into crystalline materials with cubic morphologies are highly unusual and is rarely observed for polymers. Kim reported block copolymer assemblies with bicontinuous cubic membranes[41] and Matyjaszewski reported cubosomes assembled from poly(ionic liquid) block copolymers.[42] The observation of cubic structures of block-polyIRMOFs and highly faceted morphologies in block-polyUiO-66 above demonstrates the power of block copolymer MOF formation as a general strategy to achieve non-traditional polymer morphologies. As in block-polyUiO-66 discussed above, the lower hydrodynamic radii of parent block copolymers leads to larger BCPMOF crystals. In the case of pbdc-8a-PEG_{4000}-10%, the BCPMOF crystals were small enough to perform DLS experiments, which gave hydrodynamic radii of 274 nm and 308 nm at 90° and 13° scattering angle, respectively, which indicates a narrow distribution of particle sizes (Figure 4S.80, Table 4S.7) that are consistent with the particle sizes observed by SEM (Figure 4.8f).

Controlling the shape and size of MOFs using block copolymers offers potential for new methods to prepare MOF-composite materials. Recent efforts by Johnson[11] and Kitagawa[43] demonstrated the ability to transform block copolymers into metal-organic materials with successive phase separation between MOF domains and polymer domains. Similarly, it is speculated that BCPMOFs observed in this work (Figure 4.8f) exhibit phase separation, but with larger MOF-domains. In the future, it is anticipated that the ability to control the shape and size of BCPMOFs will allow for the preparation of densely packed polymer-MOF composite materials.

Nitrogen gas adsorption confirmed that synthesis of block-polyIRMOF-1 can produce porous materials with exceptional surface areas and interesting properties. Indeed, BET surface areas of 550-1100 m^2/g were achieved for block-polyIRMOF-1 using pbdc-8a-PEG$_{Mn}$-x% type polymers (Figure 4.9). BET surface areas of ~800-900 m^2/g were achieved for polyIRMOF-1 prepared from crude pbdc-8a-PEG$_{Mn}$OMe (Fig. 4S.81), and ~300-700 m^2/g for polyIRMOF-1 prepared from pbdc-8a-COD$_{m:n}$ (Fig. 4S.82). For block-poyIRMOF-1 prepared from pbdc-8a-PEG$_{Mn}$-x% type polymers, hysteresis was observed in the N_2 isotherm, regardless of the amount or molecular weight of PEG copolymer ligand used in the synthesis. Similarly, block-polyIRMOF-1 prepared from pbdc-8a-PEG$_{Mn}$OMe also produced a hysteresis in the isotherm, indicative of a mesoporous material. In contrast, N_2 isotherms of samples prepared from pbdc-8a-COD$_{m:n}$ did not exhibit hysteresis. A possible explanation for the differences in behaviour between PEG block polyMOFs and COD block polyMOFs may be due to the size-distribution of polymer blocks in the ligands. For pbdc-8a-PEG$_{Mn}$-x% and pbdc-8a-PEG$_{Mn}$OMe, polymer ligands are prepared from PEG macromonomers that have the potential to create large regions of PEG-only domains and pbdc-8a-only domains within these copolymer ligands; in turn, PEG may be accommodated in the BCPMOF if mesopores are introduced. In contrast, pbdc-8a-COD$_{m:n}$ type

ligands are prepared from small molecule COD that is evenly distributed throughout all the polymer chains; this in turn creates smaller COD domains within pbdc-8a-COD$_{m:n}$ that do not need accommodation by mesopore formation. On the whole, these results demonstrate a promising route to the preparation of highly porous BCPMOF materials with tuneable porosity.

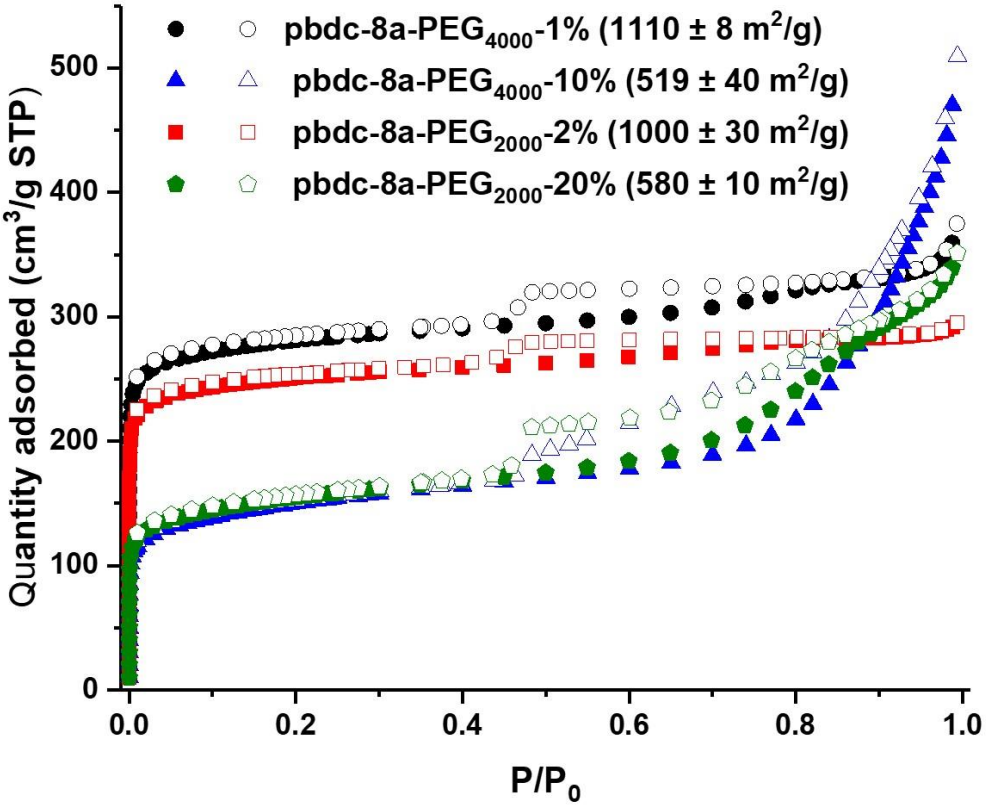

Figure 4.9. N_2 isotherms of block-polyIRMOF-1 prepared from pbdc-8a-PEG$_{Mn}$-x% polymers.

4.5 Conclusions

The use of block copolymer ligands was successfully shown to produce polyMOFs with controlled morphologies and sizes, using UiO-66 and IRMOF-1 as crystal scaffolds. This study demonstrates how block copolymer ligands with various compositions, sizes, and arrangements

can affect the formation and properties of polyMOF materials. To date, BCPMOFs are the only system where the polymer ligand is both the modulator and the provider of ditopic ligands for MOF formation, making them unique MOF-polymer hybrid materials that take advantage of block copolymer properties. This work has even encouraged the groups of others to use BCPMOF ligands as a tool to prepare colloidal MOF structures with controlled sizes and morphologies; Johnson and co-workers utilized an H_2bdc tetramer coupled with PEG to produce polyMOFs that were as small as 20 ± 1 nm in size.[44]

In future directions, it is expected that controlled polymer assemblies may be used to dictate the resultant structure of polyMOFs. As previously discussed, it is well-understood that block copolymers spontaneously self-assemble in solution, featuring constructs like micelles, nanorods, lamellae, and other unique nanostructures. Being able to capture these assemblies to dictate final polyMOF morphology may be useful to produce new and interesting materials. Ultimately, understanding the role that polymers play in polyMOFs will allow the design of materials with desirable properties.

4.6 Appendix: Supporting Information

Experimental

General Materials and Methods. Starting materials were purchased and used from commercially available suppliers (Sigma-Aldrich, Acros Organics, Matrix Scientific, and others) without further purification. Chromatography was performed using a CombiFlash R_f 200 automated system from Teledyne Isco. ^{1}H nuclear magnetic resonance (NMR) spectra were collected using a Varian spectrometer running at 400 MHz.

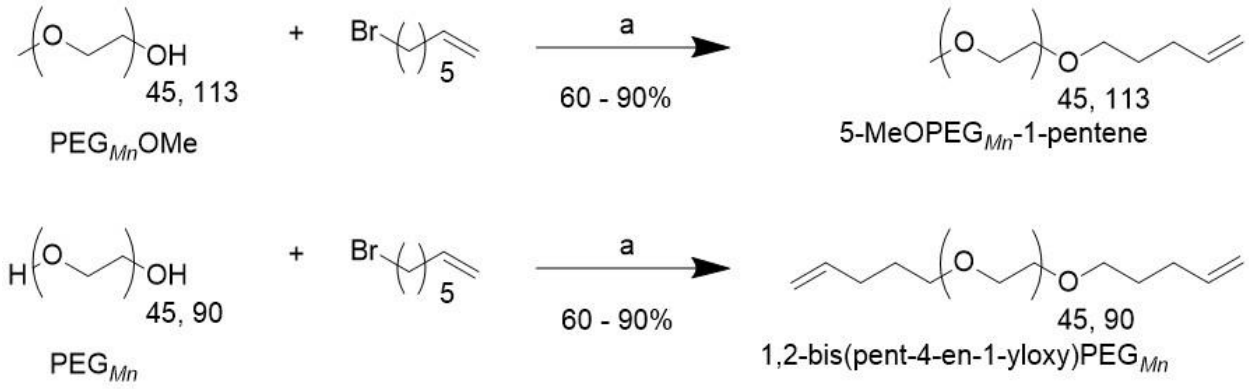

Scheme 4S.1. Synthesis of PEG macromonomers. Reagents and conditions (a): NaH, DMF, 45 °C, 4h.

Synthesis of alkene-functionalized PEG macromonomers. To a 100 mL round bottom flask was added polyethylene glycol (PEG) (2.4 mmol, 1 eq), 5-bromo-1-pentene (1.6 mL, 12 mmol, 10. eq), and dissolved in 20 mL of DMF. Then, 60% wt. NaH in mineral oil (360 mg, 9.0 mmol, 7.5 eq.) was slowly added to the solution. The reaction was stirred and heated to 45 °C for 2 h. Then, the solution was quenched using 0.6 mL of 2 M NH_4Cl solution and the solution was stirred for 30 min to ensure quenching. The mixture was filtered through a Buchner funnel to remove any precipitating salts. DMF was removed via evaporation. The functionalized polymer was dissolved in CH_2Cl_2 to precipitate any remaining salts left in the polymer mixture. The salts were filtered, and the solvent was evaporated yielding the PEG polymers. To remove any unreacted 5-bromo-1-pentene, the polymer was washed with diethyl ether. The samples were dried under vacuum at 40 °C to yield the functionalized PEG polymers.

1,2-bis(pent-4-en-1-yloxy)PEG$_{2000}$. Yield: 70 % (3.5 g, 0.88 mmol). ^{1}H NMR (400 MHz, $CDCl_3$) δ 5.80 (ddt, J = 16.9, 10.2, 6.6 Hz, 1H), 5.05 – 4.91 (m, 2H), 3.64 (s, J = 3.8 Hz, 180H), 2.20 – 1.97 (m, 4H), 1.67 (dt, J = 13.9, 6.8 Hz, 2H).

1,2-bis(pent-4-en-1-yloxy)PEG$_{4000}$. Yield: 73% (3.5 g, 0.88 mmol). ^{1}H NMR (400 MHz, DMSO-d$_6$) δ 5.79 (dt, *J* = 16.9, 8.3 Hz, 1H), 4.98 (dd, *J* = 23.8, 13.5 Hz, 2H), 3.67 (t, 2H), 3.50 (s, 246H), 2.11 – 1.99 (m, 2H), 1.63 – 1.50 (m, 2H).

5-MeOPEG$_{2000}$-1-pentene. Yield: 94% (4.5 g, 2.3 mmol). ^{1}H NMR (400 MHz, DMSO-d$_6$) δ 5.81 (ddt, *J* = 16.9, 10.2, 6.6 Hz, 1H), 5.21 – 4.90 (m, 2H), 3.50 (s, 180H), 3.23 (s, 3H), 2.13 – 1.99 (m, 2H), 1.64 – 1.50 (m, 2H). *Mn*~ 2000 g/mol.

5-MeOPEG$_{5000}$-1-pentene. Yield: 67% (8.0 g, 1.6 mmol). ^{1}H NMR (400 MHz, DMSO-d$_6$): δ 5.81 (d, *J* = 6.8 Hz, 1H), 5.25 – 4.85 (m, 2H), 3.71 – 3.65 (m, 9H), 3.50 (s, 452H), 2.06 (s, 2H),b 1.57 (dd, *J* = 14.6, 6.8 Hz, 2H).

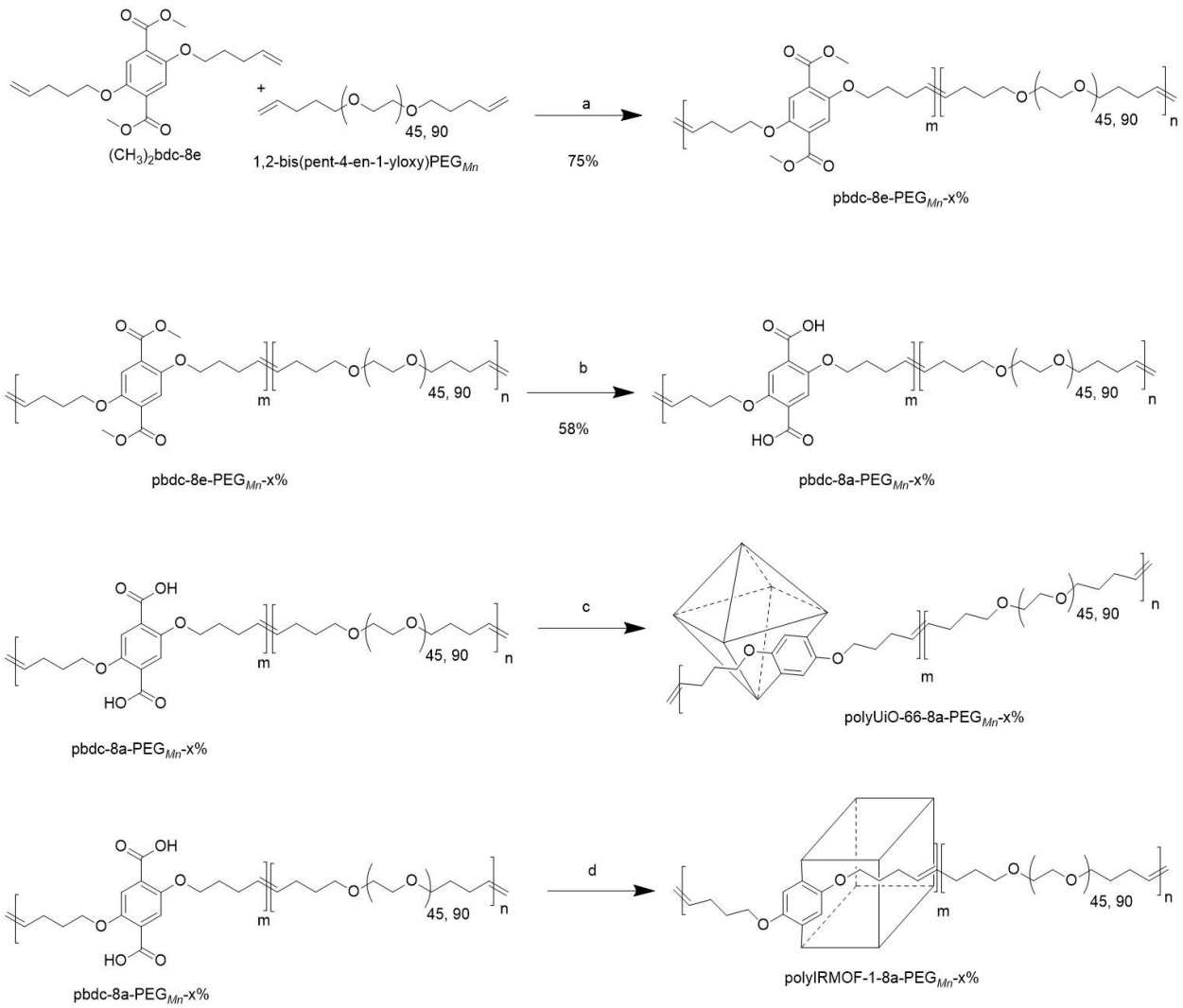

Scheme 4S.2. Synthesis of pbdc-8a-PEG$_{Mn}$-x%: a-d) Reagents and conditions: (a) Grubbs 2nd-generation catalyst, CH_2Cl_2, 50 °C, 5 h; (b) KOH, THF/H_2O, 40 °C, 12h; (c) $ZrCl_4$, 1:1 DEF/formic acid, 135 °C, 48h; (d) $Zn(NO_3)_2$*$6H_2O$, DMF, 100 °C, 24 h.

General polymerization procedure for pbdc-8e-PEG*Mn*-x% (Random AB copolymers). Dimethyl 2,5-bis(pent-4-en-1-yloxy) terephthalate (bdc-8e) (1.09 g, 3.00 mmol, 1.0 eq), 1,2-bis(pent-4-en-1-yloxy)PEG$_{Mn}$ (1-10 mol%) was added to a 10 mL round bottom flask, and dissolved in 5 mL CH_2Cl_2 and 100 µL methanol to enhance the solubility of the PEG. Grubbs second-generation catalyst was loaded neat (25 mg, 0.030 mmol, 0.01 eq). The reaction was set at 50 °C under mild nitrogen for 5 h while stirring. After 5 h, the solution was cooled to room

temperature, and 2 mL of ethyl vinyl ether was added to quench the catalyst. The solution was stirred for 30 min. The polymer was precipitated in diethyl ether, followed by centrifugation at 7000 rpm for 10 min. at 8 °C. The supernatant was decanted, and the polymer was dissolved using 5 mL CH_2Cl_2 and 2 mL of methanol. The polymer was precipitated four more times in diethyl ether. After the final wash, the polymer was dried under high vacuum for 2h.

pbdc-8e-PEG$_{2000}$-2%. Yield: 44% (540 mg, 1.0 mmol). ^{1}H NMR (400 MHz, $CDCl_3$) δ 7.33 (s, 147H), 5.73 – 5.41 (m, 138H), 4.10 – 3.96 (m, *J* = 11.8, 8.8 Hz, 309H), 3.89 (s, 406H), 3.64 (s, 180H), 2.38 – 2.12 (m, 184H), 1.86 (bs, *J* = 5.3 Hz, 193H). M_n: 18,700 g/mol, M_w/M_n: 1.3.

pbdc-8e-PEG$_{2000}$-20%. Yield: 61% (970 mg, 1.8 mmol). ^{1}H NMR (400 MHz, $CDCl_3$) δ 7.34 (s, 15H), 5.75 – 5.34 (m, 16H), 4.00 (s, *J* = 5.8 Hz, 32H), 3.89 (s, *J* = 8.2 Hz, 43H), 3.64 (s, *J* = 4.4 Hz, 180H), 2.34 – 2.12 (m, 23H), 1.97 – 1.80 (m, 23H). M_n: 14,700 g/mol, M_w/M_n: 1.4.

pbdc-8e-PEG$_{4000}$-1%. Yield: 63% (760 mg, 2.3 mmol). ^{1}H NMR (400 MHz, $CDCl_3$) δ 7.35 (s, 191H), 5.96 – 5.35 (m, 209H), 4.10 – 3.95 (m, 406H), 3.95 – 3.82 (m, *J* = 2.9 Hz, 531H), 3.64 (s, 364H), 2.40 – 2.13 (m, 265H), 2.01 – 1.75 (m, 299H). M_n: 18,700 g/mol, M_w/M_n: 1.5.

pbdc-8e-PEG$_{4000}$-10%. Yield: 50% (800 mg, 1.5 mmol). ^{1}H NMR (400 MHz, $CDCl_3$) δ 7.32 (s, 24H), 5.82 (dd, *J* = 16.9, 10.3 Hz, 1H), 5.69 – 5.32 (m, 26H), 4.99 (dd, *J* = 24.6, 13.6 Hz, 1H), 3.97 (t, *J* = 6.0 Hz, 49H), 3.86 (d, *J* = 8.0 Hz, 69H), 3.62 (s, 364H), 2.27 – 2.08 (m, 48H), 1.92 – 1.74 (m, 49H). M_n: 16,000 g/mol, M_w/M_n: 2.2.

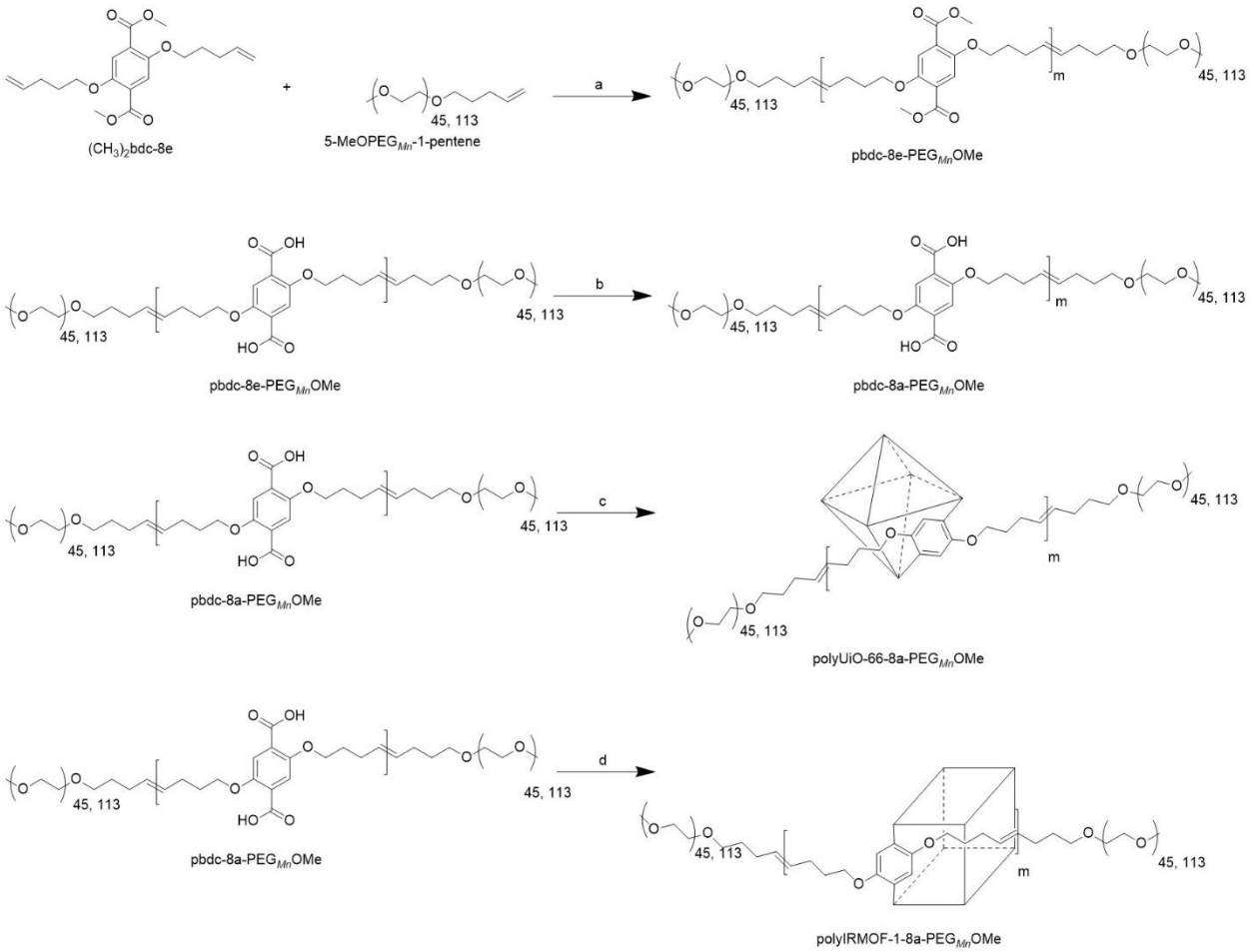

Scheme 4S.3. Synthesis of pbdc-8a-PEG$_{Mn}$OMe: a-e) Reagents and conditions: a) NaH, DMF, 45 °C, 4h; b) Grubbs 2nd-generation catalyst, CH_2Cl_2, 50 °C, 5 h, then 5-MeOPEG$_{Mn}$-1-pentene, 2 h; c) KOH, THF/H_2O, 40 °C, 12h; d) $ZrCl_4$, 1:1 DEF/formic acid, 135 °C, 48h; e) $Zn(NO_3)_2$*$6H_2O$, DMF, 100 °C, 24 h.

General polymerization procedure for pbdce-PEG$_{Mn}$OMe (AB_2 copolymers). Dimethyl 2,5-bis(pent-4-en-1-yloxy) terephthalate (bdc-8e) (1.09 g, 3.00 mmol, 1.0 eq), was added to a 10 mL round bottom flask, and dissolved in 5 mL CH_2Cl_2. Grubbs second-generation catalyst was loaded neat (25 mg, 0.030 mmol, 0.01 eq). The reaction was set at 50 °C under mild nitrogen for 5 h while stirring. After 5 h, 5-MeOPEG$_{Mn}$-1-pentene (4.0 mol%) was added to reaction, along with 100 µL methanol to enhance solubility of PEG. The mixture was stirred at 50 °C for an additional 2 h. Then, the solution was cooled to room temperature, 2 mL of ethyl vinyl ether was added to

quench the catalyst, and the solution was stirred for 30 min. The polymer was precipitated in diethyl ether, followed by centrifugation at 7000 rpm for 10 min. at 8 °C. The supernatant was decanted, and the polymer was dissolved using 5 mL CH_2Cl_2 and 2 mL of methanol. The polymer was precipitated four more times in diethyl ether. After the final wash, the polymer was dried under high vacuum for 2 h. *For purified AB_2 copolymers.* The procedure was followed as before, but after the third wash, the polymer was purified using silica gel chromatography at gradient from 0-20% methanol in CH_2Cl_2, eluting pbdc-8e at 3% methanol, and the desired AB_2 copolymers at 6% and 10% methanol in CH_2Cl_2.

pbdc-8e-PEG$_{2000}$OMe (crude). Yield: 46% (820 mg, 1.4 mmol). ^{1}H NMR (400 MHz, $CDCl_3$): δ 7.34 (s, 97H), 5.68 – 5.39 (m, 98H), 4.00 (t, J = 6.1 Hz, 200H), 3.89 (s, 279H), 3.64 (s, 180H), 2.19 (d, J = 3.6 Hz, 173H), 1.96 – 1.74 (m, 192H). M_n: 23,200 g/mol, M_w/M_n: 1.8.

pbdc-8e-PEG$_{2000}$OMe. Yield: 18% (140 mg, 0.30 mmol). ^{1}H NMR (400 MHz, $CDCl_3$) δ 7.35 (s, 56H), 5.75 – 5.34 (m, 57H), 4.00 (s, J = 15.4 Hz, 106H), 3.89 (s, J = 8.1 Hz, 143H), 3.64 (s, 180H), 2.19 (bs, 97H), 1.95 – 1.76 (m, J = 7.0 Hz, 102H). M_n: 20,300 g/mol, M_w/M_n: 1.6.

pbdc-8e-PEG$_{5000}$OMe (crude). Yield: 64% (920 mg, 1.9 mmol). ^{1}H NMR (400 MHz, $CDCl_3$) δ 7.35 (s, 133H), 5.78 – 5.37 (m, 1H), 4.00 (t, J = 6.0 Hz, 274H), 3.90 (s, 315H), 3.65 (s, 460H), 2.36 – 2.13 (m, 234 H), 1.97 – 1.74 (m, 245 H). M_n: 29,400 g/mol, M_w/M_n: 1.7.

pbdc-8e-PEG$_{5000}$OMe. Yield: 5.5% (79 mg, 0.17 mmol). ^{1}H NMR (400 MHz, $CDCl_3$) δ 7.34 (s, 30H), 5.65 – 5.35 (m, 26H), 5.02 (dd, J = 24.9, 13.6 Hz, 1H), 4.00 (t, J = 5.9 Hz, 53H), 3.88 (d, J = 8.0 Hz, 82H), 3.64 (s, 448H), 2.29 – 2.12 (m, 50H), 1.85 (d, J = 7.1 Hz, 51H). M_n: 19,900 g/mol, M_w/M_n: 1.4.

Procedure for ester deprotection of PEG copolymers. The PEG copolymer ester (300 to 800 mg) was added to a 250 mL round-bottom flask, along with potassium hydroxide (30 equiv), and

placed in 60 mL a 1:1 of THF/water solution. The mixture was heated at 45 °C overnight. The THF was reduced by evaporation. The solution was acidified to a pH value of ~1 using a 2M HCl solution. The resultant polymer suspension was collected by centrifugation at 7000 rpm for 10 min. at 8 °C. The solid was transferred to a vial and dried under high vacuum. If no solid was observed after acidification, then the water was removed by evaporation. To the resultant polymer/salt mixture was added a 20 mL solution containing 1:1 DMF/Acetone, dissolving the polymer only. The salts were removed by filtration. The remaining solution was evaporated to yield the polymer ligand.

pbdc-8a-PEG$_{2000}$-2%. Yield: 96% (210 mg, 0.41 mmol). ^{1}H NMR (400 MHz, DMSO-d$_6$) δ 7.26 (s, *J* = 6.4 Hz, 162H), 5.99 – 5.76 (m, 8H), 5.74 – 5.33 (m, 150H), 5.08 – 4.94 (m, 1H), 3.97 (d, *J* = 6.4 Hz, 295H), 3.50 (s, 180H), 2.13 (s, *J* = 6.8 Hz, 174H), 1.86 – 1.57 (m, 212H).

pbdc-8a-PEG$_{2000}$-20%. Yield: 90.1% (350 mg, 0.69 mmol). ^{1}H NMR (400 MHz, DMSO-d$_6$) δ 7.25 (s, *J* = 6.7 Hz, 15H), 5.65 – 5.36 (m, 15H), 4.08 – 3.89 (m, 30H), 3.50 (s, 180H), 2.13 (s, *J* = 39.3 Hz, 21H), 1.90 – 1.56 (m, 23H).

pbdc-8a-PEG$_{4000}$-1%. Yield: 78% (230 mg, 0.59 mmol). ^{1}H NMR (400 MHz, DMSO-d$_6$). δ 7.25 (s, *J* = 6.6 Hz, 236H), 6.02 – 5.82 (m, 4H), 5.73 – 5.23 (m, 214H), 3.97 (d, *J* = 6.4 Hz, 429H), 3.50 (s, 364H), 2.25 – 2.05 (m, 255H), 1.83 – 1.56 (m, 313H).

pbdc-8a-PEG$_{4000}$-10%. Yield: 49% (230 mg, 0.94 mmol). ^{1}H NMR (400 MHz, DMSO-d$_6$) δ 7.25 (s, 51H), 5.67 – 5.30 (m, 54H), 5.00 (dd, *J* = 25.7, 14.7 Hz, 1H), 3.96 (t, *J* = 5.7 Hz, 98H), 3.50 (s, 364H), 2.12 (s, *J* = 39.5 Hz, 97H), 1.85 – 1.51 (m, 104H).

pbdc-8a-PEG$_{2000}$OMe (crude). Yield: 87% (330 mg, 0.840 mmol) ^{1}H NMR (400 MHz, DMSO-d$_6$) δ 7.25 (s, 104H), 5.70 – 5.34 (m, 113H), 3.96 (bs, 347H), 3.50 (s, 180H), 2.12 (s, 182H), 1.71 (s, *J* = 88.2 Hz, 200H).

pbdc-8a-PEG$_{2000}$OMe. Yield: 70% (82 mg, 0. 26 mmol). ^{1}H NMR (400 MHz, DMSO-d$_6$) δ 7.25 (s, 58H), 5.68 – 5.32 (m, 58H), 3.97 (d, *J* = 6.2 Hz, 111H), 3.50 (s, 180H), 2.12 (s, 102H), 1.72 (s, 110H).

pbdca-PEG$_{5000}$OMe (crude). Yield: 89% (400 mg, 0.98 mmol). ^{1}H NMR (400 MHz, DMSO-d$_6$) δ 7.25 (s, 112H), 5.99 – 4.97 (m, 105H), 3.96 (t, *J* = 6.0 Hz, 243H), 3.50 (s, 454H), 2.12 (s, 188H), 1.84 – 1.53 (m, 203H).

pbdca-PEG$_{5000}$OMe. Yield: 33% (20 mg, 0.045 mmol). ^{1}H NMR (400 MHz, DMSO-d$_6$) δ 7.25 (s, 44H), 5.71 – 5.29 (m, 42H), 5.00 (dd, *J* = 24.0, 13.6 Hz, 1H), 3.96 (t, *J* = 6.1 Hz, 80H), 3.50 (s, 451H), 2.30 – 2.03 (m, 75H), 1.86 – 1.61 (m, 76H).

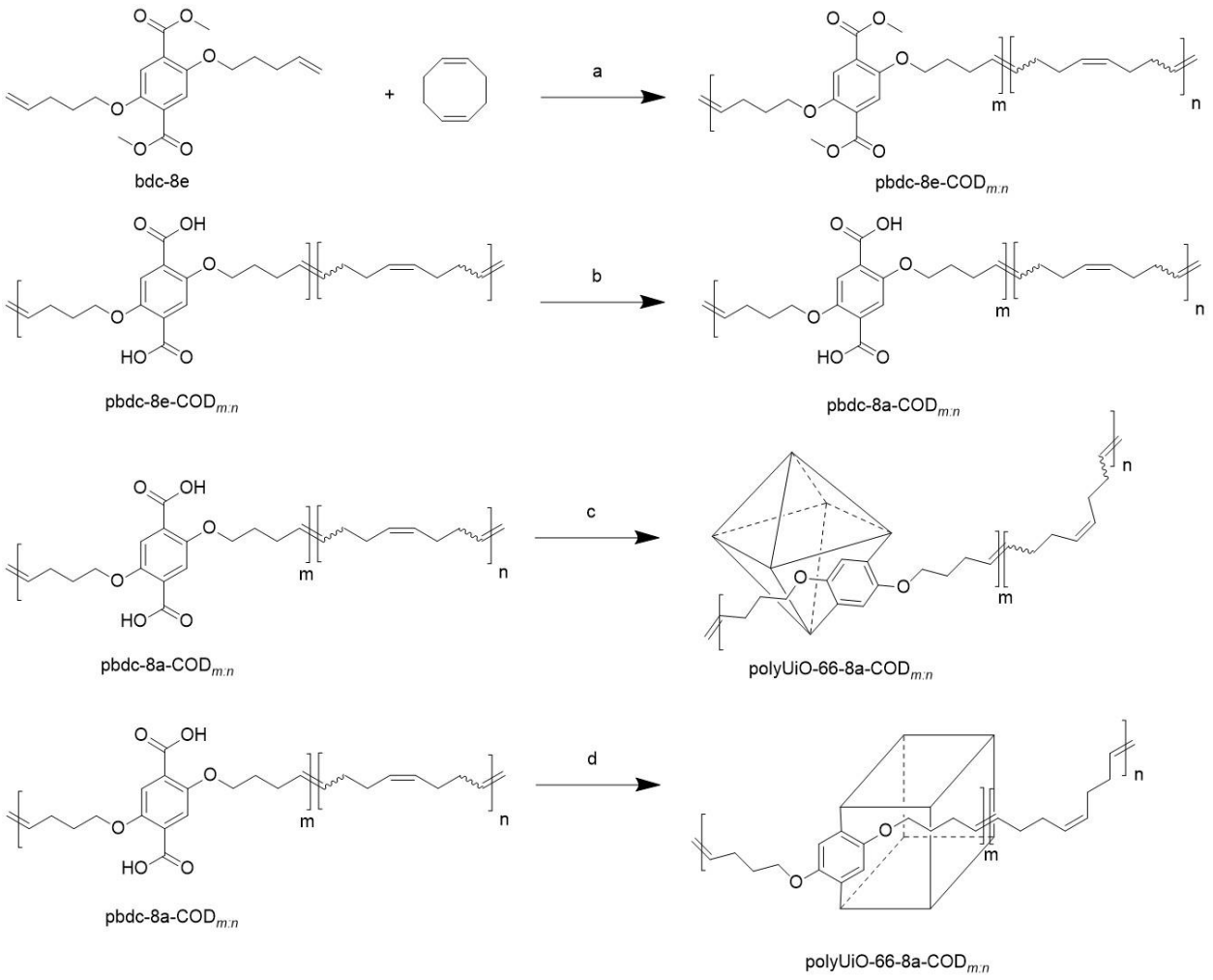

Scheme 4S.4. Synthesis of pbdc-8a-COD$_{m:n}$: a-d) Reagents and conditions: b) Hoveyda-Grubbs 2nd-generation catalyst, CH_2Cl_2, 50 °C, 5 h, then COD, 1 h; c) KOH, THF/H_2O, 40 °C, 12h; d) $ZrCl_4$, 1:1 DEF/formic acid, 135 °C, 48h; e) $Zn(NO_3)_2$*$6H_2O$, DMF, 100 °C, 24 h.

General procedure for synthesis of pbdc-8e-COD$_{m:n}$. To a 10 mL round bottom flask was added bdc-8e monomer (1.087g, 3.0 mmol, 1.00 eq), and dissolved in 5 mL of CH_2Cl_2. Hoveyda-Grubbs 2nd-generation catalyst was loaded neat (18 mg, 0.030 mmol, 0.01 eq). The reaction was set at mild reflux (45 °C) under mild nitrogen for 5 h. After 5 h, the appropriate amount of COD (0.300-6.00 mmol) along with 1 mL of CH_2Cl_2 was added to the reaction mixture, and stirred for an additional 30 min at 45 °C. The solution was cooled to room temperature, and ethyl vinyl ether (2 mL) was added to quench the catalyst, stirring for 30 min. The polymer was precipitated in

methanol, followed by centrifugation at 7000 rpm for 10 min. at room temperature. The supernatant was decanted, and the polymer was dissolved in CH_2Cl_2 and precipitated four more times in methanol. After the final wash, the polymer was transferred to a vial, and dried under vacuum for further analysis.

pbdc-8e-COD$_{10:1}$. Yield: 57% (800 mg, 1.7 mmol): ^{1}H NMR (400 MHz, $CDCl_3$) δ 7.35 (s, 2H), 5.84 – 5.23 (m, 4H), 4.00 (t, *J* = 6.0 Hz, 5H), 3.89 (s, 4H), 2.19 (s, 4H), 2.03 (s, 1H), 1.85 (d, *J* = 6.3 Hz, 4H).

pbdc-8e-COD$_{2:1}$. Yield: 60.% (880 mg, 3.00 mmol). ^{1}H NMR (400 MHz, $CDCl_3$): δ 7.35 (s, 2H), 5.90 – 4.95 (m, 4H), 4.00 (t, *J* = 5.8 Hz, 4H), 3.88 (d, *J* = 8.1 Hz, 6H), 2.18 (s, 4H), 2.02 (s, 4H), 1.86 (bs, 3H). M_n: 17,500 g/mol, M_w/M_n: 2.8.

pbdc-8e-COD$_{1:1}$. Yield: 96% (1.26 g, 2.68 mmol). ^{1}H NMR (400 MHz, $CDCl_3$): δ 7.35 (s, 2H), 5.63 – 5.33 (m, 6H), 4.00 (t, *J* = 6.0 Hz, 4H), 3.89 (s, 5H), 2.15 (bs, 4H), 2.02 (s, 8H), 1.93 – 1.76 (m, 4H). M_n: 17,200 g/mol, M_w/M_n: 2.8.

General Procedure for ester deprotection of pbdc-8e-COD$_{m:n}$. The polymer ester (600mg - 1.6g) was added to a 250-mL round-bottom flask, along with sodium hydroxide (30 equivalents), and placed in 60 mL a 1:1 of THF:water solution. The mixture was heated at 60 °C for 12h, or until the solution became clear. A biphasic solution containing THF and water was observed. The THF was reduced by evaporation. The solution was acidified *dropwise* to a pH value of ~5 using a 2M HCl solution. The resultant solid was collected by vacuum filtration.

pbdc-8a-COD$_{10:1}$. Yield: 81% (560 mg, 1.6 mmol). ^{1}H NMR (400 MHz, DMSO-d_6) δ 7.24 (s, 2H), 5.78 – 5.16 (m, 3H), 4.94 (s, 1H), 3.94 (s, 5H), 2.11 (s, 4H), 1.93 (d, *J* = 25.5 Hz, 1H), 1.70 (s, 4H).

pbdc-8a-COD$_{2:1}$. Yield: 99% (630 mg, 1.4 mmol). ^{1}H NMR (400 MHz, DMSO-d$_6$) δ 7.25 (s, 2H), 5.45 (dd, *J* = 62.1, 34.5 Hz, 4H), 3.96 (s, 4H), 2.11 (s, 3H), 1.97 (s, 4H), 1.71 (s, 3H).

pbdc-8a-COD$_{1:1}$. Yield: 93% (530 mg, 1.3 mmol). ^{1}H NMR (400 MHz, DMSO-d$_6$): δ 7.25 (s, 2H), 5.93 – 4.76 (m, 6H), 3.86 (d, *J* = 67.8 Hz, 4H), 2.07 (d, *J* = 29.1 Hz, 3H), 1.96 (s, 7H), 1.71 (s, 3H).

General procedure for Zr-polyMOF synthesis. Procedure was adapted and modified from the synthesis of polyUiO-66 discussed in Chapter 2. The polymer ligand (0.03 mmol by monomer repeat unit), $ZrCl_4$ (0.037 mmol), and 2 mL of DEF were added to a 20 mL scintillation vial. After the solution became clear, 2 mL of formic acid was added. The vial was heated at 135 °C for 48 h. The resultant film was washed by exchanging solvent with copious amounts of DMF, followed by copious amounts of methanol.

General procedure for IRMOF-type polyMOF synthesis. The IRMOF-type polyMOFs were prepared by adapting the procedure discussed in Chapter 3. The appropriate copolymer ligand (0.0250 mmol by monomer repeat unit), $Zn(NO_3)_2 \cdot 6H_2O$ (0.125 mmol), and 1.3 mL of DMF were mixed in a 20 mL scintillation vial. The vial was placed in a pre-heated oven at 100 °C for 24 h. The resultant off-white powders were cleaned by centrifugation (4000 rpm), and extensive washing by solvent-exchange of DMF (5x5 mL of DMF). The samples were kept in DMF until further studies were performed.

Analytical Characterization

Gel-permeation chromatography (GPC) conditions for analysis of copolymer esters. Gel-permeation chromatography was performed in DMF (0.7 mL/min) using a Malvern GPC equipped with D4000 single-pore column and D-6000M general-purpose mixed-bed weight divinylbenzene

column connected in series to determine molecular weights and molecular weight distributions, M_w/M_n, of our polymers. The solutions were filtered through 0.4 μm PTFE membrane before being injected into either GPC instrument. Narrow PMMA was used as the calibration standard.

PXRD Analysis. *For UiO-66 polyMOFs.* The synthesized materials were collected by filtration, washed with copious amounts of DMF, followed by copious amounts of methanol, and dried for ~20 min before data collection. *For IRMOF-1 polyMOFs.* the samples were loaded on silicon crystal sample holders while still wet with DMF. PXRD data were collected at ambient temperature on a Bruker D8 Advance diffractometer at 40 kV and 40 mA for Cu Kα (λ = 1.5418 Å), with a scan speed of 0.5 s/step, a step size of 0.02° in 2θ, and a 2θ range of 5−50°.

^{1}H NMR Digestions. *For block-polyUiO-66-PEG.* To ~5 mg of material was added 500 μL solution containing 100 μL of 1M NaOD and 400 μL DMSO-d_6. Samples were sonicated at 40 °C for 1 h. Then, samples were placed in an oven at 40 °C overnight. The remaining solids were filtered through 0.4 μm PTFE membranes and the solution was analyzed by ^{1}H NMR. *For block-polyUiO-66-COD$_{m:n}$.* Samples were filtered and washed with copious amounts of DMF, methanol, and acetone to remove any impurities. About 10 mg of material was dissolved in 600 μL DMSO-d_6 using 10 μL of 50% HF in water to digest the polyMOF. *For all polyIRMOF-1 samples.* About 5 mg of polyMOF was washed with DMF and CH_2Cl_2. To the samples was added a solution containing 600 μL of DMSO-d_6 and 5 μL of DCl. The mixture was sonicated at room temperature for 1 h. The solution was used for ^{1}H NMR analysis.

SEM Measurements. All samples were transferred to conductive carbon tape on a sample holder, and coated using a Ir-sputter coating for 7 sec. A Philips XL ESEM instrument was used for acquiring images using a 10 kV energy source under vacuum at a working distance at 10 mm.

Dynamic Light Scattering (DLS). Polymers were dissolved in *N*,*N*-diethylformamide at 5 mg/mL, sonicated for 30 min, and filtered through 0.45 micron PTFE filters into pre-cleaned quartz cuvettes prior to analysis. DLS was performed on a Malvern Zetasizer ZS90 (Malvern, UK) at both 13° and 90°. Hydrodynamic radii were determined from distribution fits to the autocorrelation functions using number-averaged weighed values.

N_2-Sorption Measurements. Prior to analysis, the materials were washed by exchanging the solvent with DMF three times for 1 d, then with methanol five times a day for 2 d, and finally with CH_2Cl_2 five times a day for 1d. About 40-50 mg of the samples were transferred to pre-weighed sample tubes, and the samples were evacuated in a vacuum line until solvent was evaporated. The crystals were activated using an ASAP 2020 Adsorption analyzer under vacuum at 70 °C for 10h. After degassing, the sample tube was reweighed to obtain an accurate mass measurement for the degassed sample. All measurements were obtained at 77K using a liquid nitrogen bath.

Supplemental Information

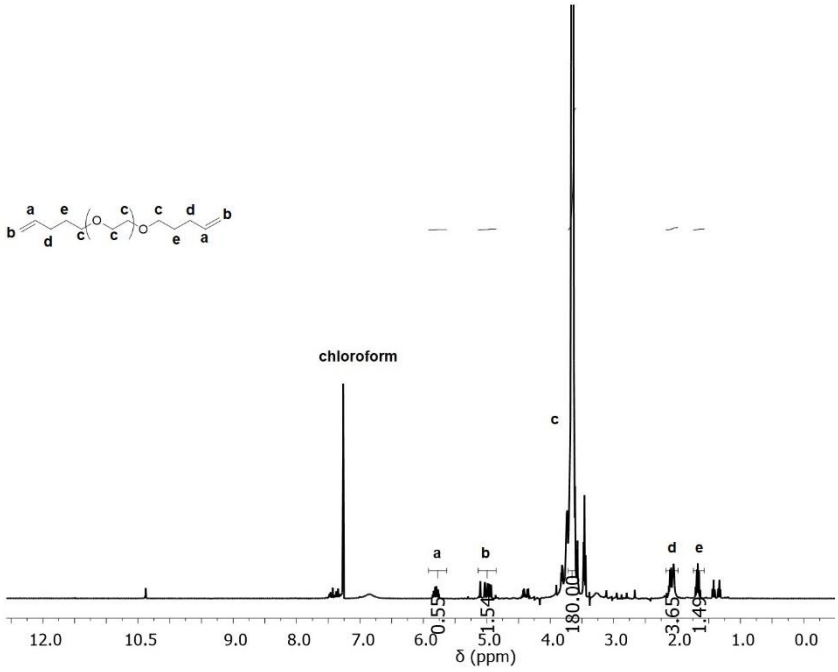

Figure 4S.1. ^{1}H NMR of 1,2-bis(pent-4-en-1-yloxy)PEG$_{2000}$.

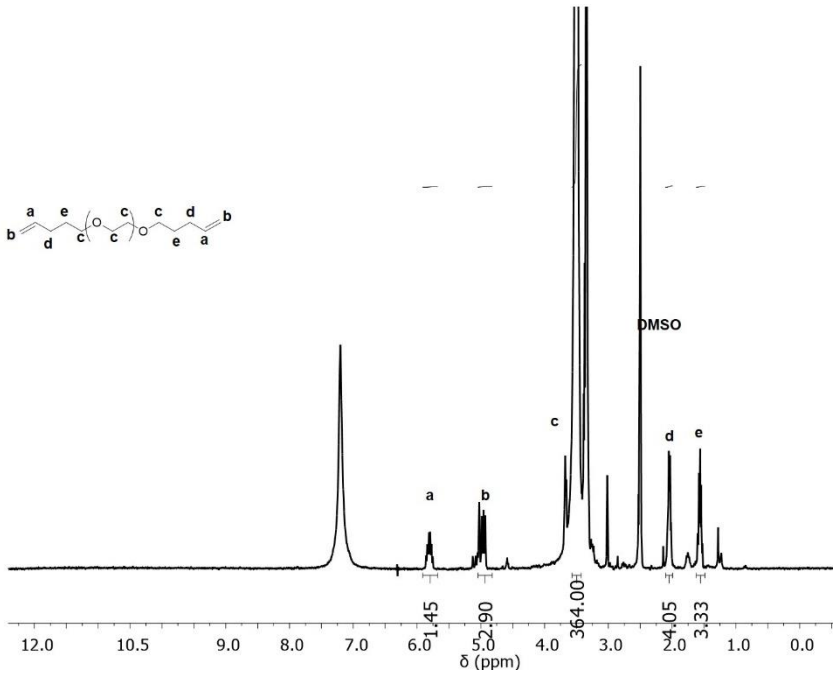

Figure 4S.2. ^{1}H NMR of 1,2-bis(pent-4-en-1-yloxy)PEG$_{4000}$.

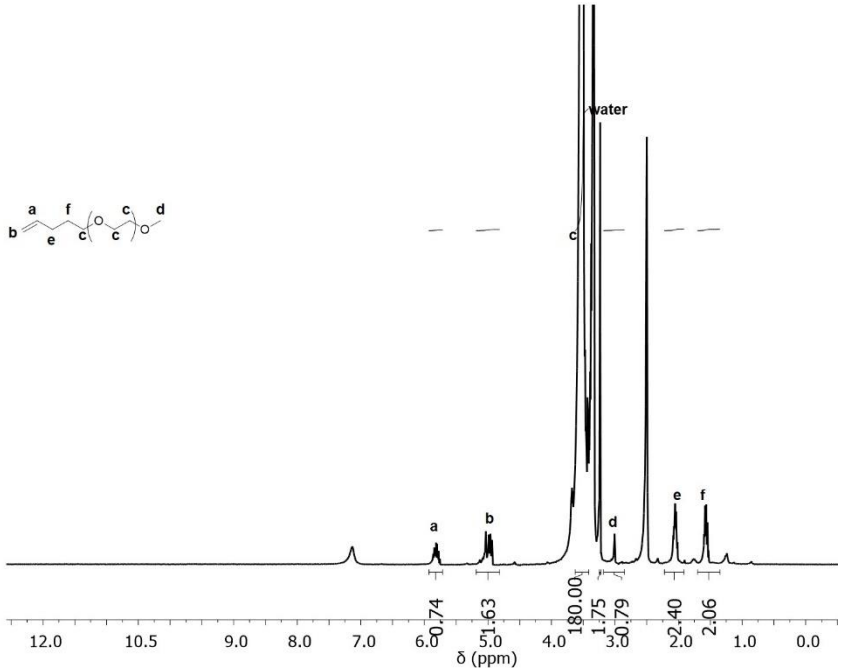

Figure 4S.3. ^{1}H NMR of 5-MeOPEG$_{2000}$-1-pentene.

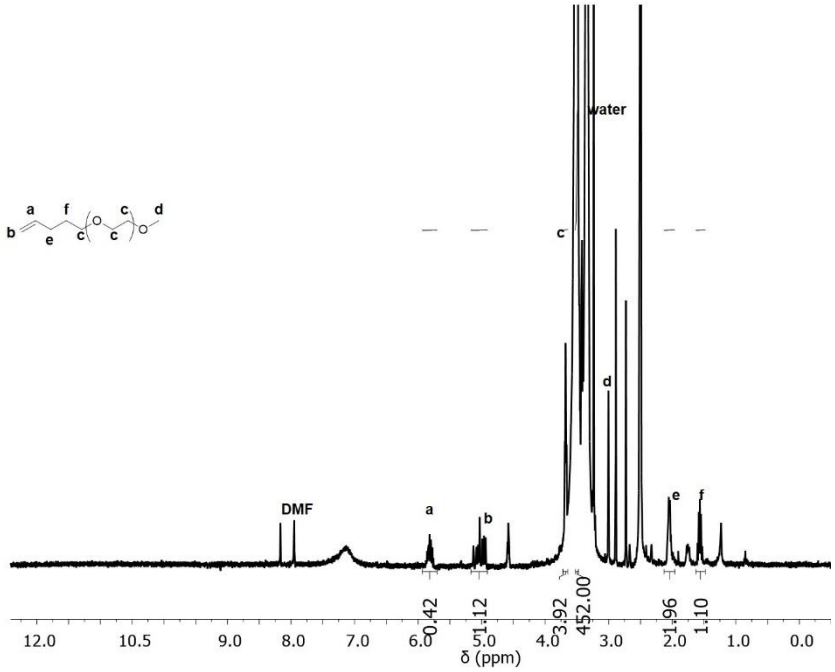

Figure 4S.4. ^{1}H NMR of 5-MeOPEG$_{5000}$-1-pentene.

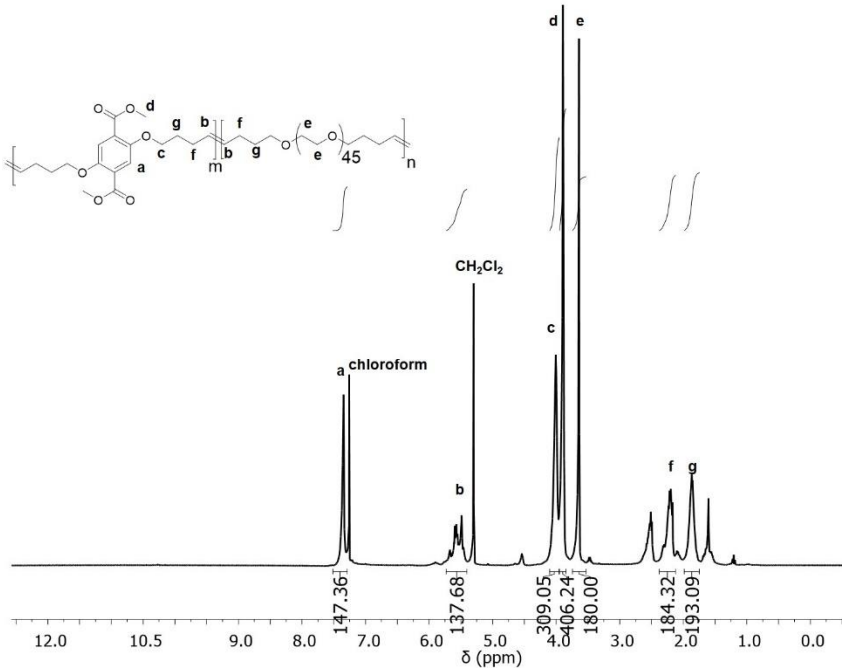

Figure 4S.5. ^{1}H NMR of pbdc-8e-PEG$_{2000}$-2%.

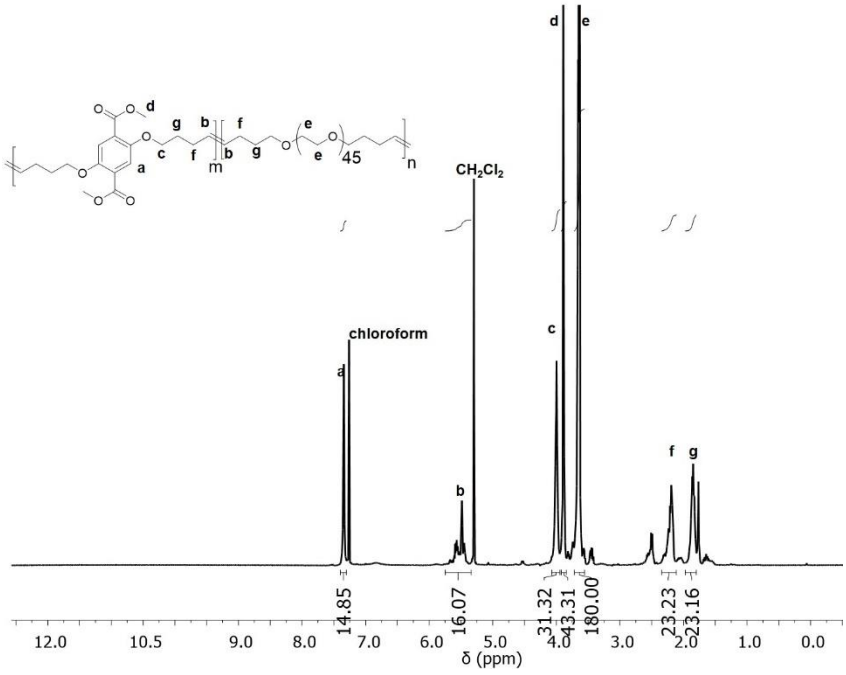

Figure 4S.6. ^{1}H NMR of pbdc-8e-PEG$_{2000}$-20%.

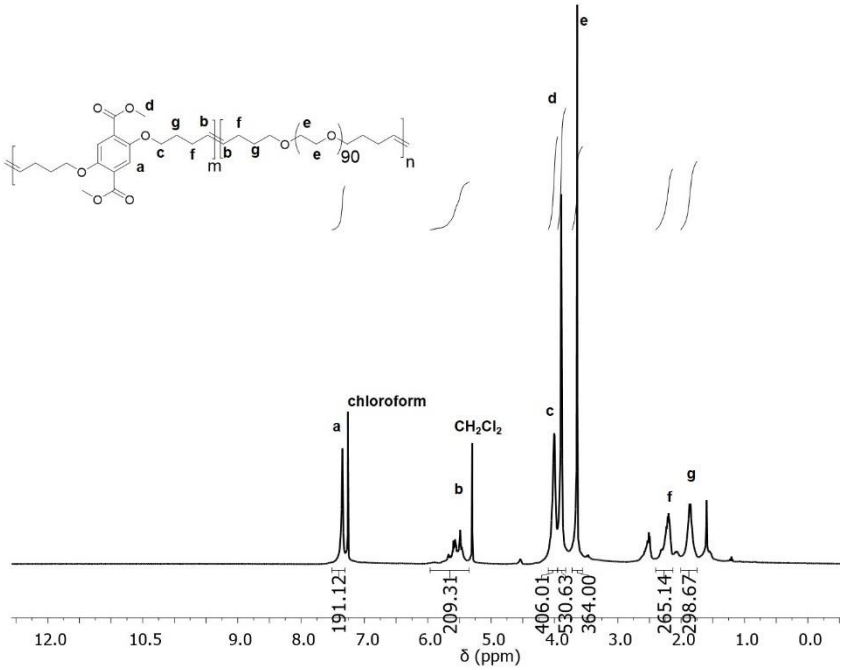

Figure 4S.7. ^{1}H NMR of pbdc-8e-PEG$_{4000}$-1%.

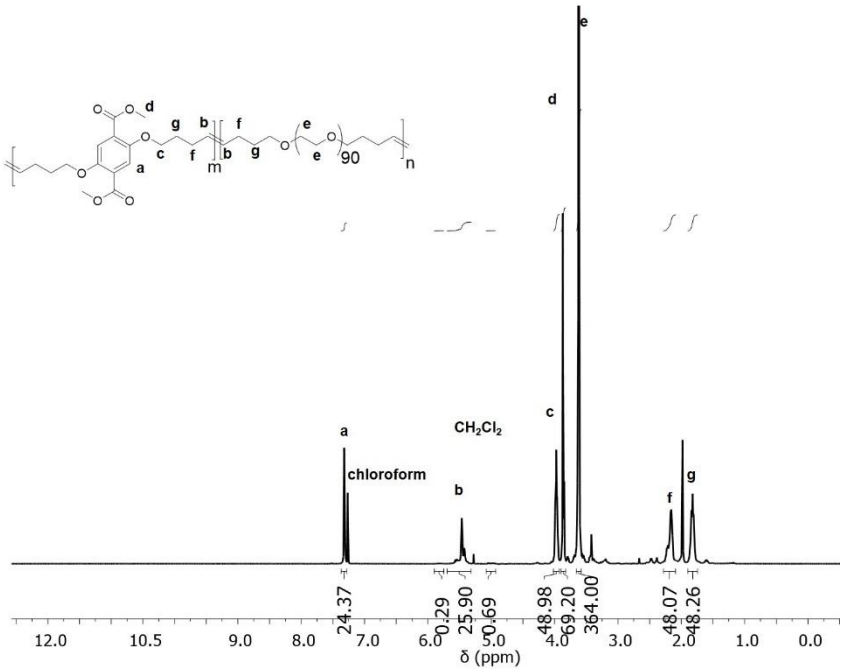

Figure 4S.8. ^{1}H NMR of pbdc-8e-PEG$_{4000}$-10%.

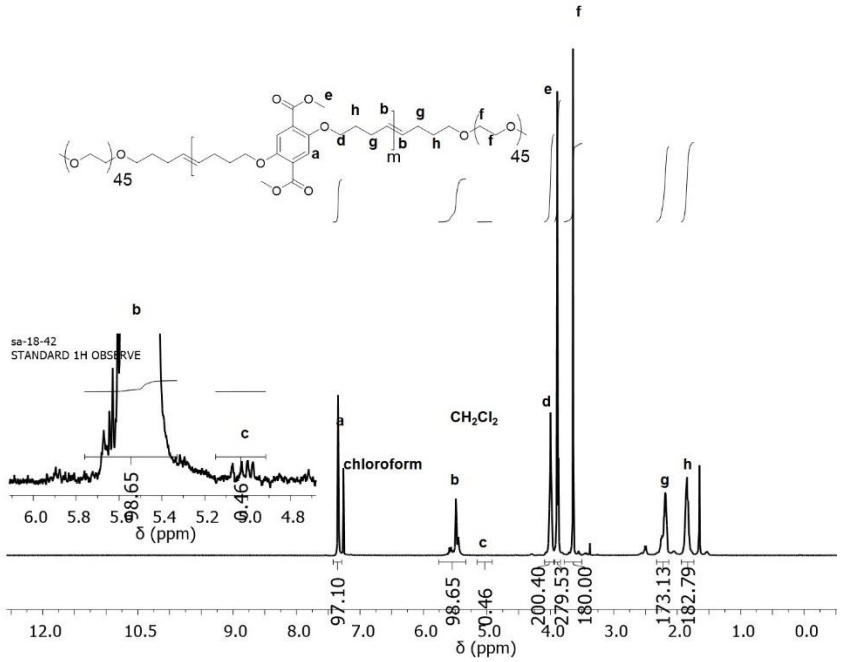

Figure 4S.9. ^{1}H NMR of crude pbdc-8e-PEG$_{2000}$OMe.

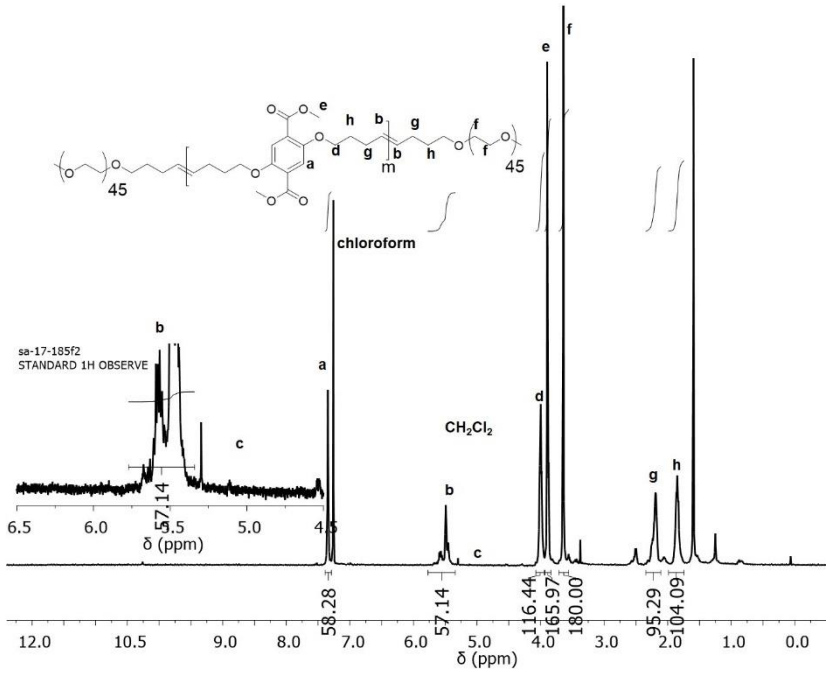

Figure 4S.10. ^{1}H NMR of pbdc-8e-PEG$_{2000}$OMe. End-group analysis was used to determine the purity of the AB_2 copolymer.

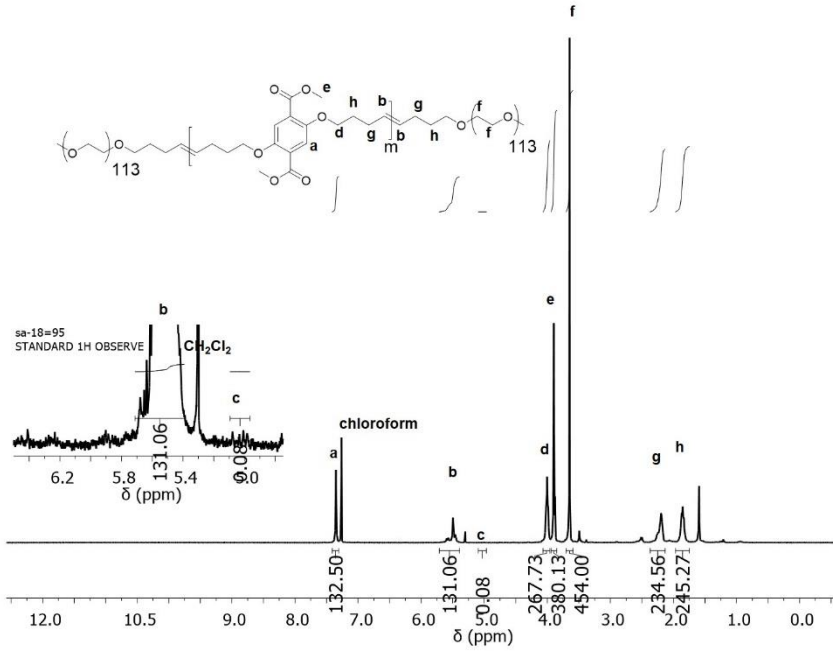

Figure 4S.11. ^{1}H NMR of crude pbdc-8e-PEG$_{5000}$OMe.

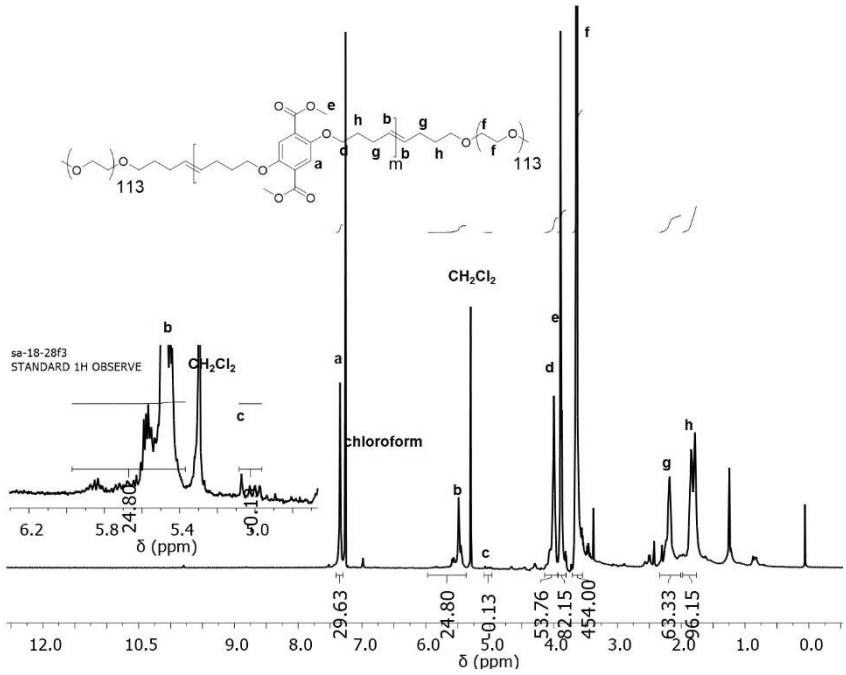

Figure 4S.12. ^{1}H NMR of pbdc-8e-PEG$_{5000}$OMe. End-group analysis was used to determine the purity of the AB_2 copolymer.

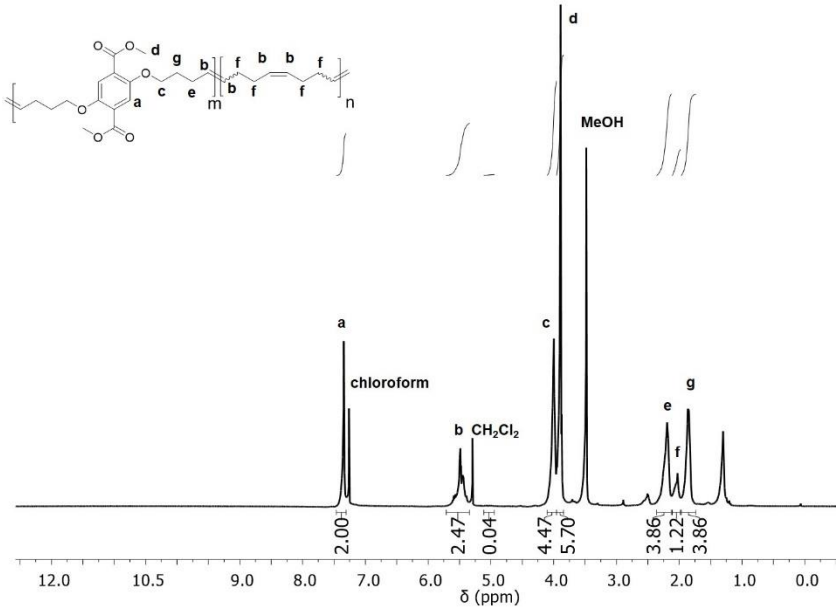

Figure 4S.13. ^{1}H NMR of pbdc-8e-COD$_{10:1}$.

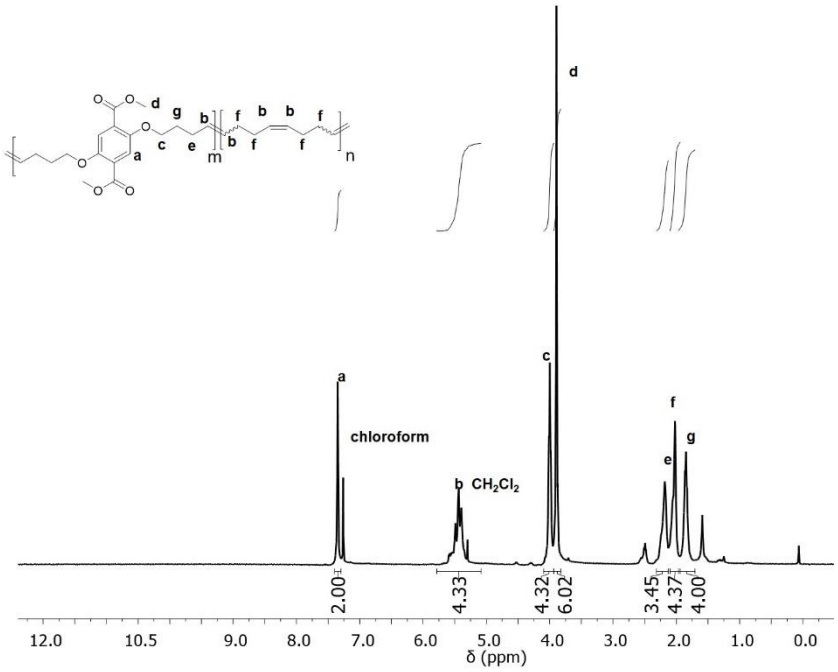

Figure 4S.14. ^{1}H NMR of pbdc-8e-COD$_{2:1}$.

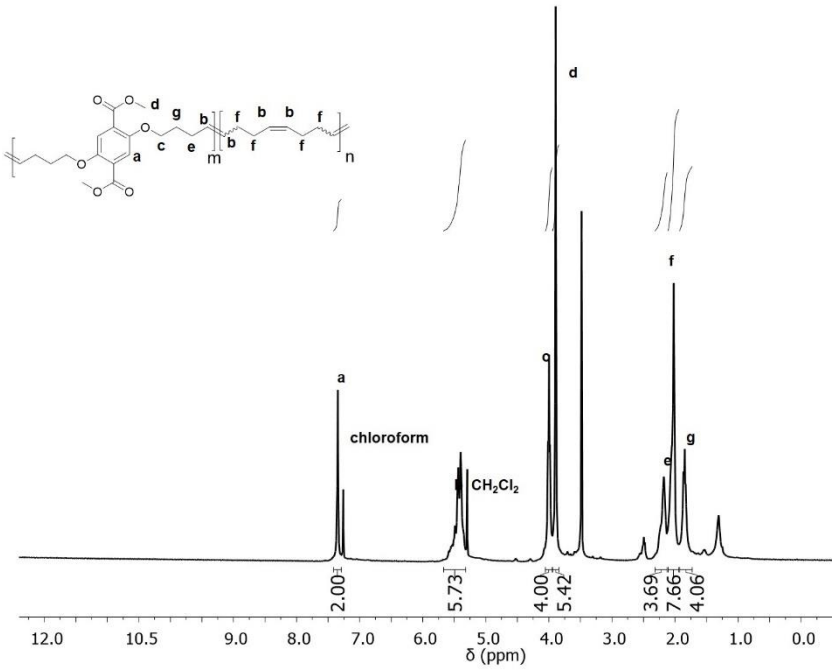

Figure 4S.15. ^{1}H NMR of pbdc-8e-COD$_{1:1}$.

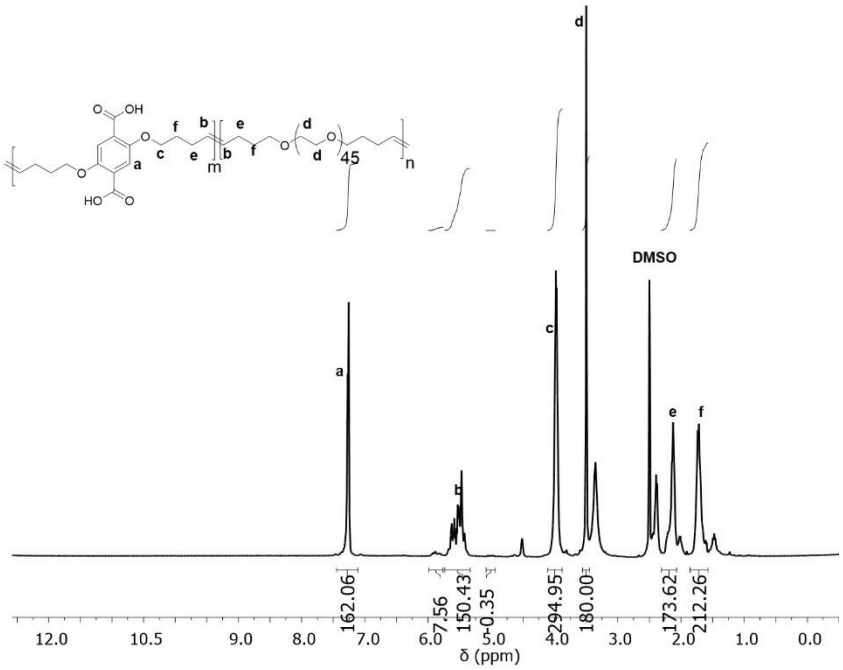

Figure 4S.16. ^{1}H NMR of pbdc-8a-PEG$_{2000}$-2%.

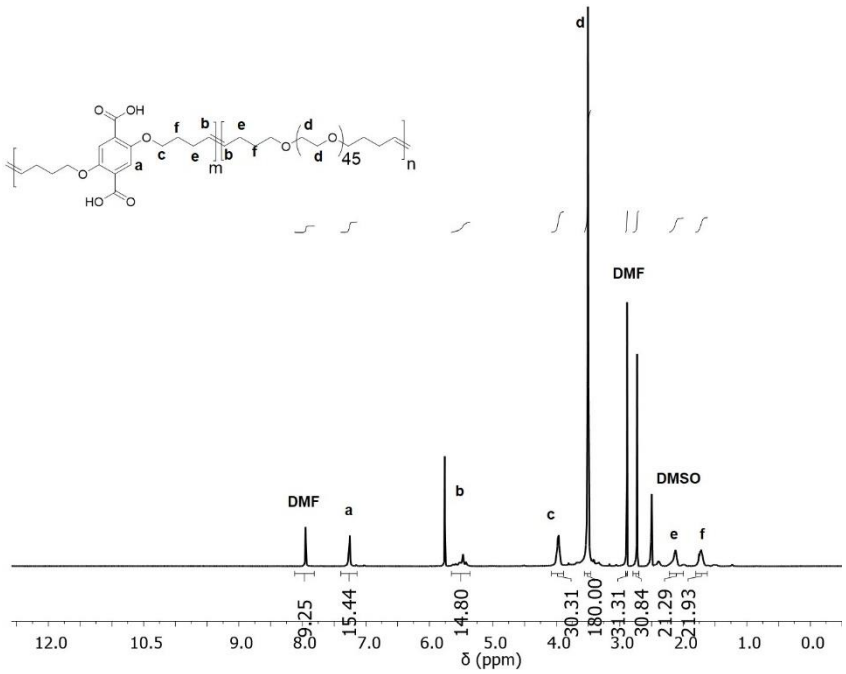

Figure 4S.17. ^{1}H NMR of pbdc-8a-PEG$_{2000}$-20%.

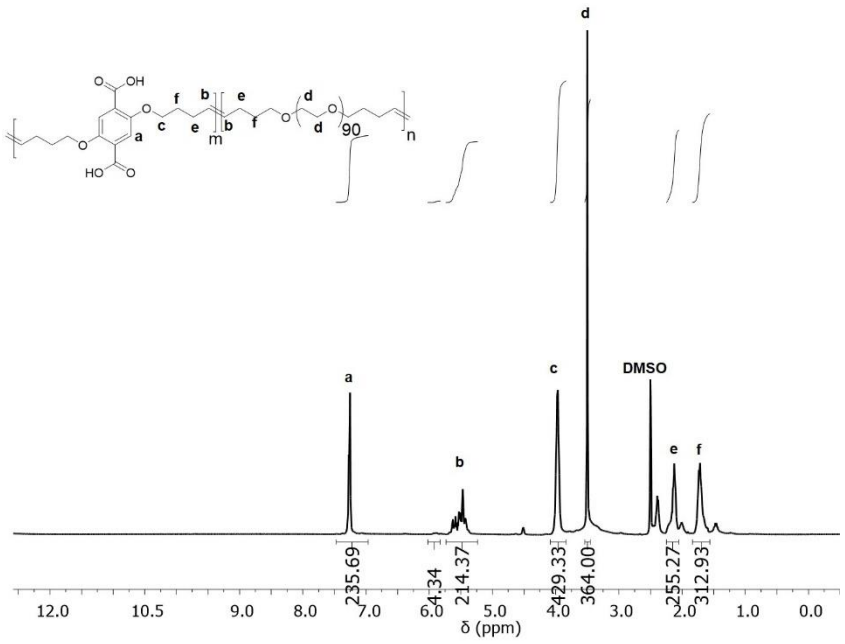

Figure 4.S18. ^{1}H NMR of pbdc-8a-PEG$_{4000}$-1%.

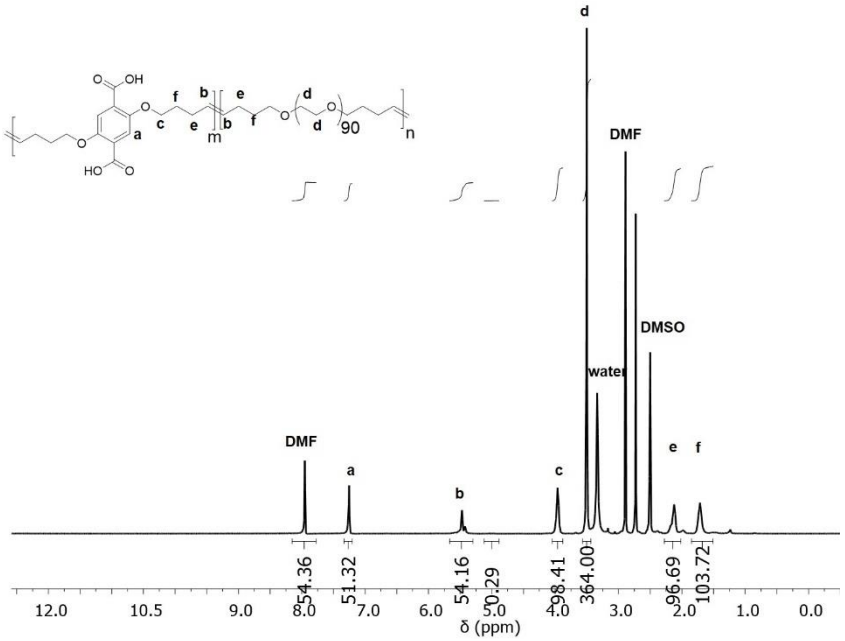

Figure 4S.19. ^{1}H NMR of pbdc-8a-PEG$_{4000}$-10%.

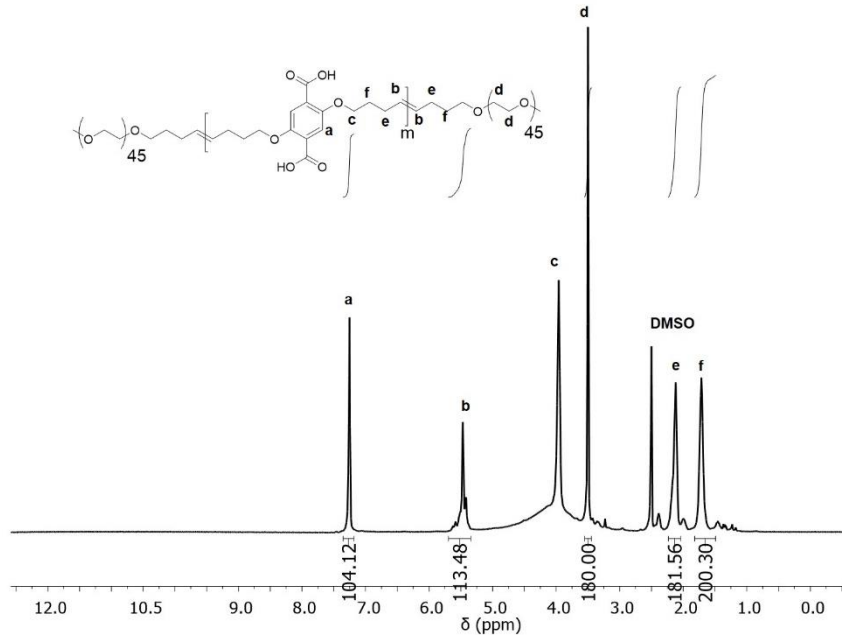

Figure 4S.20. ^{1}H NMR of crude pbdc-8a-PEG$_{2000}$OMe.

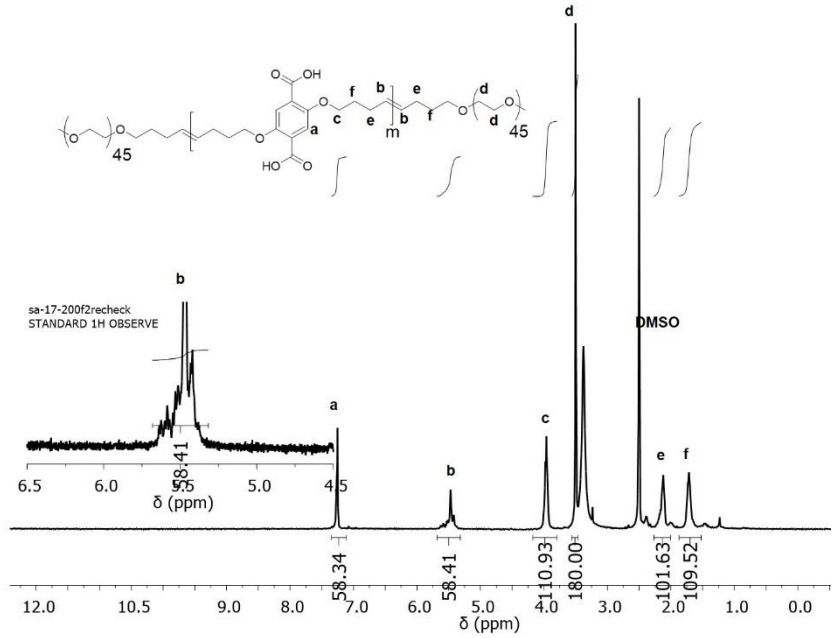

Figure 4S.21. ^{1}H NMR of pbdc-8a-PEG$_{2000}$OMe.

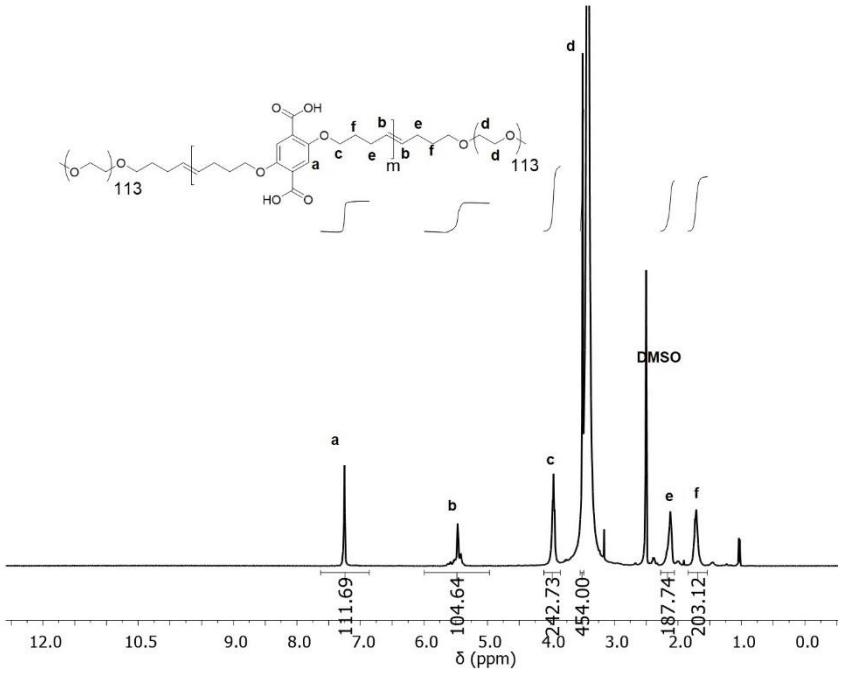

Figure 4S.22. ^{1}H NMR of crude pbdc-8a-PEG$_{5000}$OMe.

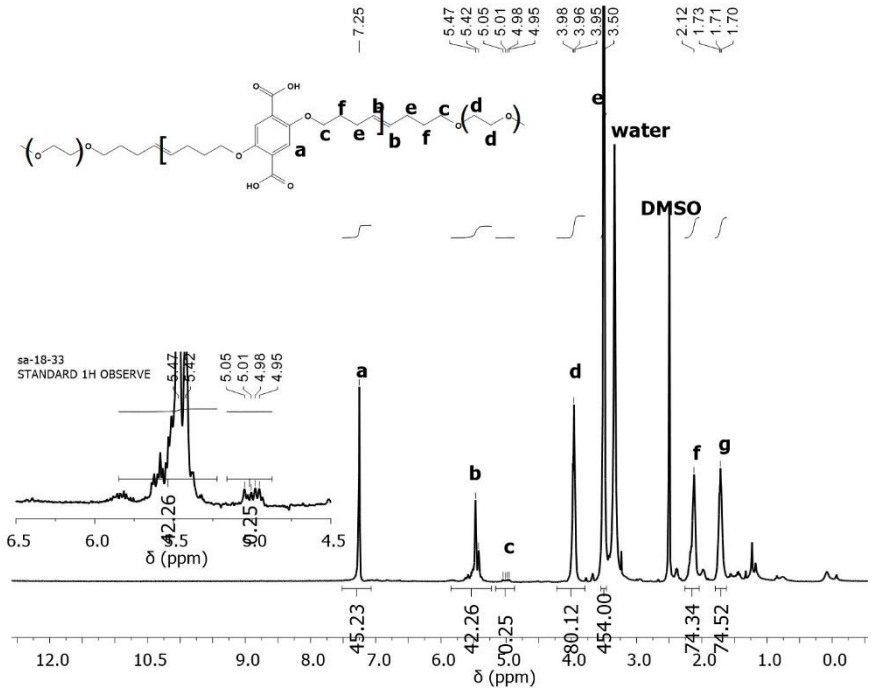

Figure 4S.23. ^{1}H NMR of pbdc-8a-PEG$_{5000}$OMe.

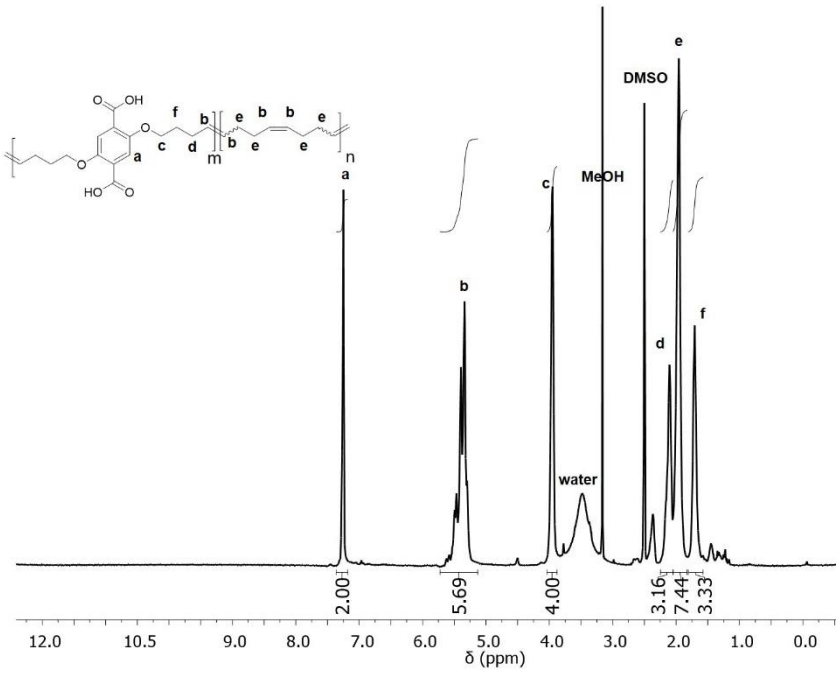

Figure 4S.24. ^{1}H NMR of pbdc-8a-COD$_{1:1}$.

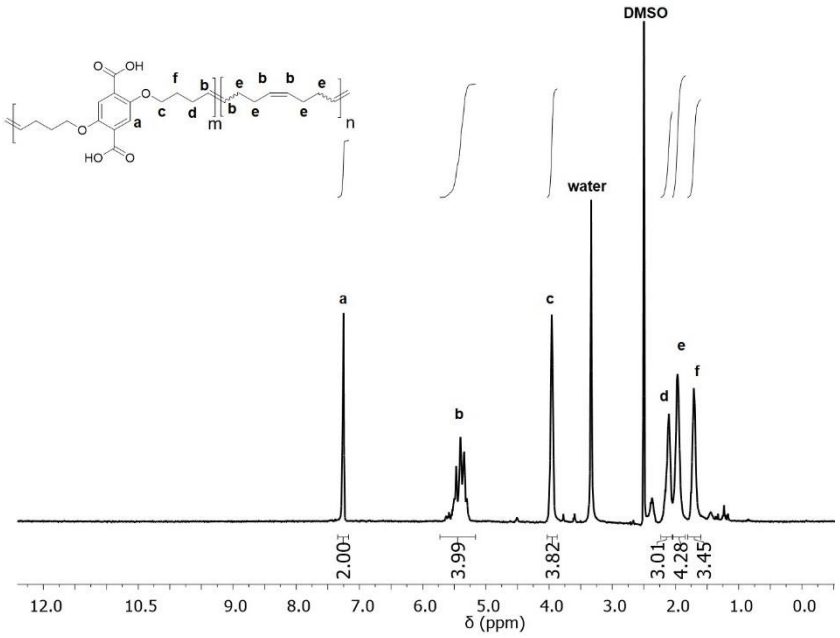

Figure 4S.25. ^{1}H NMR of pbdc-8a-COD$_{2:1}$.

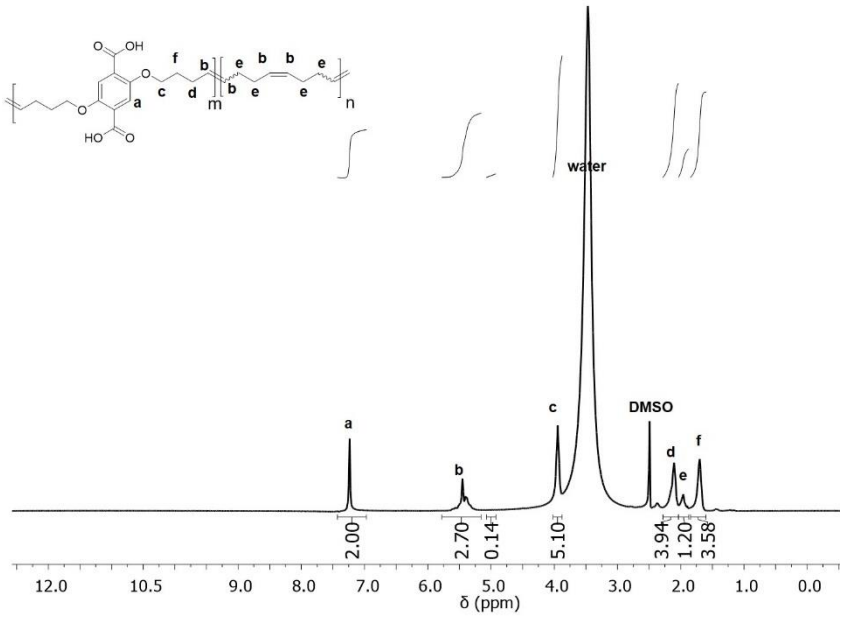

Figure 4S.26. ^{1}H NMR of pbdc-8a-COD$_{10:1}$.

Table 4S.1. Ratio of bdc-8e to co-monomer.

Ligand	Ratio of bdc-8e: co-monomer (^{1}H NMR) [a]
pbdc-8e-PEG$_{2000}$-2%	1: 0.63
pbdc-8e-PEG$_{2000}$-20%	1: 6.4
pbdc-8e-PEG$_{4000}$-1%	1: 0.91
pbdc-8e-PEG$_{4000}$-10%	1: 7.5
pbdc-8e-PEG$_{2000}$OMe (crude)	1: 0.91
pbdc-8e-PEG$_{2000}$OMe	1: 1.6
pbdc-8e-PEG$_{5000}$OMe (crude)	1: 1.6
pbdc-8e-PEG$_{5000}$OMe	1: 7.5
pbdc-8e-COD$_{1:1}$	1:1
pbdc-8e-COD$_{2:1}$	1:0.50
pbdc-8e-COD$_{10:1}$	1:0.19

[a] Ratio of bdc-8e to co-monomer (ethylene glycol or COD) was determined by ^{1}H NMR.

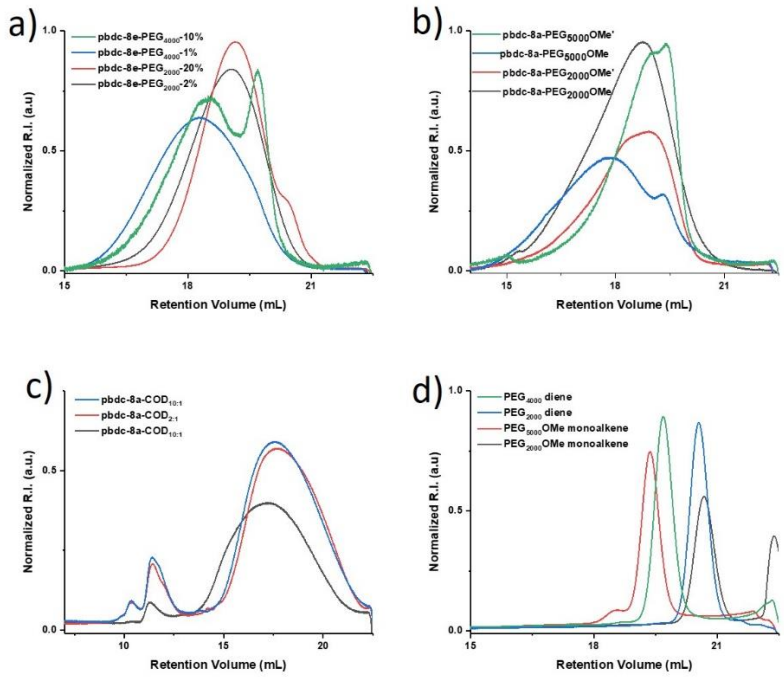

Figure 4S.27. GPC traces obtained for polymers: a) pbdc-8e-PEG$_{Mn}$-x%; b) pbdc-8e-PEG$_{Mn}$OMe; c) pbdc-8e-COD$_{m:n}$; d) alkene-functionalized PEG macromonomers.

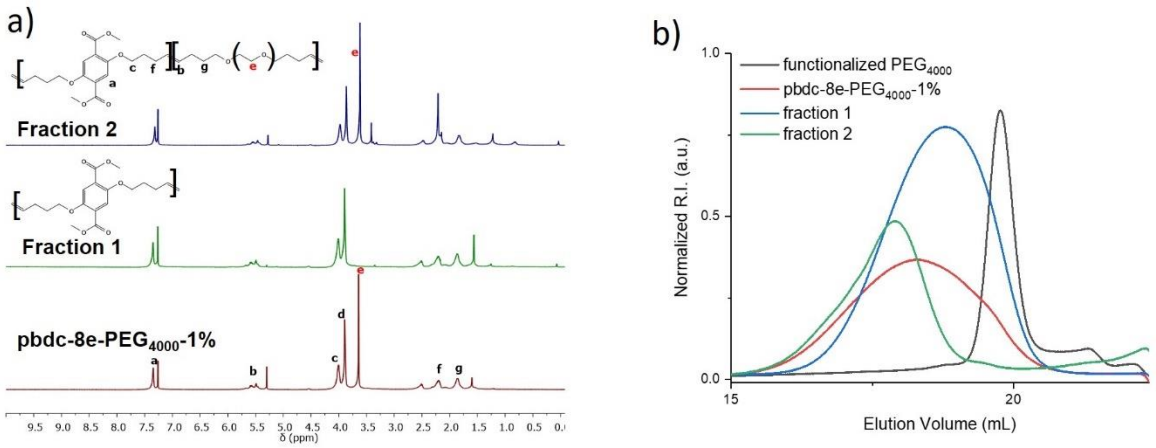

Figure 4S.28. a) ^{1}H NMR and b) GPC trace of representative fractionated sample pbdc-8e-PEG$_{4000}$-1% is presented.

Table 4S.2. Yields, compositions, and molecular weight of fractionated 8e-PEG$_{4000}$-1%.

Ligand	**Yield %**	**bdc: ethylene glycol**	M_n **(g/mol)**	M_w/M_n
Functionalized PEG$_{4000}$	-	-	10,600	1.07
pbdc-8e-PEG$_{4000}$ crude-1%	-	1.1: 1	24,300	1.44
pbdc-8e-PEG$_{4000}$-1% fraction 1	64	1:0	20,800	1.10
pbdc-8e-PEG$_{4000}$-1% fraction 2	26	1:2	38,100	1.20

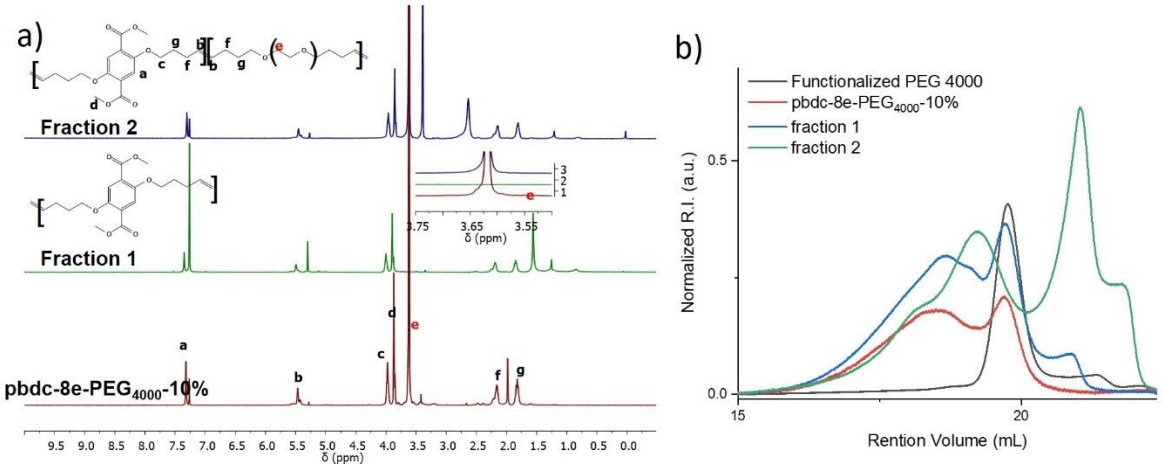

Figure 4S.29. a) ^{1}H NMR and b) GPC trace of representative fractionated sample pbdc-8e-PEG$_{4000}$-10% is presented.

Table 4S.3. Yields, compositions, and molecular weight of fractionated 8e-PEG$_{4000}$-10%.

Ligand	**Yield%**	**bdc: ethylene glycol**	***M*$_n$ (g/mol)**	***M*$_w$/*M*$_n$**
Functionalized PEG$_{4000}$	-	-	10,600	1.07
pbdc-8e-PEG$_{4000}$ crude	-	1: 7.5	18,700	1.50
pbdc-8e-PEG$_{4000}$-10% fraction 1	4	1: 0	16,000	2.15
pbdc-8e-PEG$_{4000}$-10% fraction 2	45	1: 6.1	22,000	1.54

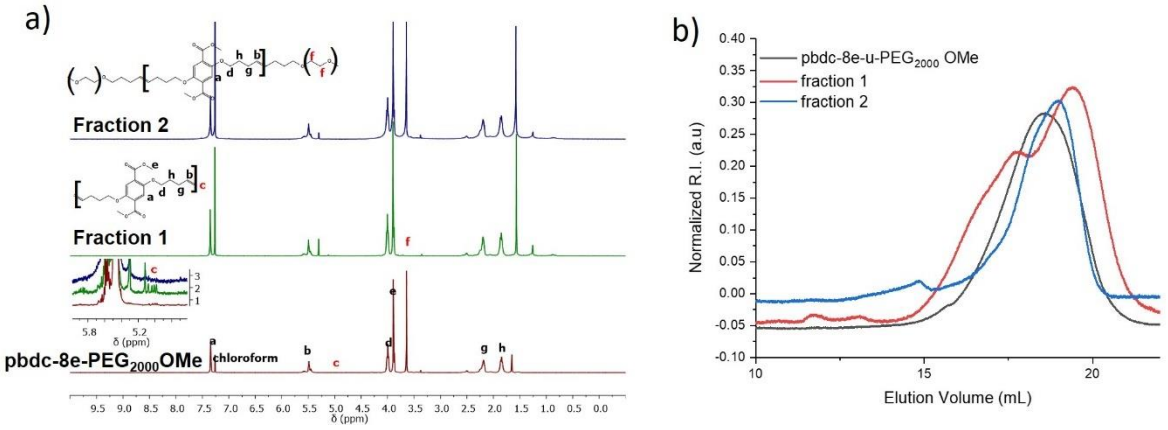

Figure 4S.30. a) ^{1}H NMR and b) GPC trace of representative fractionated sample pbdc-8e-PEG$_{2000}$OMe is presented.

Table 4S.4. Yields, compositions, and molecular weight of fractionated 8e-PEG$_{2000}$OMe.

Ligand	**Yield%**	**bdc: ethylene glycol**	M_n **(g/mol)**	M_w/M_n
pbdc-8e-PEG$_{2000}$OMe	-	1.1: 1	23,200	1.8
fraction 1	37	1: 0	17,100	2.1
fraction 2	18	1.1: 1	23,000	1.3

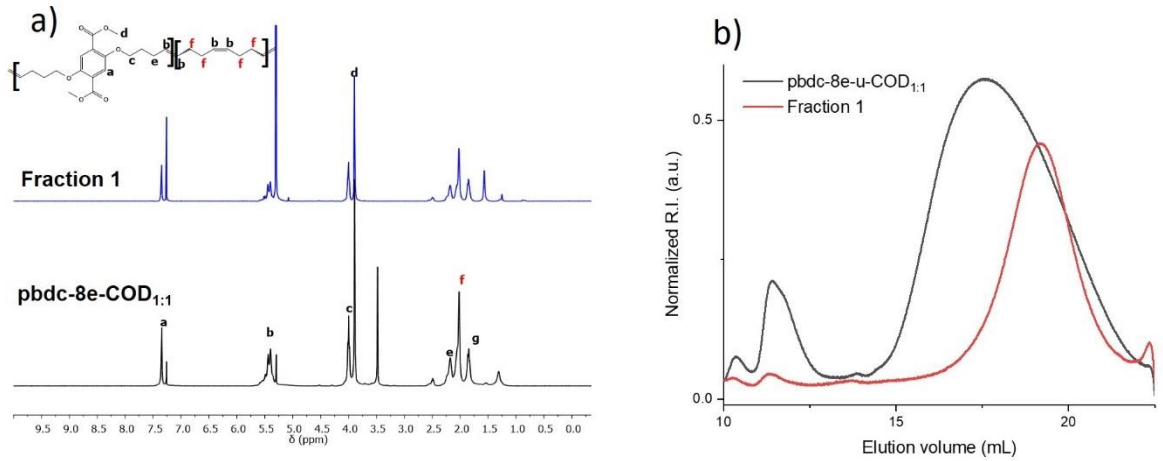

Figure 4S.31. a) ^{1}H NMR and b) GPC trace of representative fractionated sample pbdc-8e-COD$_{1:1}$ is presented.

Table 4S.5. Yields, compositions, and molecular weight of fractionated 8e-COD$_{1:1}$.

Ligand	**Yield %**	**bdc: ethylene glycol**	M_n **(g/mol)**	$Đ$
pbdc-8e-COD$_{1:1}$	-	1:1	17,200	2.8
Fraction 1	45	1:1	14,400	1.6

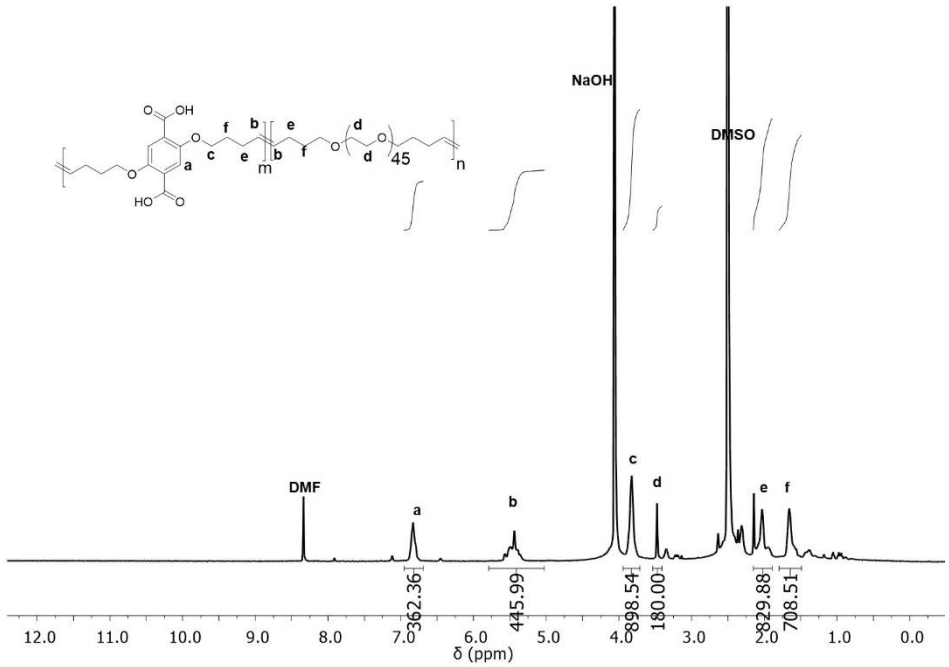

Figure 4S.32. ^{1}H NMR of digested polyUiO-66 prepared from pbdc-8a-PEG_{2000}-2%.

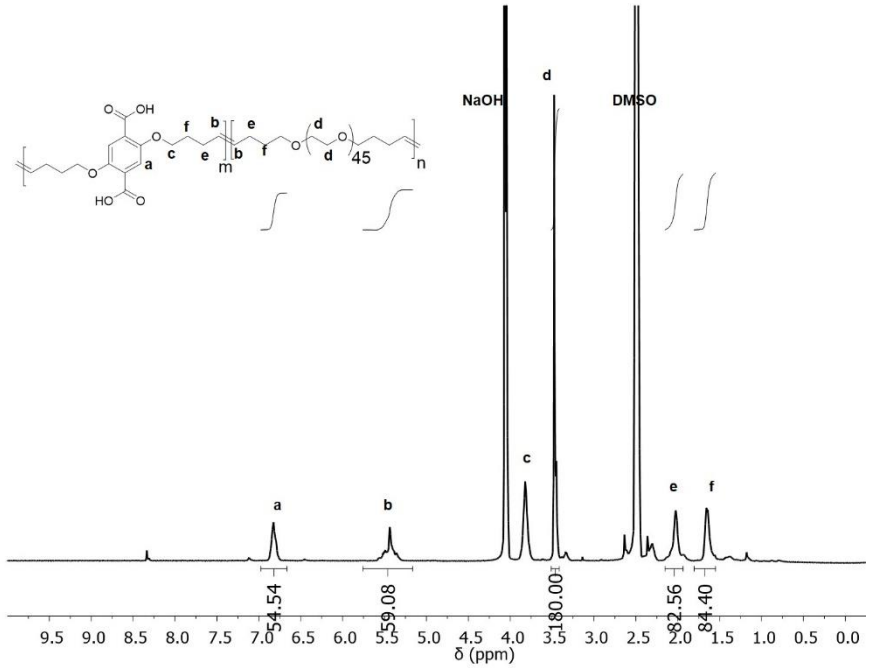

Figure 4S.33. ^{1}H NMR of digested polyUiO-66 prepared from pbdc-8a-PEG_{2000}-20%.

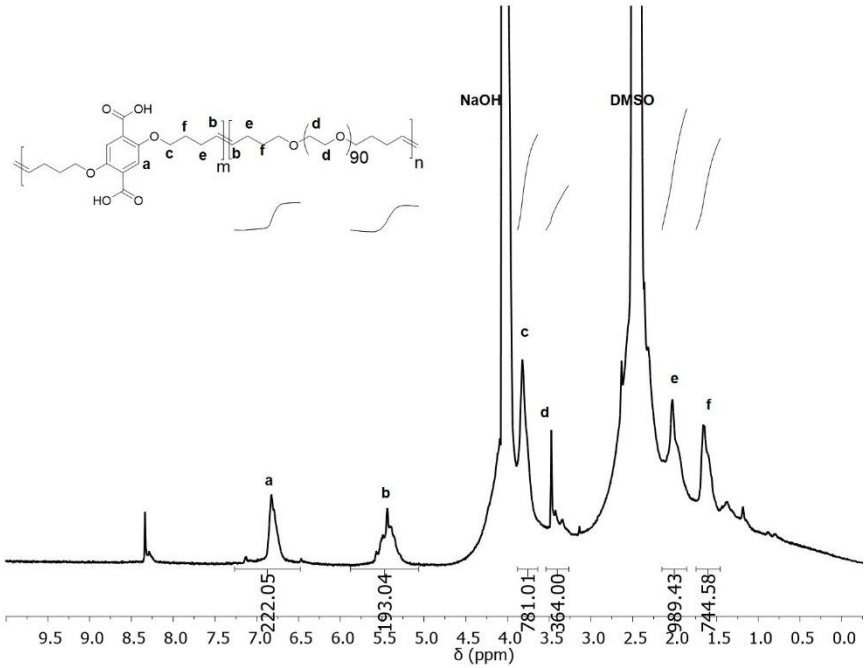

Figure 4S.34. [1]H NMR of digested polyUiO-66 prepared from pbdc-8a-PEG_{4000}-1%.

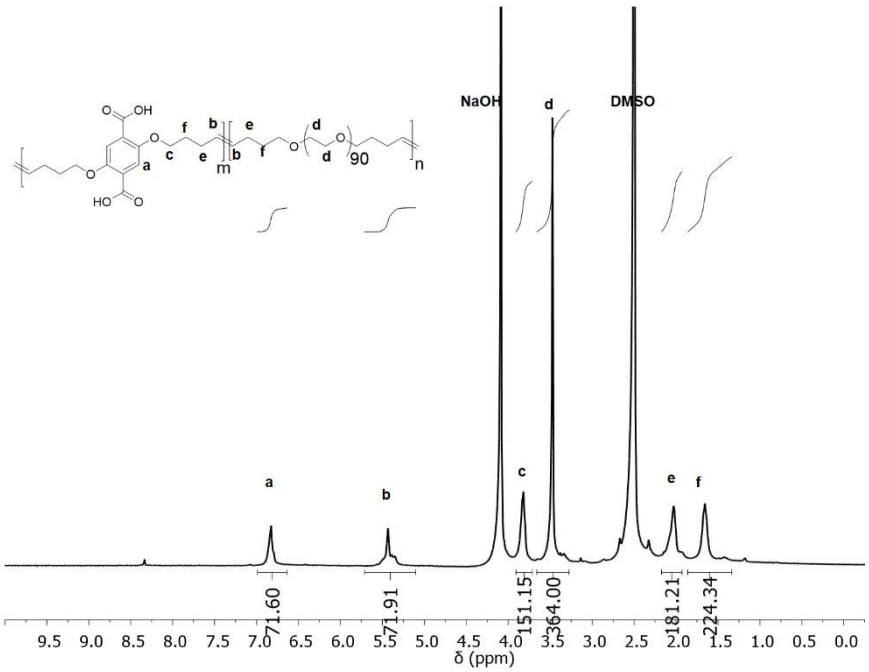

Figure 4S.35. [1]H NMR of digested polyUiO-66 prepared from pbdc-8a-PEG_{4000}-10%.

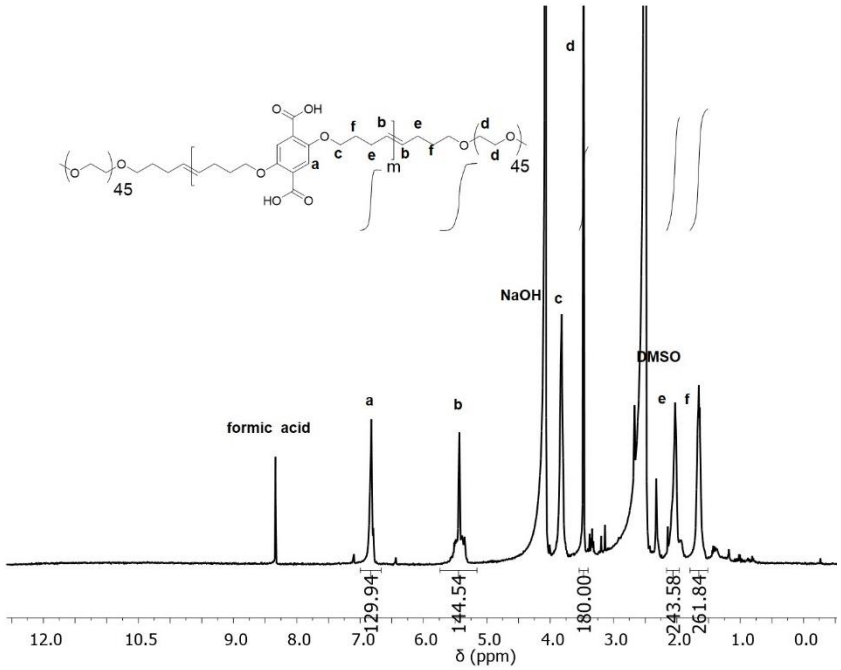

Figure 4S.36. ^{1}H NMR of digested polyUiO-66 prepared from crude pbdc-8a-PEG$_{2000}$OMe.

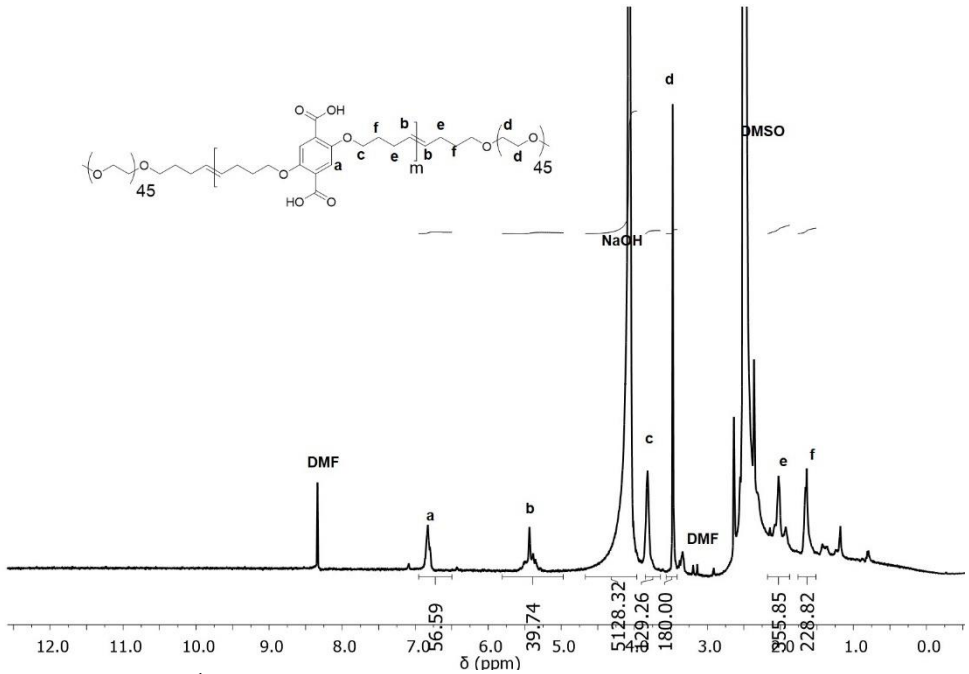

Figure 4S.37. ^{1}H NMR of digested polyUiO-66 prepared from pbdc-8a-PEG$_{2000}$OMe.

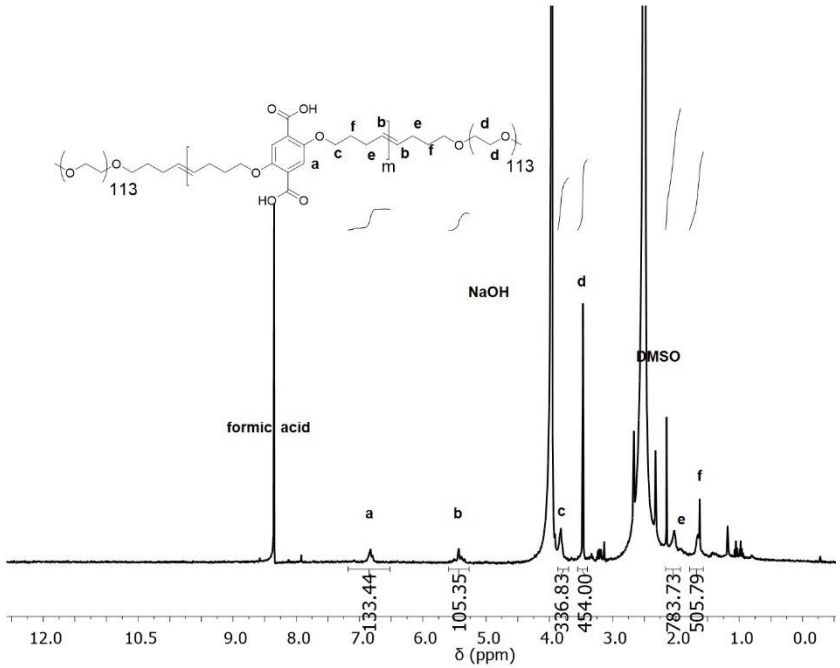

Figure 4S.38. ^{1}H NMR of digested polyUiO-66 prepared from crude pbdc-8a-PEG$_{5000}$OMe.

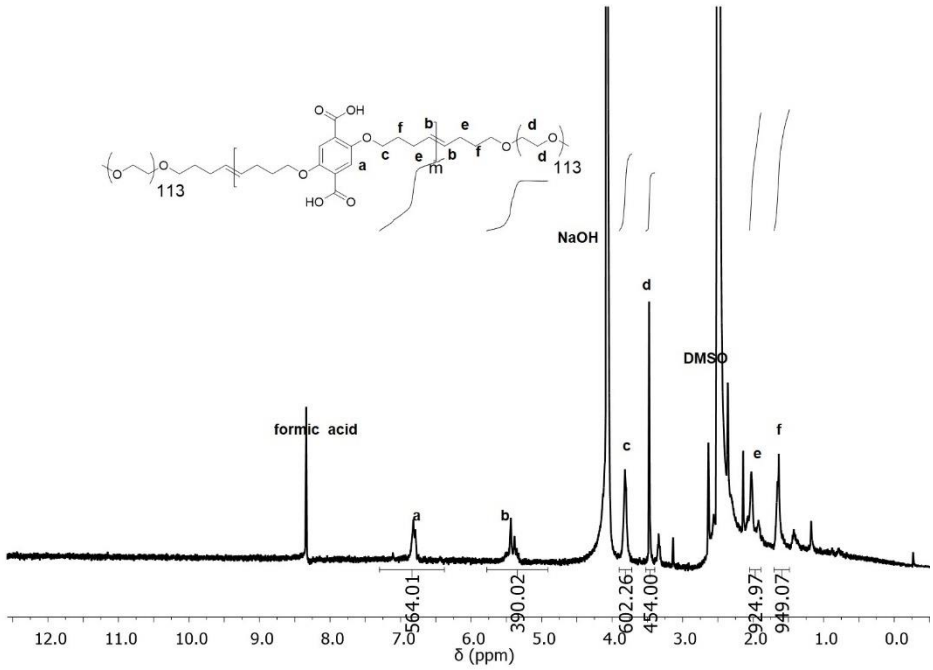

Figure 4S.39. ^{1}H NMR of digested polyUiO-66 prepared from pbdc-8a-PEG$_{5000}$OMe.

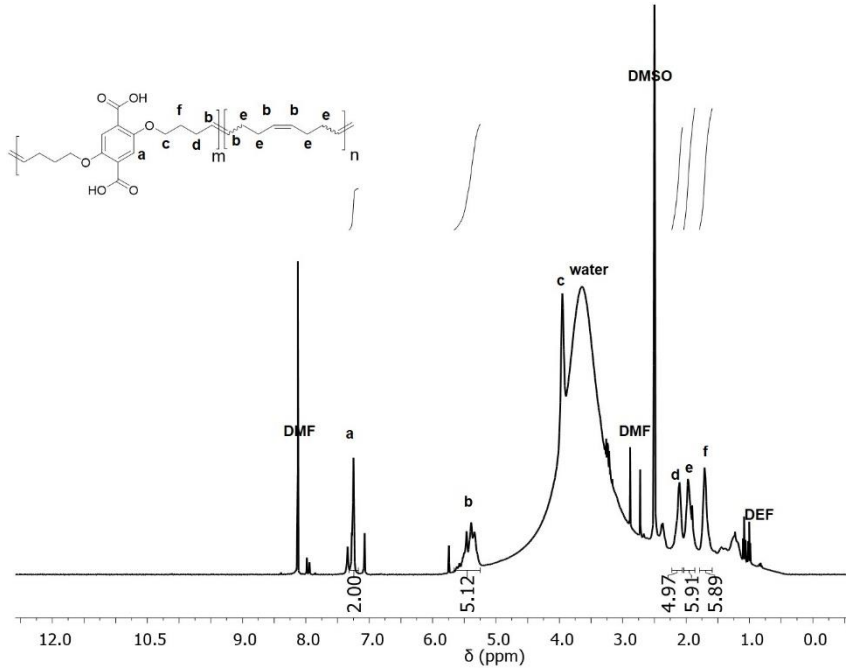

Figure 4S.40. ^{1}H NMR of digested polyUiO-66 prepared from pbdc-8a-$COD_{1:1}$.

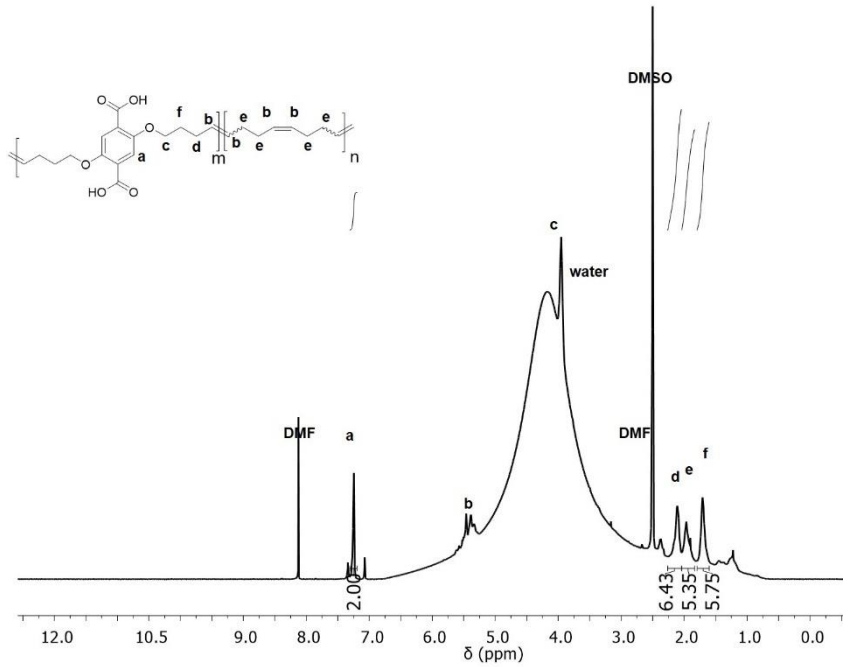

Figure 4S.41. ^{1}H NMR of digested polyUiO-66 prepared from pbdc-8a-$COD_{2:1}$.

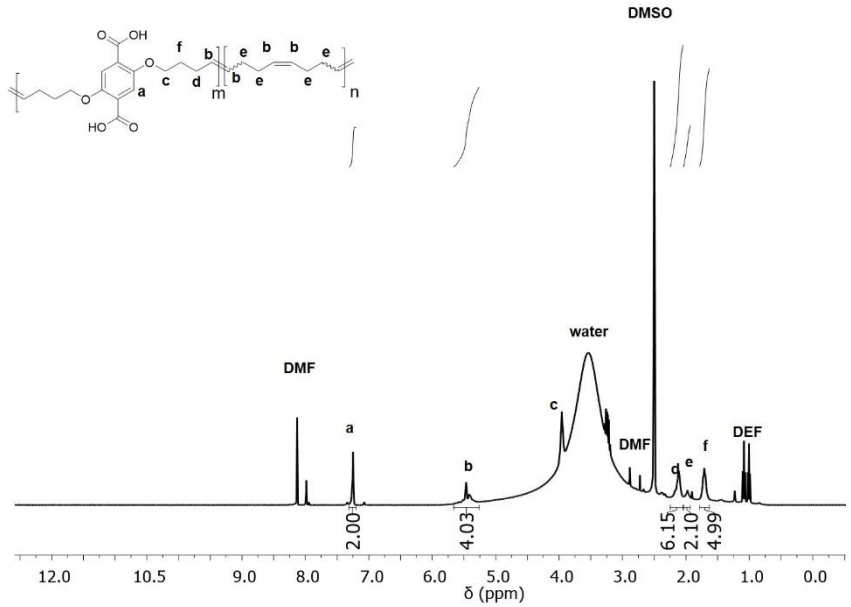

Figure 4S.42. ^{1}H NMR of digested polyUiO-66 prepared from pbdc-8a-$COD_{10:1}$.

Table 4S.6. Ratios of H_2bdc to co-monomer before and after digestion.

Ligand	**H_2bdc:co-monomer before digestion (^{1}H NMR)**	**H_2bdc:co-monomer after digestion (^{1}H NMR)**
pbdc-8e-PEG$_{2000}$-2% [a]	1.8:1	3.7:1
pbdc-8e-PEG$_{2000}$-20% [a]	1:5.8	1:1.6
pbdc-8e-PEG$_{4000}$-1%	1.3:1	1.4:1
pbdc-8e-PEG$_{4000}$-10%	1:3.3	1:2.5
pbdc-8e-PEG$_{2000}$OMe (crude) [b]	1.1:1	1.4:1
pbdc-8e-PEG$_{2000}$OMe [b]	1:1.6	1:1.8
pbdc-8e-PEG$_{5000}$OMe (crude)	1:2.0	1:1.7
pbdc-8e-PEG$_{5000}$OMe	1:5	1.7:1
pbdc-8e-COD$_{1:1}$ [c]	1:1	1.5:1
pbdc-8e-COD$_{2:1}$ [c]	2:1	2:1
pbdc-8e-COD$_{10:1}$ [c]	10:1	5:1

[a] Dissolution of polyUiO-66 prepared from pbdc-8a-PEG$_{2000}$-2% and pbdc-8a-PEG$_{2000}$-20% ligands showed that the presence of PEG had significantly decreased in comparison to the amount of PEG present in the starting block polymer ligands (Figures 4S.37-40). A possible explanation for this result may be that some of polymer chains were never incorporated into the lattice of the polyMOF and were washed prior to analysis by ^{1}HNMR digestions. [b] Digested samples of polyUiO-66 prepared from pbdc-8a-PEG$_{Mn}$OMe or pbdc-8a-PEG$_{2000}$OMe reveal that the ratio of H_2bdc to PEG in the polymer is retained even after digestion of the polymer (Figures 4S.41-44). [c] For digested samples of polyUiO-66 prepared from pbdc-8a-COD$_{m:n,}$ the ratio of H_2bdc to COD remains largely unchanged even after digestion of polyMOF samples, validating retention of structural integrity in the block polymer ligands (Figures 4S.45-46).

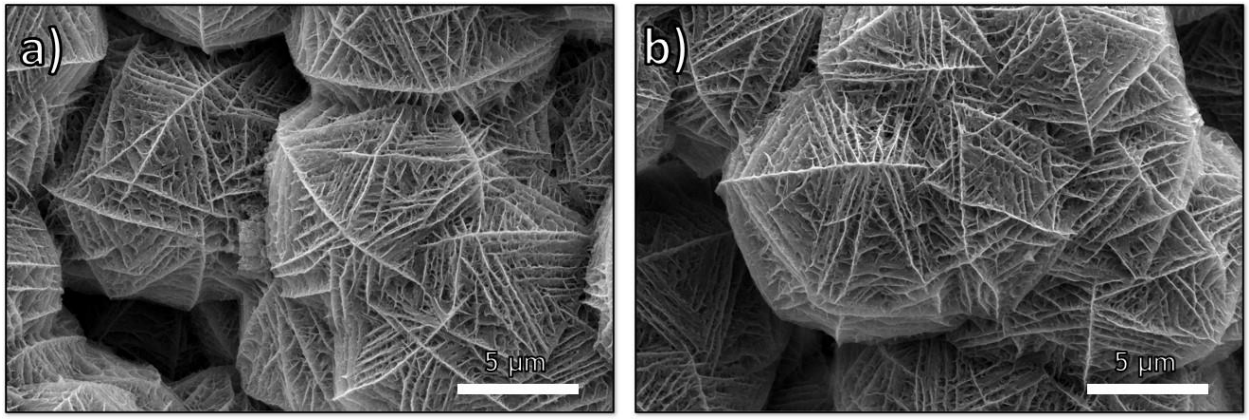

Figure 4S.43. SEM images for polyUiO-66 prepared from pbdc-8a and physically mixed PEG_{4000} at a) 1% loading and b) 10% loading.

Table 4S.7. Hydrodynamic radii at 90° and 13° scattering angle for polymer ligands, and polyIRMOF-1 derived from pbdc-8a-PEG_{4000}-10%.

	Hydrodynamic radius (nm)	
Ligand	**90°**	**13°**
pbdc-8e-PEG_{2000}-2%	4.7	26.6
pbdc-8e-PEG_{2000}-20%	5.5	101
pbdc-8e-PEG_{4000}-1%	4.8	12.5
pbdc-8e-PEG_{4000}-10%	5.3	71.5
pbdc-8e-PEG_{2000}OMe	4.3	129
pbdc-8e-PEG_{5000}OMe	5.5	33.2
pbdc-8e-$COD_{1:1}$	7.9	>500
pbdc-8e-$COD_{2:1}$	6.8	53
pbdc-8e-$COD_{10:1}$	7.5	114
MOF		
polyIRMOF-1 (pbdc-8a-PEG_{4000}-10%)	274	308

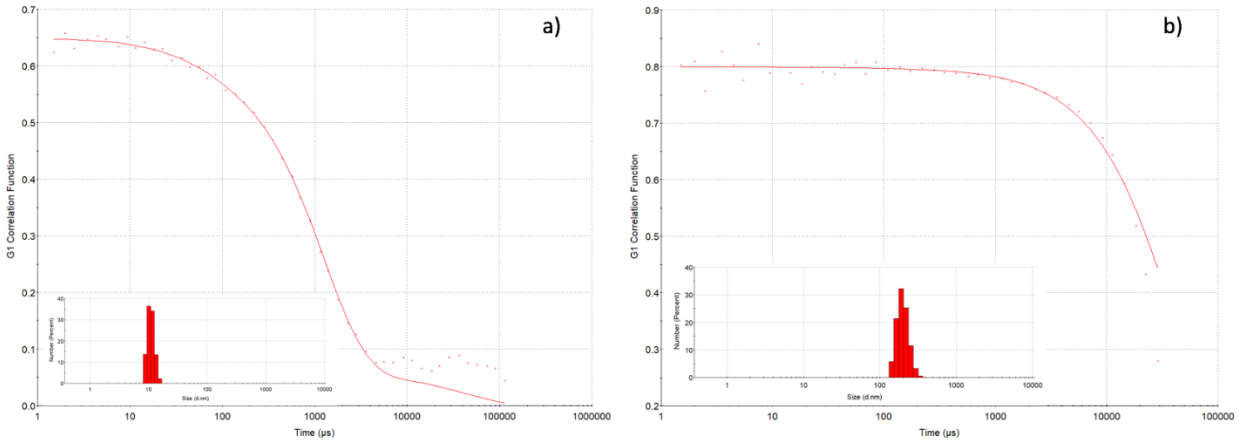

Figure 4S.44. Correlation functions, distribution fits, and number-average size distributions (inset) at 90° (a) and 13° (b) scattering angle for pbdc-8a-PEG$_{2000}$-20%.

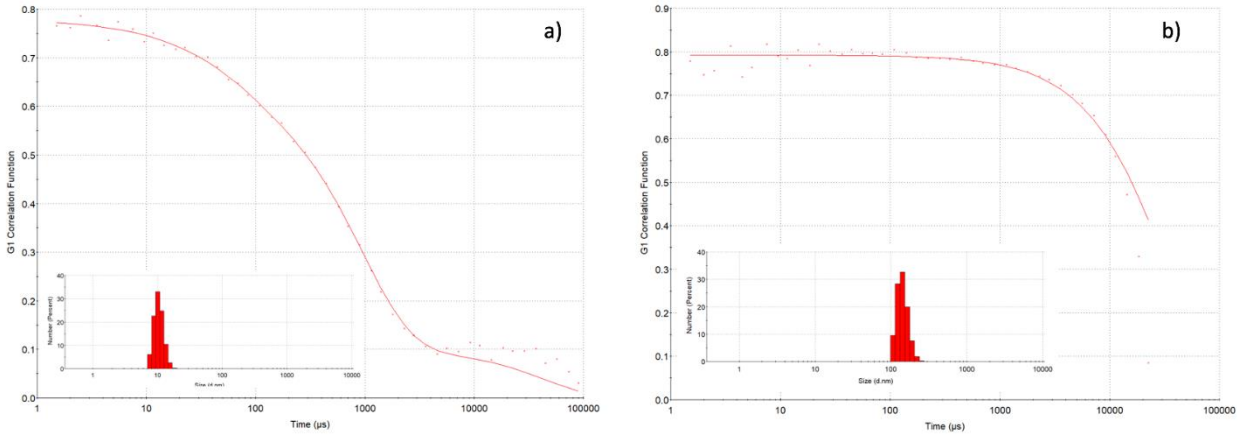

Figure 4S.45. Correlation functions, distribution fits, and number-average size distributions (inset) at 90° (a) and 13° (b) scattering angle for pbdc-8a-PEG$_{4000}$-10%.

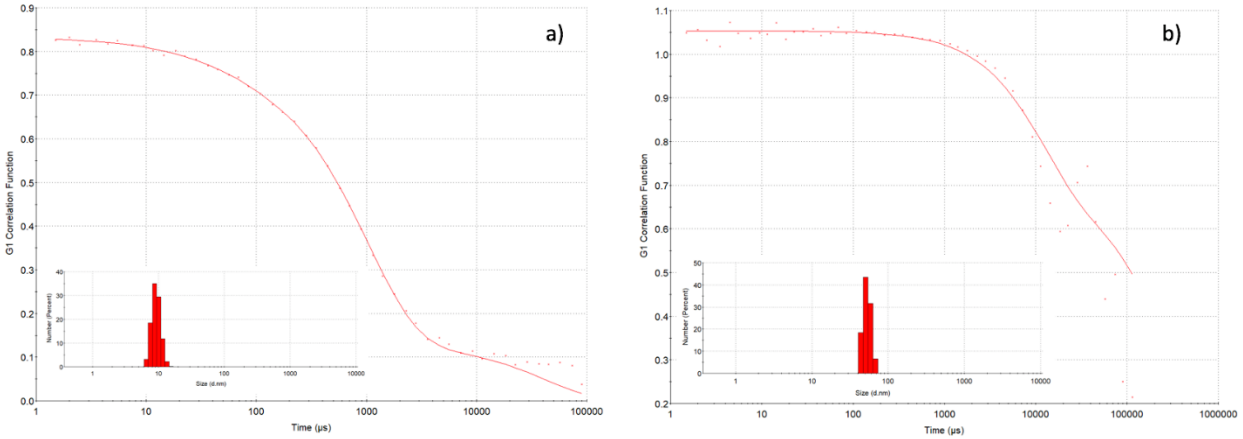

Figure 4S.46. Correlation functions, distribution fits, and number-average size distributions (inset) at 90° (a) and 13° (b) scattering angle for pbdc-8a-PEG_{2000}-2%.

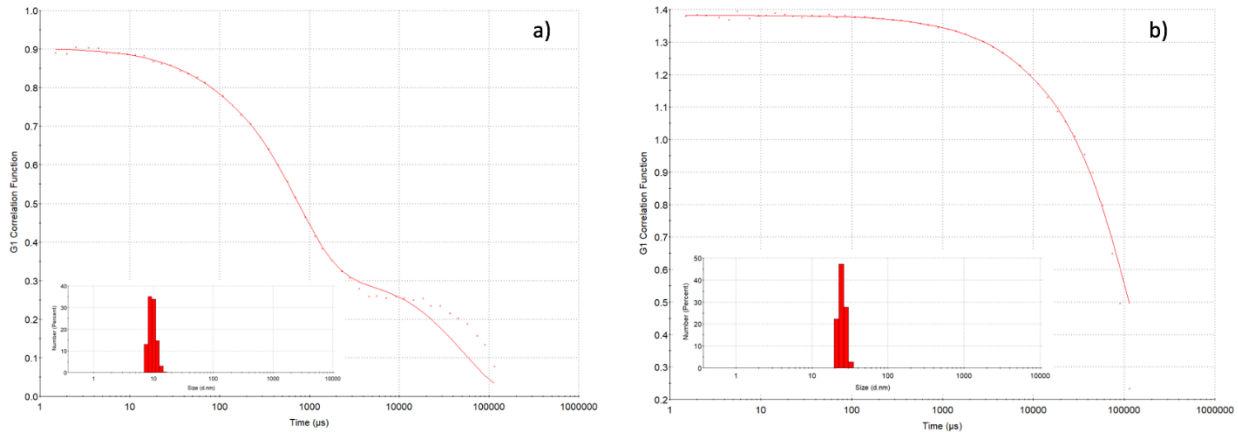

Figure 4S.47. Correlation functions, distribution fits, and number-average size distributions (inset) at 90° (a) and 13° (b) scattering angle for pbdc-8a-PEG_{4000}-1%.

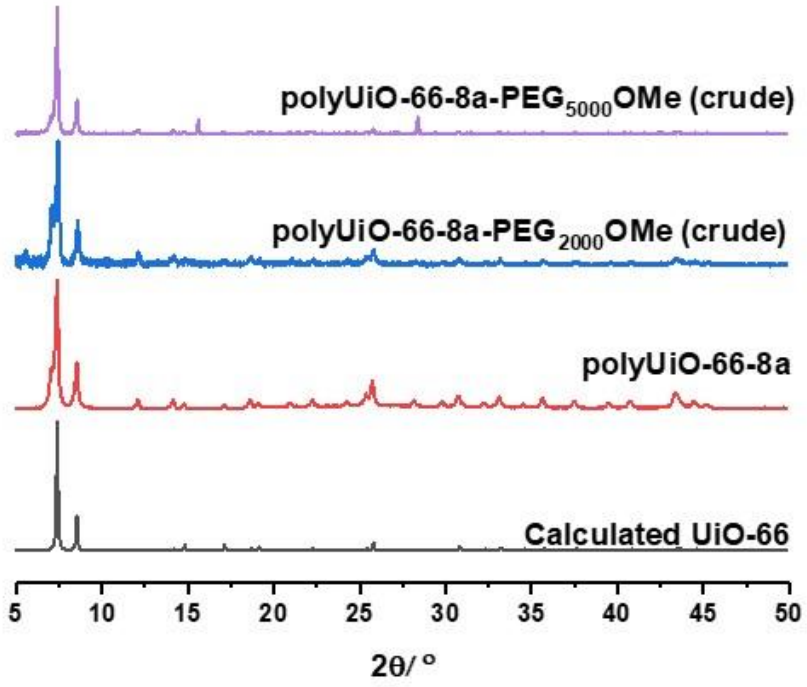

Figure 4S.48. PXRD data was obtained for polyUiO-66 prepared from crude pbdc-8a-PEG$_{Mn}$OMe.

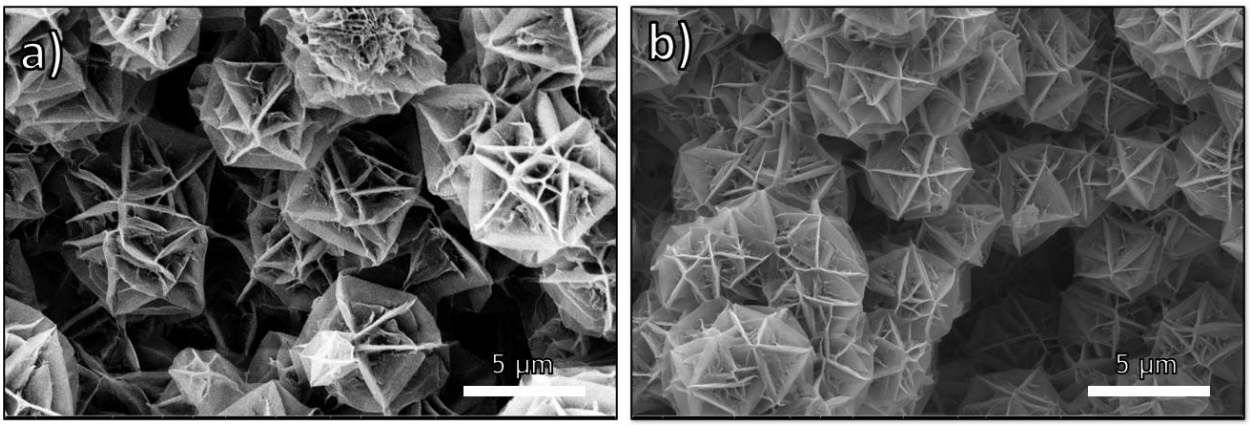

Figure 4S.49. SEM images for polyUiO-66 prepared from crude: a) pbdc-8a-PEG$_{2000}$OMe; b) pbdc-8a-PEG$_{5000}$OMe.

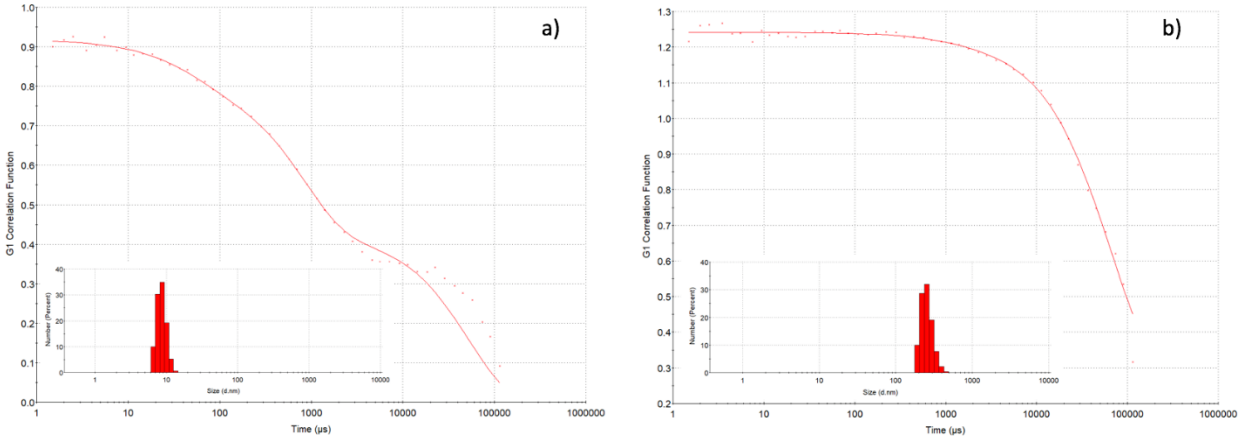

Figure 4S.50. Correlation functions, distribution fits, and number-average size distributions (inset) at 90° (a) and 13° (b) scattering angle for pbdc-8a-PEG$_{2000}$OMe.

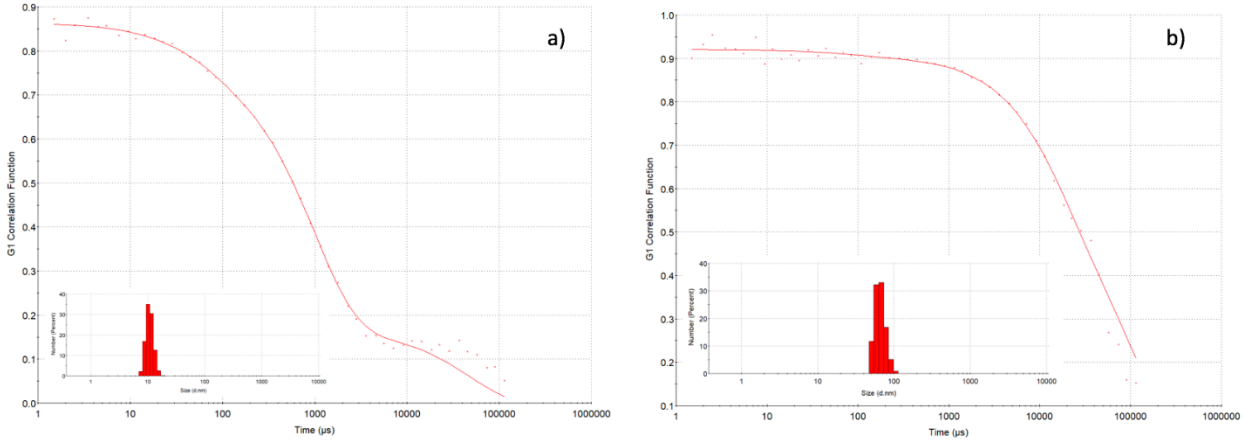

Figure 4S.51. Correlation functions, distribution fits, and number-average size distributions (inset) at 90° (a) and 13° (b) scattering angle for pbdc-8a-PEG$_{5000}$OMe.

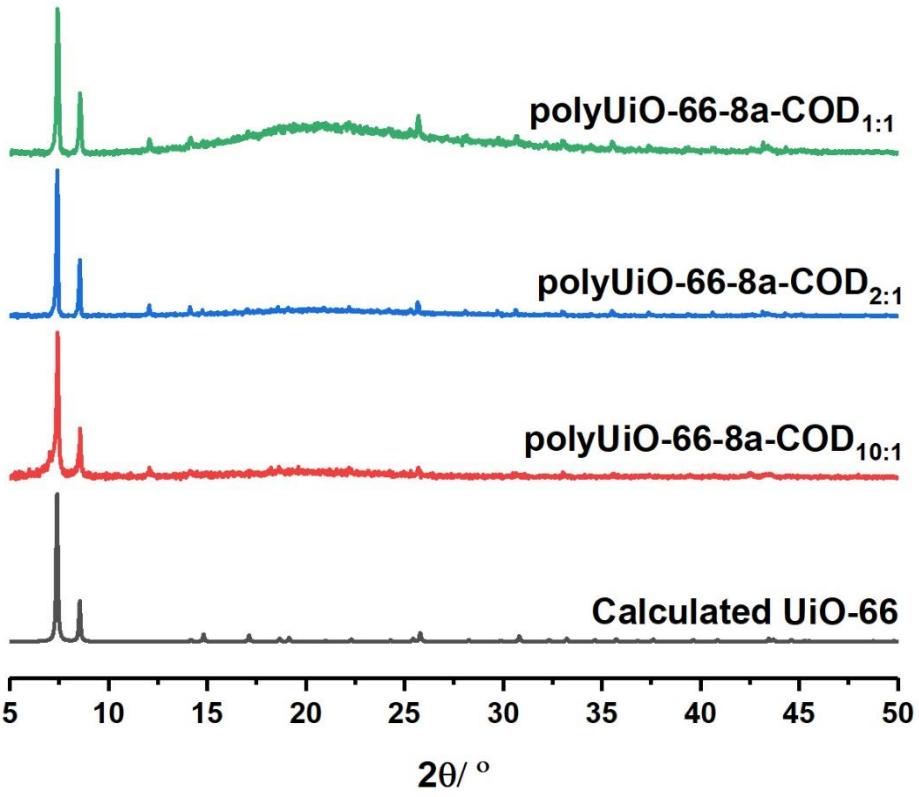

Figure 4S.52. PXRD data was obtained for polyUiO-66 prepared from pbdc-8a-COD$_{m:n}$.

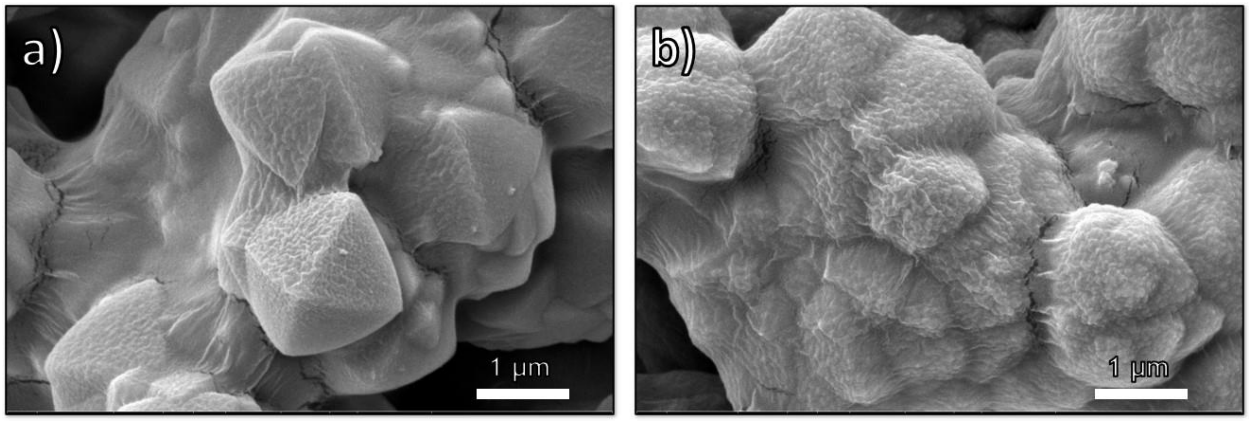

Figure 4S.53. SEM images of polyUiO-66 prepared from: a) pbdc-8a-COD$_{2:1}$; b) pbdc-8a-COD$_{1:1}$.

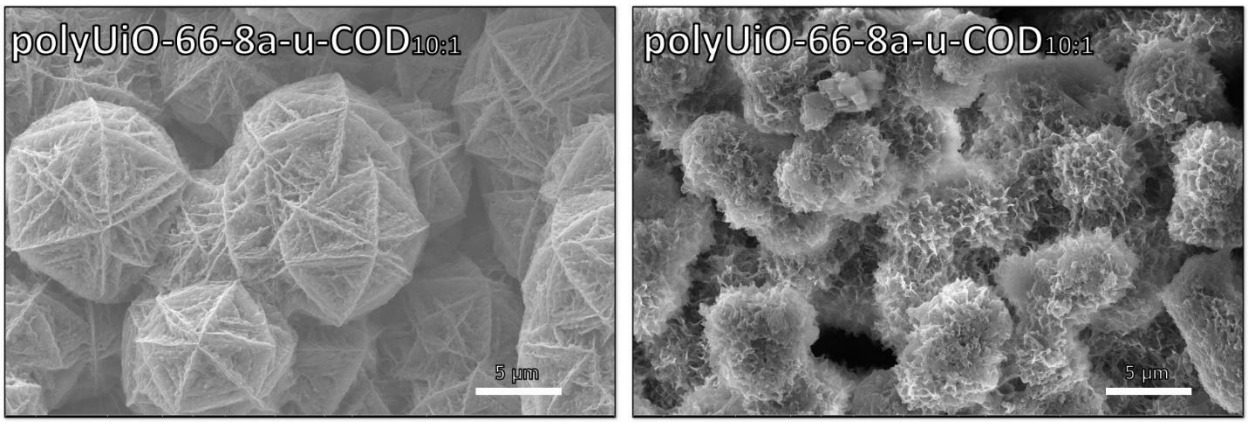

Figure 4S.54. SEM images of two different morphologies for polyUiO-66 prepared from pbdc-8a-$COD_{10:1}$.

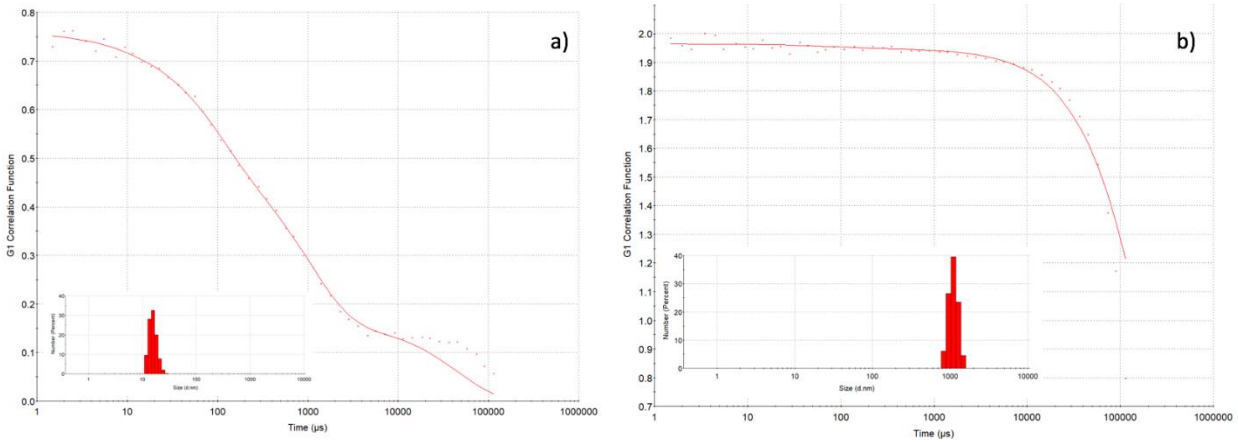

Figure 4S.55. Correlation functions, distribution fits, and number-average size distributions (inset) at 90° (a) and 13° (b) scattering angle for pbdc-8a-$COD_{1:1}$.

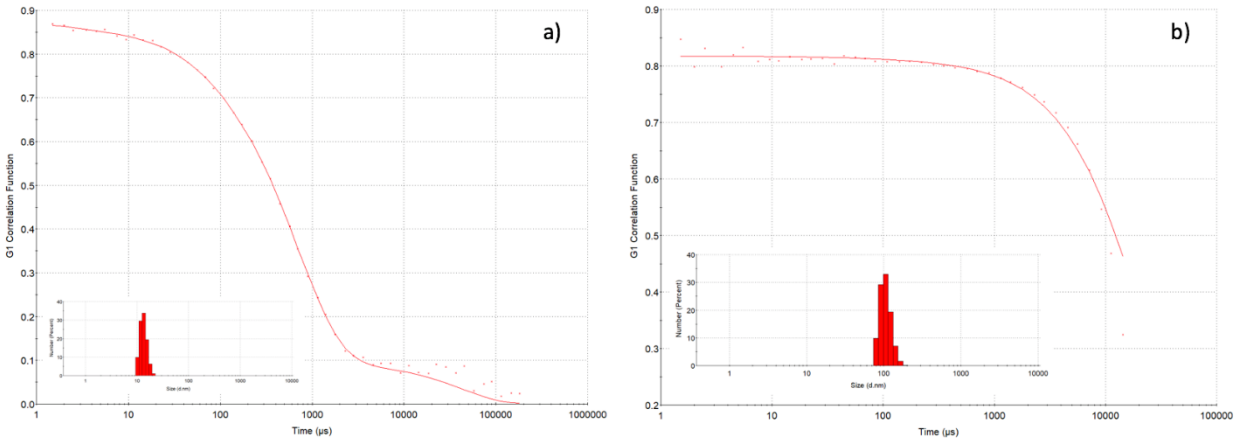

Figure 4S.56. Correlation functions, distribution fits, and number-average size distributions (inset) at 90° (a) and 13° (b) scattering angle for pbdc-8a-$COD_{2:1}$.

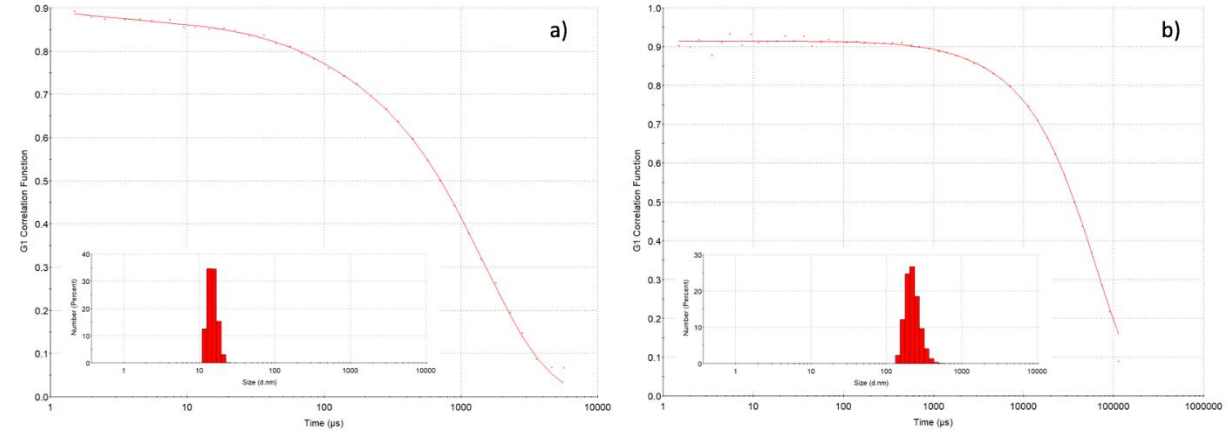

Figure 4S.57. Correlation functions, distribution fits, and number-average size distributions (inset) at 90° (a) and 13° (b) scattering angle for pbdc-8a-$COD_{10:1}$.

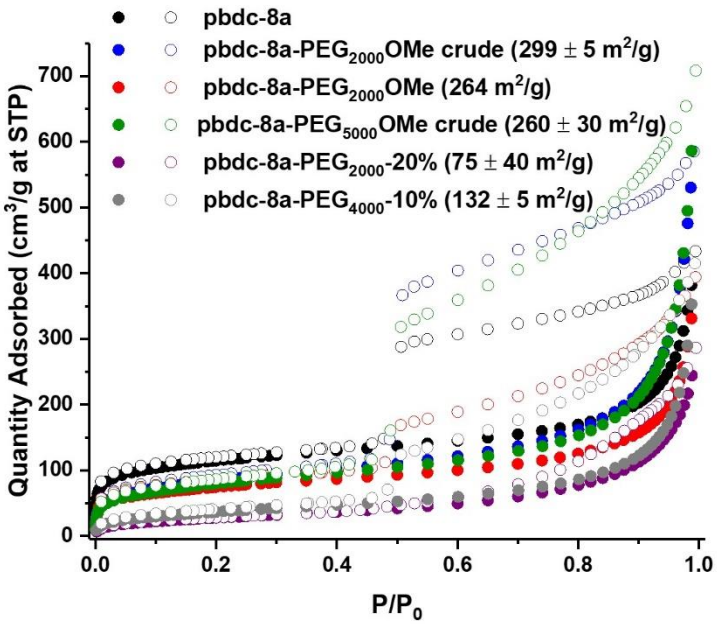

Figure 4S.58. N_2 adsorption isotherms for all block-polyUiO-66 with an interlaced morphology.

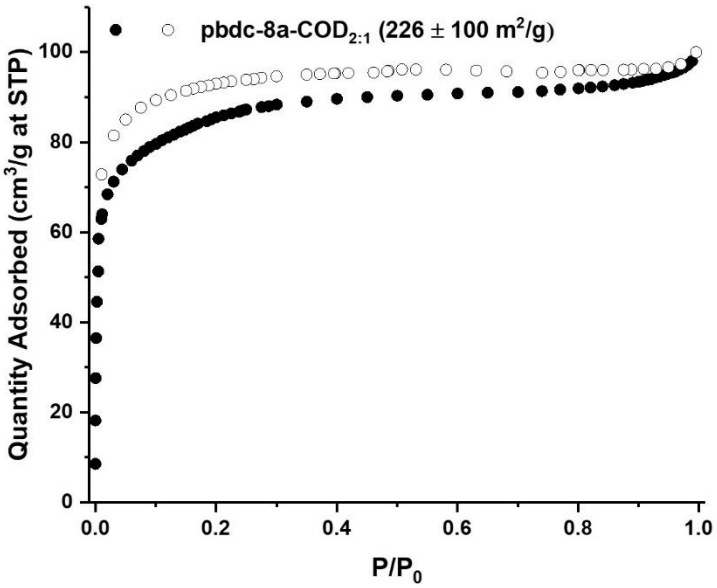

Figure 4S.59. N_2 adsorption isotherm for block-polyUiO-66 prepared from pbdc-8a-$COD_{2:1}$ is presented.

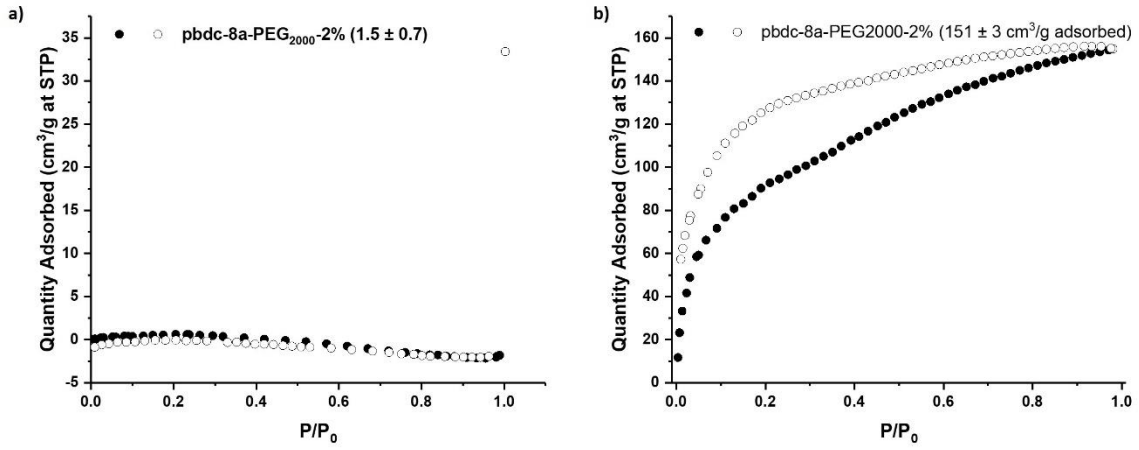

Figure 4S.60. a) N_2 adsorption isotherms and b) CO_2 adsorption for block-polyUiO-66 prepared from pbdc-8a-PEG_{2000}-2%.

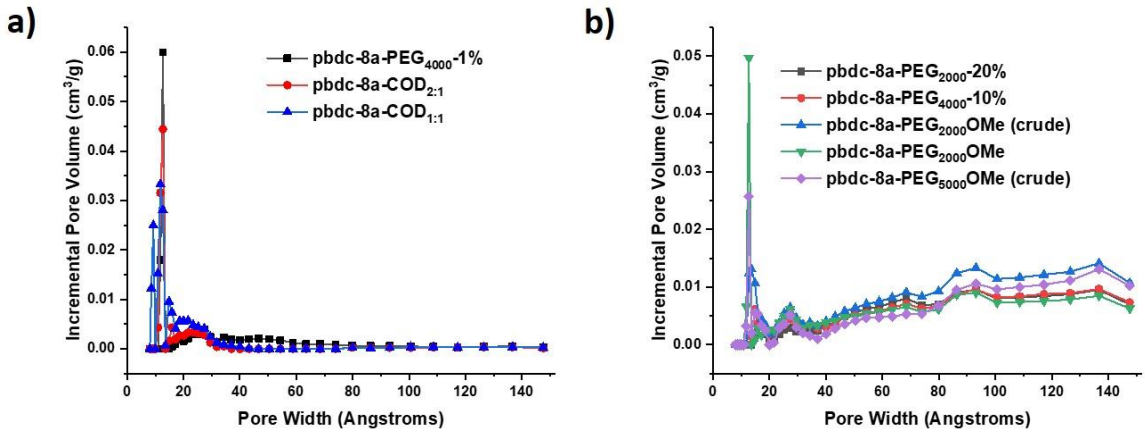

Figure 4S.61. Pore-size distribution for block-polyUiO-66 with a(n): a) octahedral morphology; b) interlaced morphology.

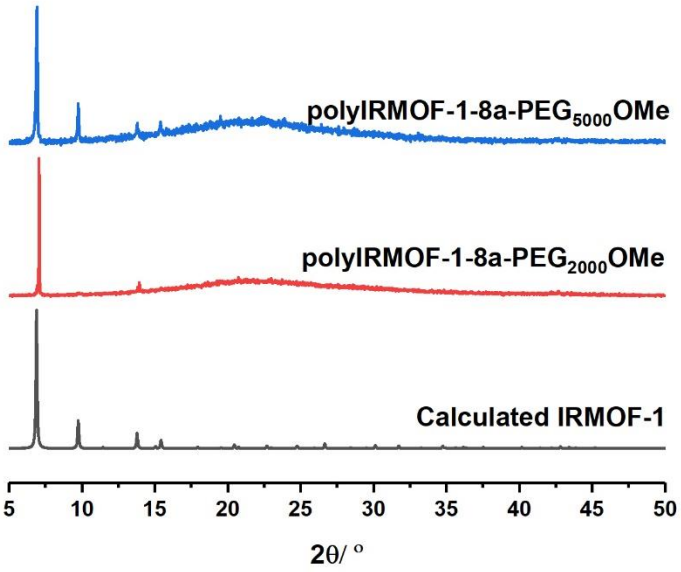

Figure 4S.62. PXRD data was obtained for polyIRMOF-1 prepared from pbdc-8a-PEG$_{Mn}$OMe.

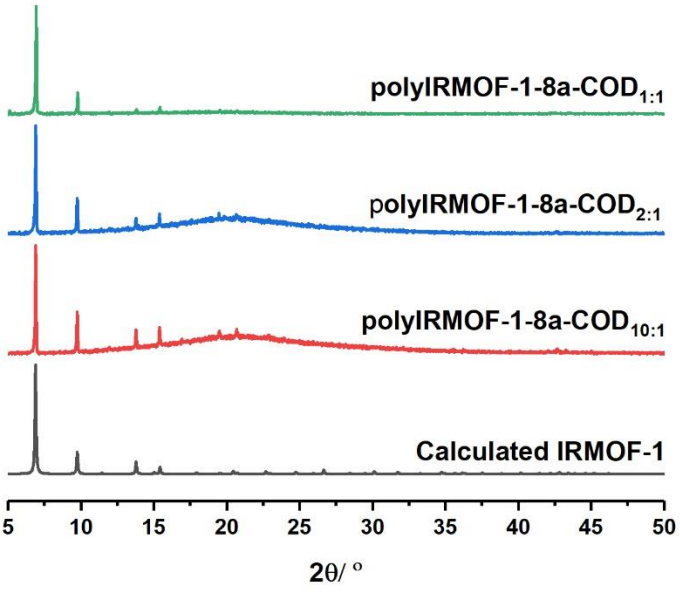

Figure 4S.63. PXRD data was obtained for polyIRMOF-1 prepared from pbdc-8a-COD$_{m:n}$.

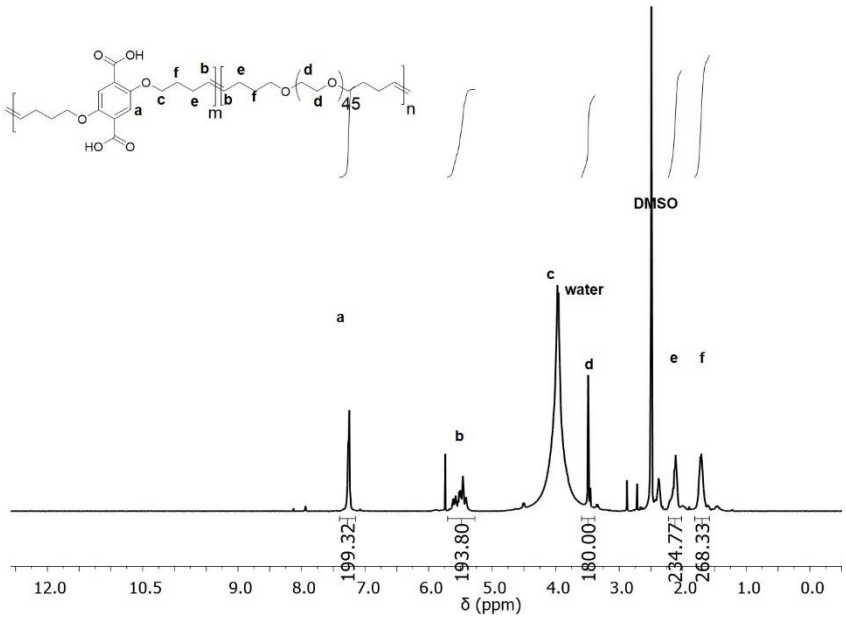

Figure 4S.64. ^{1}H NMR of digested polyIRMOF-1 prepared from pbdc-8a-PEG$_{2000}$-2%.

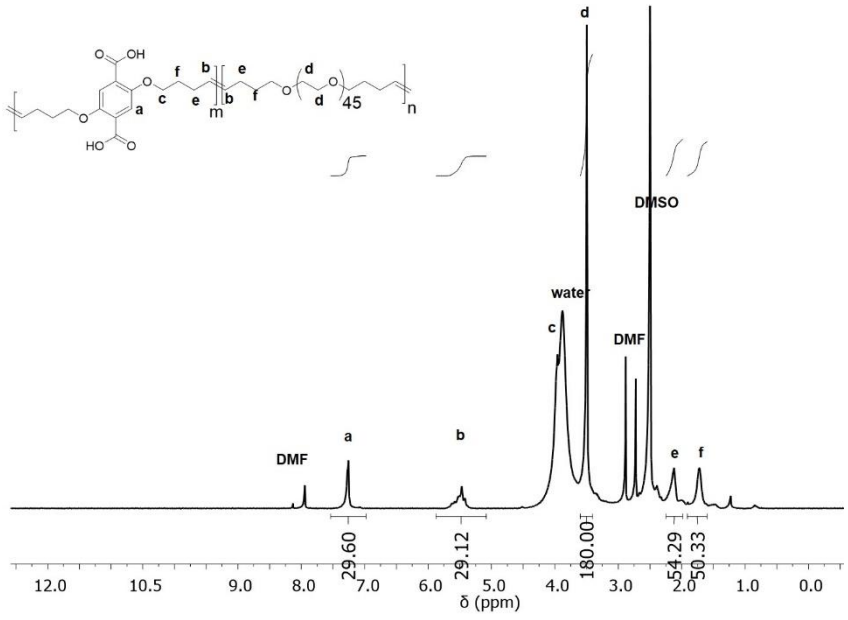

Figure 4S.65. ^{1}H NMR of digested polyIRMOF-1 prepared from pbdc-8a-PEG$_{2000}$-20%.

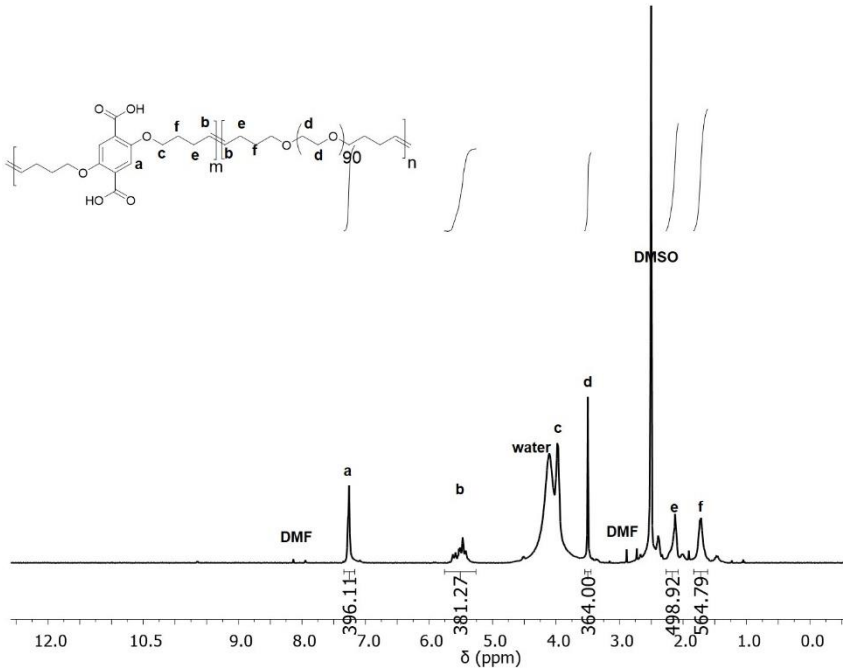

Figure 4S.66. ^{1}H NMR of digested polyIRMOF-1 prepared from pbdc-8a-PEG$_{4000}$-1%.

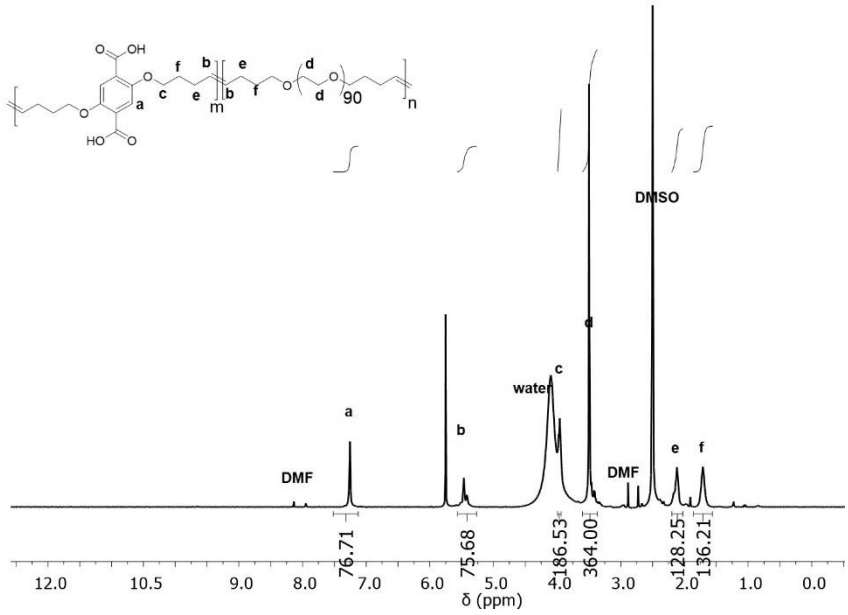

Figure 4S.67. ^{1}H NMR of digested polyIRMOF-1 prepared from pbdc-8a-PEG$_{4000}$-10%.

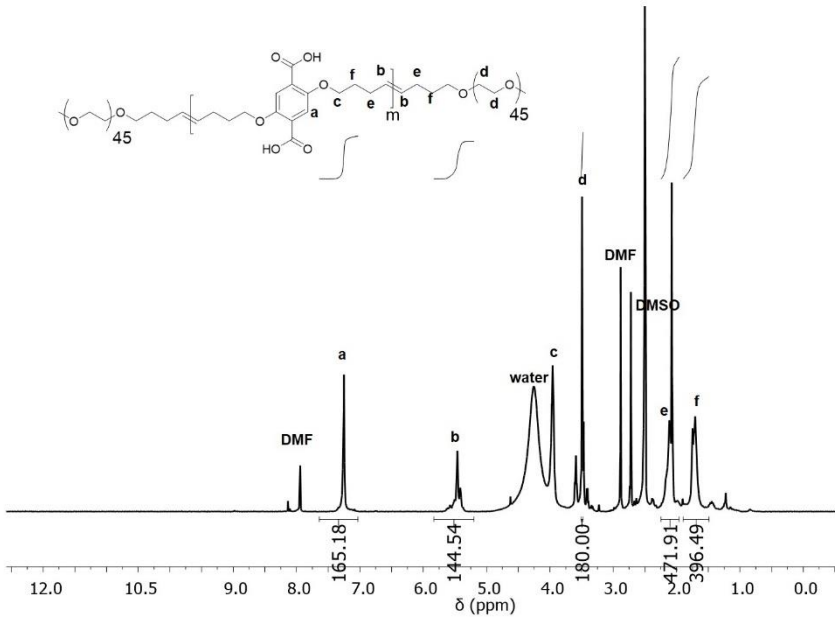

Figure 4S.68. ^{1}H NMR of digested polyIRMOF-1 prepared from pbdc-8a-PEG$_{2000}$OMe.

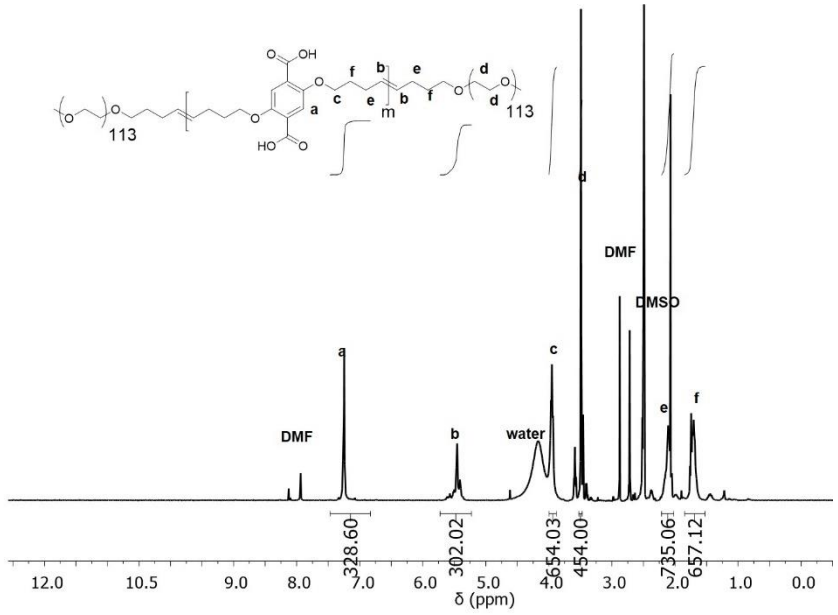

Figure 4S.69. ^{1}H NMR of digested polyIRMOF-1 prepared from pbdc-8a-PEG$_{5000}$OMe.

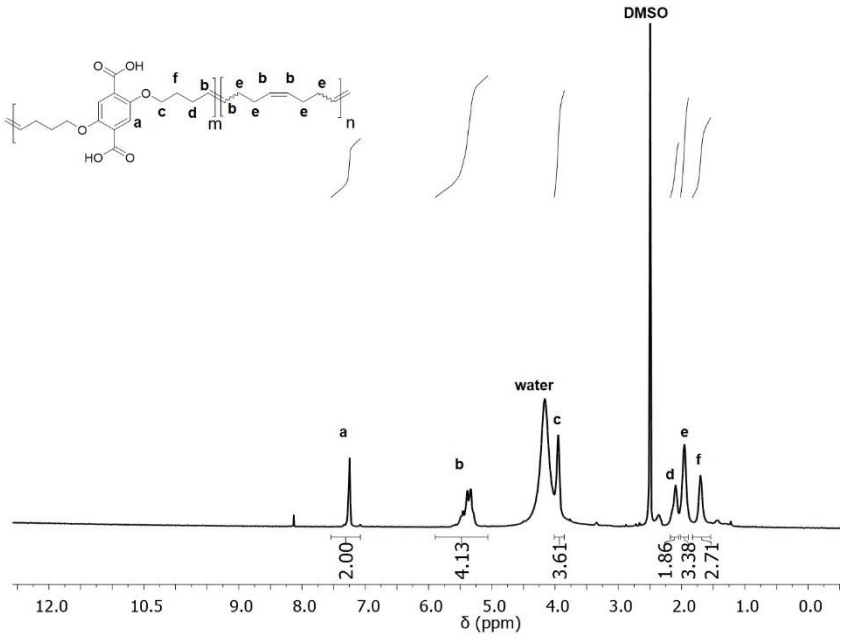

Figure 4S.70. ^{1}H NMR of digested polyIRMOF-1 prepared from pbdc-8a-COD$_{1:1}$.

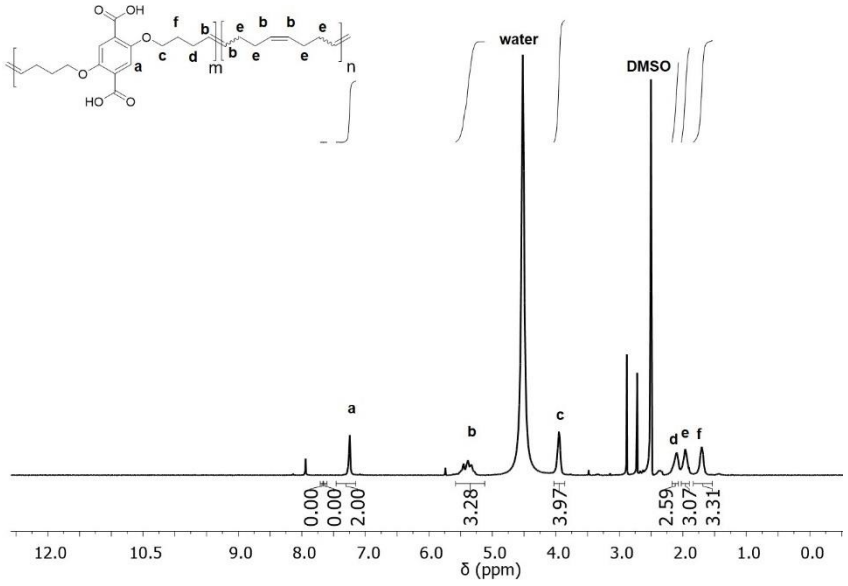

Figure 4S.71. ^{1}H NMR of digested polyIRMOF-1 prepared from pbdc-8a-COD$_{2:1}$.

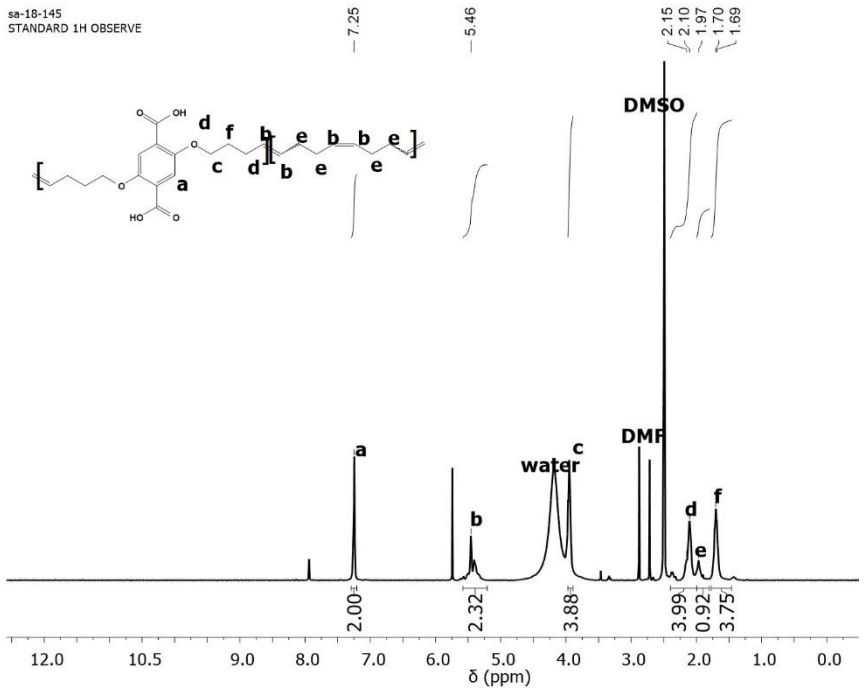

Figure 4S.72. ^{1}H NMR of digested polyIRMOF-1 prepared from pbdc-8a-$COD_{10:1}$.

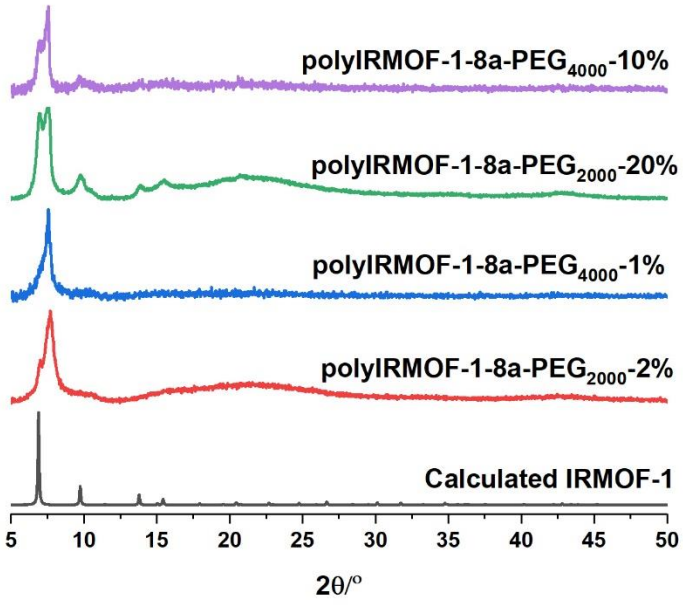

Figure 4S.73. PXRD data was obtained for polyIRMOF-1 prepared from pbdc-8a-PEG_{Mn}-x% after activation.

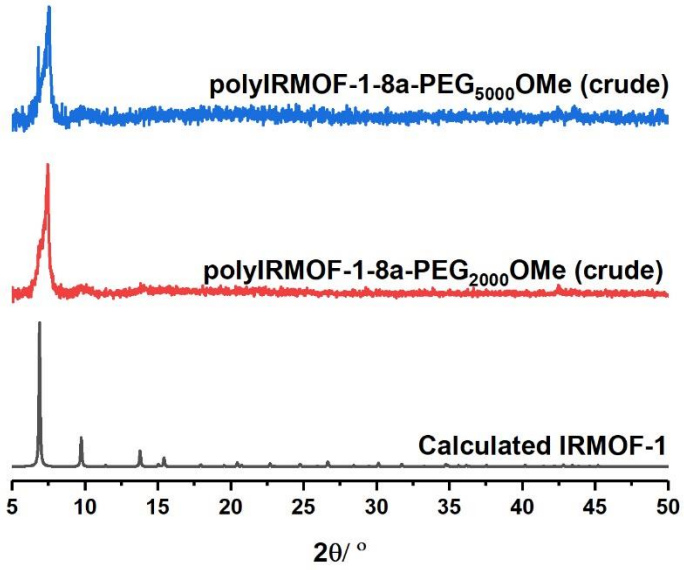

Figure 4S.74. PXRD data was obtained for polyIRMOF-1 prepared from pbdc-8a-PEG$_{Mn}$OMe after activation.

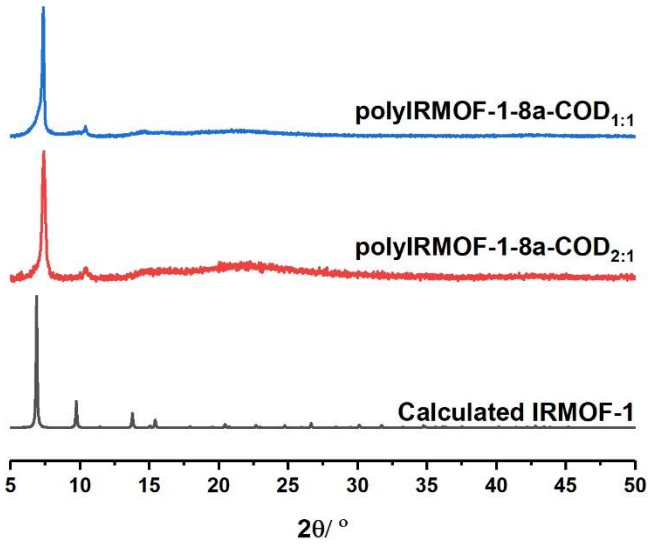

Figure 4S.75. PXRD data was obtained for polyIRMOF-1 prepared from pbdc-8a-COD$_{m:n}$ after activation.

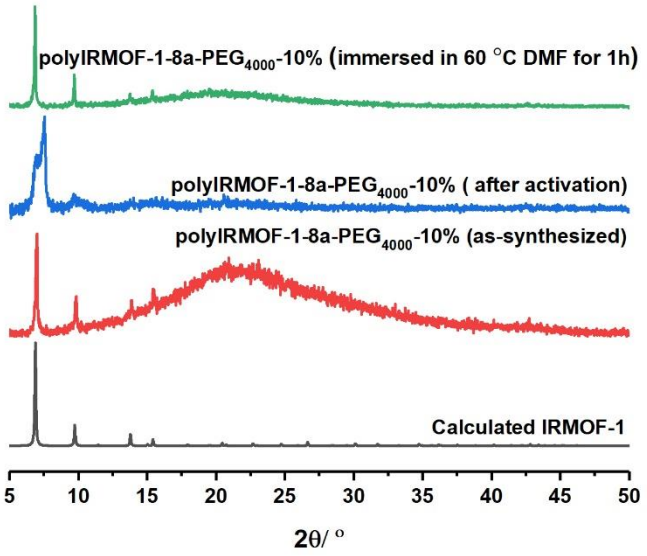

Figure 4S.76. Representative PXRD data was obtained for polyIRMOF-1 prepared from pbdc-8a-PEG$_{4000}$-10% and shown here as synthesized, after activation, and after immersion in DMF at 60 °C for 1 h.

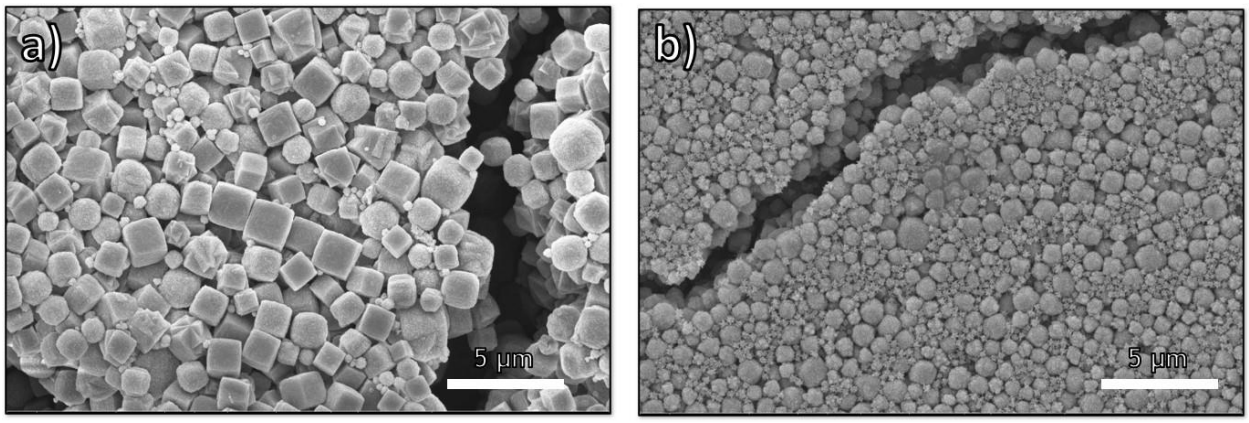

Figure 4S.77. SEM images for polyIRMOF-1 prepared from a) pbdc-8a-PEG$_{2000}$OMe and b) pbdc-8a-PEG$_{5000}$OMe.

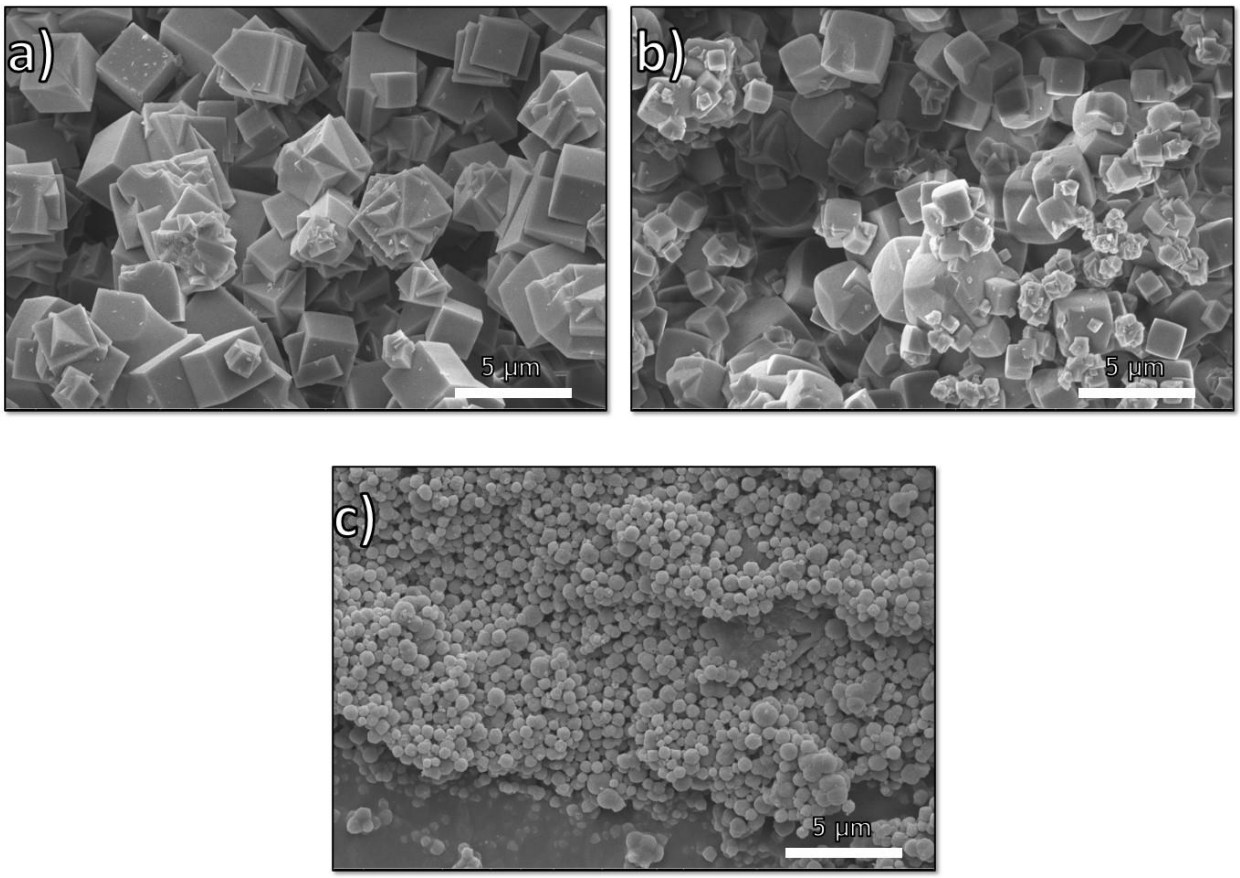

Figure 4S.78. SEM images for polyIRMOF-1 prepared from a) pbdc-8a-$COD_{10:1}$, b) pbdc-8a-$COD_{2:1}$ and c) pbdc-8a-$COD_{1:1}$.

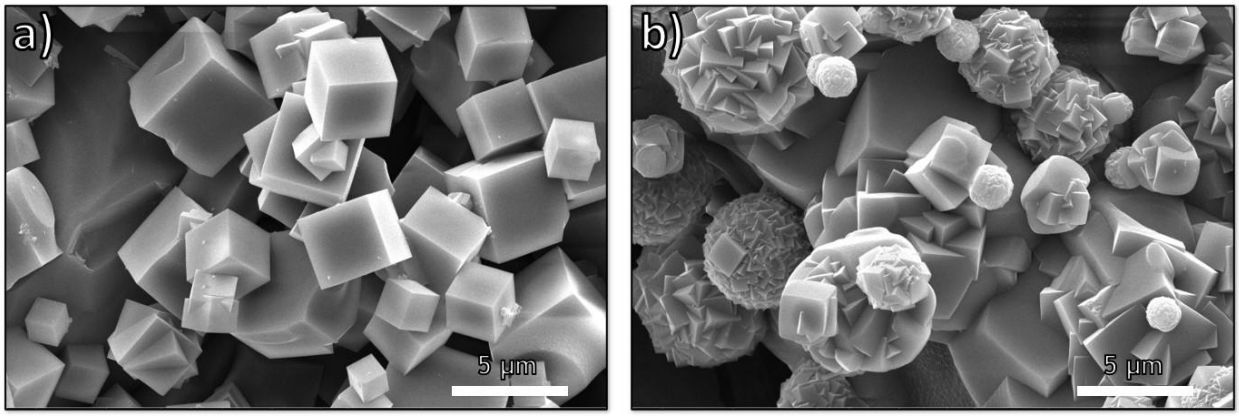

Figure 4S.79. SEM images for polyIRMOF-1 prepared from pbdc-8a and physically mixed PEG_{4000} at a)1% loading and b) 10% loading.

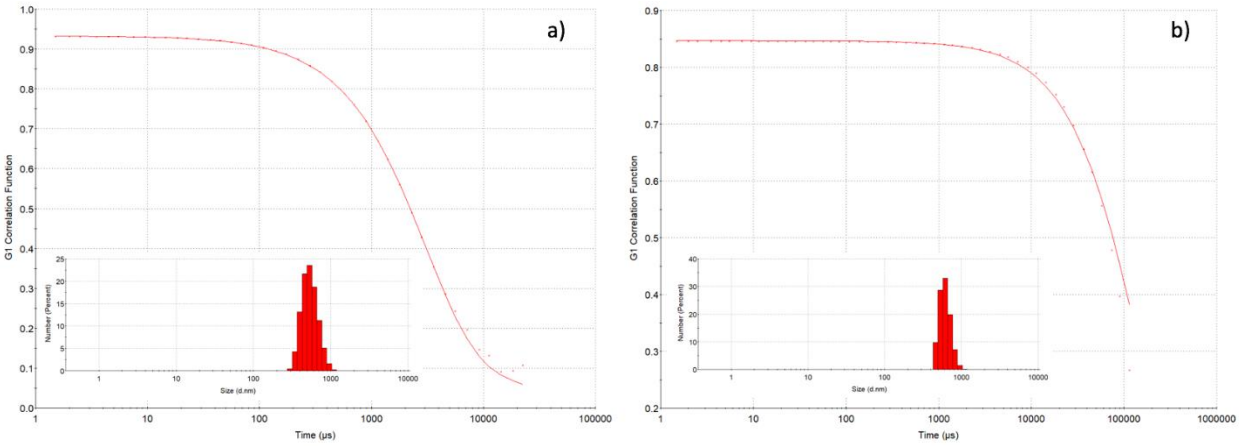

Figure 4S.80. Correlation functions, distribution fits, and number-average size distributions (inset) at 90° (a) and 13° (b) scattering angle for polyIRMOF-1 prepared from pbdc-8a-PEG$_{4000}$-10%.

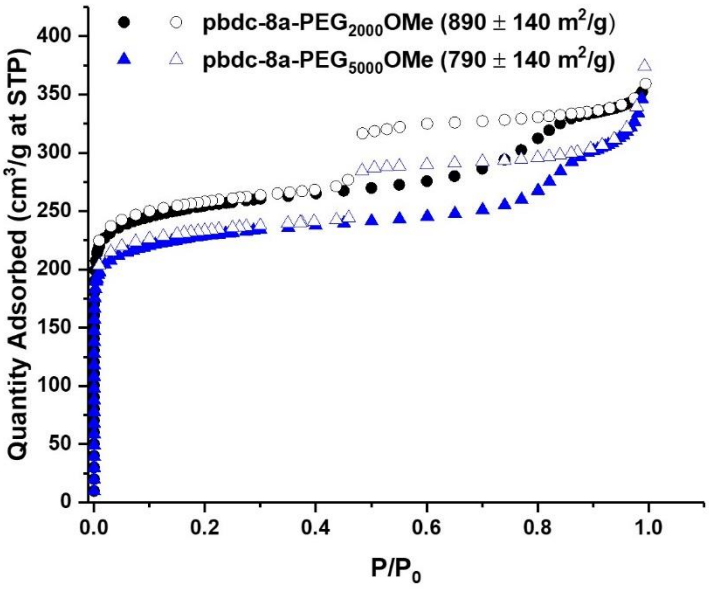

Figure 4S.81. N_2 adsorption isotherm for polyIRMOF-1 prepared from pbdc-8a-PEG$_{2000}$OMe is presented.

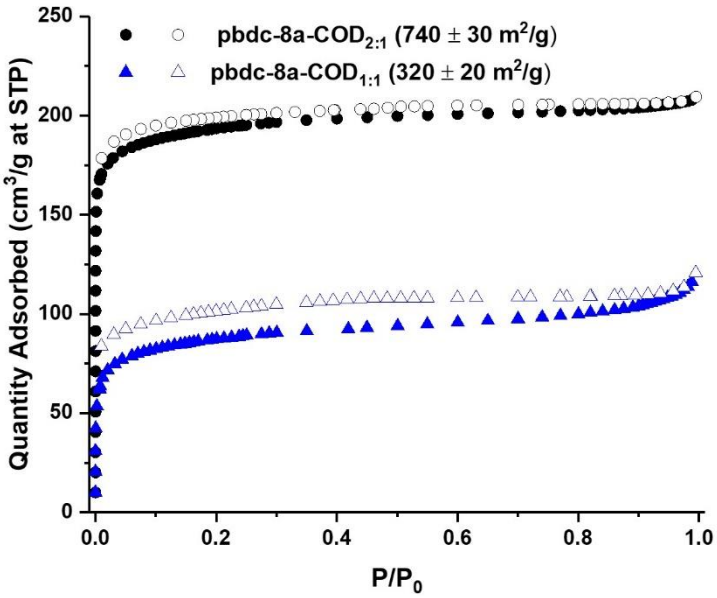

Figure 4S.82. N_2 adsorption isotherm for polyIRMOF-1 prepared from pbdc-8a-$COD_{m:n}$ is presented.

4.7 Acknowledgements

Chapter 4, in part, is a reprint of the material, "Block co-polyMOFs: morphology control of polymer–MOF hybrid materials", *Chem. Sci.* **2019**, *10*, 1746-1753. The dissertation author was the primary author of this manuscript and gratefully acknowledges the contributions of coauthors Kyle C. Bentz and Seth M. Cohen.

4.8 References

1. Ayala, S.; Zhang, Z.; Cohen, S. M., Hierarchical structure and porosity in UiO-66 polyMOFs. *Chem. Commun.* **2017,** *53*, 3058-3061.

2. Zhang, Z.; Nguyen, H. T. H.; Miller, S. A.; Cohen, S. M., polyMOFs: A Class of Interconvertible Polymer-Metal-Organic-Framework Hybrid Materials. *Angew. Chem. Int. Ed.* **2015,** *54*, 6152-6157.

3. Zhang, Z.; Nguyen, H. T. H.; Miller, S. A.; Ploskonka, A. M.; DeCoste, J. B.; Cohen, S. M., Polymer–Metal–Organic Frameworks (polyMOFs) as Water Tolerant Materials for Selective Carbon Dioxide Separations. *J. Am. Chem. Soc.* **2016,** *138*, 920-925.

4. Schukraft, G. E. M.; Ayala, S.; Dick, B. L.; Cohen, S. M., Isoreticular expansion of polyMOFs achieves high surface area materials. *Chem. Commun.* **2017,** *53*, 10684-10687.

5. Mozhdehi, D.; Ayala, S.; Cromwell, O. R.; Guan, Z., Self-Healing Multiphase Polymers via Dynamic Metal–Ligand Interactions. *J. Am. Chem. Soc.* **2014,** *136*, 16128-16131.

6. Muradyan, H.; Mozhdehi, D.; Guan, Z., Self-healing magnetic nanocomposites with robust mechanical properties and high magnetic actuation potential prepared from commodity monomers via graft-from approach. *Polym. Chem.* **2020,** *11*, 1292-1297.

7. Huang, S.; Chen, Y.; Ma, S.; Yu, H., Hierarchical Self-Assembly in Liquid-Crystalline Block Copolymers Enabled by Chirality Transfer. *Angew. Chem. Int. Ed.* **2018,** *57*, 12524-12528.

8. Pan, S.; Fu, C.; Zhu, M.; He, L.; Yang, Y.; Zhang, H.; Liu, X.; Qiu, F.; Lin, Z.; Peng, J., Hierarchical Self-Assembly of Conjugated Block Copolymers and Semiconducting Nanorods into One-Dimensional Nanocomposites. *Macromolecules* **2018,** *51*, 8833-8843.

9. Mozhdehi, D.; Neal, J. A.; Grindy, S. C.; Cordeau, Y.; Ayala, S.; Holten-Andersen, N.; Guan, Z., Tuning Dynamic Mechanical Response in Metallopolymer Networks through Simultaneous Control of Structural and Temporal Properties of the Networks. *Macromolecules* **2016,** *49*, 6310-6321.

10. Berda, E. B.; Lande, R. E.; Wagener, K. B., Precisely Defined Amphiphilic Graft Copolymers. *Macromolecules* **2007,** *40*, 8547-8552.

11. MacLeod, M. J.; Johnson, J. A., Block co-polyMOFs: assembly of polymer–polyMOF hybrids via iterative exponential growth and “click” chemistry. *Polym. Chem.* **2017,** *8*, 4488-4493.

12. Ayala Jr., S.; Cohen, S. M., PolyMOFs. In *Hybrid Metal-Organic Framework and Covalent Organic Framework Polymers*, Wang, B., Ed. The Royal Society of Chemistry: In Preparation.

13. Cheng, X.; Zhang, A.; Hou, K.; Liu, M.; Wang, Y.; Song, C.; Zhang, G.; Guo, X., Size- and morphology-controlled NH2-MIL-53(Al) prepared in DMF–water mixed solvents. *Dalton Trans.* **2013,** *42*, 13698-13705.

14. Zhang, B.; Zhang, J.; Liu, C.; Sang, X.; Peng, L.; Ma, X.; Wu, T.; Han, B.; Yang, G., Solvent determines the formation and properties of metal–organic frameworks. *RSC Adv.* **2015,** *5*, 37691-37696.

15. Falcaro, P.; Hill, A. J.; Nairn, K. M.; Jasieniak, J.; Mardel, J. I.; Bastow, T. J.; Mayo, S. C.; Gimona, M.; Gomez, D.; Whitfield, H. J.; Riccò, R.; Patelli, A.; Marmiroli, B.; Amenitsch, H.; Colson, T.; Villanova, L.; Buso, D., A new method to position and functionalize metal-organic framework crystals. *Nat. Commun.* **2011,** *2*, 237.

16. Furukawa, S.; Reboul, J.; Diring, S.; Sumida, K.; Kitagawa, S., Structuring of metal–organic frameworks at the mesoscopic/macroscopic scale. *Chem. Soc. Rev.* **2014,** *43*, 5700-5734.

17. Stock, N.; Biswas, S., Synthesis of Metal-Organic Frameworks (MOFs): Routes to Various MOF Topologies, Morphologies, and Composites. *Chem. Rev.* **2012,** *112*, 933-969.

18. Cho, W.; Lee, H. J.; Oh, M., Growth-Controlled Formation of Porous Coordination Polymer Particles. *J. Am. Chem. Soc.* **2008,** *130*, 16943-16946.

19. Guo, C.; Zhang, Y.; Guo, Y.; Zhang, L.; Zhang, Y.; Wang, J., A general and efficient approach for tuning the crystal morphology of classical MOFs. *Chem. Commun.* **2018,** *54*, 252-255.

20. Liu, Q.; Yang, J.-M.; Jin, L.-N.; Sun, W.-Y., Controlled Synthesis of Porous Coordination-Polymer Microcrystals with Definite Morphologies and Sizes under Mild Conditions. *Chem. Eur. J.* **2014,** *20*, 14783-14789.

21. Ma, M.; Zacher, D.; Zhang, X.; Fischer, R. A.; Metzler-Nolte, N., A Method for the Preparation of Highly Porous, Nanosized Crystals of Isoreticular Metal−Organic Frameworks. *Cryst. Growth Des.* **2011,** *11*, 185-189.

22. Bates, C. M.; Bates, F. S., 50th Anniversary Perspective: Block Polymers—Pure Potential. *Macromolecules* **2017,** *50*, 3-22.

23. Cölfen, H., Double-Hydrophilic Block Copolymers: Synthesis and Application as Novel Surfactants and Crystal Growth Modifiers. *Macromol. Rapid Commun.* **2001,** *22*, 219-252.

24. Cölfen, H.; Mann, S., Higher-Order Organization by Mesoscale Self-Assembly and Transformation of Hybrid Nanostructures. *Angew. Chem. Int. Ed.* **2003,** *42*, 2350-2365.

25. Meldrum, F. C.; Cölfen, H., Controlling Mineral Morphologies and Structures in Biological and Synthetic Systems. *Chem. Rev.* **2008,** *108*, 4332-4432.

26. Weber, B., Synthesis of Coordination Polymer Nanoparticles using Self-Assembled Block Copolymers as Template. *Chem. Eur. J.* **2017,** *23*, 18093-18100.

27. Jain, S.; Bates, F. S., On the Origins of Morphological Complexity in Block Copolymer Surfactants. *Science* **2003,** *300*, 460-464.

28. Pang, M.; Cairns, A. J.; Liu, Y.; Belmabkhout, Y.; Zeng, H. C.; Eddaoudi, M., Synthesis and Integration of Fe-soc-MOF Cubes into Colloidosomes via a Single-Step Emulsion-Based Approach. *J. Am. Chem. Soc.* **2013,** *135*, 10234-10237.

29. Zheng, X.-P.; Xu, S.-J.; Wu, H.-L.; Kong, Y.-F.; Wang, Y.; Shen, Q.; Xu, Z.-L.; Chen, G.-E., Effects of polyvinylidene fluoride content in the synthesis of novel zinc-based metal-organic frameworks polymer composite crystals. *Inorg. Chem. Commun.* **2018,** *92*, 91-94.

30. Chen, T.-H.; Wang, L.; Trueblood, J. V.; Grassian, V. H.; Cohen, S. M., Poly(isophthalic acid)(ethylene oxide) as a Macromolecular Modulator for Metal–Organic Polyhedra. *J. Am. Chem. Soc.* **2016,** *138*, 9646-9654.

31. Hwang, J.; Heil, T.; Antonietti, M.; Schmidt, B. V. K. J., Morphogenesis of Metal–Organic Mesocrystals Mediated by Double Hydrophilic Block Copolymers. *J. Am. Chem. Soc.* **2018,** *140*, 2947-2956.

32. Jiang, D.; Mallat, T.; Krumeich, F.; Baiker, A., Polymer-assisted synthesis of nanocrystalline copper-based metal–organic framework for amine oxidation. *Catal. Commun.* **2011,** *12*, 602-605.

33. Uemura, T.; Hoshino, Y.; Kitagawa, S.; Yoshida, K.; Isoda, S., Effect of Organic Polymer Additive on Crystallization of Porous Coordination Polymer. *Chem. Mater.* **2006,** *18*, 992-995.

34. Wang, S.; Lv, Y.; Yao, Y.; Yu, H.; Lu, G., Modulated synthesis of monodisperse MOF-5 crystals with tunable sizes and shapes. *Inorg. Chem. Commun.* **2018,** *93*, 56-60.

35. Cao, S.; Gody, G.; Zhao, W.; Perrier, S.; Peng, X.; Ducati, C.; Zhao, D.; Cheetham, A. K., Hierarchical bicontinuous porosity in metal–organic frameworks templated from functional block co-oligomer micelles. *Chem. Sci.* **2013,** *4*, 3573-3577.

36. Ayala, S.; Bentz, K. C.; Cohen, S. M., Block co-polyMOFs: morphology control of polymer–MOF hybrid materials. *Chem. Sci.* **2019,** *10*, 1746-1753.

37. Caire da Silva, L.; Rojas, G.; Schulz, M. D.; Wagener, K. B., Acyclic diene metathesis polymerization: History, methods and applications. *Prog. Polym. Sci.* **2017,** *69*, 79-107.

38. Kim, M.; Cohen, S. M., Discovery, development, and functionalization of Zr(iv)-based metal–organic frameworks. *CrystEngComm* **2012,** *14*, 4096-4104.

39. Trickett, C. A.; Gagnon, K. J.; Lee, S.; Gándara, F.; Bürgi, H.-B.; Yaghi, O. M., Definitive Molecular Level Characterization of Defects in UiO-66 Crystals. *Angew. Chem. Int. Ed.* **2015,** *54*, 11162-11167.

40. Mai, Y.; Eisenberg, A., Self-assembly of block copolymers. *Chem. Soc. Rev.* **2012,** *41*, 5969-5985.

41. Cliffe, M. J.; Wan, W.; Zou, X.; Chater, P. A.; Kleppe, A. K.; Tucker, M. G.; Wilhelm, H.; Funnell, N. P.; Coudert, F.-X.; Goodwin, A. L., Correlated defect nanoregions in a metal–organic framework. *Nat. Commun.* **2014,** *5*, 4176.

42. He, H.; Rahimi, K.; Zhong, M.; Mourran, A.; Luebke, D. R.; Nulwala, H. B.; Möller, M.; Matyjaszewski, K., Cubosomes from hierarchical self-assembly of poly(ionic liquid) block copolymers. *Nat. Commun.* **2017,** *8*, 14057.

43. Hosono, N.; Gochomori, M.; Matsuda, R.; Sato, H.; Kitagawa, S., Metal–Organic Polyhedral Core as a Versatile Scaffold for Divergent and Convergent Star Polymer Synthesis. *J. Am. Chem. Soc.* **2016,** *138*, 6525-6531.

44. Gu, Y.; Huang, M.; Zhang, W.; Pearson, M. A.; Johnson, J. A., PolyMOF Nanoparticles: Dual Roles of a Multivalent polyMOF Ligand in Size Control and Surface Functionalization. *Angew. Chem. Int. Ed.* **2019,** *58*, 16676-16681.

Chapter 5: Multivariate PolyMOFs

5.1 Introduction

As described Chapter 1, careful choice among multitopic linkers, SBUs, as well as the use of presynthetic and postsynthetic methods, can yield an incredible range of MOF structures.[1-2] In fact, efforts to compose MOFs that contain multiple linkers and SBUs within a lattice, or multivaritate MOFs (MTV-MOFs), can yield materials with intricate pore environments,[3] new lattices,[4] and even tunable porosities.[5-6] In an early example, Yaghi and co-workers prepared MTV-IRMOF-1 through a one-pot mixture of H_2bdc, H_2bdc-NH_2, H_2bdc-Br, H_2bdc-Cl_2, and other H_2bdc derivatives in combination with Zn^{2+} salts (Figure 5.1).[3] Crystals of MTV-IRMOF-1 could contain up to eight different functional groups in a single framework, and under the appropriate conditions could selectively uptake CO_2 over CO up to 400% times better than IRMOF-1 prepared only from H_2bdc. These results highlight the ability of MTV-MOFs to yield materials with intricate pore environments.

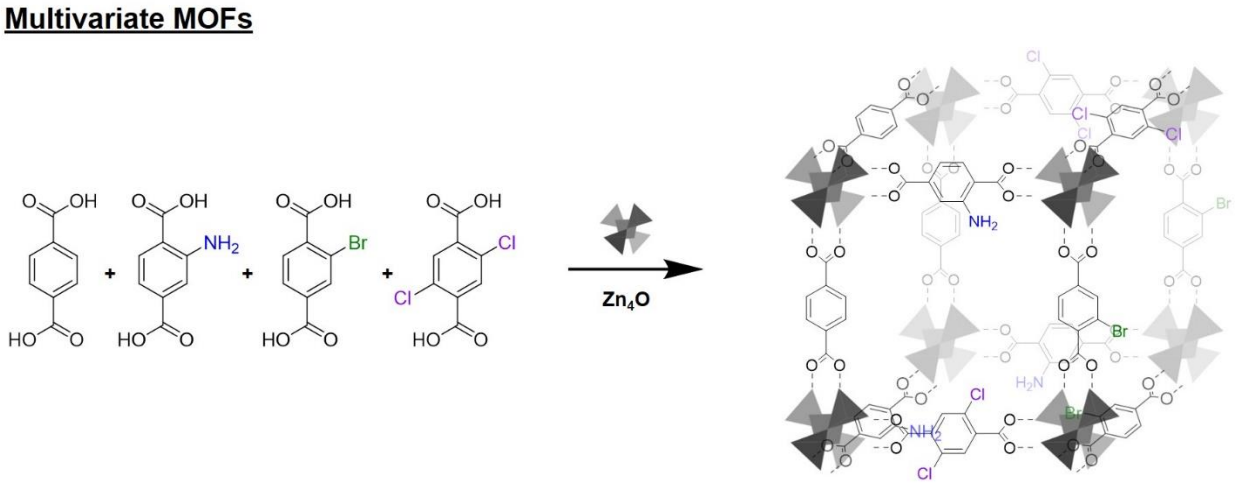

Figure 5.1. Illustrative representation of multivariate MOFs (MTV-MOFs). Ditopic H_2bdc linkers with several different functional groups can be introduced into a single MOF crystal.

The length and geometry of MTV-MOFs are often constrained by isoreticular chemistry, but can be fine-tuned when changes in the size and length of the ligands is relatively small.[7-10] For example, Zhou and co-workers recently demonstrated that UiO-type MOFs could be produced with two mixed linkers that are less than 41% different in length (Figure 5.2).[10] MOFs made of a mixture of $bpdc^{2-}$ and azobenzene-4,4′-dicarboxylate ($abpdc^{2-}$) were exceptionally homogeneous in their crystallinity and variation in the amount of each linker could be used to fine-tune the pores of MOFs; several other MTV-MOFs could be prepared this way, demonstrating the capacity to prepare MTV-MOF with gradient porosities. Despite the example presented by Zhou, multi-component MOFs with ligands of different sizes, lengths, and topologies are more commonly synthesized by core-shell methods because physically mixing multiple lattice-mismatched ligands tend to yield two separate MOF structures.[6, 11-12] For instance, Kim and co-workers demonstrated that computational screening could be used to identify matching MOF-pairs wherein the SBUs present in the surface of one type of MOF could be used as the starting coordination sites of a second framework (Figure 5.2).[12] The screening results were used to synthesize core-shell MOFs of HKUST-1@IRMOF-1 (HKUST = Hong Kong University of Science and Technology), among many other core-shell structures (Figure 5.2). Both the mixed ligand approach and the core-shell approach are effective methods to produce multi-component MOFs with mismatched ligands, and can yield MOFs with hierarchical pore sizes and extraordinary tunability.

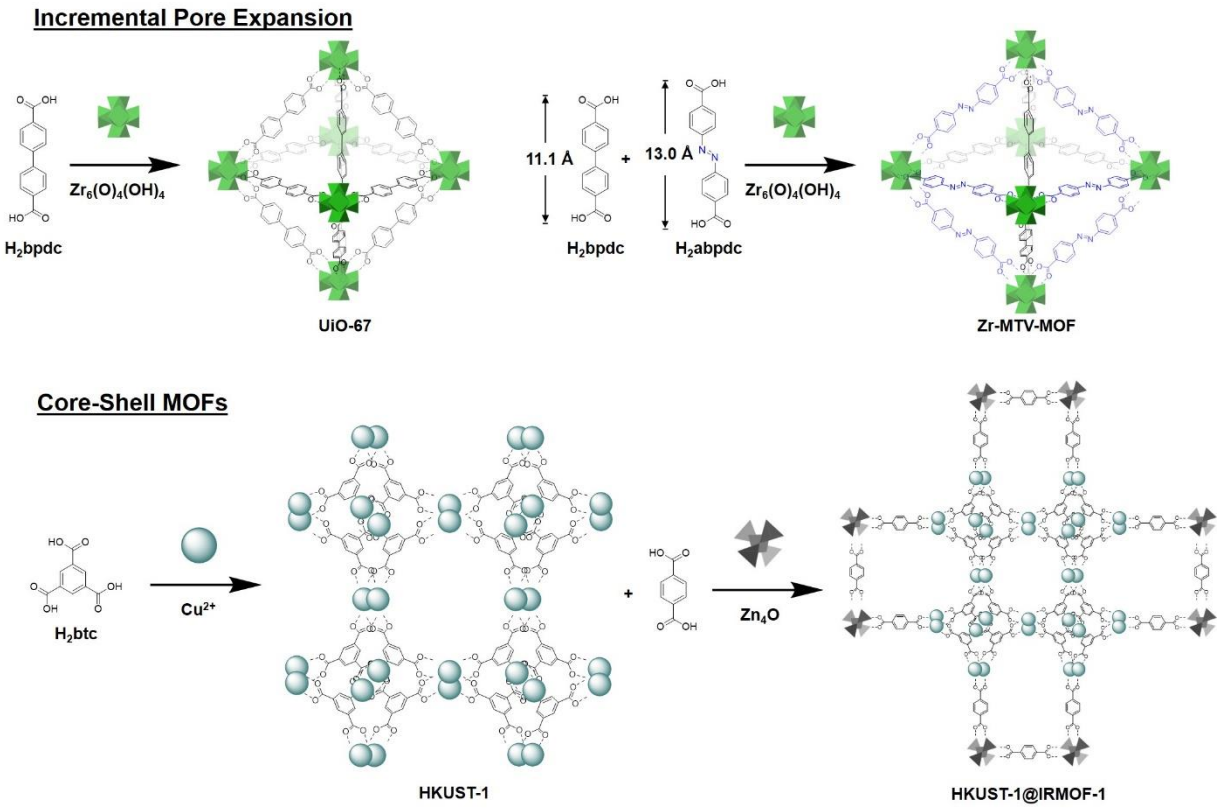

Figure 5.2. *Top*: Illustration of preparing MTV-MOFs with incremental pore expansion. Whereas H_2bdc forms UiO-67 (top left), both H_2bpdc and H_2abpdc are similar in size and can fit into a single Zr-MTV-MOF with incrementally larger pores (top right). *Bottom*: The concept of core-shell MOFs is demonstrated, wherein the core of HKUST-1 is used as a starting point to grow a shell of IRMOF-1.

Inspired by the concept of MTV-MOFs, Chapter 5 focuses on multivariate, co-polymer ligands that can serve as a method to produce MOF-polymer materials with mismatched ligands (Figure 5.3). Indeed, the use of polymer ligands provide the opportunity to attach multiple organic linkers of different lateral lengths into a single polymer chain. Preparation of 'MTV-polyMOFs' can potentially include tunable pore sizes within a single crystalline lattice, as mismatched ligands are forced to be together, and can become part of the same MOF material. In the preliminary studies discussed herein, two lattice-mismatched monomers were combined to prepare random copolymers that could be used to synthesize MTV-polyMOFs with a UiO-66 architecture and an

IRMOF-1 architecture. The ratios of the two monomers were varied to determine the capacity for which the multivariate copolymers could yield MTV-polyMOFs. Preliminary results suggest that changing the ratios of the two monomers could serve as a new method to introduce morphological changes into polyMOF materials. Success in preparing MTV-polyMOFs in the future may open a new, unprecedented avenue to controlling the porosity of MOFs at the molecular level.

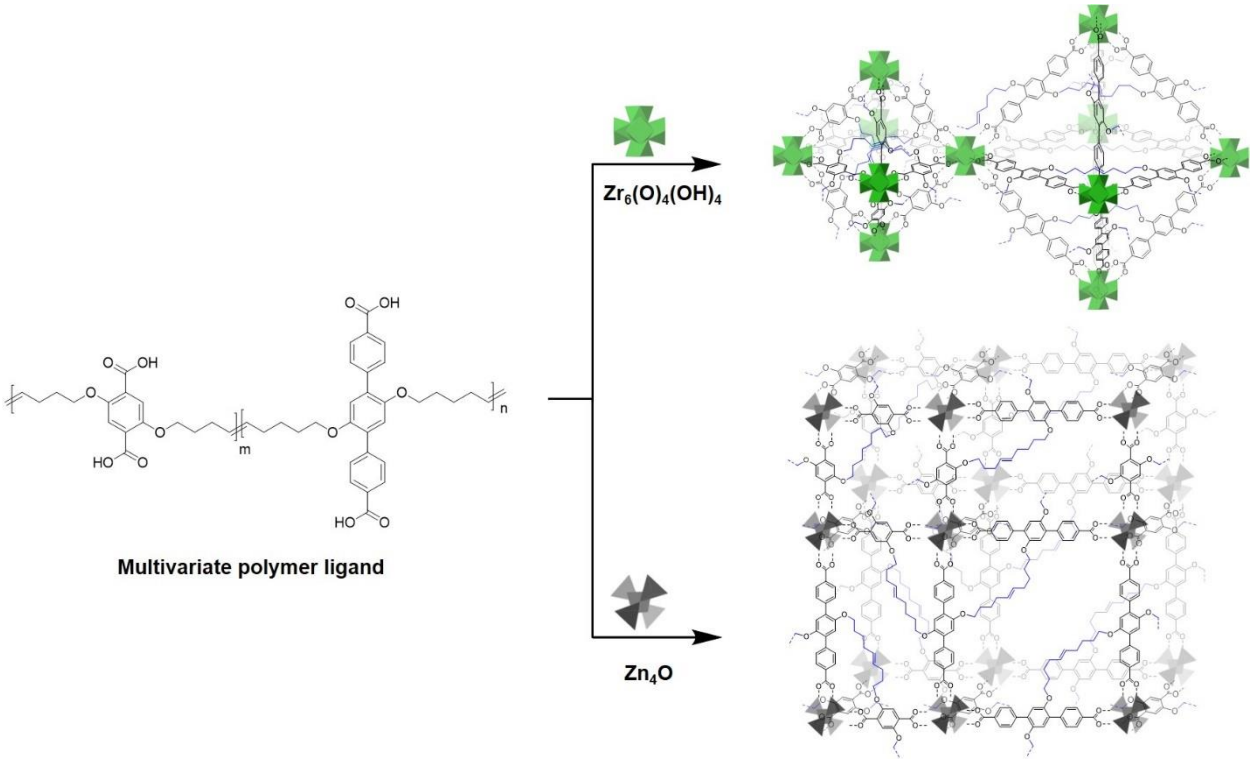

Figure 5.3. Illustrative representation of a multivariate polymer ligand used to synthesize MTV-polyMOFs.

5.2 Synthesis and Characterization of MTV Random Copolymers

Monomer syntheses were performed as described in Chapters 2 and 3, using Williamson ether condensation to yield methyl-protected bdc-8e and tpdc-10e (Scheme 5.1). The monomers were then copolymerized by ADMET polymerization using Grubbs 2nd-generation catalyst, to afford multivariate co-polymer esters of bdc-8e and tpdc-10e. These polymers are denoted as

$(CH_3)_2$-MTVP-1$_{m:n}$, where '$(CH_3)_2$' indicates the methyl-ester form of the polymer, 'MTVP' refers to multivariate polymer, and *m:n* indicates the molar ratio of bdc-8e:tpdc-10e (Figure 5S.1-4). For control experiments, homopolymers of pbdc-8e-u, and ptpdc-10e-u were also synthesized via ADMET polymerization using Grubbs 2nd-generation catalyst; these polymerization conditions are different from the optimized synthetic conditions to prepare ptpdc-10e-u discussed in Chapter 3, but for direct comparison all synthetic conditions were kept consistent for homo- and copolymer syntheses. The polymer esters were hydrolyzed to produce polymer acid ligands, denoted as MTVP-1$_{m:n}$, pbdc-8a-u, and ptpdc-10a-u (Scheme 5.1, Figures 5S.5-7).

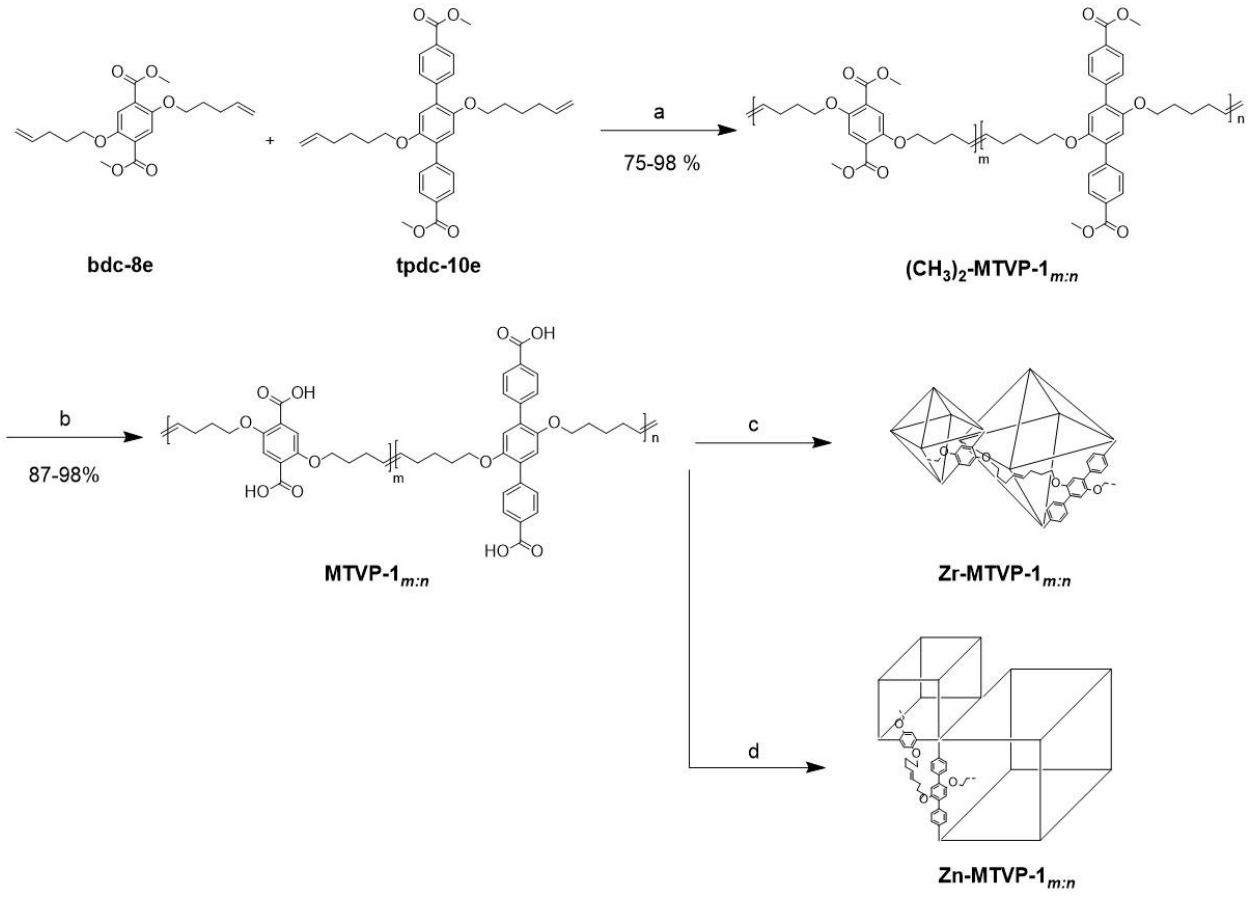

Scheme 5.1. General method for the preparation of MTV-polyMOFs is presented. Reagents and conditions: a) Grubbs 2nd-generation catalyst, CH_2Cl_2, 50 °C, 5 h; b) NaOH , 1:1 THF/H_2O, 70 °C, 12 h; c) $ZrCl_4$, 1:1 DEF/formic acid, 135 °C, 48 h; d) $Zn(NO_3)_2$, DMF, 100 °C, 24 h.

Both ^{1}H NMR and GPC were used to determine molecular weights and compositions of the multivariate co-polymer esters (Table 5.1). As expected with ADMET polymerization, all random co-polymers achieved high molecular weights with broad dispersities (determined by ^{1}H NMR and GPC, Table 5.1, Figures 5S.1-4). Moreover, ^{1}H NMR could be used to determine the ratios of bdc-8e to tpdc-10e (Figure 5S.1-3). A closer analysis of the alkenes present in the ^{1}H NMR for MTVP-1$_{m:n}$ also revealed that the multivariate co-polymer esters contained a statistical distribution of three types of arrangements: bdc-8e coupled to bdc-8e, bdc-8e coupled to tpdc-10e, and tpdc-10e coupled to tpdc-10e (Figure 5.4). The statistical distribution of these combinations could be modified by adjusting the ratios of each monomer present in the initial polymerization. It was also be noted that molecular weights of the polymers decreased with increasing amount of tpdc-10e, as determined by GPC, with the homopolymer ptpdc-10e-u containing the lowest molecular weight (Table 5.1 and Figure 5S.4). Polymers that contained more tpdc-10e were less soluble in the GPC measurement conditions than those higher in bdc-8e, so the molecular weights determined by GPC should be interpreted with care. Moreover, polymer acid ligands are too polar to evaluate by GPC, but ^{1}H NMR revealed that the compositions of the polymers were retained after hydrolysis (Figures 5S.5-7).

Table 5.1. GPC and ^{1}H NMR characterization of the multivariate polymer esters.

Ligand	M_n (GPC)	M_w/M_n	DP bdc-8e (^{1}HNMR) [a]	DP tpdc-10e (^{1}HNMR) [a]
pbdc-8e-u	17,900	2.2	111	-
MTVP-$1_{3:1}$	18,400	2.0	77	24
MTVP-$1_{1:1}$	15,700	1.7	90	80
MTVP-$1_{1:3}$	8,800	2.0	44	114
ptpdc-10e-u	7,600	1.6	-	230

[a] The number of repeating units was determined using end-group analysis by ^{1}HNMR.

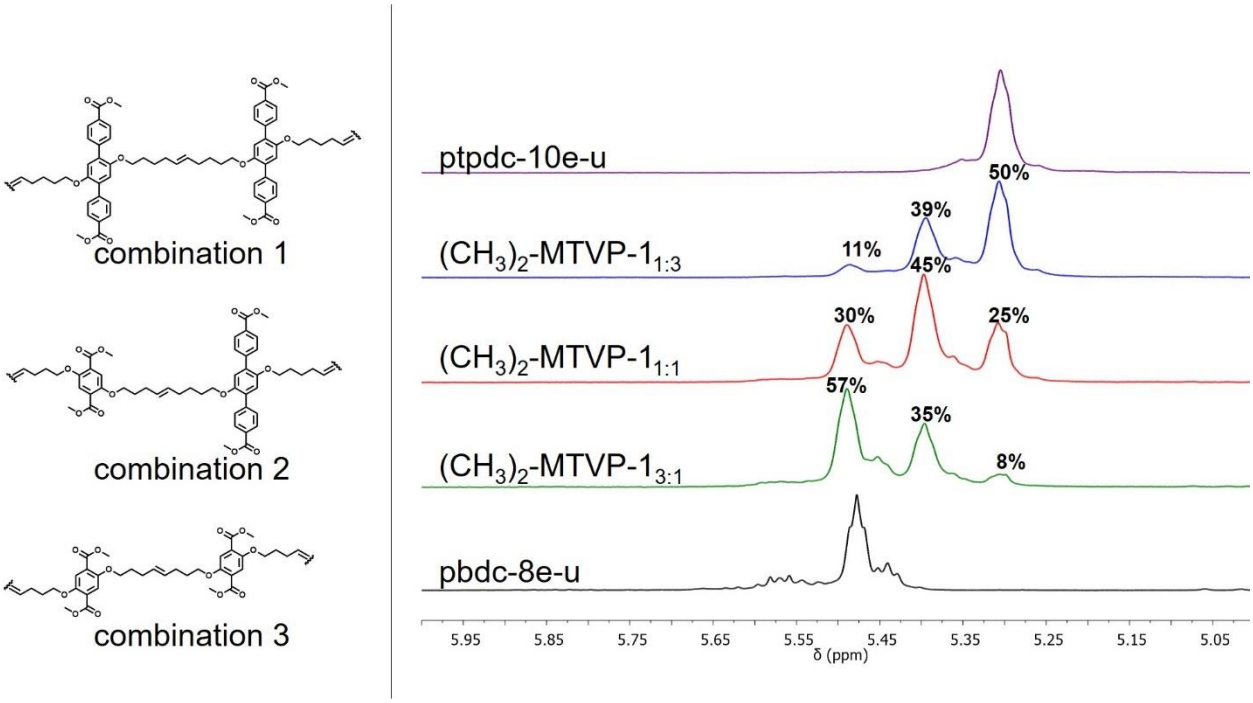

Figure 5.4. *Left*: Three possible arrangements are illustrated, wherein bdc-8e can be coupled to bdc-8e, bdc-8e can be coupled to tpdc-10e, and tpdc-10e can be coupled to tpdc-10e. *Right*: ^{1}H NMR analysis in the alkene region of MTVP-$1_{m:n}$ reveals these three combinations can be adjusted by changing the ratio of the starting precursors before polymerization.

5.3 Synthesis and Characterization of MTV-polyMOFs

Initially, MTV-polyMOFs were prepared with a UiO-66 architecture because the framework is highly stable and tolerant to defects. These materials, denoted as Zr-MTVP-$1_{m:n,}$ were synthesized using $ZrCl_4$ under the same solvothermal conditions described in Chapter 2. The

structural integrity of all polymers was retained after polyMOF formation, as confirmed by ^{1}H NMR digestion of the materials (Figures 5S.8-10).

All Zr-MTVP-1$_{m:n}$ displayed a mixture of reflections predicted in both UiO-66 and UiO-68 diffraction patterns, but the reflections were broad (Figure 5.5a). The diffraction broadening may be attributed to a combination of nanocrystalline regions of polyUiO-66 and polyUiO-68 within these materials, embedded within regions where neither lattice is dominant and both types of linkers (bdc^{2-} and $tpdc^{2-}$) intertwine. Moreover, the ratio of pbdc-8a-u:ptpdc-10a-u did not change the dominant reflections observed in each Zr-MTVP-1$_{m:n}$. For instance, Zr-MTVP-1$_{3:1}$ displayed a dominant reflection typically observed in UiO-66 (2θ ~7.4°), but no reflections that suggest domains of UiO-68 in this material. In contrast, Zr-MTVP-1$_{1:3}$ predominantly displayed primary reflections typically observed in UiO-68 (2θ ~4.7° and 5.4°). Materials prepared from a physical mixture of separately prepared pbdc-8a-u and pbdc-10a-u also displayed similar diffraction patterns with broad reflections (Figure 5.5b). Though these results are encouraging for the preparation of MTV-polyMOFs, much larger crystalline domains would be needed to improve the interpretation of the crystalline habits of these materials.

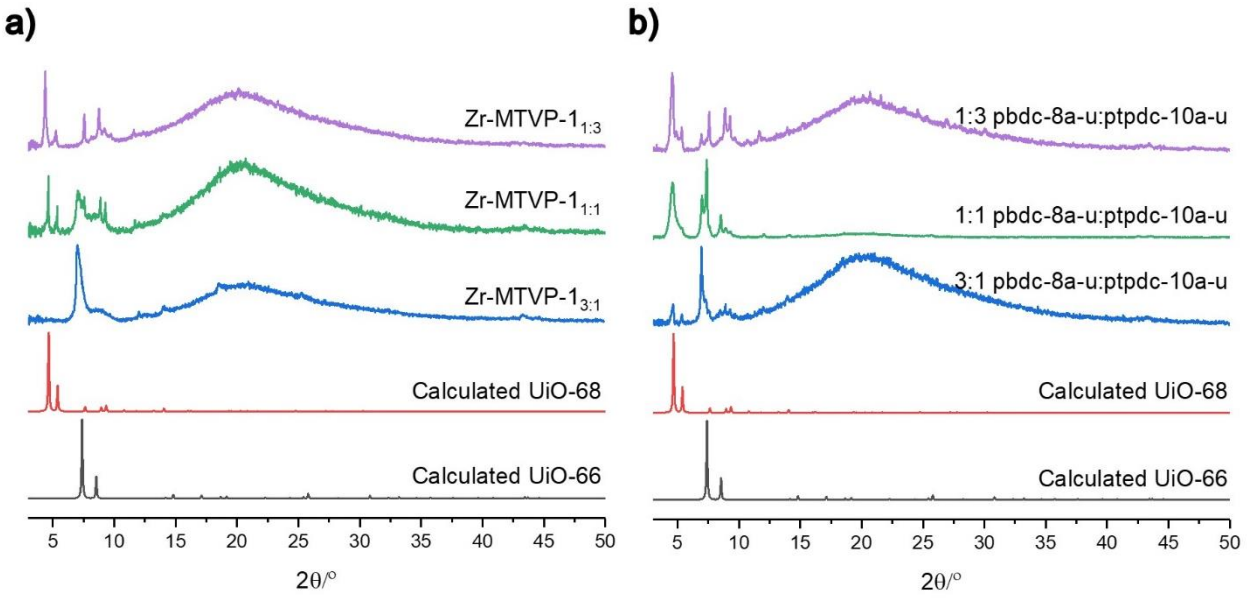

Figure 5.5. PXRD patterns of calculated UiO-66, UiO-68, and experimental Zr-polyMOFs prepared from (a) MTVP-1$_{m:n}$ and (b) physical mixtures of pbdc-8a-u and ptpdc-10a-u.

SEM images of Zr-MTVP-1$_{m:n}$ revealed that depending on the ratio of bdc^{2-}:$tpdc^{2-}$, these materials display morphologies that are similar, but distinguishable from polyUiO-66-8a-u or polyUiO-68-10a-u (Figure 5.6). Specifically, Zr-MTVP-1$_{3:1}$ yields microcrystalline films with an interlaced morphology like polyUiO-66-8a-u, but with less hexagonal features (Figures 5.6a, 5.6b). Increasing the ratio of $tpdc^{2-}$ in Zr-MTVP-1$_{1:1}$ yielded a mixture of microcrystalline spheres and hexagonal plates (Figure 5.6c); in Zr-MTVP-1$_{1:3}$, hexagonal plates are produced that are similar in morphologies to polyUiO-68-10a, but smaller in size (Figures 5.6d, 5.6e). By stark contrast, all Zr-polyMOFs prepared from physically mixed pbdc-8a-u and pbdc-10a-u displayed an interlaced, hexagonal morphology, but with smaller facets than parent polyUiO-66-8a-u and polyUiO-66-10a-u (Figures 5.6f, 5.6g, 5.6h). Results obtained from physically mixed UiO-polyMOFs are especially interesting, as it is normally expected that two physically mismatched ligands would yield MOF materials with distinguishable morphologies,[10]; however, physically mixing two mismatched polymer ligands may produces hybrid crystals that are nearly

indistinguishable from each other (Figures 5.6f, 5.6g, 5.6h). Overall, preliminary results by SEM suggest that multivariate co-polymer ligands may serve as a new strategy to control morphology of polyMOFs.

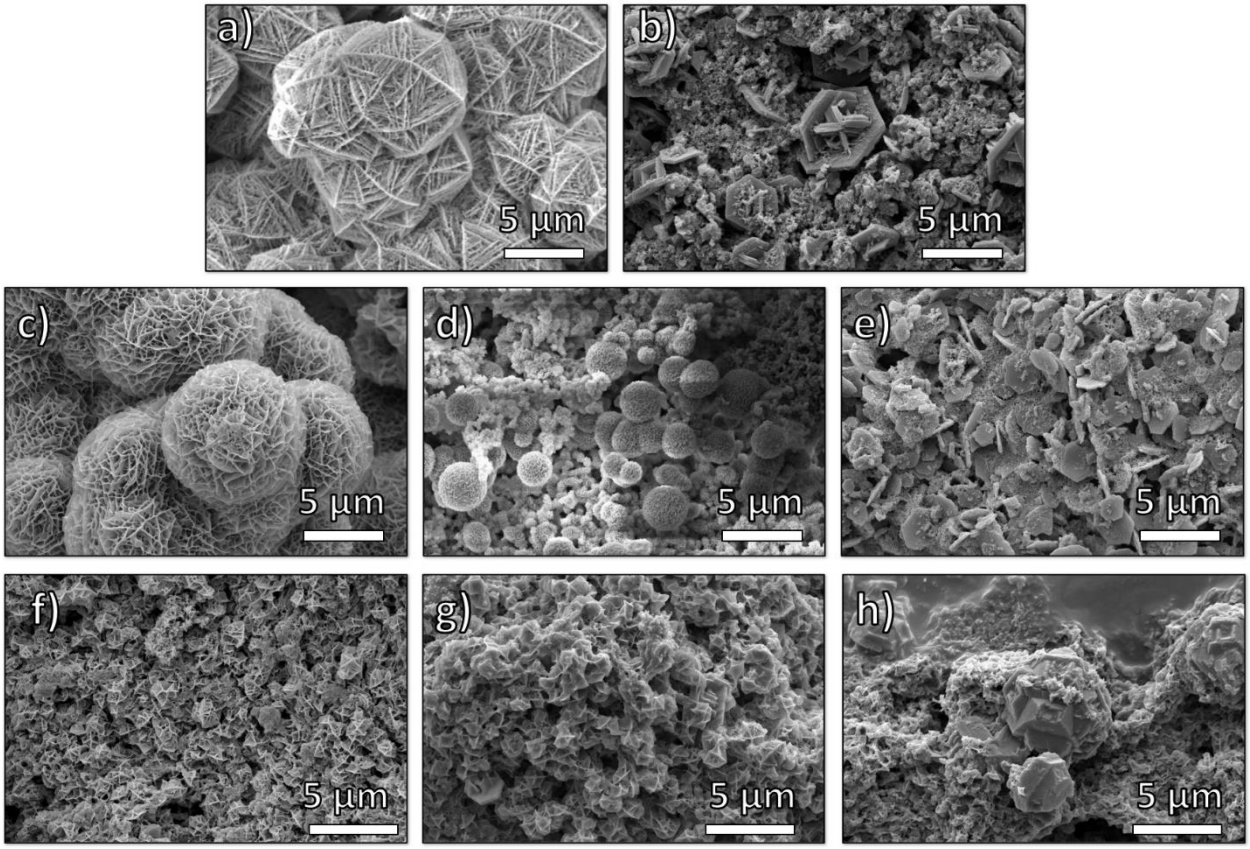

Figure 5.6. SEM images of Zr-polyMOFs prepared from homopolymer and MTVP polymer ligands: (a) polyUiO-66-8a-u; (b) polyUiO-68-10a-u; (c) Zr-MTVP-$1_{3:1}$; (d) Zr-MTVP-$1_{1:1}$; (e) Zr-MTVP-$1_{1:3}$; (f) 3:1 ratio of polyUiO-66-8a-u and polyUiO-68-10a-u; (g) 1:1 ratio of polyUiO-66-8a-u and polyUiO-68-10a-u; (h) 1:3 ratio of polyUiO-66-8a-u and polyUiO-68-10a-u.

MTV-polyMOFs were also prepared from an IRMOF-1 architecture because this simpler framework has fewer configurational restraints than UiO-66. These materials were synthesized under solvothermal conditions as described in Chapter 3 and denoted as Zn-MTVP-$1_{m:n}$. Most of Zn-MTVP$_{m:n}$ yielded poor crystallinity as gauged by PXRD (Figure 5.7). At best, only materials

prepared from Zn-MTVP-$1_{3:1}$ displayed moderate crystallinity, with a PXRD pattern that matched IRMOF-1. For all other Zn-MTVP-$1_{m:n}$, broad diffraction regions could be observed at 2θ ~5.0° and 8.3°. These broad diffraction regions are different from the primary reflections of IRMOF-1 (2θ ~6.8° and 9.7°) and IRMOF-16 (2θ ~4.1° and 9.7°) and may correspond an average of nanocrystalline domains where bdc^{2-} and $tpdc^{2-}$ intermix in a single lattice. As with the Zr-MTV-polyMOFs, improving the crystallinity of these materials could help improve the interpretation between. In contrast to Zn-MTVP-$1_{m:n}$, polyIRMOF materials prepared from mixtures of pbdc-8a-u and ptpdc-10a-u yielded solids that contained reflections consistent with IRMOF-1 and IRMOF-16 (Figure 5S.11); this result is consistent with results observed in the literature, as lattice-mismatched ligands generally yield two separate MOF materials.[10]

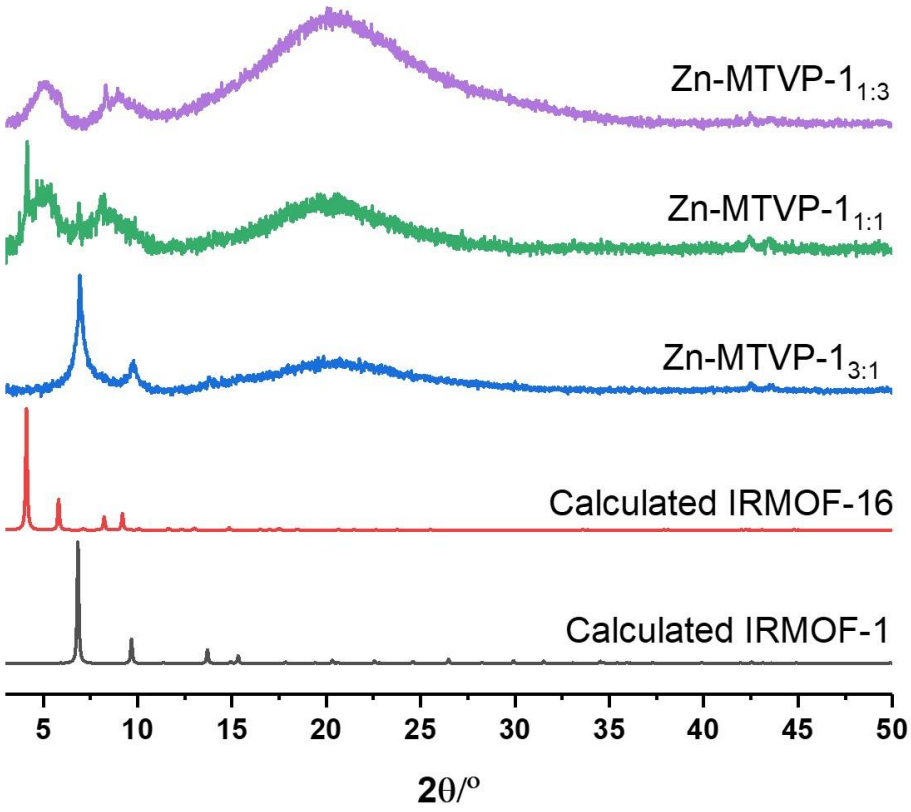

Figure 5.7. PXRD patterns of calculated IRMOF-type patterns and experimental Zn-MTVP-1$_{m:n}$.

Despite the poor crystallinity of Zn-MTVP-1$_{m:n}$, SEM revealed that these materials still displayed largely regular facets (Figure 5.8). In fact, Zn-MTVP-1$_{1:1}$ produced tetragonal, intergrown solids that were comparable in shape to crystals prepared from polyIRMOF-1-8a-u and polyIRMOF-16-10a-u materials (Figure 5.8a, 5.8b, 5.8c). For comparison, MTV-polyIRMOF materials prepared from a mixture of a 1:1 ratio of pbdc-8a-u and ptpdc-10a-u also yielded intergrown, cubic crystals (Figure 5.8d); however, it is clear from the image that two populations of crystals exist in the sample, and coincides with results observed by PXRD (see above). The ability to see regular facets to these materials is promising for future MTV-polyIRMOF-1

materials, but new strategies to observe short-range order would aid in better interpretation of the regular arrangements in these materials.

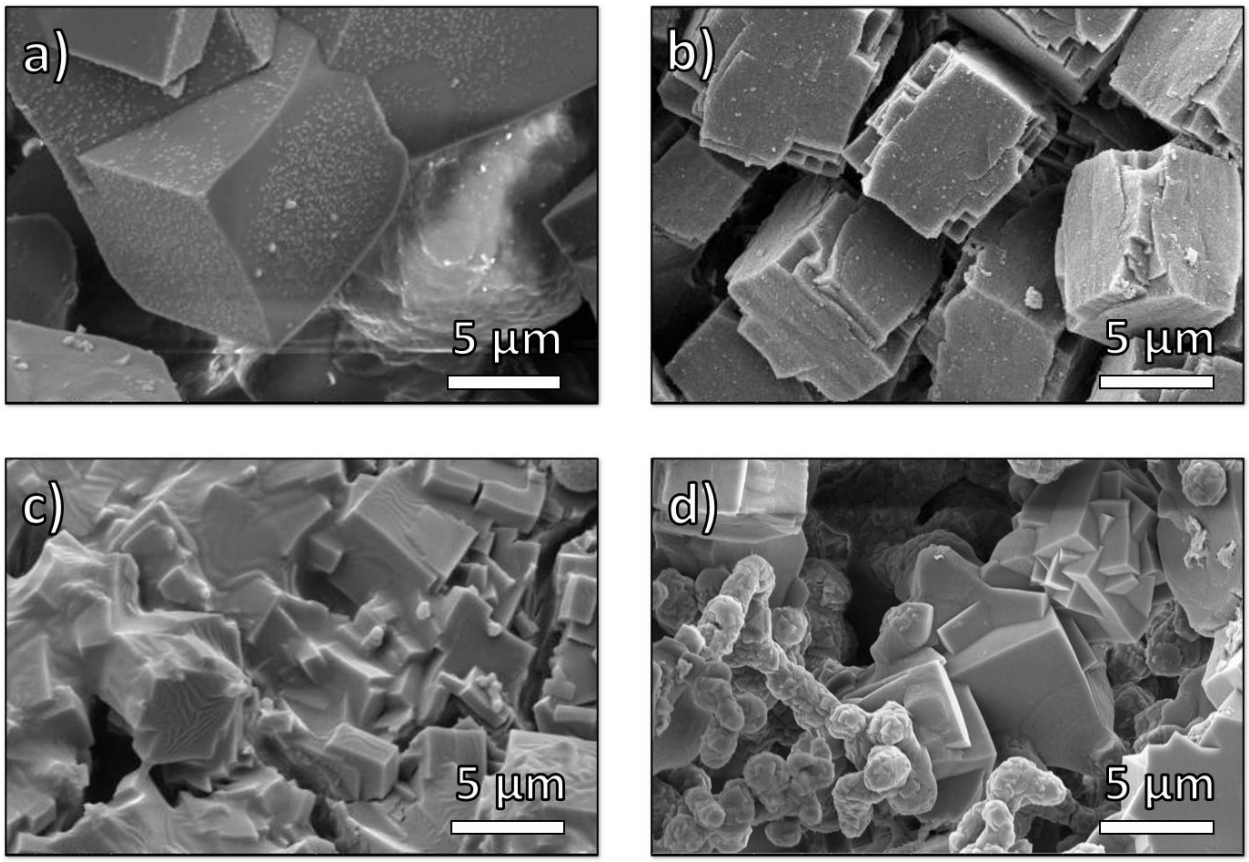

Figure 5.8. SEM images of Zn-polyMOFs prepared from homopolymer and MTVP polymer ligands: (a) polyIRMOF-1-8a-u; (b) polyIRMOF-16-10a-u; (c) Zn-MTVP-$1_{1:1}$; (d) 1:1 ratio of polyIRMOF-1-8a and polyIRMOF-16-10a-u.

5.4 Conclusions and Outlook

Chapter 5 presents initial efforts to prepare MTV-polyMOFs from polymer ligands that contain organic linkers of mismatched lengths. As discussed in Section 5.2, multivariate, random copolymers containing H_2bdc units and H_2tpdc units were synthesized in different ratios to determine the capacity to which lattice mismatched polymer ligands could afford polyMOFs. Two of the common polyMOF structures, UiO-66 and IRMOF-1, were investigated in Section 5.3, and

although the materials yielded poor crystallinity, the morphological changes suggest that the multivariate polymers may have the capacity to produce crystalline MTV-polyMOFs with new and interesting features like enhanced porosity. In the future, adsorption measurements will provide insight as to whether crystallinity affects the porosity of these materials. Moreover, characterization methods like solid-state NMR and small-angle X-ray scattering may provide more insight to the structures obtained from these materials.

One potential direction to improve MTV-polyMOFs may be to produce small, incremental changes to the lattice of the framework, as reported by Zhou and Rosi.[8, 10] Similarly to their work, monomer precursors of H_2bpdc and H_2abpdc could be prepared, copolymerized by ADMET polymerization, and used to synthesize common polyMOF lattices; the difference in length between these two monomers is only 2 Å, making them promising candidates for MTV-polyMOF materials. These materials may produce interesting, new pore environments that have not been observed in other MOF materials.

The development of block co-polymers will also serve as an improvement to future MTV-polyMOF systems. Several studies by Nomura and co-workers have shown that alkene-terminated polymers can be functionalized exclusively at the end groups using Schrock's molybdenum catalyst.[13-14] Lattice-mismatched polymer ligands can be functionalized using this strategy, and coupled through conventional methods like copper assisted alkyne-azide click chemistry (Figure 5.9). In contrast to the random polymers, these materials may have improved crystallinity with nanophase separation between the two disparate lattices. With additional investigations, MTV-polyMOFs may bring about a new class of porous materials with highly tunable porosity.

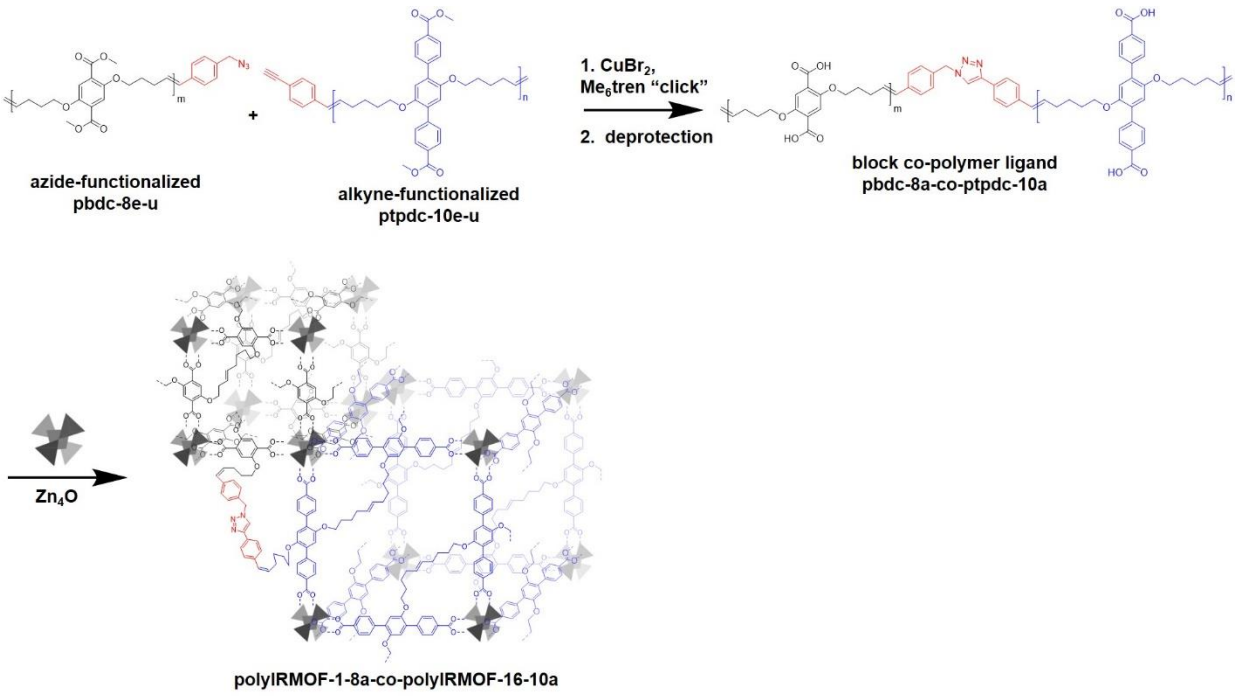

Figure 5.9. A general strategy for the synthesis of MTV-polyMOFs using block copolymers is presented, using pbdc-8e-u and ptpdc-10e-u as examples. Exclusive end-functionalized polymers can be coupled by alkyne-azide copper "click" chemistry to yield block copolymer ligands. These new ligands may have the potential to yield polyMOFs with nanophase separations between two disparate lattices.

5.5 Appendix: Supporting Information

Experimental

General Materials and Methods. Starting materials were purchased and used from commercially available suppliers (Sigma-Aldrich, Acros Organics, Matrix Scientific, and others) without further purification. ^{1}H nuclear magnetic resonance (NMR) spectra were collected using a Varian spectrometer running at 400 MHz.

General polymerization procedure for $(CH_3)_2$-MTVP-1$_{m:n}$. Dimethyl 2,5-bis(pent-4-en-1-yloxy) terephthalate (bdc-8e, 230-690 µmol, 1-3 eq) and dimethyl 2',5'-bis(hex-5-en-1-yloxy)-[1,1':4',1"-terphenyl]-4,4"-dicarboxylate (tpdc-10e, 230-690 µmol, 1-3 eq) were added to a 5 mL round bottom flask, and dissolved in 1.0 mL CH_2Cl_2. Grubbs 2nd-generation catalyst was loaded

neat (7.8 mg, 0.0092 mmol, 0.04 eq). The reaction was set at 50 °C under mild nitrogen for 5 h while stirring. After 5 h, the solution was cooled to room temperature, and 1 mL of ethyl vinyl ether was added to quench the catalyst. The solution was stirred for 30 min. The polymer was precipitated in methanol, followed by centrifugation at 7000 rpm for 10 min. at 8 °C. The supernatant was decanted, and the polymer was dissolved using 5 mL CH_2Cl_2. The polymer was precipitated four more times in methanol. After the final wash, the polymer was dried under high vacuum at 8 °C for 2 h.

$(CH_3)_2$-MTVP-$1_{3:1}$. Yield: 75% (375 mg). ^{1}H NMR (400 MHz, $CDCl_3$) δ 8.07 (s, *J* = 7.5 Hz, 92H), 7.65 (s, *J* = 7.7 Hz, 92H), 7.35 (s, 152H), 6.98 (s, 47H), 5.41 (dd, *J* = 48.0, 25.5 Hz, 212H), 5.10 – 4.91 (m, 4H), 4.00 (s, 317H), 3.93 (s, 130H), 3.89 (s, *J* = 7.1 Hz, 527H), 2.19 (s, 305H), 1.97 (s, 117H), 1.85 (s, 301H), 1.67 (s, 105H), 1.40 (s, 96H). M_n: 18,400 g/mol, M_w/M_n: 1.95.

$(CH_3)_2$-MTVP-$1_{1:1}$. Yield: 78% (315 mg). ^{1}H NMR (400 MHz, $CDCl_3$) δ 8.10 (d, *J* = 24.4 Hz, 331H), 7.65 (s, *J* = 5.4 Hz, 332H), 7.31 (d, *J* = 24.9 Hz, 186H), 6.98 (s, 163H), 5.70 – 5.15 (m, 361H), 5.10 – 4.88 (m, 4H), 4.16 – 3.70 (m, 1768H), 2.17 (s, 360H), 1.96 (s, *J* = 25.2 Hz, 353H), 1.83 (s, *J* = 5.2 Hz, 360H), 1.66 (d, *J* = 6.6 Hz, 369H), 1.40 (s, 335H). M_n: 15,700 g/mol, M_w/M_n: 1.68.

$(CH_3)_2$-MTVP-$1_{1:3}$. Yield: 98% (452 mg). ^{1}H NMR (400 MHz, $CDCl_3$) δ 8.23 – 7.87 (m, 473H), 7.66 (s, *J* = 5.5 Hz, 474H), 7.33 (s, 84H), 6.97 (s, 228H), 5.59 – 5.16 (m, 336H), 4.95 (s, 4H), 4.07 – 3.77 (m, 1614H), 2.13 (d, *J* = 30.9 Hz, 179H), 1.95 (s, 473H), 1.83 (s, 183H), 1.73 – 1.62 (m, 446H), 1.40 (d, *J* = 6.3 Hz, 475H). M_n: 8,800 g/mol, M_w/M_n: 2.00.

Procedure for ester deprotection of $(CH_3)_2$-MTVP-$1_{m:n}$. The MTV polymer ester (220 mg – 360 mg) was added to a 250 mL round-bottom flask, along with potassium hydroxide (30 equiv), and placed in 60 mL a 1:1 of THF/water solution. The mixture was heated at 70 °C overnight.

The THF was reduced by evaporation. The solution was acidified to a pH value of ~1 using a 2M HCl solution. The resultant polymer suspension was collected by centrifugation at 7000 rpm for 10 min. at 8 °C. The solid was transferred to a vial and dried under high vacuum at 40 °C.

MTVP-1$_{3:1}$. Yield: 98% (210 mg). ^{1}H NMR (400 MHz, DMSO-d_6) δ 7.97 (s, 5H), 7.69 (s, 5H), 7.25 (s, 8H), 7.09 (s, 2H), 5.80 – 5.08 (m, 10H), 3.96 (s, 20H), 2.11 (s, 14H), 1.91 (s, 5H), 1.83 – 1.48 (m, 31H).

MTVP-1$_{1:1}$. Yield: 89% (210 mg). ^{1}H NMR (400 MHz, DMSO-d_6) δ 7.96 (s, 3H), 7.69 (s, 3H), 7.24 (s, 2H), 7.07 (s, 2H), 5.55 – 5.15 (m, 4H), 3.94 (s, 7H), 2.09 (s, 4H), 1.91 (s, 4H), 1.69 (s, 4H), 1.57 (s, 3H).

MTVP-1$_{1:3}$. Yield: 87% (293 mg). ^{1}H NMR (400 MHz, DMSO-d_6) δ 7.95 (s, 10H), 7.66 (s, 9H), 7.23 (s, 2H), 7.05 (s, 4H), 5.29 (d, J = 37.6 Hz, 6H), 3.92 (s, 13H), 2.08 (s, 3H), 1.88 (s, 10H), 1.67 (s, 3H), 1.56 (s, 9H), 1.33 (d, J = 15.5 Hz, 10H).

General procedure for Zr-polyMOF synthesis. Procedure was adapted from the synthesis of polyUiO-66 discussed in Chapter 2. The appropriate amount of MTVP-1$_{m:n}$ (0.06 mmol of total carboxylate linkers), $ZrCl_4$ (0.037 mmol), and 2 mL of DEF were added to a 20 mL scintillation vial. After the mixture was sonicated for 15 min, 2 mL of formic acid was added. The vial was heated at 135 °C for 48 h. The resultant film was washed by exchanging solvent with copious amounts of DMF, followed by copious amounts of methanol. Samples were stored dry until further use.

General procedure for IRMOF-type polyMOF synthesis. The IRMOF-type polyMOFs were prepared by adapting the procedure discussed in Chapter 3. The appropriate amount of MTVP-1$_{m:n}$ (0.050 mmol of total carboxylic acid), $Zn(NO_3)_2 \cdot 6H_2O$ (0.125 mmol), and 1.3 mL of DMF were mixed in a 20 mL scintillation vial. The vial was placed in a pre-heated oven at 100 °C for

24 h. The resultant off-white powders were cleaned by centrifugation (4000 rpm), and extensive washing by solvent-exchange of DMF (5x5 mL of DMF). The samples were kept in DMF until further studies were performed.

Analytical Characterization

Gel-permeation chromatography (GPC) conditions for analysis of copolymer esters. Gel-permeation chromatography was performed in THF (1.0 mL/min) using an Agilent GPC equipped with Wyatt multidetectors (RI, DLS, Viscomer) and a general-purpose mixed-bed weight divinylbenzene column connected in series to determine molecular weights and molecular weight distributions, M_w/M_n, of our polymers. The solutions were filtered through 0.4 μm PTFE membrane before being injected into either GPC instrument.

PXRD Analysis. *For UiO-66 polyMOFs.* The dries, synthesized materials were loaded on a small-well sample holder. *For IRMOF-1 polyMOFs.* The samples were loaded on silicon crystal sample holders while still wet with DMF. PXRD data were collected at ambient temperature on a Bruker D8 Advance diffractometer at 40 kV and 40 mA for Cu Kα (λ = 1.5418 Å), with a scan speed of 0.5 s/step, a step size of 0.02° in 2θ, and a 2θ range of 5−50°.

^{1}H NMR Digestions. *For Zr-MTVP-1$_{m:n}$.* Samples were filtered and washed with copious amounts of DMF, methanol, and acetone to remove any impurities. About 10 mg of material was dissolved in 600 μL DMSO-d_6 using 10 μL of 50% HF in water to digest the polyMOF. *For Zr-MTVP-1$_{m:n}$.* About 5 mg of polyMOF was washed with DMF and CH_2Cl_2. To the samples was added a solution containing 600 μL of DMSO-d_6 and 5 μL of DCl. The mixture was sonicated at room temperature for 1 h. The solution was used for ^{1}H NMR analysis.

SEM Measurements. All samples were transferred to conductive carbon tape on a sample holder, and coated using a Ir-sputter coating for 7 sec. A Philips XL ESEM instrument was used for acquiring images using a 10 kV energy source under vacuum at a working distance at 10 mm.

Supplemental Figures

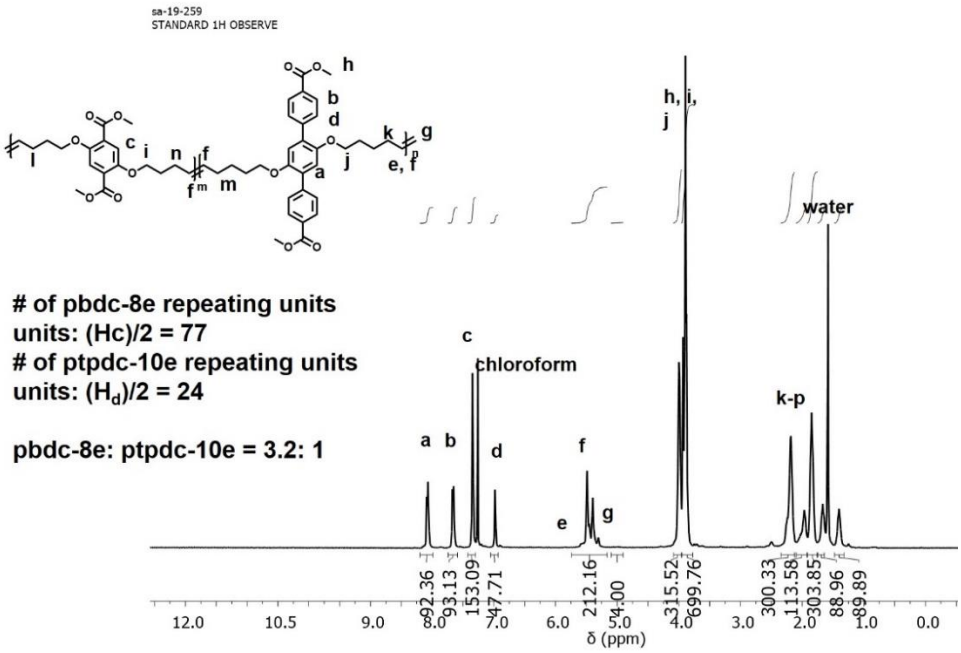

Figure 5S.1. ^{1}H NMR of $(CH_3)_2$-MTVP-$1_{3:1}$. End-group analysis was used to quantify the repeating units of bdc-8a and tpdc-10e.

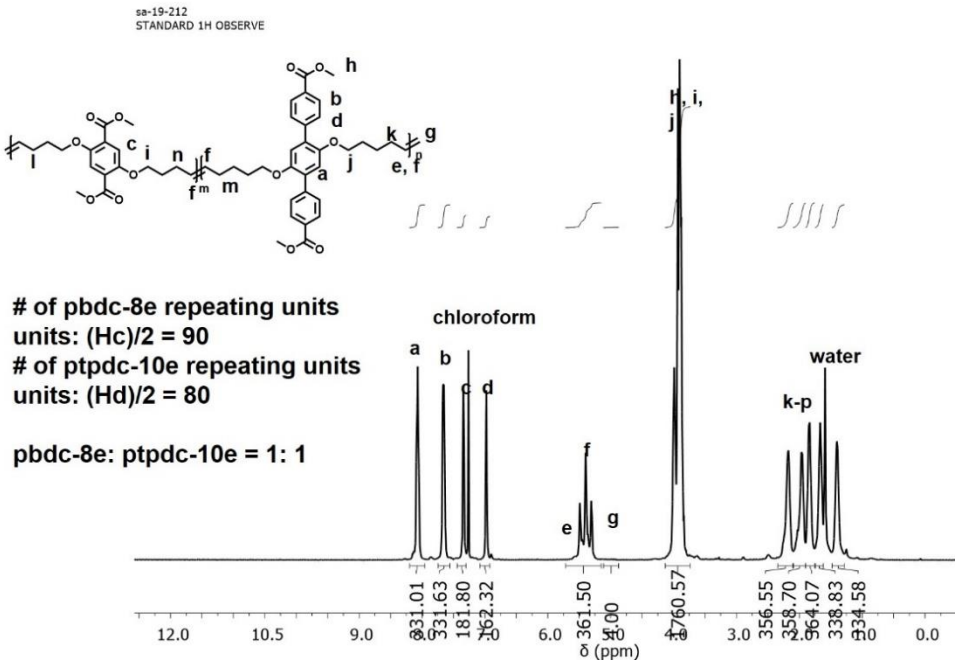

Figure 5S.2. ^{1}H NMR of $(CH_3)_2$-MTVP-$1_{1:1}$.

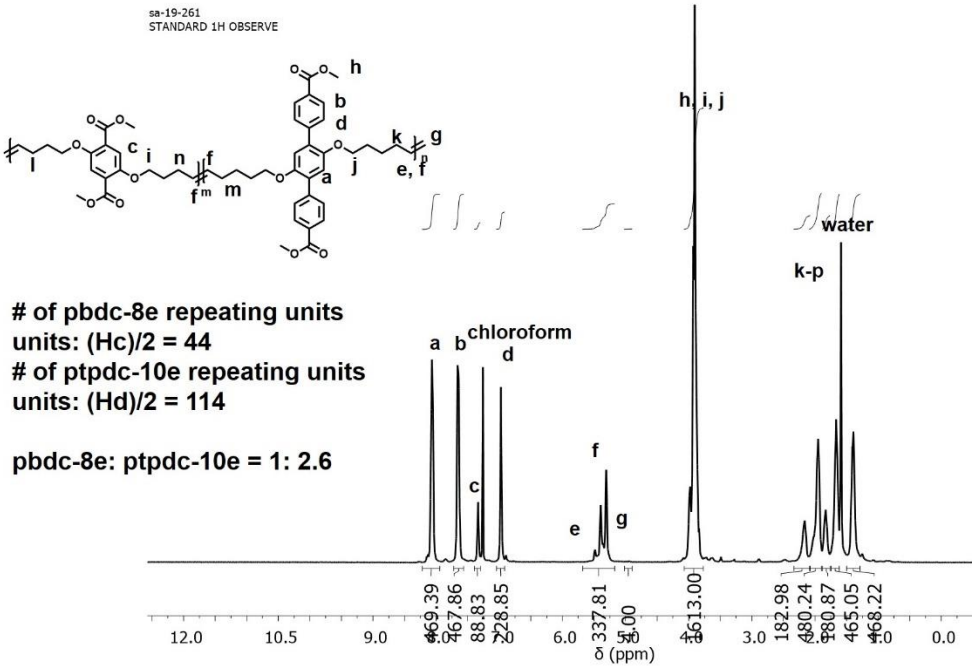

Figure 5S.3. ^{1}H NMR of $(CH_3)_2$-MTVP-$1_{1:3}$.

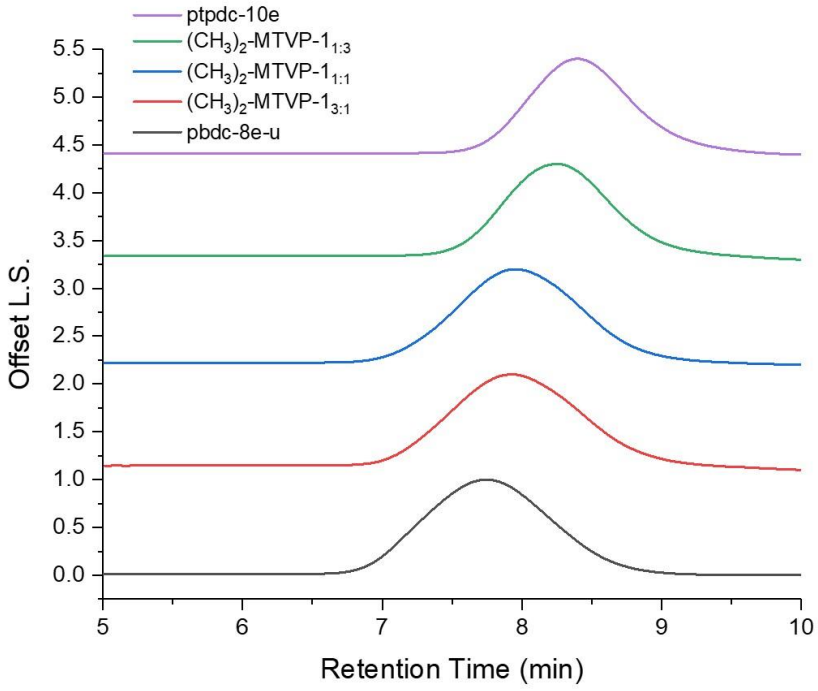

Figure 5S.4. GCP traces of $(CH_3)_2$-MTVP-$1_{m:n}$, pbdc-8e-u and ptpdc-10e-u.

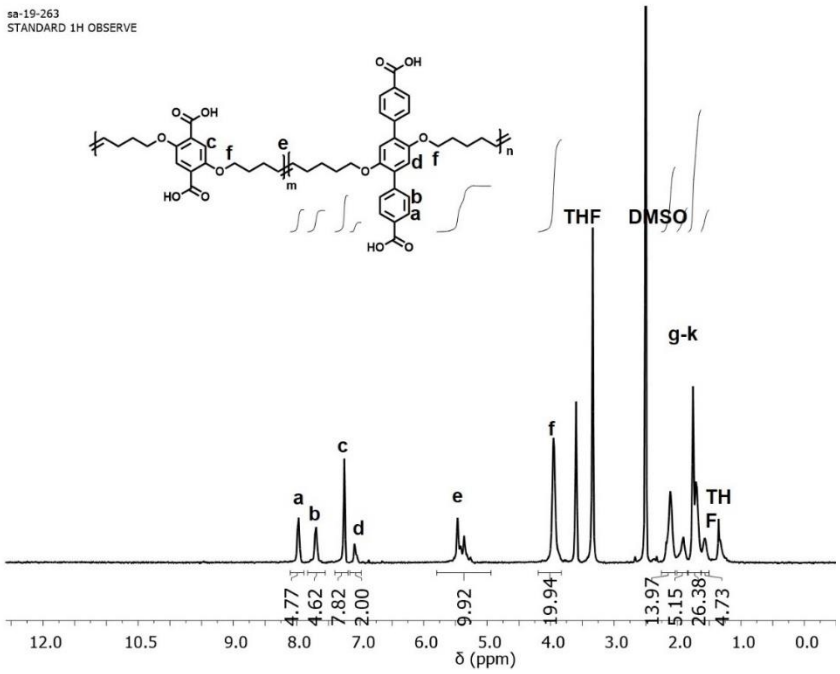

Figure 5S.5. ^{1}H NMR of MTVP-$1_{3:1}$.

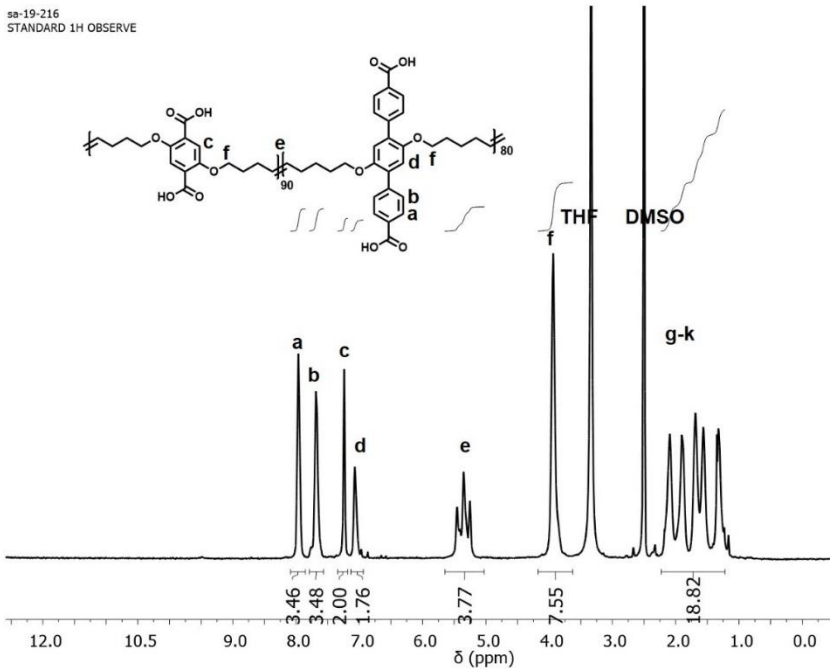

Figure 5S.6. ^{1}H NMR of MTVP-$1_{1:1}$.

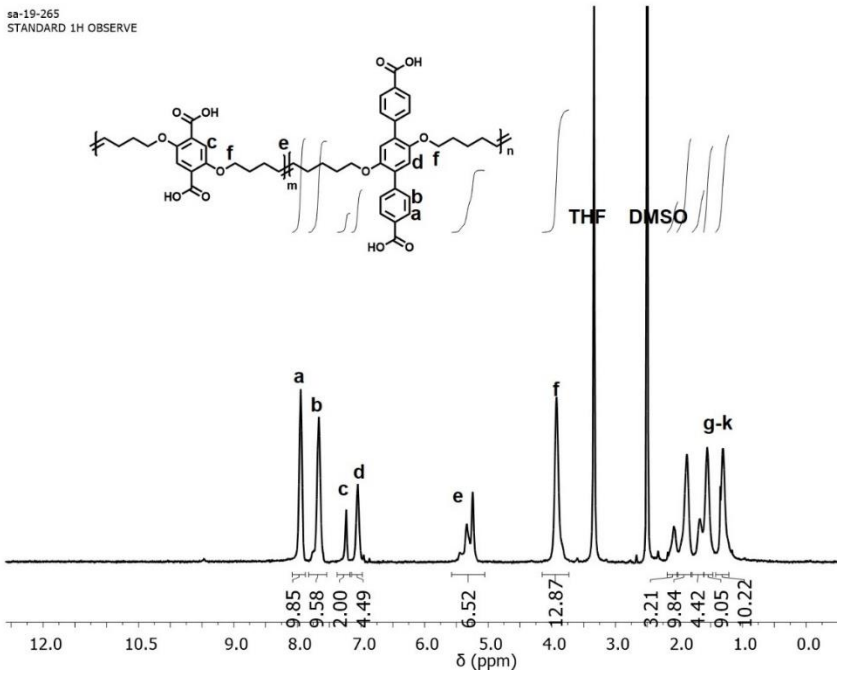

Figure 5S.7. ^{1}H NMR of MTVP-$1_{1:3}$.

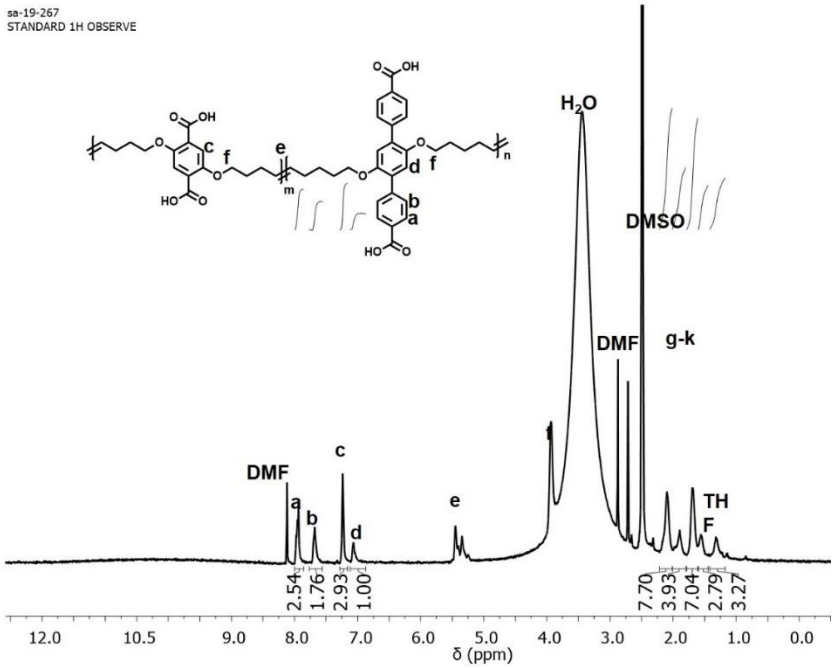

Figure 5S.8. ^{1}H NMR of digested Zr-MTVP-$1_{3:1}$.

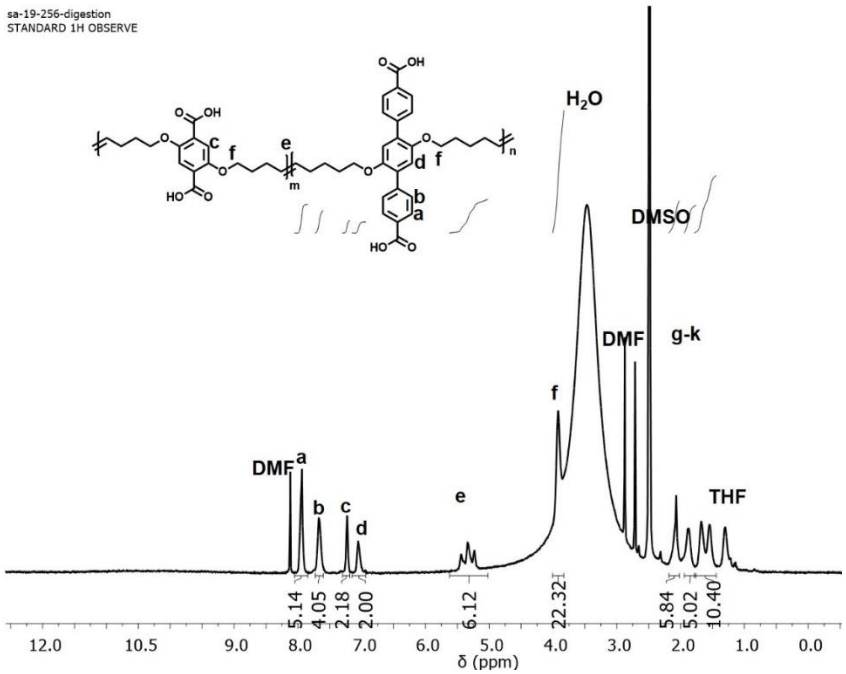

Figure 5S.9. ^{1}H NMR of digested Zr-MTVP-$1_{1:1}$.

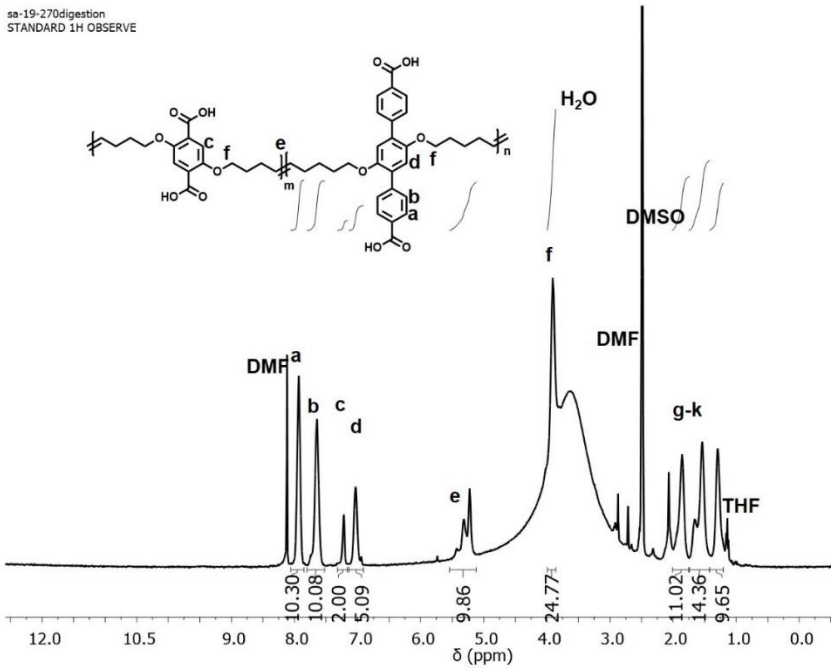

Figure 5S.10. ^{1}H NMR of digested Zr-MTVP-$1_{1:3}$.

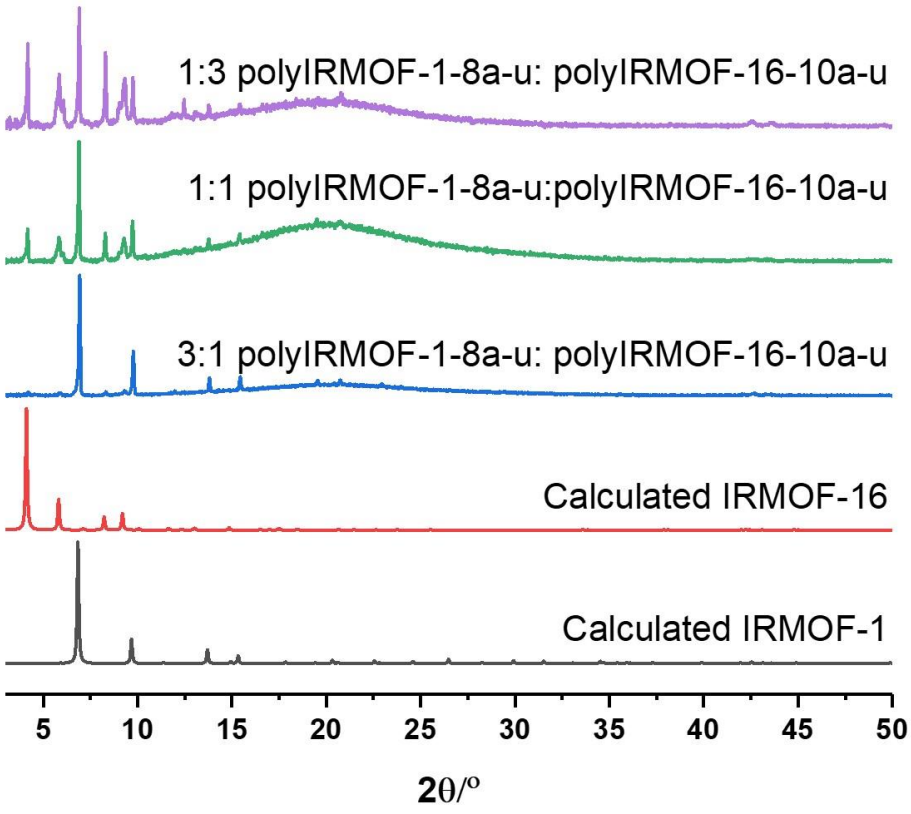

Figure 5S.11. PXRD patterns of Zn-polyMOFs prepared from a mixture of homopolymers pbdc-8a-u and ptpdc-10a-u in three different ratios.

5.5 Acknowledgements

The dissertation author gratefully acknowledges the MOF subgroup, and Seth M. Cohen for their helpful discussions regarding the project presented in Chapter 5.

5.6 References

1. Altintas, C.; Avci, G.; Daglar, H.; Nemati Vesali Azar, A.; Erucar, I.; Velioglu, S.; Keskin, S., An extensive comparative analysis of two MOF databases: high-throughput screening of computation-ready MOFs for CH4 and H2 adsorption. *J. Mater. Chem. A* **2019,** *7*, 9593-9608.

2. Moghadam, P. Z.; Li, A.; Wiggin, S. B.; Tao, A.; Maloney, A. G. P.; Wood, P. A.; Ward, S. C.; Fairen-Jimenez, D., Development of a Cambridge Structural Database Subset: A Collection of Metal–Organic Frameworks for Past, Present, and Future. *Chem. Mater.* **2017,** *29*, 2618-2625.

3. Deng, H.; Doonan, C. J.; Furukawa, H.; Ferreira, R. B.; Towne, J.; Knobler, C. B.; Wang, B.; Yaghi, O. M., Multiple Functional Groups of Varying Ratios in Metal-Organic Frameworks. *Science* **2010,** *327*, 846.

4. Koh, K.; Wong-Foy, A. G.; Matzger, A. J., A Crystalline Mesoporous Coordination Copolymer with High Microporosity. *Angew. Chem. Int. Ed.* **2008,** *47*, 677-680.

5. Feng, L.; Wang, K.-Y.; Day, G. S.; Zhou, H.-C., The chemistry of multi-component and hierarchical framework compounds. *Chem. Soc. Rev.* **2019,** *48*, 4823-4853.

6. Feng, L.; Wang, K.-Y.; Willman, J.; Zhou, H.-C., Hierarchy in Metal–Organic Frameworks. *ACS Cent. Sci.* **2020,** *6*, 359-367.

7. Liu, C.; Rosi, N. L., Ternary gradient metal–organic frameworks. *Faraday Discuss.* **2017,** *201*, 163-174.

8. Liu, C.; Zeng, C.; Luo, T.-Y.; Merg, A. D.; Jin, R.; Rosi, N. L., Establishing Porosity Gradients within Metal–Organic Frameworks Using Partial Postsynthetic Ligand Exchange. *J. Am. Chem. Soc.* **2016,** *138*, 12045-12048.

9. Luo, T.-Y.; Liu, C.; Gan, X. Y.; Muldoon, P. F.; Diemler, N. A.; Millstone, J. E.; Rosi, N. L., Multivariate Stratified Metal–Organic Frameworks: Diversification Using Domain Building Blocks. *J. Am. Chem. Soc.* **2019,** *141*, 2161-2168.

10. Yuan, S.; Huang, L.; Huang, Z.; Sun, D.; Qin, J.-S.; Feng, L.; Li, J.; Zou, X.; Cagin, T.; Zhou, H.-C., Continuous Variation of Lattice Dimensions and Pore Sizes in Metal–Organic Frameworks. *J. Am. Chem. Soc.* **2020,** *142*, 4732-4738.

11. Koh, K.; Wong-Foy, A. G.; Matzger, A. J., MOF@MOF: microporous core–shell architectures. *Chem. Commun.* **2009**, 6162-6164.

12. Kwon, O.; Kim, J. Y.; Park, S.; Lee, J. H.; Ha, J.; Park, H.; Moon, H. R.; Kim, J., Computer-aided discovery of connected metal-organic frameworks. *Nat. Commun.* **2019,** *10*, 3620.

13. Haque, T.; Nomura, K., ADMET Polymerization: Greener Method for Synthesis of End-Functionalized Poly(Arylene Vinylene)s. *Green and Sustainable Chemistry* **2017,** *Vol.07No.01*, 19.

14. Miyashita, T.; Kunisawa, M.; Sueki, S.; Nomura, K., Synthesis of Poly(arylene vinylene)s with Different End Groups by Combining Acyclic Diene Metathesis Polymerization with Wittig-type Couplings. *Angew. Chem. Int. Ed.* **2017,** *56*, 5288-5293.